Università degli Studi del Piemonte Orientale

Dipartimento di Scienze e Innovazione Tecnologica

Dottorato di Ricerca in Chemistry & Biology

curriculum: Drug Discovery and Development

XXIX ciclo a.a. 2015-2016

SSD: CHIM/03

Passive drug targeting and delivery of antitumor Pt(IV) prodrugs

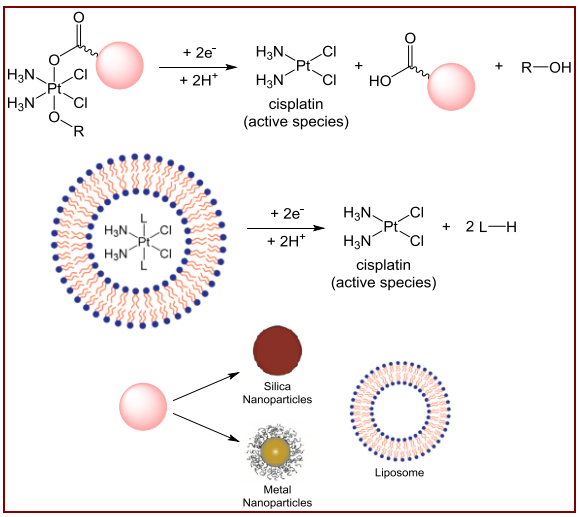

Elena Perin

Supervised by Prof. Mauro Ravera

PhD program co-ordinator: Prof. Domenico Osella

Università degli Studi del Piemonte Orientale

Dipartimento di Scienze e Innovazione Tecnologica

Dottorato di Ricerca in Chemistry & Biology
curriculum: Drug Discovery and Development
XXIX ciclo a. a. 2015-2016
SSD: CHIM/03

Passive drug targeting and delivery of antitumor Pt(IV) prodrugs

Elena Perin

Supervised by Prof. Mauro Ravera

PhD program co-ordinator: Prof. Domenico Osella

Contents

Chapter I

The Tumor

1.1 The Origin of the Tumor

A tumor (from the Latin *tumor*, “swelling”), also defined as neoplasia (from the Greek *néos*, “new”, and *plàsis*, “formation”), is an abnormal mass of tissue growing upon a pathological proliferation of the cells in a part of the body. The main feature of these cells is the uncontrolled and uncoordinated growth with respect to the healthy ones and this behavior is due to the fact that they do not respond to the mechanisms of cellular control and, in turn, this is due to alterations of their genetic heritage.

Although tumors are characterized by a common origin mechanism, they can undergo different evolution and symptoms pathways while sharing a steady and progressive cancerous cells increase, owing to a more rapid cellular reproduction. Therefore, a continuous multiplication of the majority of tumor cells is observed and only few cells do not survive and die.

A neoplasia usually grows and develops obeying a geometric law: in the early stages, the growth is slow and then it accelerates when the tumor mass increases. In addition, when the tumor reaches a critical size (about 1 cm^3), it grows more and more rapidly and the symptoms can be felt (*Figure 1.1*).

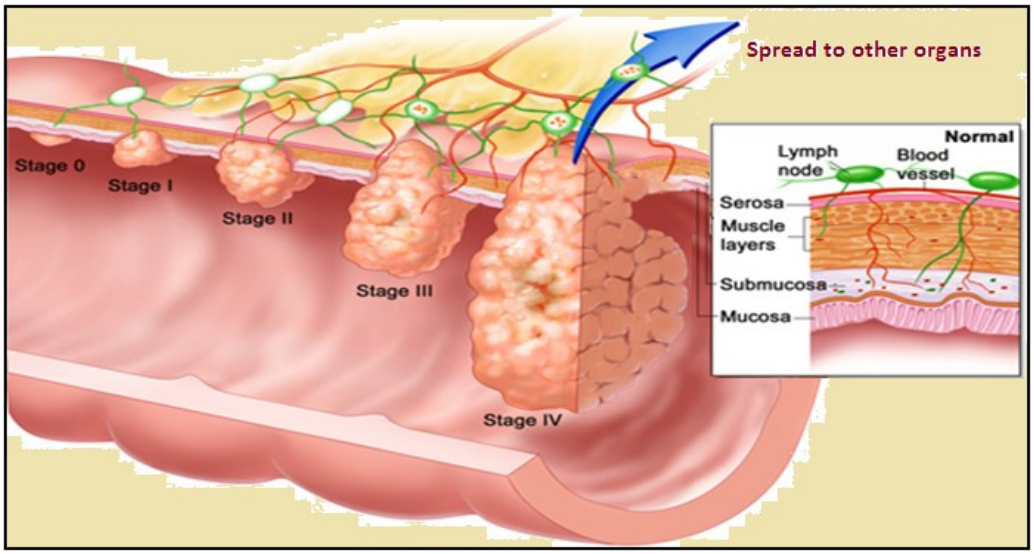

Figure 1.1: Scheme of the growth phases of a tumor process.
The picture is a modification of that reported in literature [1]

The term cancer (from the Latin *cancer*, "crab") was introduced by observing neoplastic cells behavior. In fact, in the multiplication phase, they form ramifications that entrap and destroy the surrounding healthy cells; metaphorically, in the same way, a crab destroys its prey with its claws.

The genes responsible for cellular control are located inside each cell and they have to prevent diseased cells to survive; the beginning of a tumoral process is the result of a failure of these genes. Therefore, since the mechanism responsible for the replication does not work anymore, the cells behave abnormally and multiply themselves forming daughter cells characterized by the same problems. Into the cells a series of changes happens, in particular as regards the genes. The neoplasia can have a benign or malignant biological behavior, depending on the features of the neoplastic cells. A benign tumor has a structure in which the cells mostly preserve the morphological and functional original tissue features, it has a growth speed usually slow and this is an expansive but not infiltrative growth. The tumor, indeed, is localized and enclosed in a wrapping of connective fibrous tissue, which allows it to distinguish itself from the other tissues, and, although

expanding, it does not invade the surrounding tissues but it only compresses them. On the contrary, a malignant tumor, commonly defined cancer, consists of cells which are morphologically and functionally different from the original tissue and this kind of neoplasia rapidly grows, also by infiltrating into the surrounding tissues, thus destroying them. The infiltration of these cancerous cells does not stop and continues its way into the human body through blood and lymphatic systems, giving rise to the metastasis (or secondary tumors). Moreover, the cancer has a high risk of reformation after surgery, unlike a benign tumor.

Finally, some anomalies characterize the neoplastic cells:

- an excess of sodium;
- a lack of potassium;
- an excess of water.

In particular, water is about 90%, unlike 66% of the healthy cells: this excess is due, in turn, to the high sodium content in the blood, indeed sodium, being aggressive, attracts protective liquid around itself.

The medical nomenclature of tumors provides their classification on the basis of the tissue where they start growing and of their biological behavior (i.e. benign or malignant) (*Table 1.1*).

Tissue of origin	**Benign tumor**	**Malignant tumor**
Connective tissue, Cartilage, Bone, Muscle	Fibroma, Chondroma, Osteoma, Leiomyoma, Rhabdomyoma	Sarcoma
Leukocytes		Leukemia
Glandular epithelial and coating	Adenoma, Papilloma	Carcinoma
Nervous tissue		Blastoma

Melanocytes	Melanocytic nevus	Melanoma
Lymphatic glands		Lymphoma

Table 1.1: Classification and medical nomenclature of tumors

Moreover, there are several methods employed to classify a neoplasia according to its stage. In particular, some methods consider the tumor size (T), the degree of regional spread or node involvement (N), or distant metastasis (M): this is the TNM staging method [2]. The T and N stages range from 0 to 4, e.g. T 0 means no cancer evidence, N 0 no nodal involvement, and T and N increase with the tumor size and the degree of lymph nodes involvement increasing, respectively. As regards metastasis, M 0 and M 1 are used and indicate no evidence or evidence of metastasis.

The neoplasia formation is divided into different phases, such as hyperplasia and dysplasia.

The hyperplasia is characterized by an increase of the tissue volume due to an abnormal multiplication of the cells that compose it: this is the expression of the adaptive response of a tissue to those stimuli that lead to an increase of its functional activity.

An anomaly of the development of a tissue or a system is observed in the dysplasia and this behavior is often accompanied by deviations of the function and deformity. Therefore, the anomalous proliferative process involves a volume increase and an alteration of the affected area architecture. Thus, these diseases can be distinguished because the former leads to the increase of the cells number, while the latter to variations of their shape and organization.

1.2 Antitumor Therapies

The immune system of the patient is not able to distinguish cancerous cells from healthy ones or the reaction against them is not enough. Antibiotics and antiviral drugs administered have no effect on tumor cells because from a structural point of view, they are still substantially human cells; neoplastic drugs must be highly selective and able to recognize a cancerous tissue respect to healthy ones. Therefore, a tumor needs to be cured by means of one of the following treatments:

- radiotherapy;
- surgical excision;
- chemotherapy;
- hormone therapies.

The rapid reproduction of tumor cells makes them more vulnerable to radiations than the healthy ones and this aspect can be exploited for the treatment of some kinds of tumor with gamma rays (radiotherapy) to physically destroy the majority of malignant cells.

By means of early diagnosis, some types of still embryonic tumors can be identified and therefore, in these cases, it may be necessary only surgical excision or the irradiation with high energy sources.

In the case of advanced stage diseases and, in particular, when malignant cells have already spread in the body, giving rise to metastasis, chemotherapy is exploited. This treatment is based on specific chemical compounds (antiproliferative or antineoplastic chemotherapeutics). The antineoplastic (or antiblastic) drugs are substances able to stop or to slow down tumoral processes. Although physical therapy and surgery are the best tumor treatments, antineoplastic drugs, especially in particular cases, allow to obtain remarkable

results, even though not definitive. Among them, antimitotic and antimetabolites must be considered.

Since its first administration, in half a century, the antitumor chemotherapy saw the study of thousands chemical compounds. However, only few reached the stage of trials in animals (*in vivo*) and a lower number showed to be tolerable and effective in order to allow clinical trials in patients. A small part of the drugs tested in patients demonstrated to be useful in cancer therapy.

Moreover, usually, radiotherapy and chemotherapy were employed after a surgical excision as a preventive measure, in order to reduce the risk of a relapse.

Another possible cure can be obtained by means of hormone therapies. It is known that the occurrence of some kinds of neoplasia (such as breast and prostate tumors) is stimulated by hormones (such as estrogen and androgen). Therefore, hormone therapy aims to limit/avoid hormone production or their proliferative actions on cancer.

The requirements of an effective antitumoral treatment are numerous and some of them are mentioned below. In particular, the drug must be selectively sent to the tumor tissue and a reasonable amount of it must remain into the cells for a defined time, without degrading. The tumor itself must be sensitive to the drug treatment and the patient must tolerate the drug side effects. The employed strategy of administration should be specific for each case, being monochemotherapy, which includes the use of a single drug, or combination chemotherapy (or polychemotherapy), when a combination of more antineoplastics is exploited. It is known that a combination of antitumor drugs is more effective than the use of single ones because these latter, with rare exceptions, are not able to completely eradicate cancer. The clinical superiority of combination chemotherapy can be ascribed to several causes:

- a single drug leads to the maximum cellular destruction within the tolerated dose;
- the efficacy against resistant cells is larger;
- the development of resistant clones, from cells which initially were sensitive to the therapy, can be prevented or slowed down.

Over the years, some useful principles have been identified in order to guide the choice of drugs to be combined for the development of new therapeutic combinations, even though the drugs are still combined on mainly empirical basis. In general, however, only singularly active drugs, which do not show overlapping toxicities, must be chosen.

In today therapy, the dose is administered for a period ranging from one to five days per cycle and the interval between two cycles of chemotherapy is established according to the recovery time from the toxicity of normal tissues or organs, sensitive to the drug. These considerations have induced to define a two-weeks free period between two cycles of treatment: the new cycle begins in the 21^{st} day, if the drugs are administered on the 1^{st} and the 8^{th} days, and on the 29^{th} day, if the administration is on the 1^{st} and the 14^{th} days. In some rapidly growing tumors (such as lymphomas and leukemias), however, this therapeutic scheme is not appropriate because the tumor can grow again during the period without treatment and different schedules of drugs administration must be used. Actually, in the clinical practice is often necessary to change the drugs dose in order to adapt the treatment to the tolerability of the individual patient. In doing so, it should be considered that a decrease of the dose intensity can result in a significant decrease of the treatment efficacy. For this purpose, it can be useful to use hematopoietic growth factors in order to maintain the dose intensity and, anyway, to make any modifications of dose in a standardized way, according to the commonly accepted guidelines, in order to avoid alterations of the chemotherapy regimen.

Another modality of therapy involves the use of combinations with variable drug composition, which is defined alternating or sequential polychemotherapy. Among the side effects that may occur, fever, nausea and vomit can be kept under control by means of the most modern drugs, but the most widespread adverse effect is myelosuppression. This medical condition occurs when the bone marrow produces blood components in smaller quantities: this is defined anemia when concerns the red blood cells, leukopenia as regards the white blood cells, and thrombocytopenia in the case of platelets. The effects that may occur are characteristic of the individual patient but, if the chemotherapy is accompanied by hyperthermia, the side effects can be made less pronounced and the positive ones for the tumor treatment are enhanced.

1.3 New Generation Therapies

Other therapeutic methods allow to reduce the neoplastic mass and some of them are mentioned below. In the radiotherapy field, a new methodology defined Boron Neutron Capture Therapy (BNCT) is gradually earning importance (*Figure 1.2*). This particular technique involves the penetration of a thermal neutrons beam in the brain tissue thus reaching the tumor mass: the low energy neutrons (about 0.025 eV), therefore, react with ^{10}B (previously introduced into the neoplastic cells by means of drugs), giving origin to ^{11}B, able to emit alpha radiations that destroy the tumor.

$$ {}^{10}_{5}B + {}1^{1}_{0}n \rightarrow \{{}^{11}_{5}B\} \rightarrow {}^{7}_{3}Li + {}^{4}_{2}\alpha + \gamma $$

Similarly to boron, in the organism there are many other elements able to capture neutrons, with consequent radiations emission. Their impact section (i.e.

the probability of capturing neutrons), however, is several orders of magnitude lower than the boron one (*Table 1.2*).

Element	**Impact section (expressed in Barn)**
boron	**3838.00**
oxygen	0.0002
carbon	0.0037
magnesium	0.069
phosphorus	0.19
hydrogen	0.332
calcium	0.44
sulfur	0.52
sodium	0.536
nitrogen	1.75
potassium	2.07
iron	2.62
chlorine	33.8

Table 1.2: Neutron capture impact section of the main elements in the organism

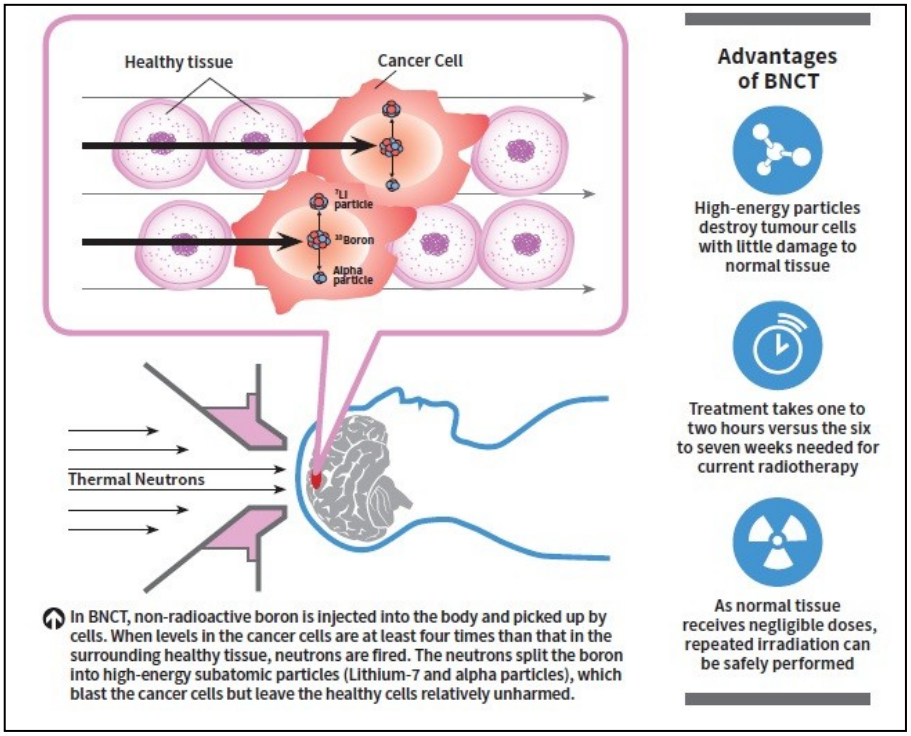

Figure 1.2: Application and advantages of Boron Neutron Capture Therapy. The picture is a modification of that reported in literature [3]

This method is appropriate for surface tumors: indeed, the penetration of the thermal neutrons is limited and, therefore, this technique is ideal for cutaneous neoplasias, such as melanomas. Neoplastic cells, then, must be enriched with boron and this can be carried out by using boron compounds, bound to antibodies, or by using boronic acid, injected near the melanoma itself.

Other developed techniques are Immunoscintigraphy (ISG) and Radioimmunotherapy (RIT), which are able to early identify neoplastic cells and to block the tumor, by means of a targeted action, avoiding the damage to the surrounding tissues. The tumoral tissues are characterized by the alteration of some biochemical processes, among which an increase of both cellular metabolism and nucleic acids synthesis must be recalled. Furthermore, the cancerous cells have antigens that are not expressed by normal tissues or are

present only in smaller amount. In this regard, the use of radiolabelled antibodies, specific for each antigen, allows the identification of diseased tissues by means of external detection; this is the purpose of Immunoscintigraphy. This treatment enables the detection of different types of tumor, among which melanoma, gastrointestinal, brain, breast, ovarian and lung tumors.

The principle on which the previously discussed method is based can also be extended to Radioimmunotherapy. It directs its action towards specific targets (cancerous cells) by identifying them and by stopping their progress. With this purpose, it employs radiolabelled antibodies and specific peptides and, thanks to the radiations produced *in situ*, it makes possible the damage to the DNA of neoplastic cells.

Another form of non-surgical treatment is Photodynamic Therapy (PDT), the principle of which is a photodynamic reaction able to selectively destroy tumoral cells. A photodynamic reaction involves the absortion of laser light by a photosensitive substance, based on metal-porphyrin groups, administered to the patient, and the subsequent localized formation of singlet oxygen $^1O_2$, i.e. oxygen in its reactive form (which is one of the so-called ROS, Reactive Oxygen Species). The species thus formed are toxic for the cell that generated them and cause its death; therefore, according to the purpose of this method, these tissues are destroyed. Among the requirements for the choice of a photosensitizer, it is important that it must be a molecule which does not show any toxic effects in humans, with limited size in order to allow its penetration through the skin, and able to distinguish and, therefore, to select diseased cells from healthy ones.

1.4 Cell Proliferation

The reproduction of human cells occurs by means of the duplication of their DNA, which is followed by the division of the parental cell into two daughter cells. In physiological conditions, the equilibrium of the cells number of the tissues is guaranteed by another equilibrium, the harmonic one among cell proliferation, senescence and cell death. The cell constantly receives signals of proliferation or death from the microenvironment, elaborates them by means of mechanisms of signals transduction, and, ultimately, transmits them to the nucleus, where the last phase of the cell cycle regulation occurs. In order to ensure the identity of the genetic heritage transmitted to the daughter cells, every individual cell includes appropriate mechanisms of DNA repair that, in the case of the occurrence of spontaneous mutations or induced by mutagens, provides for the correction. After the completion of a predefined number of mitotic cycles, the cells, except those stem, enter a phase of irreversible senescence.
In contrast to normal cells homeostasis, which is regulated by a complex net of molecular pathways that supervise a rigid control of cell cycle, DNA repair and cell death, the neoplasias are characterized by specific genetic lesions which cause a genomic instability and alter the control of cell cycle and apoptosis.

1.5 Cell Cycle

The administration of cytotoxic drugs has the main purpose of preventing cell division and, in particular, the substances can act in a targeted way on a phase or indiscriminately on several cycle phases.
The cell cycle is an event of great importance and possible mistakes could compromise the life of the cells themselves: for this reason, it is regulated in all

its phases. In particular, the cycle consists of five distinct phases [4] (*Figure 1.3* and *Table 1.3*):

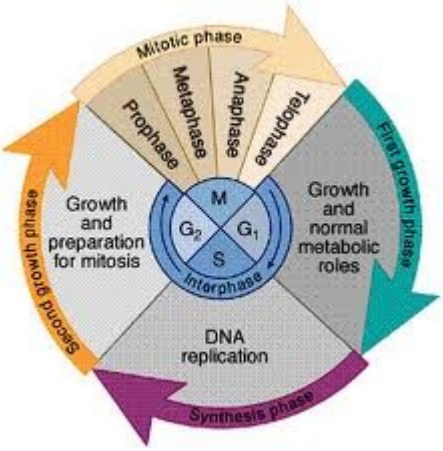

Figure 1.3: Cell division cycle of a eukaryotic cell [5]

G_0 phase	resting state, in which cells have stopped dividing (temporarily or irreversibly) (*not shown in Figure 1.3*)
G_1 phase	state that follows mitosis and in which it is possible to assist to the synthesis of proteins and RNA, necessary to duplicate chromosomes
S phase	chromosomes duplication occurs and, therefore, DNA synthesis
G_2 phase	state that precedes cell division and in which proteins are synthesized again
M phase	divided into mitosis and cytodieresis (or cytokinesis), in which it is possible to assist to the division of chromosomes and cytoplasm of the cell

Table 1.3: Main phases of the cell cycle and their biological function

The points where the process control occurs in order to avoid mistakes during the cycle, defined as "checkpoints", are located in correspondence with G_1-S and G_2-M transitions.

The genetic information must be correctly transmitted from mother to daughter cells (the latter are genetically identical to the progenitor cell) and, for this reason, at first the genome must be duplicated during the S phase and then chromosomes must be confined into the two daughter cells during the M phase. This latter phase is divided into two processes, closely related: mitosis and cytodieresis (or cytokinesis). During the first phase, cell chromosomes are divided between the two daughter cells, while in the second one it is possible to assist to the physical division of the cell cytoplasm.
At the end of M phase and at the beginning of G_1 phase, cells can leave the cell cycle and enter a quiescence phase (G_0 phase), in which they can remain for an indefinite time, following a path that leads to the terminal differentiation, or for a limited period of time, returning to be a part of the cycle. At this point a strict genetic control exists and tumoral cells, which are less differentiated than healthy ones, can be induced to terminal differentiation, thus reducing the malignancy of the tumor.

1.6 Cell Death

The cytotoxicity of a molecule can be defined as the ability to kill a cell. A cell that starts to die modifies its structure. Below, two different types of cell death are described: apoptosis and necrosis (*Figure 1.4*).

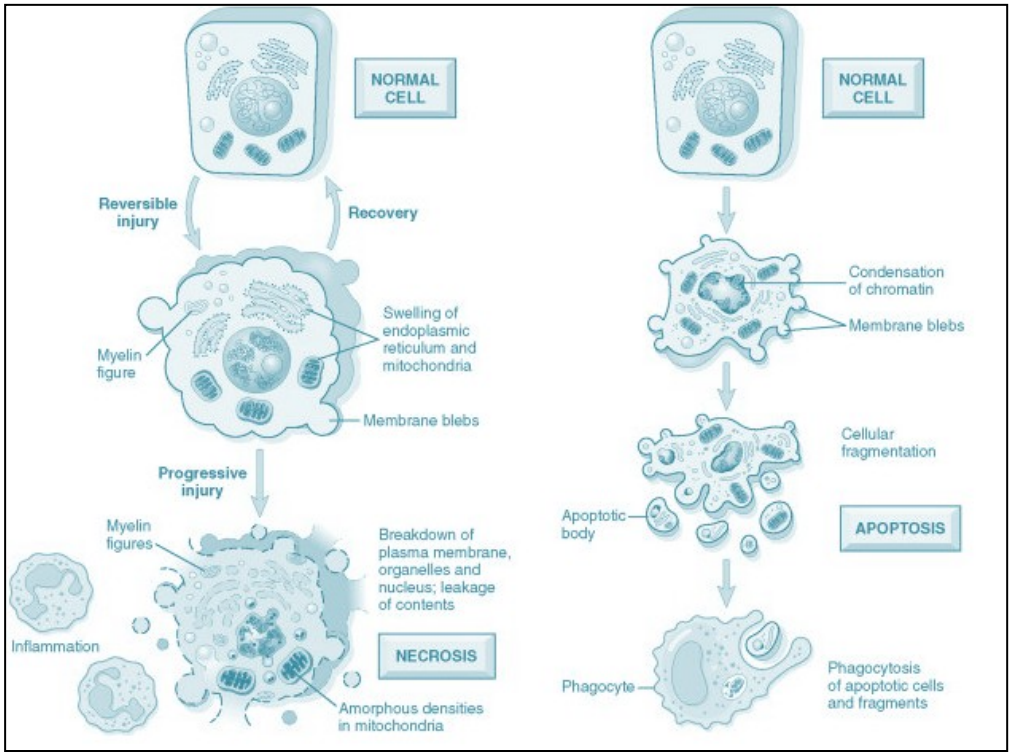

Figure 1.4: Schematic representation of apoptosis and necrosis mechanisms

The necrosis is an accidental cell death, which involves at the same time more or less large groups of cells that are part of an organ or a tissue. This pathological phenomenon occurs when a cell undergoes violent chemical or physical attacks or violent variations of the physiological conditions, due, for example, to hypothermia or hypoxia, which result in a irreversible damage to the cell membrane.

The necrosis may occur due to considerable osmotic variations, to the stopping of oxygen or nutrients supply, or to the proteins denaturation.

The necrosis is a passive process (ATP-independent) and it begins when a loss of the homeostatic abilities occurs. We can assist to an unregulated influx of water and extracellular ions, to an increase of the cellular and mitochondrial size until reaching the rupture (*Figure 1.5*). This necrotic cells explosion is followed

by the overflow of their content on the nearby cells and by an inflammatory response (phlogosis), loading to the area occupied by the debris of dead cells. Then this is followed by the chemotactic recall of leukocytes and this has a double function: the debris phagocytosis and the release of lysosomal enzymes, which act on the dead cells favoring their dissolution.

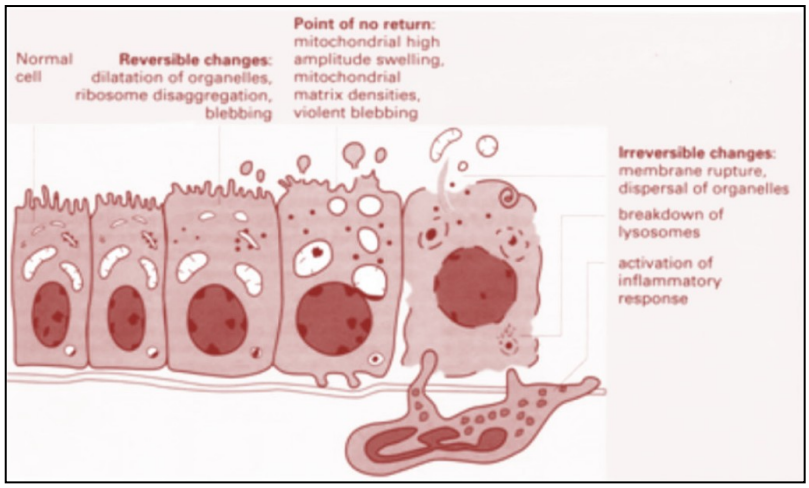

Figure 1.5: Main steps which lead a healthy cell to necrosis [6]

The apoptosis is an active process (ATP-dependent), which affects isolated cells in viable tissues, during which the cell begins a specific program which determines the death (it is defined, in fact, as a suicide of the cell itself).

The term apoptosis derives from the Greek and is employed to describe the fall of the flowers petals or the leaves. This etymology, however, is related to the characteristics of the cell death process: apoptotic cells condense and detach from the tissue support structures on which they are growing, as well as the tree leaves which fall in autumn.

It can manifest in a spontaneous way or by induction and the resulting events may be a cellular contraction, a change in the distribution of membrane phospholipids (in fact, phosphatidylserine (PS) moves from the cytoplasmic to

the extracellular area of the plasma membrane), and the chromatin condensation (due to its organization collapse), during which bubbles are formed (phenomenon defined Blebbing) that, separating from the cell itself, give rise to apoptotic bodies (which contain cytoplasm and organelles) that are subsequently phagocyted (*Figure 1.6*).

The process begins when an alteration of the mitochondrial membrane permeability occurs and this is followed by the release of cytochrome c into the cytosol, which caused the activation of enzymatic substances (the Caspases) giving rise to the cutting of cytoplasmic and nuclear substrates. The DNA fragmentation is not random, unlike what occurs in necrosis.

As regards the apoptotic bodies phagocytosis, it occurs very rapidly and efficiently so that avoids any inflammatory response because it prevents the release of their content outside.

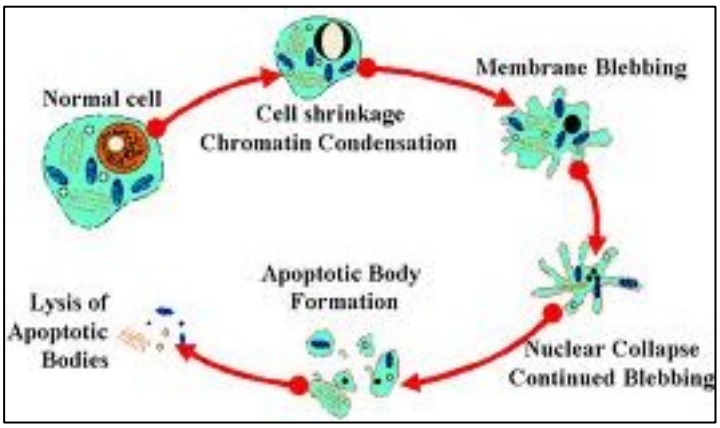

Figure 1.6: Main step which lead a healthy cell to apoptosis [7]

It is a fundamental phenomenon in physiological processes because it removes not functional or structurally not useful cells. The apoptosis, in fact, has a complementary and reverse function respect to that of mitosis and cell proliferation in the regulation of cell populations.

In the embryonic phase, it proceeds to the removal of the interdigital membranes, to the formation of the lumen of hollow organs, to the numeric scaling of nerve cells and to the opening of the eyelids during the development of nervous and immune systems.
In adult it is responsible for the atrophy observed in some tissues and for the endometrial cells destruction during the menstrual cycle, for the atresia of the ovarian follicles during the menopause and for the breast regression after the weaning.
The apoptosis, therefore, is involved in many physiological cellular processes, not only in the pathological ones, unlike necrosis, which has mainly a pathological nature.

References

[1] Liquidarea.com website, Tumore del colon retto: è difficile guarire senza gli screening.
[2] A. Mandal, Cancer Classification, News Medical, Life Science & Medicine.
[3] National Cancer Center Singapore website, The next big thing in radiotherapy.
[4] GM. Cooper, The Cell: A Molecular Approach. The Eukaryotic Cell Cycle, 2000.
[5] epertutti.com website, Divisione Cellulare negli eucarioti - Ciclo cellulare, Regolazione della divisione cellulare.
[6] SlidePlayer, Patologia cellulare. Cause di danno Virchow (il padre della patologia moderna) nell'800: tutte le forme di danno di organo, cominciano con alterazioni.
[7] Vincenzo Piazza, L'apoptosi nella tiroide di Hashimoto.

Chapter II

The Platinum Chemistry

2.1 The Chemistry of Platinum Complexes

Platinum was discovered in 1748 by the Spaniard Antonio de Ulloa in the gold mines of Colombia and the name with which it is currently known was disparangingly attributed to it: in fact, “platinum” is the short for “plata”, i.e. small silver. The explanation for this name is that, although it looked like silver, it had not its properties.

It is a not very abundant metal on the Earth crust (0.015 ppm) and it can be found in its native state or associated with sulfur compounds of copper and nickel.

Although it is noble (resistant to chemical attack), platinum can be dissolved in *aqua regia* (a mixture of nitric and hydrochloric concentrated acids in a volumetric ratio 1:3) and at elevated temperature it can also react with F_2 to obtain PtF_4 or PtF_6, according to the reaction conditions, and with Cl_2 in order to obtain $PtCl_2$ or $PtCl_4$, according to the temperature at which the process is carried out.

It may form compounds in the oxidation states 0, II, IV, V and VI, and the last two, in particular, with oxygen and fluorine derivatives.

The most important oxidation states in aqueous solution and, therefore, in the biological environments are II and IV: in the +2 oxidation state the complexes show a square-planar geometry (that corresponds to a coordination number of 4), whereas in the +4 oxidation state the geometry is octahedral (the coordination number is 6) and this is the most stable.

Since the platinum in the +2 oxidation state, according to the Hard Soft Acid Base (HSAB) classification of Pearson, is a “soft” acid, the most stable complexes will be realized in the presence of “soft” bases, such as S, Se, P and As-donor ligands and also the complexes with *N*-donor ligands are very significant.

The most important anionic compound of platinum(II) for the preparative chemistry is $[PtCl_4]^{2-}$, which is synthesized by reduction of $[PtCl_6]^{2-}$ with hydrazine, and, in turn, $[PtCl_6]^{2-}$ is prepared by means of the reaction of the metal with *aqua regia*.

Among the cationic complexes, $[Pt(H_2O)_4]^{4+}$ is relevant and it can be easily obtained by treating $[PtCl_4]^{2-}$ with a solution of $AgNO_3$.

Moreover, there are numerous neutral complexes with a stoichiometry [PtXYLL'], where X and Y are anions such as halides, hydrides and alkyls, whereas L and L' are neutral ligands such as NH_3, amines, nitrogen heterocycles and phosphines.

In the IV oxidation state, the compounds can be prepared by means of substitution reaction of the halide ion in the most significant anionic complex $[PtCl_6]^{2-}$, by oxidative reactions of the corresponding Pt(II) compounds (by using oxidants such as hydrogen peroxide, *N*-chlorosuccinimide [1], *N*-bromosuccinimide [2], iodobenzene dichloride [3, 4], etc.), by substitution of hydroxyl groups in axial position in neutral complexes of general formula $[PtA_2L(OH)X_2]$ (A = amine, L = -OH, -OR, halide, -COOH, and X = -COOR, halide).

2.2 History of Cisplatin

The merit of having synthesized and, therefore, discovered one of the main drugs employed in antitumoral therapy, the complex *cis*-diamminedichloroplatinum(II) (cisplatin), is assigned to Michele Peyrone; for this reason, cisplatin was originally defined "Peyrone's chloride" (1845). After nearly half a century, it was possible to distinguish the compound into two subgroups, defined isomers. The isomers are species with the same chemical formula but different arrangements of the atoms in the space or different ways in

which the atoms are bound to each other. The isomers can be classified in many types and, in this regard, it is possible to introduce the *cis-trans* geometric isomerism concept, according to which the two species are defined geometric isomers. Alfred Werner, a theoretical of coordination chemistry, attributed the prefix *cis* to the Peyrone's chloride to indicate the presence of two identical ligands on the same side of the complex. In doing this, he distinguished this geometric isomer from the other one (*trans*, *Figure 2.1*).

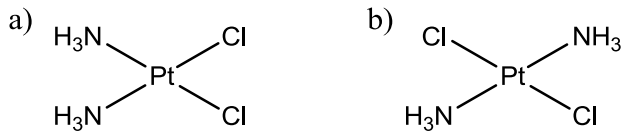

Figure 2.1: Geometric isomers of the diamminedichloroplatinum(II).
a) Cisplatin and b) Transplatin

The structure of cisplatin, however, was determined by means of X-ray diffraction in 1966.

In the 60s, Barnett Rosenberg, physics professor at the Biophysics Laboratory of the Michigan State University, by observing the similarity between the force lines of the electric fields and the mitotic spindles (i.e. microtubules chains that go from the centrioles, which are located at the poles, till the chromosomes located at the equator of a cell, during the mitosis), dealt with the influence of the electric fields on the cell growth in *Escherichia coli* bacteria.

In his experiment, current was made to pass into the growth medium of the bacterial population (a solution also containing ammonium chloride as electrolyte) by means of a pair of metal electrodes (in particular, platinum, characterized by a high chemical inertness in normal conditions).

One or two hours after the application of the electric field, the bacterial cells interrupted their normal division process, even if they continued their growth until they formed long filaments. After the removal of the previously applied

electric field, the elongation of filaments continued for about two hours, at the end of which the cells division began again. Therefore, Rosenberg observed that bacteria were not able to reproduce themselves because the division (and, therefore, the replication of their DNA) was impossible, but they were subject to a growth leading to a length of more than three orders of magnitude higher than in normal conditions.

Rosenberg, therefore, focused on the possible cause of the process and, in doing this, he realized that it was not due to the presence of the electric field but to new chemical compounds generated in solution.

Afterwards, the responsible species for this process was identified and attributed to a platinum complex: *cis*-diamminedichloroplatinum(II).

Since the cancer is a pathology derived from the uncontrolled division process, that discovery allowed Rosenberg to think that the effect of the platinum compounds, observed on *Escherichia coli*, could probably occur also in tumor cells.

The antitumor efficacy of cisplatin was then tested on tumors, such as sarcoma 180 implanted in mice. The results obtained were striking: the tumor growth stopped and, in some cases, also the regression of the tumor itself occurred as a result of the administration of the platinum complex [5].

In the following decade (in particular, in 1972), the trials of cisplatin on humans began. However, its clinical use was not authorized immediately: in fact, there was the risk of no longer being employed because, within a short time, the antitumor action of the drug was accompanied by serious toxic effects (especially if the administration provides high doses). Among the side effects, alterations in renal function till the nephrotoxicity, neuropathologies, peripheral neuropathy and alterations in liver function may occur. Due to these negative aspects, its approval and clinical application occurred only after the emanation

of a therapeutic scheme, which can mitigate the problem by using pre- and post-hydration of the patient and induced diuresis.
The search for the best methods is still an active investigation field that tries to develop new protective agents to be administered with cisplatin, able to reduce its side effects but not its efficacy.
In 1978 the clinical use of this drug was approved in the United States of America and, only later, in Japan and Europe. Since then, it represents the most employed antineoplastic drug and it shows its efficacy, in particular, in testicular cancer. It is successful also for other types of neoplasia, such as prostate, ovarian, bladder, head and neck tumors.
The *trans*-diamminedichloroplatinum(II) has no significant antitumor effects. It is kinetically more reactive and more labile than the *cis* isomer and, therefore, it has an average life shorter than cisplatin: this explains the fact that it is not employed as antitumor drug.

2.3 Cisplatin Mechanism of Action

Cisplatin is administered intravenously. In the bloodstream, the complex does not dissociate due to the high concentration of chloride ions (about 0.1 M).
In the blood plasma, cisplatin can react with human serum albumin (HSA). This latter is a single-chain protein of 64 kDa that contains several methionines (Met) and one cysteine (Cys), which can form stable N,S-chelates with cisplatin inactivating it. This ability is due to the high affinity of platinum(II) for sulfur.
The cisplatin is able to cross the cell membrane by means of a passive diffusion mechanism of the neutral molecule, although some facilitated transport mechanisms (CTR1) seem to be operative [6, 7].
When the cisplatin molecule arrives in the cytoplasm, where the chloride ions concentration in very low (about 3 mM), hydrolysis processes occur in order to

obtain aqua- and hydroxido-complexes and, in particular, the cisplatin aqua-complexes represent its active forms.

The rate constant for the substitution of the first chloride ion, at 37 °C, is 7×10^{-3} min^{-1}, which corresponds to a half-life time of about 2 hours. The hydrolysis of the first chloride ligand is twice faster than the substitution of the second chloride ion.

At acidic pH (< 6), about 50% of cisplatin is in the diaquacomplex form.

At neutral and alkaline pH, the equilibrium is shifted towards the deprotonation of the coordinated water molecule: therefore, hydroxido and aquahydroxidocomplexes are obtained.

Once into the cell, the complex is in its hydrolyzed form and its final pharmacological target is the DNA; moreover, it is able to interact with several fundamental proteins for the DNA replication itself and for the mitosis.

The hydrated active species is a bifunctional electrophilic reagent, therefore able to bind a nucleophilic site present on the DNA strand. The antitumoral function of cisplatin depends on its activation inside the cell as diammineplatinum species, by the dissociation of the two chloride ions and by the formation of inter- and intra-strand crosslinks, respectively on the opposite strands and on the same strand of DNA (*Figure 2.2*). These crosslinks cause the DNA replication arrest and, as a result, the cell death, if a mechanism of repair does not occur.

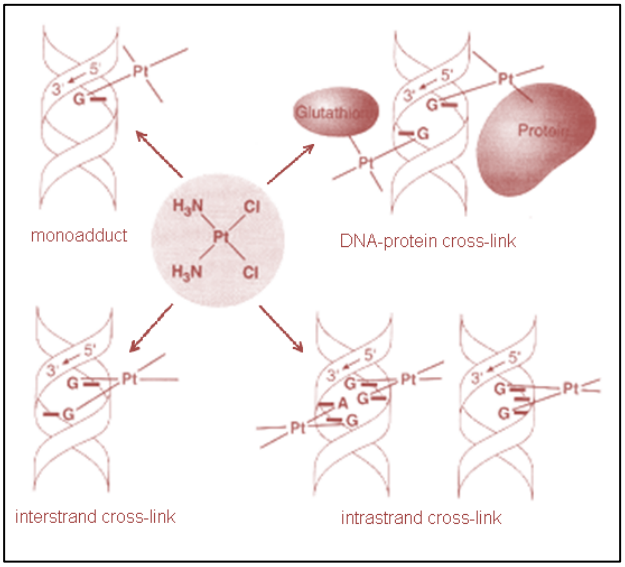

Figure 2.2: Crosslink processes of the hydrolyzed cisplatin with the DNA

The characteristics of the main DNA platination sites are (*Figure 2.2*):

1. monofunctional bond with a Guanine (*Figure 2.3*), defined as monoadduct,
2. bifunctional bond with both a Guanine and a donor atom of a protein,
3. inter-strand crosslink by means of two Guanines,
4. intra-strand crosslink by two adjacent Guanines,
5. intra-strand crosslink by means of two Guanines, separated by a third nitrogenous base,
6. intra-strand crosslink by a Guanine and an adjacent Adenine (*Figure 2.3*).

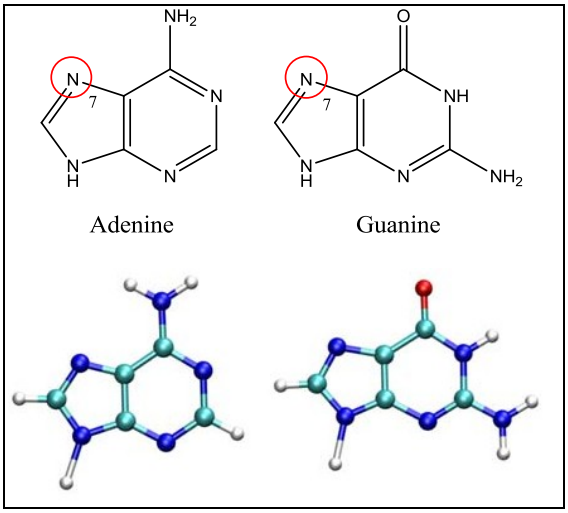

Figure 2.3: The Purines Adenine and Guanine represent the nucleophilic binding sites for the active form of cisplatin

In the case of cisplatin, the type 4 adducts represent 50-60% of metallated sites, the type 5 adducts 20-30%, the type 5 adducts only 10% of the coordinated platinum. As regards the types 1, 2 and 3 adducts, they represent a percentage lower than 4%. Therefore, the main coordination way of cisplatin to DNA is by intra-strand crosslinks with two adjacent Guanines or with a Guanine and an adjacent Adenine (*Figure 2.4*).

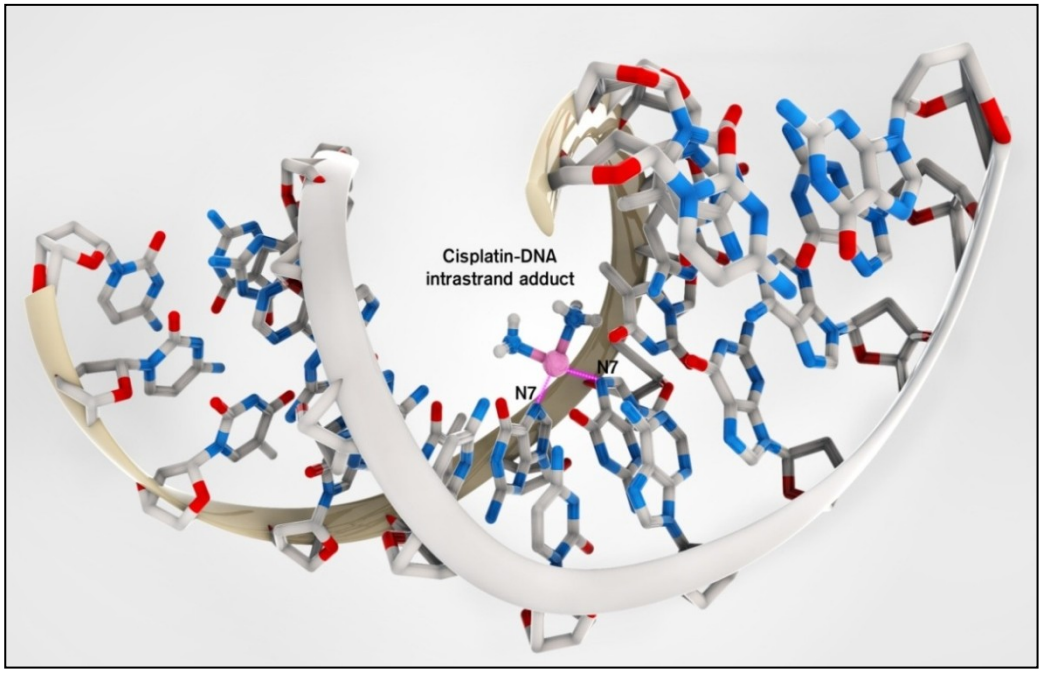

Figure 2.4: Intra-strand adduct of cisplatin with DNA, by means of the N-7 of two adjacent Guanines [8]

The mechanism of cisplatin activation is summed below. In the first phase, it loses the first chloride ligand, which is replaced by a water molecule, and it undergoes the first aquation reaction or "hydrolysis". Afterwards, the aquacomplex can bind the nitrogen in the 7th position (N-7) of a Guanine. At this stage, the complex undergoes a second "hydrolysis" and bind a second adjacent Purine.

When cisplatin binds DNA, it is possible to assist to a deformation of the hydrogen bonds present between the two DNA helices, which are weaker than the coordination bond, and this leads to a consequent distortion of the platinated helix.

In the final phase, the part of the complex that does not bind to DNA is excreted, and therefore degraded, through the liver: only about 50% of the initially

administered cisplatin is eliminated from the organism within 48 hours; the remaining part is excreted in a period that goes from 2 to 8 weeks.

2.4 Second Generation of Platinum Complexes: Features and Cytotoxic Activity

The administered dose of an antitumoral drug is related to different factors. At first, it is necessary to evaluate the activity of the drug itself and, therefore, the maximum dose tolerated by the organism. Another very important requirement is the solubility of the compound: a solubility of about 1 mg/mL, as in the case of cisplatin, is close to the limit of chemotherapeutic agent parenterally administrable, i.e. by injection.

The increase of the solubility in water of the cisplatin derivatives was the first target for the creation of a second generation of chemotherapeutic drugs.

The most of the platinum complexes containing two chlorides as "leaving groups", defined "leaving" because they detached before the compound reaches its biochemical target, is usually not much soluble in water. For this reason, it was decided to replace them with a carboxylate anion, preferably a chelating agent, i.e. a dicarboxylate, such as oxalate, glycolate, lactate or 1,1'-cyclobutanedicarboxylate.

The leaving groups of a complex must be coordinated to the metal by means of medium strength bonds. If this does not occur, the ligands weakly retained will lead to the formation of very toxic complexes, whereas those strongly bound will generate inactive compounds. For this reason, the carboxylates are the leaving groups preferred to make longer the half-life times of the resulting complexes.

The oxidation state of the metal is another important factor: in general, the Pt(IV) complexes are less active than those of Pt(II) but are more soluble in

water and can be activated only when they are reduced to platinum(II) species by biological reducing agents, such as cysteine, ascorbic acid, reduced glutathione, cytochrome c, etc.

Another fundamental requirement for a cytotoxic complex to be employed consists in being neutral so that it can more easily cross the cell membrane by passive diffusion.

It is possible to summarize the SAR (Structure-Activity Relationship) rules, enunciated in 1973 by Cleare and Hoeschele [9], which should allow a more focused design of new drugs:

- the complex must be neutral (in order to avoid interactions with charged species present into the cells and to facilitate the crossing through the cell membrane),
- the oxidation state must be +2,
- the geometric isomer must be the *cis* one,
- the complex must have two leaving groups with modulable hydrolysis rate (e.g. halides or dicarboxylates) and two carrier groups with modulable steric hindrance (e.g. aliphatic or aromatic *N*-donors, often chelating agents such as diamines).

For the cancer treatment, two dicarboxylate Pt(II) complexes are worldwide employed: carboplatin (or *cis*-diammine-(1,1'-cyclobutanedicarboxylato)platinum(II), CBDCA) and oxaliplatin (or *cis*-(1*R*,2*R*-cyclohexanediammine)oxalatoplatinum(II)). On the contrary, the approval of other Pt(II) complexes is restricted to some States: in particular, lobaplatin (or (1,2-di(aminomethyl)cyclobutane)lactatoplatinum(II)) in China, nedaplatin (or *cis*-diammineglycolatoplatinum(II)) in Japan, and heptaplatin (or *cis*-malonato[(4*R*,5*R*)]-4,5-bis(aminomethyl)-2-isopropyl-1,3-dioxolane] platinum(II)) in Korea (*Figure 2.5*).

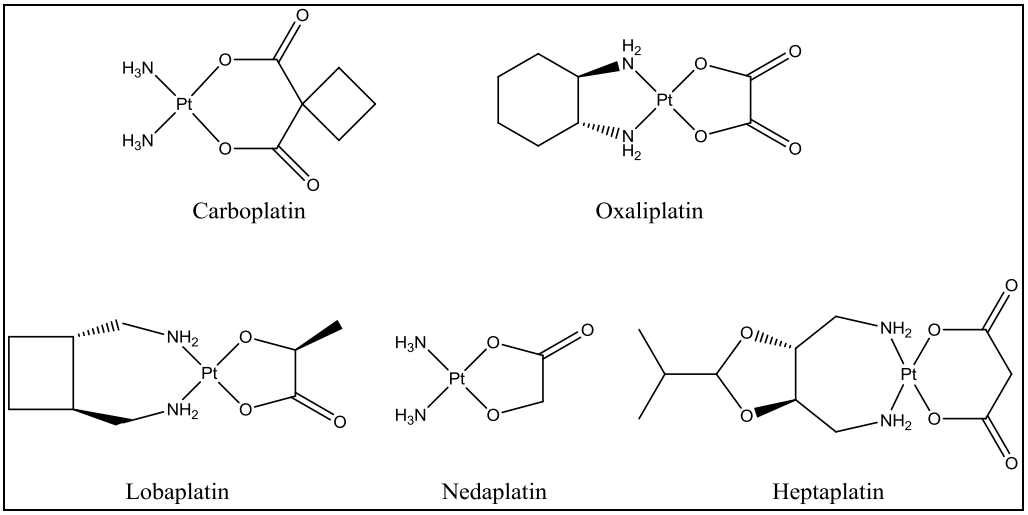

Figure 2.5: Main platinum complexes of II generation

The choice of carboplatin is related to several favorable characteristics that allow to reduce side effects. This compound reacts like cisplatin does: it forms intra-strand and inter-strand crosslinks with the nucleophilic sites of DNA. The replacement of the two chloride ligands has the main function of making carboplatin more resistant (even hundred times) to the hydrolysis reactions and this allows the drug to have a higher life time. In fact, the cyclobutanedicarboxylate ring makes the ligand more stable than the chloride groups in cisplatin: as a consequence, the nephrotoxic potential of the molecule is significantly reduced, due to the decrease of the complex reactivity.

In vivo tests, carried out in order to determine the antitumoral characteristics of the several derivatives of cisplatin, led to the conclusion that carboplatin gives rise to a series of side effects, such as nephrotoxicity, myelosuppression, vomiting, neurotoxicity but, anyway, it shows a minimal non-haematologic toxicity if compared to cisplatin.

The more limited toxicological profile of carboplatin allows to perform studies in which a much higher chemotherapeutic drug dose, than the standard cisplatin dose, was employed.

Pharmacokinetic studies indicate that cisplatin and carboplatin behaviors are different and this difference is clearly correlated to the different chemical stability of the two drugs.

In vitro test with plasma showed that cisplatin rapidly decomposes with a half-life time of about 2 hours at 37 °C. Carboplatin, instead, is much more stable and has a half-life time of about 30 hours. Therefore, cisplatin is inactivated mainly by the binding to plasma proteins which, after about 4 hours from the intravenous infusion, bind more than 90% of the administered cisplatin. On the contrary, carboplatin binds much less to blood proteins and, after 4 hours from the infusion, only 24% of the total platinum is bound to the proteins.

The drug elimination occurs by glomerular filtration through the kidneys. For a period ranging from 4 to 6 hours after the administration, the carboplatin present in plasma remains intact and, only later, there is the formation of crosslinks between platinum and proteins. Moreover, about 65% of the administered carboplatin dose can be found in the urine within 24 hours, whereas for cisplatin only about 15%: this demonstrates that cisplatin-proteins crosslink can be formed more easily than the one between carboplatin and proteins.

The introduction of carboplatin in clinical trials minimized the necessity of hyper-hydration or the use of antiemetics, and the consequence of this was a decrease of nephrotoxicity, neurotoxicity and ototoxicity. The suppression of the spinal cord activity, however, is its main side effect and this restricts the doses of this drug.

After several studies, it is possible to state that carboplatin is 10-40 times less effective than cisplatin: in fact, in order to obtain tumoral cell growth inhibition

effects similar to those of cisplatin, carboplatin requires a 10 times higher concentration.

However, carboplatin inhibits the hemopoietic cells growth as effectively as cisplatin does: therefore, carboplatin is a drug with a higher antiproliferative activity on hemopoietic cells, although the mechanism that explains this higher sensitivity is not completely clear.

Clinically carboplatin can be replaced by cisplatin in the treatment of ovarian and lung cancers but is less effective than cisplatin in genitourinary system, head, neck and esophagus tumors.

Oxaliplatin is a platinum complex different from both cisplatin and carboplatin and it shows no cross-resistance on the Pt-resistant tumoral cell lines. The oxaliplatin toxicity profile, more similar to cisplatin than to carboplatin, includes nausea, vomiting, diarrhea and hematological effects. Alopecia and nephrotoxicity, instead, are not associated with oxaliplatin. Neurological toxicity is the dose-limiting effect. As regards the clinical activity, oxaliplatin is the first platinum complex that shows cytotoxic activity towards colorectal cancer; moreover, it is also effective to the Pt-resistant ovarian tumors.

2.5 Platinum(IV) Prodrugs: Characteristics and Mechanism of Action

Even though the early SAR rules (see *paragraph 2.4*) pointed out that Pt(II) complexes are preferred, the antitumoral drugs based on Pt(IV) show several advantages, if compared to their Pt(II) analogues. In particular, they are less reactive and, therefore, they can undergo fewer side reactions, produce fewer side effects and they may be orally administered (because of their stability in biological fluids). Furthermore, they make possible many structural modifications, which are reflected on important physical and chemical

properties for the activity of these compounds, such as reduction potential, lipophilicity and, therefore, the cell uptake.

Platinum(IV) compounds have an octahedral geometry and an electronic configuration [Xe] $4f^{14}$ $5d^6$ and their higher inertness is due to the fact that they remain intact until their arrival into the cells and, only in the hypoxic and reducing tumor site, they can be activated by biological reducing agents. In particular, the generally accepted intracellular mechanism by which Pt complexes exert their antitumoral effects can be divided into four main phases [10]:

- cell membrane crossing and entrance into the cells,
- activation, i.e. reduction for Pt(IV) compounds and following aquation reactions of the Pt(II) metabolites,
- interaction with the main biological target, i.e. DNA,
- cell response to the DNA damage.

The axial ligands (L) are released only at a cellular level, where substances such as ascorbate and reduced glutathione (GSH), present in higher concentration than in the extracellular fluid, reduce platinum from +4 to +2 oxidation states. For this reason, Pt(IV) mechanism of action is defined as "activation by reduction" and platinum(IV) compounds are defined as "prodrugs" because they are reduced to the more reactive Pt(II) species. Afterwards, the corresponding Pt(II) complexes, after their aquation reaction, can rapidly bind DNA [11] (*Figure 2.6*).

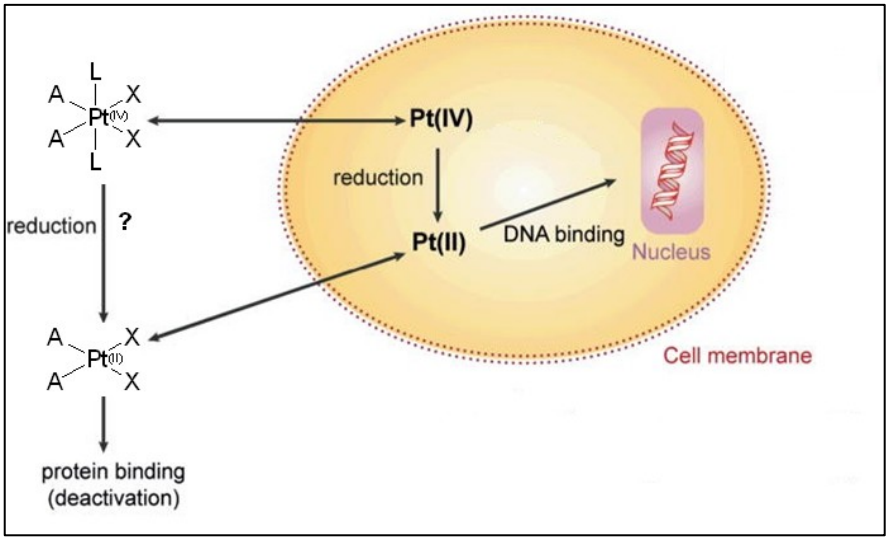

Figure 2.6: Mechanism of action of Pt(IV) complexes, the "activation by reduction" (A = carrier ligands, X = leaving ligands, L = axial ligands). The picture is a modification of that reported in literature [11]

The ease with which a complex may be reduced will affect its biological activity and, in order to ensure the activity, the analogue Pt(II) compound must be active [12].

As regards the biological reducing agents, there is a higher concentration of these species into the cells: in particular, ascorbic acid concentration in blood plasma is 50-150 μM, whereas in the intracellular site is about 1 mM. The same considerations can be made also for GSH: about 900 μM in the extracellular fluid and about 2 mM into the cells [13].

The direct crosslink of the Pt(IV) complex to DNA was observed *in vitro* in a reductant free environment, but mechanistically these reactions are negligible because the half-life times are much higher than those of the reduction: in fact, it is unlikely that a platinum(IV) compound can resist the large amount of reducing agents present *in vivo* and arrive intact to the nucleus [14].

If the reduction process occurs in the extracellular site, the Pt(II) complex, after the replacement of the leaving groups with two water molecules, binds to proteins and, therefore, it is deactivated.

Although Pt(IV) compounds have been investigated less than those of Pt(II), some of them proved to be promising as antitumoral drugs for clinical trials. The most studied were iproplatin, tetraplatin and JM216 (satraplatin) (*Figure 2.7*).

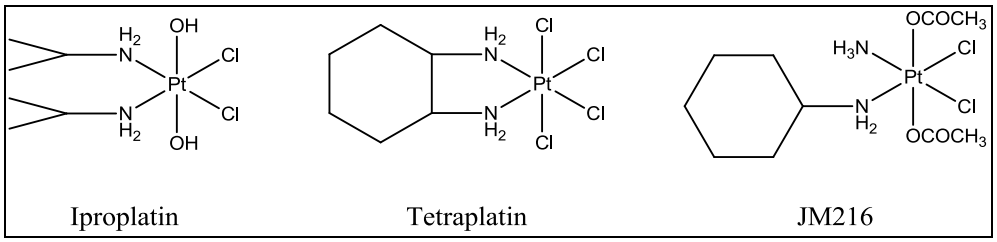

Figure 2.7: The most studied Pt(IV) complexes

Iproplatin (JM9 or *cis,trans,cis*-$[PtCl_2(ipa)_2OH_2]$, where ipa is isopropylamine) was selected for its high solubility from a series of compounds synthesized by Tobe. It is well tolerated, entered the II and III phases [15] but then was abandoned because it is less active than cisplatin [16].

Tetraplatin (or $[PtCl_4(DACH)]$, where DACH is 1*R*,2*R*-diminocyclohexane) demonstrated to be very promising in preclinical studies but it was abandoned in the I phase, due to a severe induced neurotoxicity [17].

JM216 (satraplatin or *cis,trans,cis*-$[Pt(c\text{-}C_6H_{11}NH_2)Cl_2(NH_3)(OCOCH_3)_2]$) has recently arrived in the III phase [18]. It was selected because it represents a compromise among the oral activity (similar to the intravenously administered carboplatin in most of the models), few emetic properties (studied on ferrets, since mice do not have any emetic responses) and favorable physicochemical properties, such as a good solubility in water. Furthermore, the complex shows a good stability in acidic solutions, with a half-life time of some hours in 1 M

HCl: this fact tends to decrease the risk of possible transformations in the stomach before the absorption.

The fact that none of the clinically tested compounds revealed to be significantly more active than cisplatin was particularly disappointing for researchers, since the *in vitro* results obtained by Kelland *et al.* [19] demonstrated that JM216 analogues are up to 840 times more active than cisplatin. This high activity was put in relation with the high cell uptake, but the *in vivo* reduction alters the pharmacological properties and, therefore, also the efficacy. Probably, the studied drugs are reduced too early in the bloodstream.

2.6 Drug Targeting and Delivery

The Drug Targeting and Delivery (DTD) methods [20] aim at synthesizing drugs selective towards tumoral tissues and administrable at lower doses with fewer side effects and with a high therapeutic index (TI, i.e. the ratio between the average lethal dose (LD_{50}) and the effective dose, which causes a 90% reduction in tumor mass (ED_{90})).

The DTD allows to achieve these aims by using vectors able to selectively lead cytotoxic agents to the tumoral cells, thus avoiding damages to the healthy ones, by exploiting the biochemical differences between neoplastic and normal cells/tissues, and limiting drug resistance.

A century ago Paul Ehrlich introduced the concept of drug targeting and it considered a “magic bullet” as an entity composed of two components: the former recognizes and binds the target, whereas the latter provides a therapeutic action. At present, the concept of magic bullet includes a combined action of three components: the drug, the targeting moiety and the pharmaceutical carrier, employed in order to increase the number of drug molecules per single targeting moiety [21].

Depending on the nature of the carrier substances, it is possible to distinguish active and passive targeting strategies [20].

2.6.1 Active Strategies

The active drug targeting is the result of a specific biomolecular interaction between the drug and the cell/tissue. By definition, a molecular agent targeted (MTA) is a biomolecule characterized by specific properties in respect of a well-defined molecular target, involved in disease processes.

An active targeting strategy involves drugs transported by biologically active molecules, in which the specific functionality leads the drug towards the tumor site, due to its binding affinity (a nutrient in respect of its carrier, an antibody for its antigen or a ligand for its receptor). For example, the cell proliferation process requires high amounts of energy. A decrease of the contribution of nutrients leads to the cell death if the cell proliferation cannot be limited, such as in the case of tumors. In mammals, the cell proliferation is controlled by signals transduction pathways stimulated by specific growth factors, but in tumors an excessive activation of these pathways, through oncogenic mutations, leads to a significant increase of the nutrients uptake, in particular glucose, amino acids and their derivatives.

In the 20s, Otto Warburg demonstrated that ascite tumor cells have high glucose consumption rate: the Warburg effect is considered a metabolic distinctive feature of aggressive tumors. For this reason, sugars and also amino acids (in particular glutamine) are useful as active vectors. Other types of employed biovectors are hormones, antimetabolites, bile acids and bisphosphonates.

2.6.2 Passive Strategies

The passive drug targeting, instead, exploits the so-called Enhanced Permeability and Retention (EPR) effect (*Figure 2.8*): in the solid tumors, the tissue, being in rapid and uncontrolled growth, shows a high permeability of the blood vessels and an inefficient or absent lymphatic drainage [20].

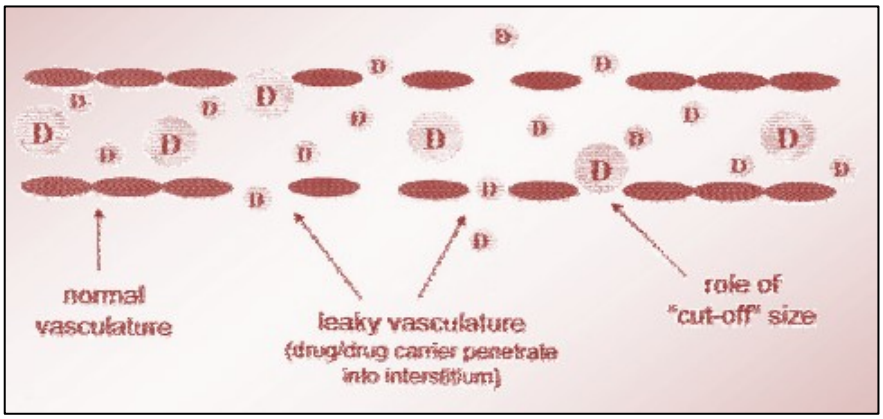

Figure 2.8: Schematic representation of the EPR effect

The vascular endothelium in tumors rapidly proliferates and is discontinuous with a high number of fenestrations in the blood vessels, where the endothelium is substantially quiescent. As a result, the particles with small enough dimensions (i.e. 50-200 nm) can passively cross the endothelial barrier of the tumor through the fenestrations.

In addition, the absence of an efficient lymphatic drainage prevents the removal of the excess fluid from the solid tumor tissue.

The combination of these two effects makes the tumor iperpermeable to circulating macromolecules (such as albumin, micelles, nanoparticles, liposomes, etc.), which come out and are accumulated, due to the inefficient lymphatic drainage.

In addition to the EPR effect, the tumor cells show a higher uptake of the macromolecules present in the peritumoral fluid by endocytosis than normal cells, as a result of their high metabolic activity.

2.6.3 The Choice of Passive DTD Vectors

In the last years, several potential passive DTD systems were employed, such as inorganic nanoparticles, polysaccharides, liposomes, polymeric micelles, etc. (*Figure 2.9*).

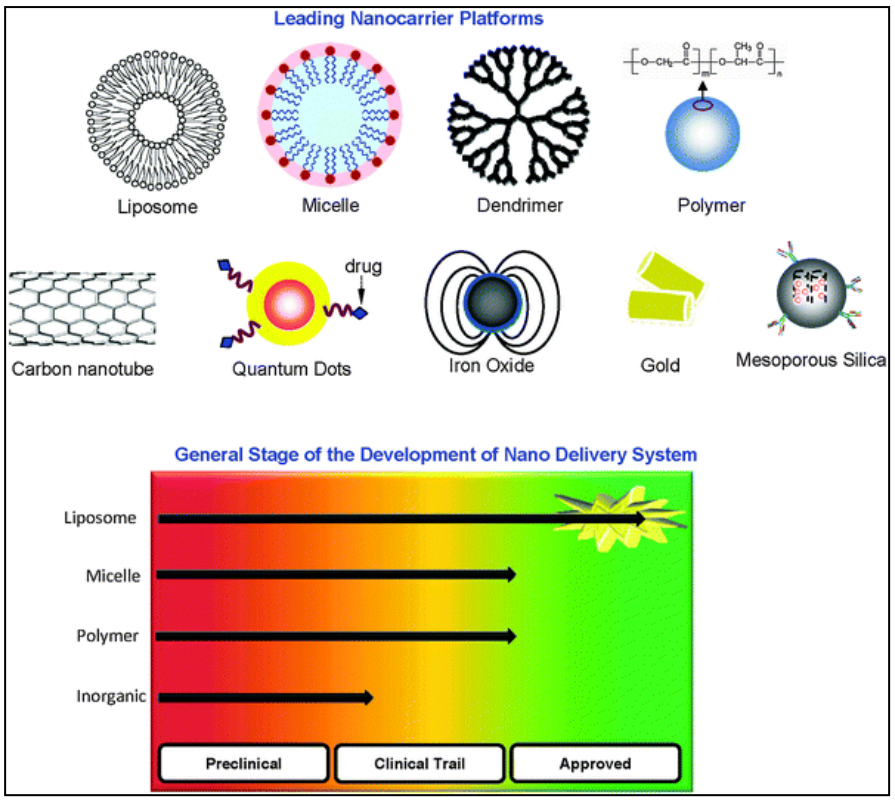

Figure 2.9: Main passive DTD vehicles and their general stage of development [22]

Several types of inorganic nanoparticles were employed as carrier, such as silica nanoparticles (NPs) (both mesoporous and non porous), gold nanoparticles, magnetic iron oxide nanoparticles, quantum dots and carbon nanotubes.

Silica nanoparticles obtained a significant interest because of their versatile silane chemistry (as regards the surface functionalization), their biocompatibility, ease of large-scale synthesis and low-cost of production. As previously mentioned, they can be distinguished into mesoporous and nonporous NPs: the former type is based on physical or chemical adsorption of the drug (and the release can be modulated by the use of the so-called "gatekeeper"), and the latter is based on drug conjugation and the release can be controlled by the use of appropriate linkers [23]. A detailed description is provided in *Chapters IV* and *V*.

Gold nanoparticles are interesting vehicle because they are inert, nontoxic, biocompatible and easy to be prepared and functionalized. Some studies were carried out by employing this type of NPs functionalized with thiolated 28-mer oligonucleotides containing a terminal dodecyl amine for the Pt coupling, which is a *cis,cis,trans*-$[Pt(NH_3)_2Cl_2(OH)(O_2CCH_2CH_2CO_2H)]$ [24].

Magnetic iron oxide NPs are investigated since they have a double function: Magnetic Resonance Imaging (MRI) contrast agents and carrier platform for DTD strategies. Moreover, their biocompatibility and biodegradability are significant features that make these nanoparticles widely used in biomedical applications [25]. More details are reported in *Chapter VII*.

As reported by Peer *et al.* [26], polysaccharides, which are polymers of monosaccharides linked by glycosidic bonds, are very versatile platforms: they have many reactive sites that can be exploited for further chemical modifications, such as esterification, amidation, grafting, etc. Moreover, another advantage is the bioadhesion, in particular for mucosal surfaces. Among the

polysaccharides employed, chitosan, dextran, alginate can be mentioned and, in particular, chitosan is discussed in *Chapter VI*.

Liposomes, term derived from the Greek *lipo*, "fat", and *soma*, "body", to describe their phospholipids composition, were introduced in England in 1961 by the haematologist Alec D. Bangham. In particular, they are concentric vesicles composed of a phospholipid bilayer and can be used to incorporate drugs within their structure. Some formulations of liposomes containing platinum complexes was successful in clinical trials: Lipoplatin™ and Aroplatin™, which contain cisplatin and *cis*-bis(neodecanoato)-(*trans*-*R,R*-1,2-diaminocyclohexane)platinum(II), respectively [27]. More details as regards liposomes are shown in *Chapter VIII*.

Polymeric micelles allow to incorporate drugs into their inner core by chemical conjugation or physical entrapment. Wang *et al.* reported a significant example, NC-6004 which is a block copolymer of PEG and poly(glutamic acid) (PGlu) coordinated with *cis*-diammineplatinum moieties: the hydrophilic PEG chain is the outer shell, whereas the PGlu-Pt complex chain is the inner core [27]. It is in phase III clinical trial in Asia for pancreatic cancer, in phase I in Japan and USA for head and neck tumors and in phase II in USA for non-small cell lung (NSCL), bladder and bile duct cancers [28].

2.6.4 Nanoparticles Properties

As previously described, small particles can extravasate and accumulate into the interstitial spaces but, since the cut off size of the fenestrations can vary from case to case, the conjugates dimensions (and the NPs stability) must be controlled in order to achieve the highest efficiency. Bae *et al.* [29] summed up the relationship between NPs size and presumed bioactivities in the body (*Table 2.1*).

Size	Biological systems and remarks
4.5 nm	Abundant small pores present in normal tissue endothelium
25 nm	Relatively few large pores present in normal tissue endothelium
20 - 50 nm	Average size of polymeric micelles without loaded drugs
100 nm	Frequently tested size of drug-loaded polymeric micelles
150 nm	Proposed cutoff size for particle extravasation in liver. This latter has blood vessels with fenestrations of 100–175 nm
200 nm	Nanoparticles less than 200 nm have significantly longer circulation time due to low uptake by the reticuloendothelial system (RES)
380 nm	A tumor-dependent functional pore cutoff size ranges from 200 nm to 1.2 μm, but the pore cutoff size of porous blood vessels in majority tumors is known to be 380 - 780 nm. Thus, the range for the EPR effect should be similar.
400 nm	Sterically stabilized liposomes of 400 nm in diameter were able to penetrate into tumor interstitium. Accumulation of hyaluronic acid-coated nanoparticles (400 nm) in the tumor tissue
500 nm	The maximum size of nanoparticles allowing penetration through cell membranes is known to be 500 nm
1 μm	Particles below 1 μm were taken up by Peyer's patches and then migrated to mesenteric lymph nodes
5 μm	The upper limit for rigid particles circulating within the smallest capillaries
40 μm	Particles larger than 40 μm have been used for embolization therapy

Table 2.1: NPs size and their presumed bioactivity in the body [29]

2.6.5 The Drug Release

An ideal DTD system is based on four main concepts: efficient drug loading on a vehicle (which should be non-toxic, non-immunogenic, biodegradable and physically and chemically stable *in vitro* and *in vivo*), prolonged circulation time in the blood vessels allowing the achievement of the prefixed target, retention into the targeting site and drug release within a time that allows an efficient drug function [29].

The targeting ensures the high efficiency of the drug and reduces side effects, but an efficient release at the target site is fundamental [20]. In this regard, the characteristics of the neoplastic tissue can be exploited. The microenvironment is highly hypoxic, since the hemoglobin in the erythrocytes is depleted of oxygen, and acidic. This latter is due to the fact that tumoral cells are in rapid growth, have not sufficient amount of oxygen for their methabolism and, therefore, use anaerobic glycolysis for their energy requirements. It is possible to assist to a high production of lactic acid, responsible for the acidification of the peritumoral environment: its pH is lower by about one unit than the one of normal cells. The pH gradient, therefore, can be exploited, from a therapeutic point of view, with antitumoral species which contain hydrolysable groups at acidic pH.

When the drug arrives into the cells, it must be released from the carrier in order to exert its function. The release can occur by the cleavage of hydrolyzable bond at the tumoral cells pH or of an amide bond, after the attack of hydrolytic enzymes. In the framework of antitumor metal drugs, this is the case of Pt(II) complexes carried by nanovectors. On the contrary, in the case of Pt(IV) prodrugs, hydrolyzable groups are not required. In fact, the hypoxic and reducing features of the neoplastic site can be used for the “activation by

reduction" of the prodrugs producing the Pt(II) active species that are released from the NPs if they are linked in axial position (*Figure 2.10*).

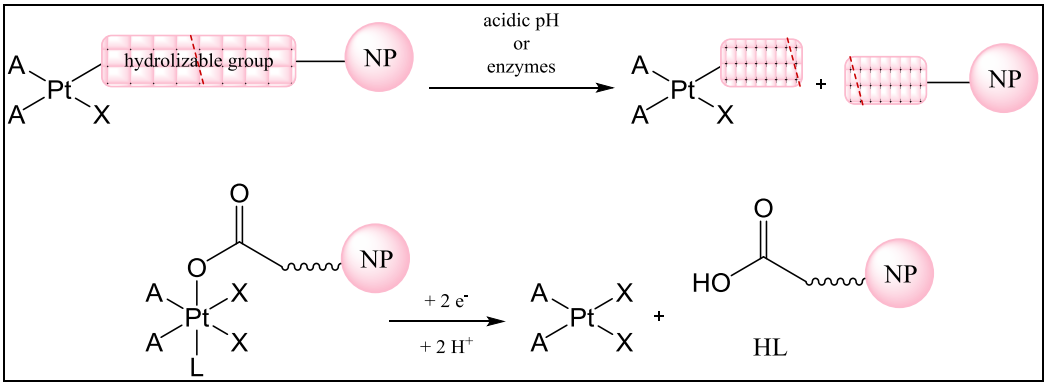

Figure 2.10: Schematic representation of the drug release from the vector

References

[1] M. Ravera, E. Gabano, G. Pelosi, F. Fregonese, S. Tinello, D. Osella, A New Entry to Asymmetric Platinum(IV) Complexes via Oxidative Chlorination, *Inorg. Chem.*, 53 (2014), 9326-9335.

[2] Z. Xu, Z. Wang, S-M. Yiu, G. Zhu, Mono- and di-bromo platinum(IV) prodrugs via oxidative bromination: synthesis, characterization, and cytotoxicity, *Dalton Trans.*, 44 (2015), 19918-19926.

[5] B. Rosenberg, L. Vancamp, J. E. Trosko, V. H. Mansour, Platinum Compounds: a New Class of Potent Antitumour Agents, *Nature*, 222 (1969), 385-386.

[6] X. Lin, T. Okuda, A. Holzer, S. B. Howell, The copper transporter CTR1 regulates cisplatin uptake in Saccharomyces cerevisiae, *Mol. Pharmacol.*, 62 (2002) 1154-1159.

[7] S. Ishida, J. Lee, D. J. Thiele, I. Herskowitz, Uptake of the anticancer drug cisplatin mediated by the copper transporter Ctr1 in yeast and mammals, *PNAS*, 99 (2002), 14298–14302.

[8] Durham University website, Biomedical research and biological tracing.

[9] M. J. Cleare, J. D. Hoeschele, Studies on the Antitumor Activity of Group VIII Transition Metal Complexes, Part I. Platinum(II) Complexes, *Bioinorg. Chem*, 2 (1973), 187-210.

[10] H. Kostrhunova, J. Kasparkova, D. Gibson, V. Brabec, Studies on Cellular Accumulation of Satraplatin and Its Major Metabolite JM118 and Their Interactions with Glutathione, *Mol. Pharmaceutics*, 7 (2010), 2093-2102.

[11] N. Graf, S. J. Lippard, Redox activation of metal-based prodrugs as a strategy for drug delivery, *Adv. Drug Deliv. Rev.*, 64 (2012), 993-1004.

[12] T. W. Hambley, The influence of structure on the activity and toxicity of Pt anti-cancer drugs, *Coord. Chem. Rev.*, 166 (1997), 181-223.

[13] E. Wexselblatt, D. Gibson, What do we know about the reduction of Pt(IV) pro-drugs?, *J. Inorg. Biochem.*, 117 (2012), 220-229.

[14] M. D. Hall, T. W. Hambley, Platinum(IV) antitumour compounds: their bioinorganic chemistry, *Coord. Chem. Rev.*, 232 (2002), 49-67.

[15] V. H. C. Bramwell, D. Crowther, S. O'Malley, R. Swindell, R. Johnson, E. H. Cooper, N. Thatcher, A. Howell, Activity of JM9 in advanced ovarian cancer: a phase I-II trial, *Cancer Treat. Rep.*, 69 (1985), 409-416.

[16] M. Gordon, S. Hollander, Review of platinum anticancer compounds, *J. Med.*, 24 (1993), 209-265.

[17] M. C. Christian, Abstracts, 7th International Symposium on Platinum and other Metal Coordination Compounds in Cancer Chemotherapy (1995), S128.

[18] M. J. McKeage, F. Raynaud, J. Ward, C. Berry, D. O'Dell, L. R. Kelland, B. Murrer, P. Santabarbara, K. R. Harrap, I. R. Judson, Phase I and

pharmacokinetic study of an oral platinum complex given daily for 5 days in patients with cancer, *J. Clin. Oncol.*, 15 (1997), 2691-2700.

[19] L. R. Kelland, B. Murrer, G. Abel, C. M. Giandomenico, P. Mistry, K. R. Harrap, Ammine/Amine Platinum(IV) Dicarboxylates: A Novel Class of Platinum Complex Exhibiting Selective Cytotoxicity to Intrinsically Cisplatin-resistant Human Ovarian Carcinoma Cell Lines, *Cancer Res.*, 52 (1992), 822-828.

[20] E. Gabano, M. Ravera, D. Osella, The Drug Targeting and Delivery Approach Applied to Pt-Antitumour Complexes. A Coordination Point of View, *Curr. Med. Chem.*, 16 (2009), 4544-4580.

[21] V. P. Torchilin, Drug targeting, *Eur. J. Pharm. Sci.*, 11 Suppl. 2 (2000), S81-S91.

[22] W. X. Mai, H. Meng, Mesoporous silica nanoparticles: A multifunctional nano therapeutic system, *Integr. Biol.*, 5 (2013), 19-28.

[23] L. Tang, J. Cheng, Nonporous Silica Nanoparticles for Nanomedicine Application, *Nano Today*, 8 (2013), 290–312.

[24] T. C. Johnstone, K. Suntharalingam, S. J. Lippard, The Next Generation of Platinum Drugs: Targeted Pt(II) Agents, Nanoparticle Delivery, and Pt(IV) Prodrugs, *Chem. Rev.*, 116 (2016), 3436–3486.

[25] C. Sun, J. S.H. Lee, M. Zhang, Magnetic nanoparticles in MR imaging and drug delivery, *Adv. Drug Deliv. Rev.*, 60 (2008), 1252–1265.

[26] S. Mizrahy, D. Peer, Polysaccharides ad building blocks for nanotherapeutics, *Chem. Soc. Rev.*, 41 (2012), 2623-2640.

[27] X. Wang, Z. Guo, Targeting and delivery of platinum-based anticancer drugs, *Chem. Soc. Rev.*, 42 (2013), 202-224.

[28] NanoCarrier Co., Ltd.

[29] Y. H. Bae, K. Park, Targeted drug delivery to tumors: Myths, reality and possibility, *J. Control Release*, 153 (2011), 198-205.

Chapter III

Outline of the Thesis

The aim of this Ph.D. work is focused on the exploration of several passive Drug Targeting and Delivery (DTD) methods in order to selectively carry Pt(IV) antitumor prodrugs to the tumor site, in which the corresponding Pt(II) active metabolite (obtained after the so-called activation by reduction, favoured in the hypoxic and reducing *milieu* of tumors) can exert its antitumor action.

The first step of such work project consists in the synthesis of Pt(IV) complexes, containing suitable functionalities to be exploited in coupling reactions with nanosized vectors. Alternatively, platinum complexes can be encapsulated into lipophilic systems. Then, the work includes the loading of selected nanocarriers with the metal complexes and the biological evaluation of the resulting conjugates.

In particular, the below reported projects have been developed:

- synthesis and characterization of Pt(IV) complexes, their subsequent coupling reactions with different kinds of amino-functionalized core-shell silica nanoparticles and, finally, *in vitro* studies of the corresponding conjugates;
- coupling reactions of the previously prepared Pt(IV) complexes with chitosan and chitosan derivatives;
- synthesis and characterization of Pt(IV) prodrugs able to link magnetic iron oxide nanoparticles and their coupling reactions with such vectors;
- encapsulation of antitumor drugs into liposomes and their *in vitro* studies.

Chapter IV

Synthesis and Characterization of Pt(IV) Complexes and Coupling Reactions with Amino-Functionalized Fluorescent Core-Shell Silica Nanoparticles

4.1 Introduction

Cisplatin represents the starting point for all the platinum(IV) complexes synthesized in this work.

The oxidation of cisplatin (which involves the transition from the square-planar geometry to the octahedral one) was carried out by using hydrogen peroxide, as an oxidizing agent, and the reaction product depended on the mixture solvent. In fact, it is possible to assist to the coordination of two hydroxyl groups in axial position in the presence of water, or of a hydroxyl and an ethoxy functionalities in ethanol. In the first case, both of the axial groups can further react with other species (such as anhydrides, acyl chlorides, etc.), in order to form two esterified bonds. On the contrary, in the presence of an alkoxide, it remains inert during the subsequent synthetic procedures, whereas only the hydroxyl functionality can be further esterified.

The synthesized Pt(IV) complexes show one or two free carboxylic groups and these functionalities can be exploited to form amidic bonds by reaction with amines. In particular, the mono- or di-functionalizable compounds can be coupled to the primary amines present on the surface of several vectors (such as silica nanoparticles, chitosan and iron oxide nanoparticles), suitable for passive Drug Targeting and Delivery (DTD) strategies.

The synthesized platinum compounds and conjugates are here reported:

- (SP-4-2)-diamminedichloridoplatinum(II), cisplatin,
- (OC-6-33)-diamminedichloridodihydroxidoplatinum(IV) (**1**),
- (OC-6-33)-diamminebis(4-carboxypropanoato)dichloridoplatinum(IV) (**2**),
- Activated *N*-hydroxysuccinimidyl diester of **2** (**3**),
- (OC-6-33)-diamminebis(4-oxo-4-(propylamino)butanoato)dichlorido platinum(IV) (**4**),

- Difunctionalized Pt(IV) complex - silica NPs conjugates (**5a**-**5d**),
- (OC-6-44)-diamminedichloridoethanolatohydroxidoplatinum(IV) (**6**),
- (OC-6-44)-diammine(4-carboxypropanoato)dichloridoethanolato platinum(IV) (**7**),
- Activated *N*-hydroxysuccinimidyl ester of **7** (**8**),
- (OC-6-44)-diamminedichloridoethanolato(4-oxo-4-(propylamino) butanoato)platinum(IV) (**9**),
- Monofunctionalized Pt(IV) complex - silica NPs conjugates (**10a**-**10d**).

Each complex was characterized by High Performance Liquid Chromatography coupled with Mass Spectrometry (HPLC-MS), spectroscopic techniques such as Nuclear Magnetic Resonance Spectroscopy (multinuclear NMR) and Infrared Spectroscopy (IR), and Elemental Analysis (EA).

In this chapter, compounds **3** and **8** were coupled with amino-functionalized nonporous core-shell silica nanoparticles, after checking their reaction with a primary amine (propylamine) as a model. Moreover, the behavior of a mono- and a di-functionalizable complexes was compared in order to evaluate the stability of the final NPs suspension and to verify the possibility of cross-links between nearby NPs (in the case of the presence of two available carboxylic functionalities), causing aggregation.

As previously mentioned (*Chapter II*), in recent years, silica NPs have been highly employed for biochemical applications and two different types of particles are currently used: mesoporous and nonporous NPs. Such NPs are different as regards the anchoring of the drugs, another difference consists in the lower toxicity of the nonporous ones respect to the others [1], even though the cytotoxicity of the NPs is often cell type dependent and is related to geometry, surface functionalities and colloidal stability. For this reason, in this work, four types of nonporous silica NPs (which differ in size) were employed. These

particles show a core-shell structure based on a silica core, surrounded by a fluorescent dye and by another shell of silica. Finally, the surface was functionalized with alkyl chains ending with primary amino groups, which can be exploited in coupling reactions with Pt(IV) complexes and allow to pursue the DTD aims. The presence of a fluorophore (e.g. rhodamine B or fluorescein) is important to follow, by means of imaging techniques, the path of the drug - NP conjugates inside the cells and, then, *in vivo*.

4.2 Instrumental Information

The chromatographic analysis were performed by using a Waters HPLC-MS instrument equipped with an Alliance 2695 separations module, a 2487 dual lambda absorbance detector and a mass spectrometer 3100, as the second detector. The stationary phase consisted (except for the reduction kinetics studies, see *paragraph 4.17.1.2*) of a C18 Phenosphere-NEXT column 5 μm, 250 × 4.60 mm ID. The mobile phase was a mixture of eluants, i.e. an aqueous solution of formic acid 15 mM and pure methanol, in different percentages (depending on the analyzed complex). The flow rate was 0.500 mL/min, isocratic elutions were performed and the analysis temperature was set at 37 °C. The UV-Visible detector was fixed at 210 nm wavelength.

The Electrospray Ionization (ESI) mass spectra were collected by setting the source and the desolvation temperatures at 150 °C and 250 °C, respectively. In particular, the ESI source temperature was set to a higher value than the employed solvent boiling temperature, in order to avoid its condensation. Nitrogen was used with a double function: drying and nebulizer gas. Furthermore, the cone and the capillary voltages were fixed at 30 V or 20 V and at 2.70 kV, respectively. The internal pressure was 10^{-5} mbar and the employed

scan mode was “centroid”, i.e. the signal intensities are proportional to the ionic abundance.

The NMR spectra were measured by using a NMR Bruker Avance III, operating at 500 MHz (^{1}H), 125.7 MHz (^{13}C) and 107.2 MHz (^{195}Pt, with a spectral window of 2000 ppm), and a JEOL Eclipse Plus, operating at 400 MHz (^{1}H), 100.6 MHz (^{13}C) and 86.0 MHz (^{195}Pt, with a spectral window of 2000 ppm). ^{1}H and ^{13}C NMR chemical shifts were reported in ppm, referenced to solvent resonances, and, in the case of measurements in D_2O, 1% methanol was added as internal reference. ^{195}Pt NMR spectra were registered by using a solution of K_2PtCl_4 in saturated aqueous KCl, as external reference. The K_2PtCl_4 chemical shift was set at -1628 ppm from Na_2PtCl_6 (δ = 0 ppm).

The elemental analyses were performed by means of a EA3000 CHN Elemental Analyzer (EuroVector, Milano).

Particle size, size distribution and ζ potential were measured by scanning electron microscopy (SEM) and by dynamic light scattering (DLS), respectively. The Field Emission Gun-SEM micrographs were obtained by using an Inspect F SEM-FEG (FEI, Hillsboro, USA) with a beam diameter of 3 nm. From 200 to 250 individual nanosphere diameters were measured for each sample and the images were elaborated by using the Scion Image processing program (Scion Corp., Frederick, USA).

DLS and ζ potential analyses were performed at 25 °C, at a fixed ionic strength, with a Malvern Zetasizer Nano ZS (Malvern Instruments Ltd., Malvern, UK) at a fixed scattering angle of 173°, using a He–Ne laser and DLS software for Windows (version 6.11, Malvern, UK). The instrument was checked with a standard polystyrene latex with a diameter of 100 nm.

The mineralization of Pt-loaded silica nanoparticles was performed by means of a microwave assisted acid digestion apparatus Milestone Start D with an internal temperature sensor.

The quantification of the platinum content in conjugates and biological samples was performed by means of inductively coupled plasma-optical emission spectrometry (ICP-OES) with a Spectro Genesis ICP-OES spectrometer (Spectro Analytical Instruments, Kleve, Germany) equipped with a cross flow nebulizer, or by inductively coupled plasma-mass spectrometry (ICP-MS) with a Thermo Optek X Series 2. By ICP-OES the Pt concentration was determined by selecting the Pt 299.797 nm line, whereas by ICP-MS the most abundant isotopes of platinum and indium (used as internal standard) were measured at m/z 195 and 115, respectively. The calibration curve was prepared by dilution with 1.0% v/v nitric acid of a 1000 ppm platinum standard stock solution.

4.3 Synthesis of the Nonporous Core-Shell Silica Nanoparticles

In 1956 Gerhard Kolbe observed the formation of spherical silica particles when tetraethoxysilane (TEOS) was hydrolyzed in the presence of ammonia. In 1968, in particular, Stöber *et al.* took up and improved this process in order to observe exceptional monodispersed silica particles [2].

In this work, four types of NPs (defined as **a**, **b**, **c** and **d**) were synthesized by using a modified Stöber method [3, 4]. In particular, as reported by Ravera *et al.* [5], in a round-bottomed flask, equipped with a reflux condenser, a thermometer and a mechanical stirrer, a mixture of water (37.5 mL for **a**, 25 mL for **b** and **c**, 30 mL for **d**) and ammonia (6.2 mL for **a**, 21 mL for **b** and **c**, 13 mL for **d**) were introduced and diluted with methanol to the final volume of 320 mL. The solution was heated to 30 °C in an oil bath at a stirring rate of 200 rpm, then tetraethoxysilane (TEOS, 20 mL, 90 mmol) was added and the reaction was carried out for 2.5 hours. Subsequently, the fluorescent layer was grown by adding a mixture of TEOS and the prepared fluorophore, i.e. rhodamine B isothiocyanate (RhBITC, for **a** and **c**) or fluorescein isothiocyanate (FITC, for **b**

and **d**). In particular, such fluorophore (3.6 mg of RhBITC and 2.7 mg of FITC, respectively, 6.7 µmol) were covalently bound to the silane coupling agent (3-aminopropyl)trimethoxysilane (APTMS, 119 µL, 681 µmol) in 2 mL of ethanol. This mixture was stirred for 3 hours at room temperature and then added to the reaction flask with TEOS (340 µL, 1.5 mmol). The reaction was performed for 16 hours and, after the established time, NPs were collected by centrifugation (900 rpm, 10 minutes) and washed by three cycles of suspension in ethanol and centrifugation. The external silica shell was obtained by reacting, for 8 hours at 30 °C, 5.0 g of NPs with 2 mL of TEOS in a mixture of ammonia (4 mL), water (35 mL) and ethanol to a final volume of 320 mL. Then, APTMS (400 µL, 2.29 mmol) were added to the suspension and the reaction was carried out for 16 hours. The NPs were collected by centrifugation (900 rpm, 10 minutes) and purified by at least three cycles of dispersion in ethanol and centrifugation.

In *Figure 4.1* a scheme of the several procedures carried out to synthesize the silica nanoparticles is shown.

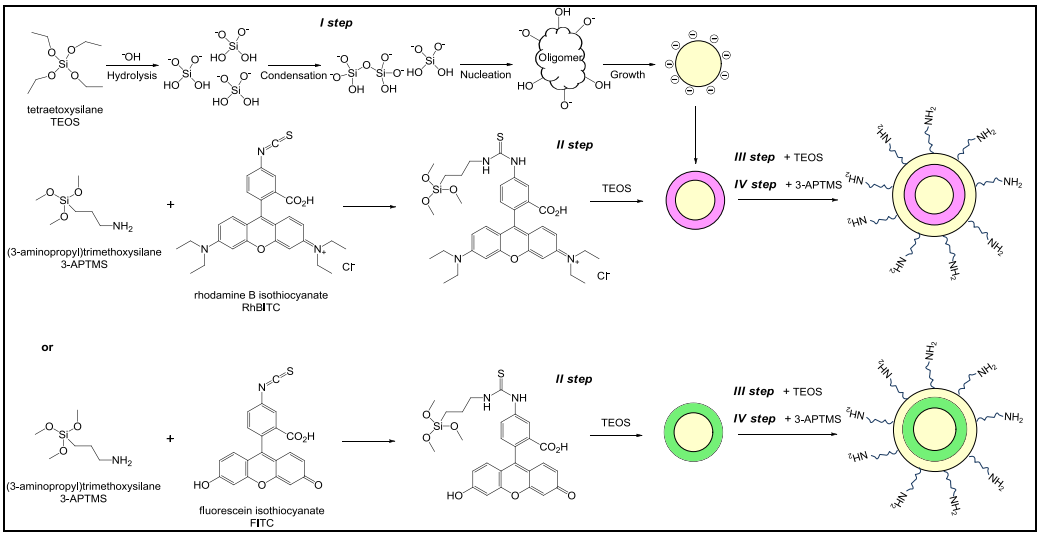

Figure 4.1: Synthetic scheme to prepare silica NPs

The nanoparticles were then stored as an ethanol suspension: in fact, this is the only way to maintain their stability and to prevent their aggregation (which occurs in the case of lyophilized samples).

In *Figure 4.2*, SEM images of one of the NPs samples (**b**) are shown in order to observe their size growth by adding shells.

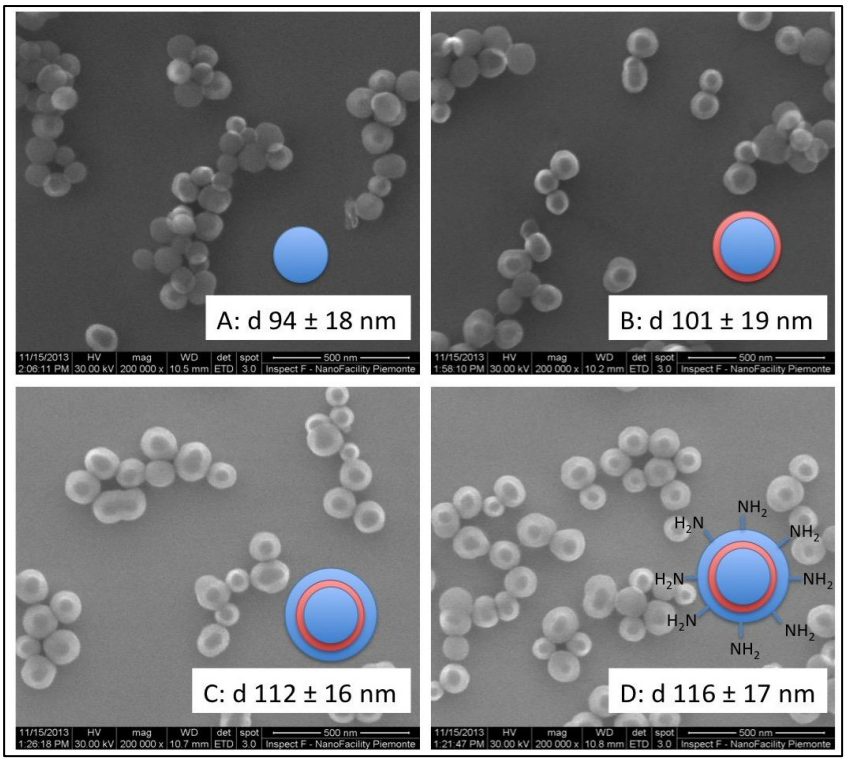

Figure 4.2: SEM micrographs at different growth phases of NPs **b**

For each sample, in order to proceed with a quantitative determination of the fluorophore and of the exposed amino groups, the silica nanoparticles density (expressed as g NPs/mL of ethanol suspension) was measured. In particular, 1 mL of each ethanol suspension was dried in an oven and, then, the dried product was weighed: the results obtained are shown in *Table 4.1*.

NPs	NPs density (g NPs/mL)
a	0.0350
b	0.0206
c	0.0128
d	0.0137

Table 4.1: **a**-**d** NPs suspensions density

4.3.1 Quantification of the Fluorophore

For the quantification of the fluorescent dye [5], 0.02 g of NPs were suspended (by means of 2 hours of sonication in an ultrasonic bath) in a mixture of 1 mL of ethanol and 1 mL of 1 M aqueous NaOH and it was stirred overnight. Then, it was centrifuged (10000 rpm, 5 minutes) to obtain a clear solution, whose absorbance value at 550 nm (for rhodamine B) or at 497 nm (for fluorescein) was measured and related to the fluorophore concentration using experimentally determined molar extinction coefficients ε (85434 M^{-1} cm^{-1} for fluorescein and 109359 M^{-1} cm^{-1} for rhodamine B). Each value is the mean of at least three independent measurements. Data are expressed as fluorophore loading (μmol fluorophore/g NPs) and shown in *Table 4.2*. For all the samples, the fluorophore loading efficiency ranges from 16 to 38% and this value represents the molar ratio between the fluorophore molecules incorporated in the NPs and the ones employed in the synthesis.

NPs	Fluorophore	Fluorophore loading (µmol/g NPs)
a	Rhodamine B	0.250 ± 0.011
b	Fluorescein	0.403 ± 0.006
c	Rhodamine B	0.183 ± 0.003
d	Fluorescein	0.261 ± 0.004

Table 4.2: **a**-**d** NPs fluorophore loading

4.3.2 Quantification of the Amino Functionalities

As regards the quantification of the amino groups [5], 0.5 g of NPs were washed with ethanol for at least five times in order to remove unreacted ammonia and APTMS. The pellet was then dispersed in 20 mL of an aqueous solution containing 0.2 M HCl and 0.5 M NaCl in order to allow complete protonation of amino groups, centrifuged and dispersed in 20 mL of water and then it was suspended in 20 mL of a 1 M aqueous KNO_3. The suspension was left overnight under stirring to allow displacement of chloride by nitrate anions. The suspension was then centrifuged and the solution (containing chlorides) was directly titrated with a 0.01 M aqueous solution of $AgNO_3$. In particular, the titration was based on the precipitation reaction of AgCl, which, being a very poorly soluble salt in the aqueous mixture (Kps at 25 °C = 1.1×10^{-10}), precipitated. The titration was monitored by using an Ag^+-selective electrode, by registering and studying the potential of the solution at 25 °C after each titrant addition, and it was considered complete when all the AgCl was precipitated. The titration curve of NPs **a** is shown in *Figure 4.3*, as an example. Then the data were processed, expressed as amino group density (mmol NH_2/g NPs) and reported in *Table 4.3*.

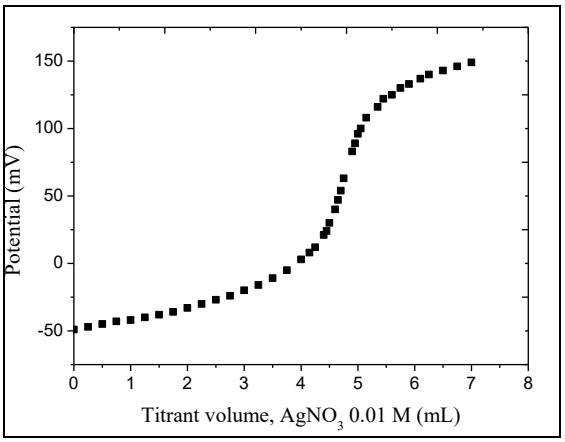

Figure 4.3: Titration curve of silica NPs sample **a**

NPs	amino groups density (mmol NH_2/g NPs)
a	9.34×10^{-2}
b	2.32×10^{-1}
c	2.20×10^{-1}
d	2.80×10^{-1}

Table 4.3: **a-d** NPs amino functionalities density

4.3.3 Size and Stability Investigations

For each sample, SEM and DLS analyses were carried out in order to evaluate the NPs dimensions. In the first technique, a drop of the ethanol suspension was deposited on a sample holder, the alcohol was let evaporate and then the analysis was performed, after the introduction of the sample holder into the instrument and after the setting of the required parameters.

On the contrary, for DLS measurements, the NPs ethanol suspension was centrifuged and the pellet was dispersed in a 0.2 M aqueous solution of HCl (in order to reach a higher stability), centrifuged and suspended in 20 mL of a 10 mM KNO_3 solution (in order to perform the analyses at fixed ionic strength). About 1 mL of the prepared suspension was transferred into a plastic disposable cuvette which, in turn, was introduced into the instrument for the analysis.
The same suspension prepared for the DLS was employed for the ζ potential analysis, which allows to evaluate the suspension stability. In this case, the sample was transferred into a cuvette suitable for ζ potential measurements and then introduced into the instrument for the analysis. All the results are summarized in *Table 4.4*.

NPs	SEM diameter (nm)	DLS diameter (nm)	ζ potential (mV)
a	262 ± 16	380.6 ± 5.6	37.9 ± 2.5
b	116 ± 17	161.0 ± 1.3	58.0 ± 2.8
c	96 ± 13	178.9 ± 0.6	57.3 ± 2.4
d	48 ± 5	122.8 ± 1.1	54.5 ± 1.1

Table 4.4: **a**-**d** NPs dimensions and suspensions stability results

The ζ potential is a measure of the stability of a suspension: a system is stable if an equilibrium between electrostatic interactions of opposite sign (i.e. attractive and repulsive forces) among the particles is established. As reported in literature [6], ζ potential ≥ |30| mV indicates a stable suspension, due to the electrostatic repulsion, among the nanoparticles, that avoid their aggregation. If the value is ≥ |60| mV the system shows a very high stability. Values < |20| mV, instead, are a measure of a limited stability because the attractive forces begin to prevail over the repulsive ones. When ζ potential < |5| mV aggregation occurs.

In this case (*Table 4.4*), all the four types of NPs exceed the threshold of stability, since their ζ potential values are higher than +30 mV.

As regards the size, DLS diameter are bigger than those determined by SEM (*Figure 4.4*).

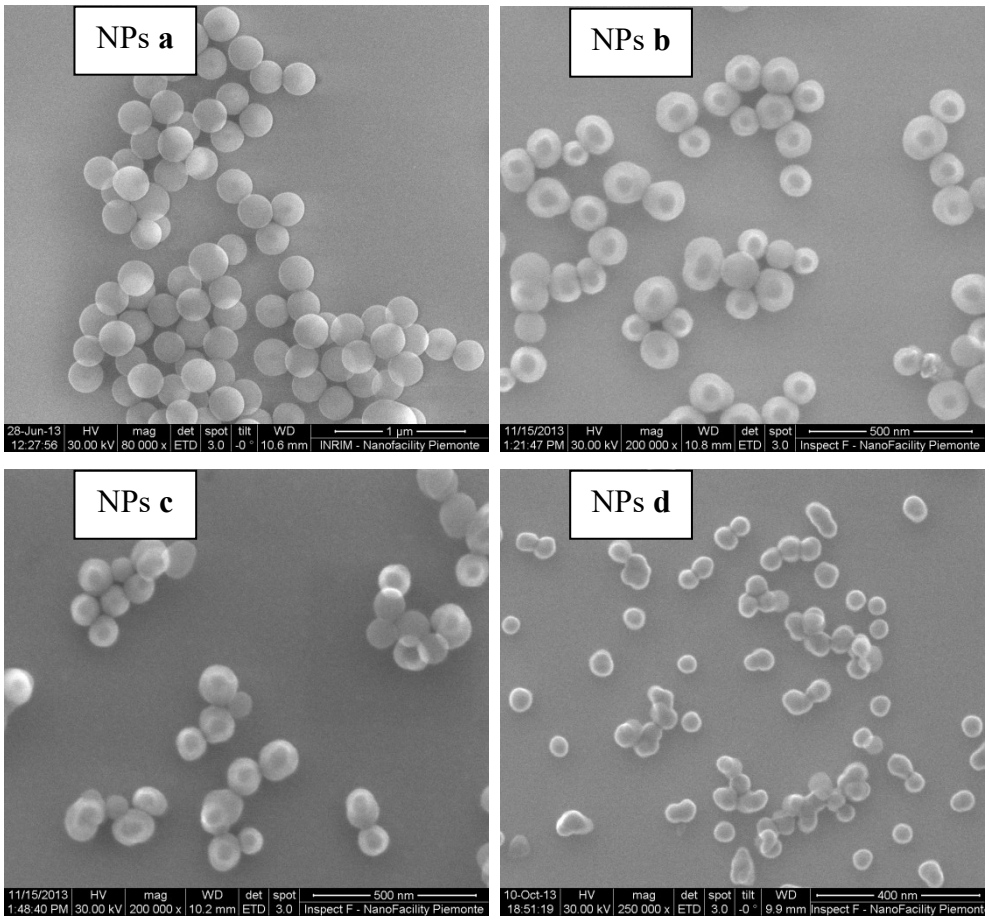

Figure 4.4: SEM micrographs of the synthesized silica nanoparticles **a-d**

This can be explained considering that, in solution, each nanoparticle is surrounded by water molecules, which form a solvation shell. Therefore, the DLS data take into account the hydrodynamic radius (considering the solvent effect), which is slightly bigger than the one of the particle itself: this justifies

the higher dimensions observed by DLS. In particular, the hydrodynamic radius is related to the ionic strength: the higher the ionic strength, the less expanded the hydrodynamic radius and, therefore, the smaller the NPs size.

4.4 Synthesis of Cisplatin

The cisplatin synthesis was carried out according to the Dhara's method [7].
In the first synthetic phase, potassium tetrachloroplatinate(II) reacts with potassium iodide to allow the formation of potassium tetraiodoplatinate(II) and potassium chloride

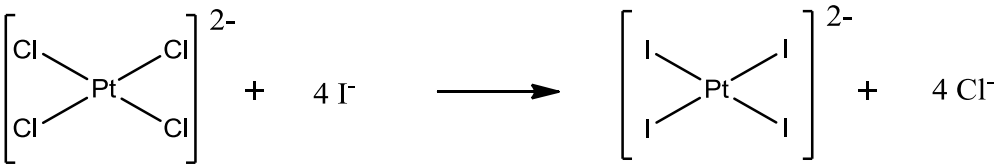

The product reacts with an ammonia solution 30% in order to synthesize the (SP-4-2)-diamminediiodidoplatinum(II). It is not possible to obtain the other geometric isomer, the *trans* one. In fact, when the first ammonia molecule replaces one of the ligands in the complex, giving rise to the monoamminetriiodidoplatinate(II) intermediate, the second ammonia molecule will place in *trans* mode with respect to one of the remaining iodides. This is due to the high *trans*-orienting effect of the iodide ligands. Therefore, we can assist to the formation of a *cis* complex.

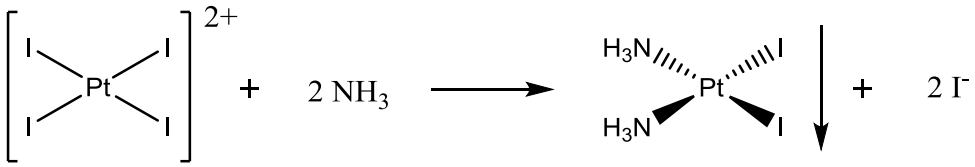

The (SP-4-2)-diamminediiodidoplatinum(II) reacts with silver nitrate: the role of silver(I) ions consists in precipitating iodide ions in the form of silver iodide

and, therefore, in replacing them with two molecules of water, as coordinated to the metal ligands.

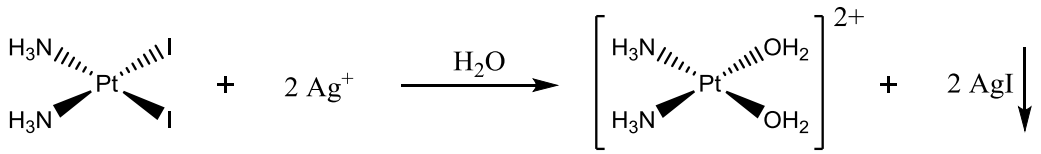

In the next phase the complex in aqueous solution reacts with potassium chloride: the water molecules are moved away from the coordination sphere of the metal and replaced by chloride ligands, thus obtaining cisplatin.

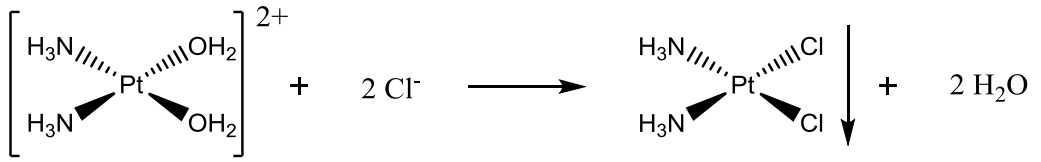

4.4.1 Synthesis of (SP-4-2)-diamminediiodidoplatinum(II)

1.00×10^3 mg (2.41 mmol) of $K_2[PtCl_4]$ was dissolved in 10 mL of ultrapure water, in the dark. Then, a 6-fold molar excess (respect to $K_2[PtCl_4]$) of potassium iodide (2.40×10^3 mg, 14.45 mmol) was added and the reaction mixture was magnetically stirred at room temperature, in the dark, for 40 minutes: during this period, we can assist to a change of color from red to brown.

The next phase involves the dropwise addition of an ammonia solution 30%, 3.3-fold molar excess respect to $K_2[PtCl_4]$ (7.95 mmol), and after 30 minutes it was possible to observe the precipitation of a yellow compound: (SP-4-2)-diamminediiodidoplatinum(II). The reaction product was separated from the solution by means of centrifugation and, then, it was washed with cold ultrapure water, ethanol and diethyl ether. Subsequently, it was properly dried and the reaction yield was calculated.

Yield: 1.12×10^3 mg, 2.32 mmol, 96.3%.

4.4.2 Synthesis of (SP-4-2)-diamminedichloridoplatinum(II)

To the previously synthesized complex (1.12×10^3 mg, 2.32 mmol), dissolved in 10 mL of ultrapure water, a 1.96-fold molar excess of silver nitrate (772 mg, 4.55 mmol) respect to (SP-4-2)-diamminediiodidoplatinum(II) was added. The reaction was carried out at 50 °C for 24 hours in the dark. Then, the solution was centrifuged and filtered with a syringe microfilter (Regenerated Cellulose, porosity of 0.20 μm) to remove the precipitated silver iodide. The solution, when necessary, was also concentrated by means of a rotary evaporator in order to reduce its volume to some mL.
Subsequently, a 21-fold molar excess of potassium chloride (3.63×10^3 mg, 48.7 mmol) with respect to (SP-4-2)-diamminediiodidoplatinum(II) was added to the previously concentrated solution and the reaction mixture was stirred for 24 hours at room temperature in the dark. In this phase the precipitation of (SP-4-2)-diamminedichloridoplatinum(II) occurred and this yellow compound was then separated from the solution by means of centrifugation, washed with cold ultrapure water, ethanol and diethyl ether and, finally, dried *in vacuo*.
Yield: 546 mg, 1.82 mmol, 78.2%.

4.4.2.1 Characterization of the Complex

RP-HPLC-ESI-MS

The analysis was performed by employing a stationary phase consisting of a C18 Phenosphere-NEXT column 5 μm, 250 × 4.60 mm ID, a mobile phase composed by a 70:30 mixture of a 15 mM aqueous solution of formic acid and

pure methanol (by isocratic elution), a flow rate of 0.500 mL/min, a temperature of 37 °C and the UV-Visible detector set at 210 nm. The complex showed a retention time of 5.22 minutes and its identity was attributed by the corresponding ESI-MS spectrum (*Figure 4.5*).

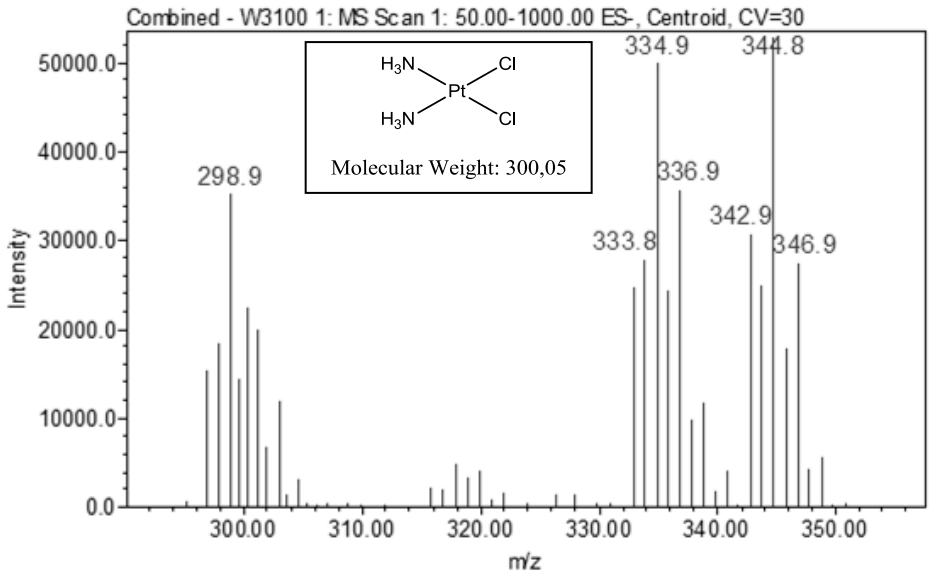

Figure 4.5: ESI-MS spectrum of cisplatin, prepared in ultrapure water

Figure 4.5 shows the cisplatin ESI-MS spectrum corresponding to the HPLC peak and registered in negative ion mode with a cone voltage (CV) of 30V: it confirmed the success of the synthesis since it contained the pseudo-molecular ion $[M-H]^-$ peak at 298.9 m/z and the peaks of adducts $[M+Cl]^-$ and $[M+formate]^-$ at 334.9 m/z and 344.8 m/z, respectively (the formate ion derived from the eluant).

^{195}Pt-NMR

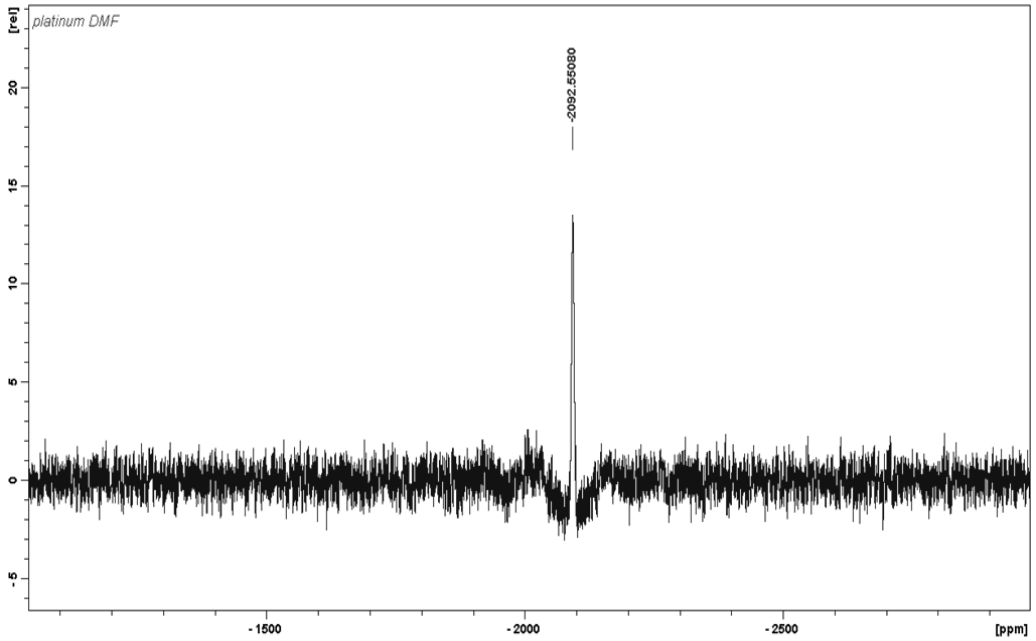

Figure 4.6: ^{195}Pt-NMR spectrum of cisplatin, registered in DMF-d_7

The cisplatin ^{195}Pt-NMR spectrum (*Figure 4.6*) was registered in DMF-d_7 (at a 107.2 MHz NMR frequency) and shows a signal with a chemical shift value of -2093 ppm, which is consistent with a Pt(II) with two chlorides and two amines.

4.5 Synthesis of (OC-6-33)-diamminedichloridodihydroxidoplatinum(IV) (1)

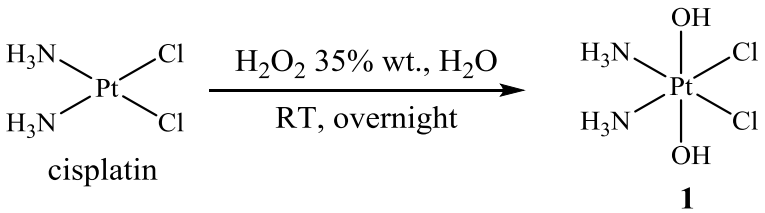

To a mixture of cisplatin (450 mg, 1.50 mmol) in 8 mL of ultrapure water, 35% w/w aqueous hydrogen peroxide (657 µL, 7.50 mmol) was added dropwise. The

reaction was carried out in continuous magnetic stirring at room temperature overnight. The precipitation of **1** was then favored by cooling the reaction mixture to -18 °C for 20 minutes. The resulting bright yellow solid was washed with cool ultrapure water, methanol and diethyl ether and, finally, dried *in vacuo*.

Yield: 348 mg, 1.04 mmol, 69.5%.

Elemental analysis calculated for $Cl_2H_8N_2O_2Pt$: H 2.41, N 8.39, Pt 58.40 %. Found: H 2.37, N 8.22, Pt 58.51 %.

4.5.1 Characterization of the Complex

RP-HPLC-ESI-MS

The analysis was performed by employing a stationary phase consisting of a C18 Phenosphere-NEXT column 5 μm, 250 × 4.60 mm ID, a mobile phase composed by a 70:30 mixture of a 15 mM aqueous solution of formic acid and pure methanol (by isocratic elution), a flow rate of 0.500 mL/min, a temperature of 37 °C and the UV-Visible detector set at 210 nm. Compound **1** showed a retention time of 4.16 minutes and its identity was attributed by the corresponding ESI-MS spectrum (*Figure 4.7*).

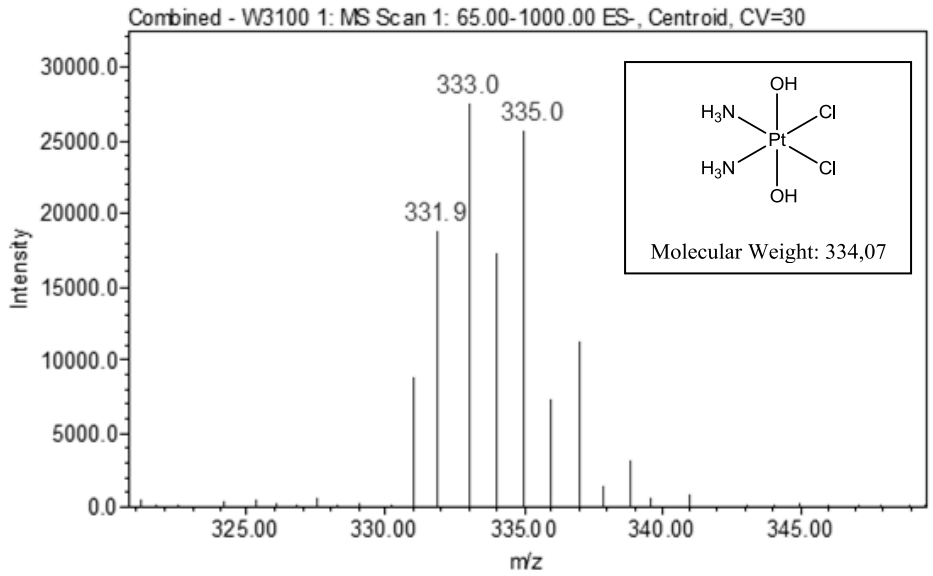

Figure 4.7: ESI-MS spectrum of complex **1**, prepared in ultrapure water

The ESI-MS spectrum of complex **1**, registered in negative ion mode with a cone voltage of 30V, shows the pseudo-molecular ion $[M-H]^-$ at 333.0 m/z.

^{195}Pt-NMR

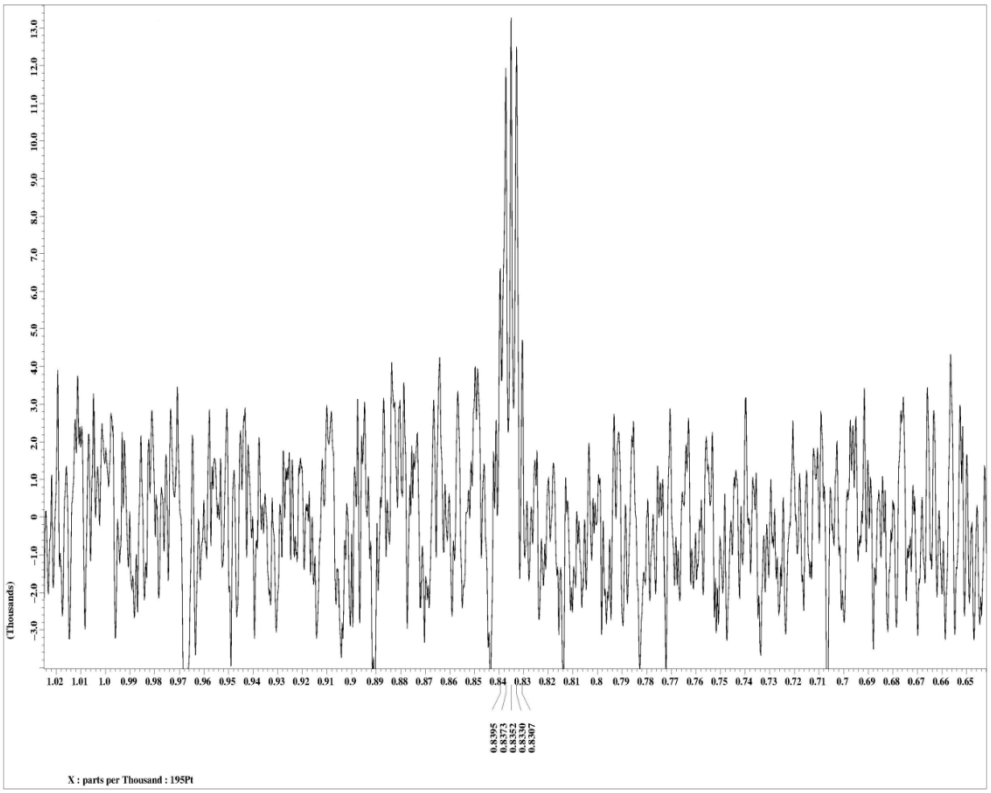

Figure 4.8: ^{195}Pt-NMR spectrum of complex **1**, registered in D_2O

The ^{195}Pt-NMR spectrum of complex **1** (*Figure 4.8*) was registered in D_2O (at a 86.0 MHz NMR frequency) and shows a signal at 835 ppm (qt, ^{1}J = 185.76 Hz), which is consistent with a Pt(IV) complex containing two chlorides, two amines and two hydroxido ligands. The signal multiplicity is typical for the coupling of ^{195}Pt (spin quantum number I = ½) with two ^{14}N atoms (I = 1). The signal is quite broad, due to the coupling with the quadrupolar nucleus ^{14}N.

4.6 Synthesis of (OC-6-33)-diamminebis(4-carboxypropanoato)dichloridoplatinum(IV) (2)

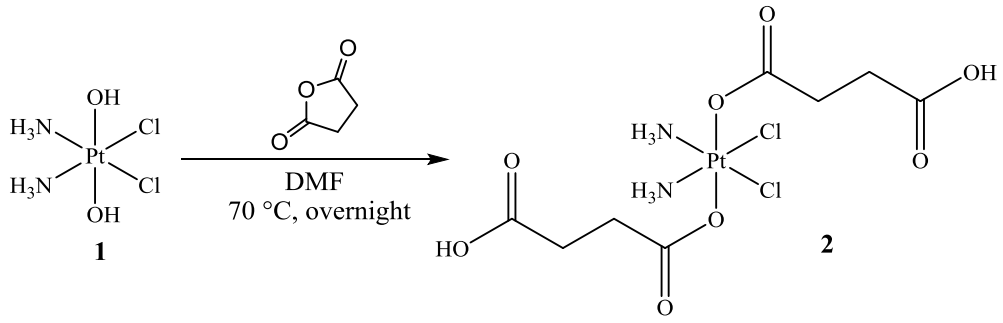

Succinic anhydride (120 mg, 1.20 mmol) and complex **1** (100 mg, 0.299 mmol) were dissolved in 5 mL of anhydrous *N,N*-dimethylformamide (DMF). The reaction mixture was stirred at 70 °C overnight. The yellow solution obtained was filtered to eliminate possible unreacted starting reagents and then DMF was removed under reduced pressure. The addition of acetone (1 mL) and, subsequently, of cool diethyl ether led to the precipitation of a yellow solid, which was washed with diethyl ether and then dried *in vacuo*.

Yield: 102 mg, 0.191 mmol, 63.8%.

Elemental analysis calculated for $C_8H_{16}Cl_2N_2O_8Pt$: C 17.99, H 3.02, N 5.24, Pt 36.52 %. Found: C 17.67, H 3.25, N 5.32, Pt 36.25 %.

4.6.1 Characterization of the Complex

RP-HPLC-ESI-MS

The analysis was performed by employing a stationary phase consisting of a C18 Phenosphere-NEXT column 5 μm, 250 × 4.60 mm ID, a mobile phase composed by a 70:30 mixture of a 15 mM aqueous solution of formic acid and

pure methanol (by isocratic elution), a flow rate of 0.500 mL/min, a temperature of 37 °C and the UV-Visible detector set at 210 nm. Compound **2** showed a retention time of 6.33 minutes and its identity was attributed by the corresponding ESI-MS spectrum (*Figure 4.9*).

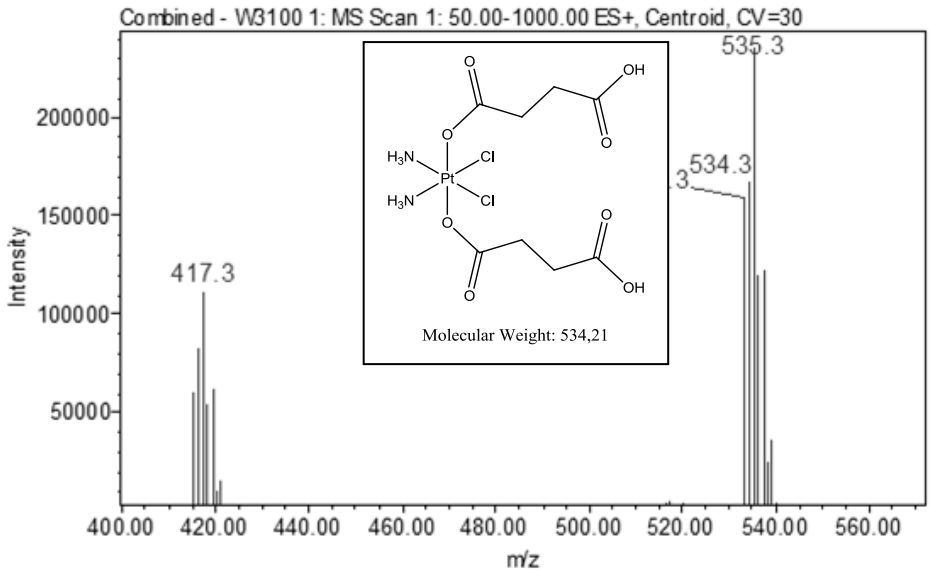

Figure 4.9: ESI-MS spectrum of complex **2**, prepared in ultrapure water

In the ESI-MS spectrum reported in *Figure 4.9*, registered in positive ion mode with a CV of 30V, the presence of complex **2** is confirmed by the peaks of the pseudo-molecular ion $[M+H]^+$ at 535.3 m/z and of its fragment $[M-O_2C(CH_2)_2CO_2H]^+$ at 417.3 m/z.

[1]H-NMR

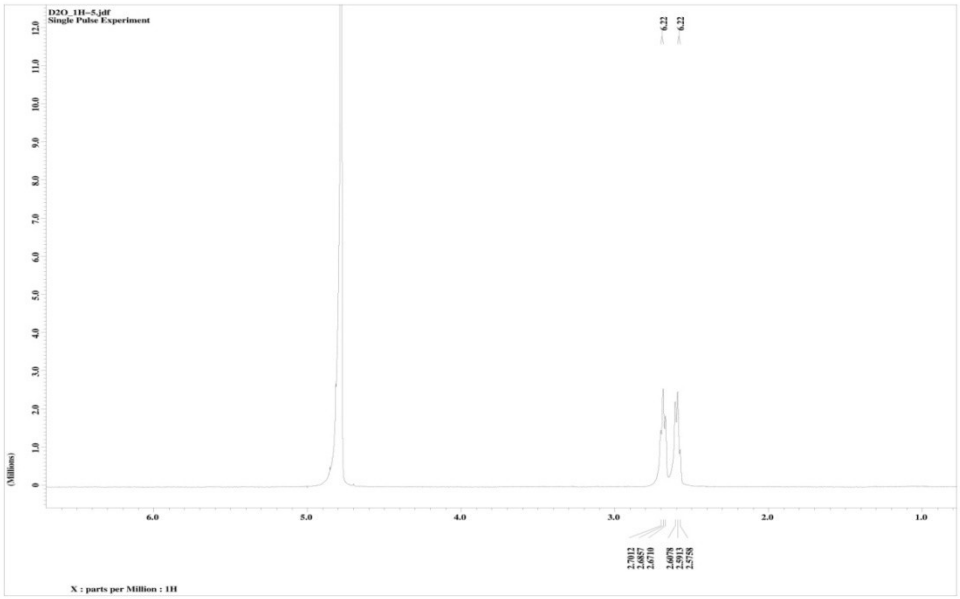

Figure 4.10: [1]H-NMR spectrum of complex **2**, registered in D_2O

The [1]H-NMR (400 MHz, D_2O) spectrum of complex **2** shows the following signals, δ: 2.59 (t, 4H, -C*H*$_2$CO$_2$H, ^{3}J = 6.22 Hz), 2.69 (t, 4H, -C*H*$_2$CO$_2$, ^{3}J = 6.22 Hz) ppm.

^{13}C-NMR

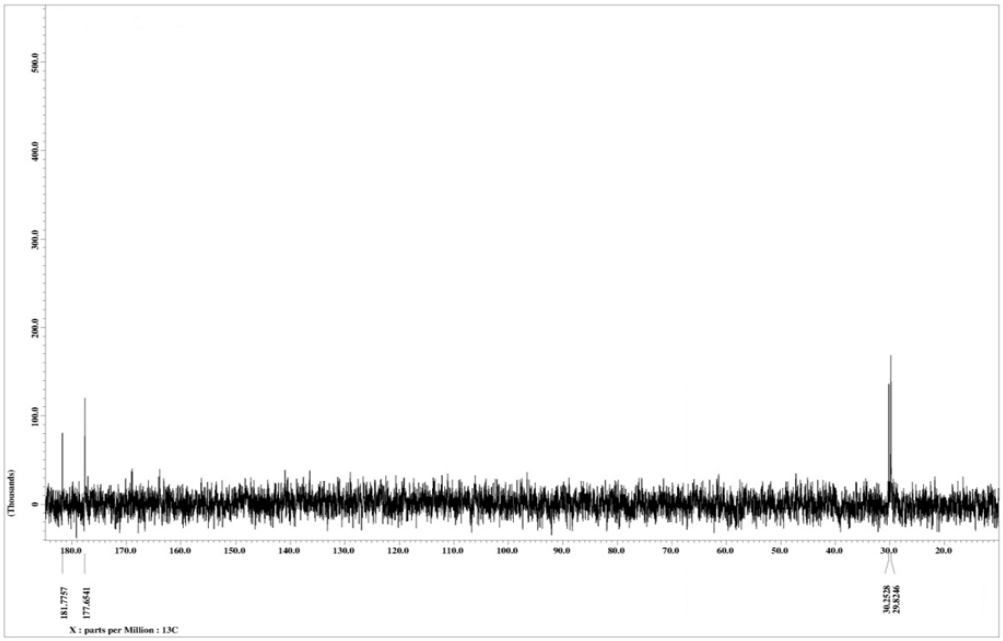

Figure 4.11: ^{13}C-NMR spectrum of complex **2**, registered in D_2O

The ^{13}C-NMR (100.6 MHz, D_2O) spectrum of complex **2** shows the following signals, δ: 29.8 (-*C*H_2CO_2H), 30.3 (-*C*H_2CO_2), 177.7 (-*C*OOH), 181.8 (-O*C*O) ppm.

^{195}Pt-NMR

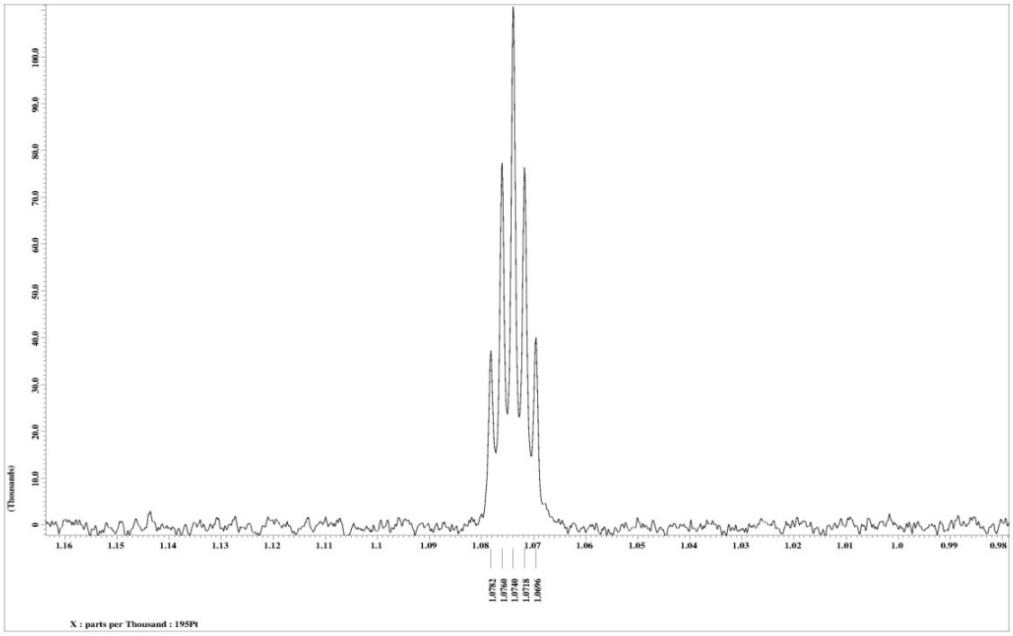

Figure 4.12: ^{195}Pt-NMR spectrum of complex **2**, registered in D_2O

Figure 4.12 shows the ^{195}Pt-NMR spectrum of complex **2**. It was registered in D_2O (at a 86.0 MHz NMR frequency) and it shows a signal at 1074 ppm (qt, ^{1}J = 189.42 Hz), which is consistent with a Pt(IV) complex with two chlorides, two amines and two carboxylato ligands. Also in this case, the multiplicity and the broadness of the signal are due to the coupling of ^{195}Pt with quadrupolar ^{14}N.

4.7 Synthesis of the Activated N-hydroxysuccinimidyl Diester of 2 (3)

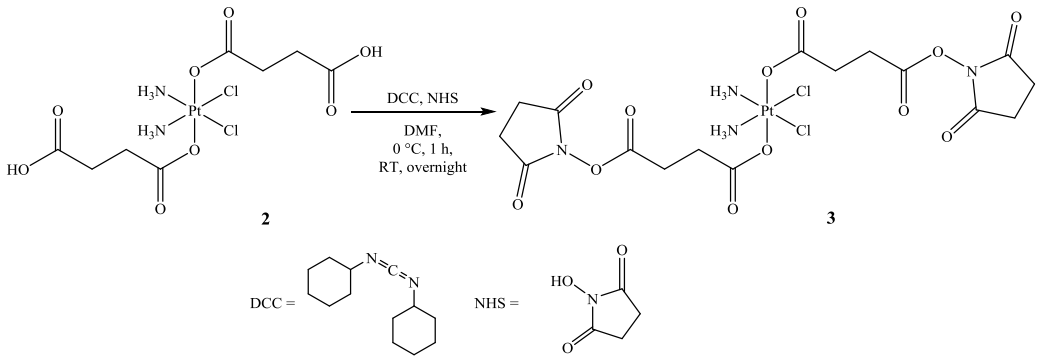

A mixture of **2** (100 mg, 0.187 mmol), *N,N'*-dicyclohexylcarbodiimide (DCC, 85.0 mg, 0.412 mmol) and *N*-hydroxysuccinimide (NHS, 47.4 mg, 0.412 mmol) in anhydrous DMF was stirred at 0 °C for 1 hour and then overnight at room temperature. After that, the solution was cooled to -18 °C and the byproduct dicyclohexylurea was removed by filtration. DMF was eliminated under reduced pressure to form a brown oil. The compound was then precipitated with diethyl ether, yielding a pale yellow solid.

Yield: 97.6 mg, 0.134 mmol, 71.6%.

Elemental analysis calculated for $C_{16}H_{22}Cl_2N_4O_{12}Pt$: C 26.38, H 3.04, N 7.69, Pt 26.78 %. Found: C 26.17, H 3.37, N 7.39, Pt 26.51 %.

4.7.1 Characterization of the Complex

RP-HPLC-ESI-MS

The analysis was performed by employing a stationary phase consisting of a C18 Phenosphere-NEXT column 5 μm, 250 × 4.60 mm ID, a mobile phase

composed by a 50:50 mixture of a 15 mM aqueous solution of formic acid and pure methanol (by isocratic elution), a flow rate of 0.500 mL/min, a temperature of 37 °C and the UV-Visible detector set at 210 nm. Compound **3** showed a retention time of 5.71 minutes and its identity was attributed by the corresponding ESI-MS spectrum (*Figure 4.13*).

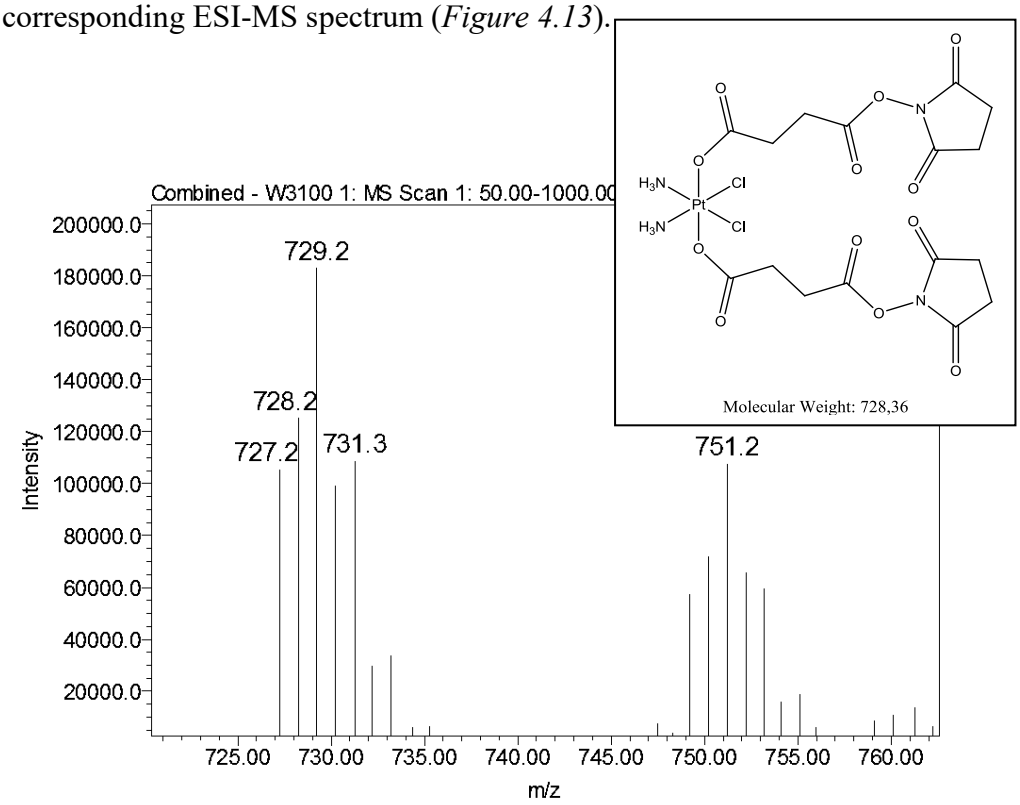

Figure 4.13: ESI-MS spectrum of complex **3**, prepared in a 50:50 mixture of ultrapure water and methanol

Figure 4.13 shows the ESI-MS spectrum of complex **3**, registered in positive ion mode with a cone voltage of 30V: the pseudo-molecular ion $[M+H]^+$ at 729.2 m/z and the adduct $[M+Na]^+$ at 751.2 m/z can be observed.

^{1}H-NMR

The ^{1}H-NMR (500 MHz, DMSO-d_6) spectrum of complex **3** shows the following signal, δ: 2.64 (t, 4H, -C*H*$_2$CO$_2$N, ^{3}J = 7.15 Hz), 2.81 (s, 8H, -C*H*$_2$CON), 2.82 (t, 4H, -C*H*$_2$CO$_2$, ^{3}J = 7.15 Hz), 6.47 (m, 6H, -N*H*$_3$) ppm.

^{13}C-NMR

The ^{13}C-NMR (125.7 MHz, DMSO-d_6) spectrum of complex **3** shows the following signals, δ: 25.7 (-*C*H$_2$CO$_2$N), 25.9 (-*C*H$_2$CON), 27.2 (-*C*H$_2$CO$_2$), 168.9 (-*C*OON), 170.7 (-*C*ON), 178.6 (-O*C*O) ppm.

^{195}Pt-NMR

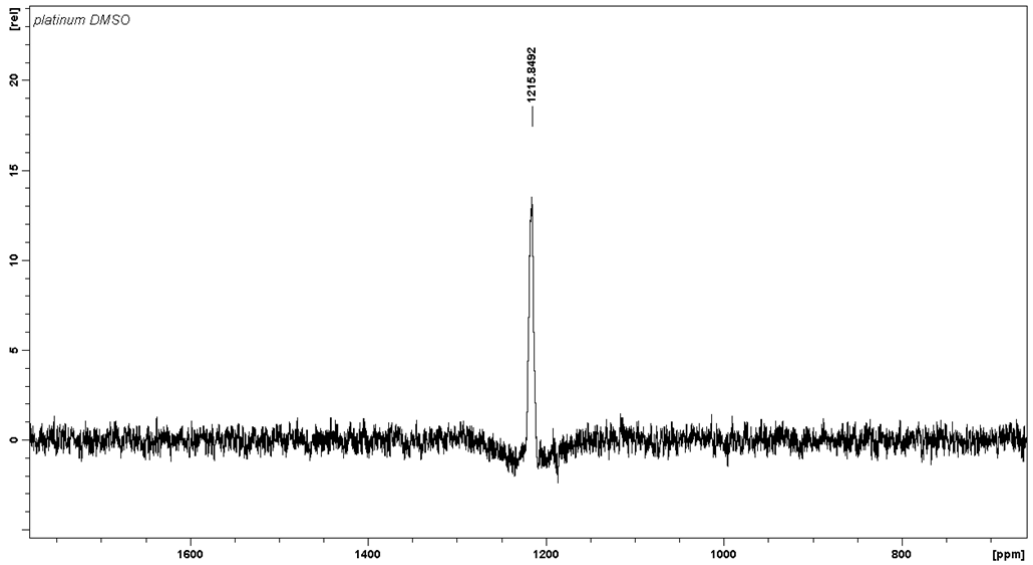

Figure 4.14: ^{195}Pt-NMR spectrum of complex **3**, registered in DMSO-d_6

The complex **3** ^{195}Pt-NMR spectrum (*Figure 4.14*) was registered in DMSO-d_6 (at a 107.2 MHz NMR frequency) and shows a signal corresponding to a

chemical shift value of 1216 ppm, which is consistent with a Pt(IV) complex with two chlorides, two amines and two carboxylato ligands.

4.8 Synthesis of (OC-6-33)-diamminebis(4-oxo-4-(propylamino)butanoato)dichloridoplatinum(IV) (4)

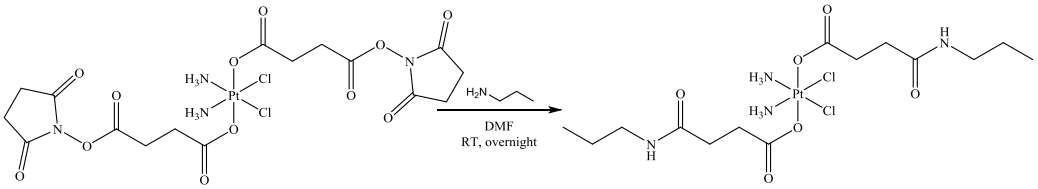

3 4

To a solution of **3** (50.0 mg, 0.0686 mmol) in 4 mL of anhydrous DMF, propylamine (56.7 µL, 0.686 mmol) was added and the mixture was stirred at room temperature for 24 hours.. The yellow solution was then cooled to -18 °C and then filtrated. The solvent was eliminated under reduced pressure and, during this phase, a pale yellow solid was formed and it was washed with diethyl ether. The product was washed with cool acetonitrile and diethyl ether and then dried *in vacuo*.

Yield: 33.4 mg, 0.0542 mmol, 78.9%.

Elemental analysis calculated for $C_{14}H_{30}Cl_2N_4O_6Pt$: C 27.28, H 4.91, N 9.09, Pt 31.65 %. Found: C 27.00, H 4.71, N 9.31, Pt 31.91 %.

4.8.1 Characterization of the Complex

RP-HPLC-ESI-MS

The analysis was performed by employing a stationary phase consisting of a C18 Phenosphere-NEXT column 5 μm, 250 × 4.60 mm ID, a mobile phase composed by a 50:50 mixture of a 15 mM aqueous solution of formic acid and pure methanol (by isocratic elution), a flow rate of 0.500 mL/min, a temperature of 37 °C and the UV-Visible detector set at 210 nm. Compound **4** showed a retention time of 9.06 minutes and its identity was attributed by the corresponding ESI-MS spectrum (*Figure 4.15*).

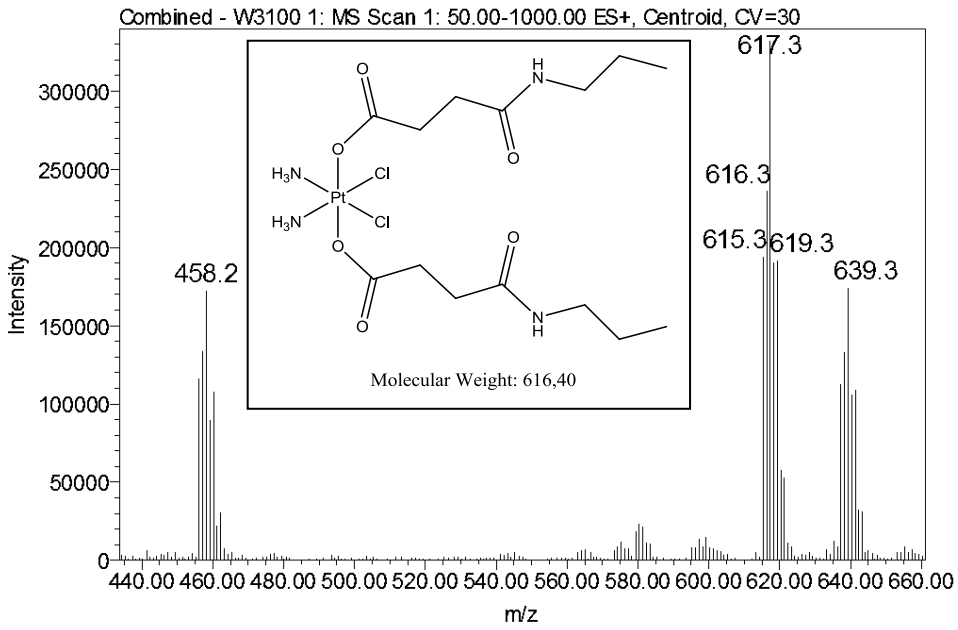

Figure 4.15: ESI-MS spectrum of complex **4**, prepared in a 50:50 mixture of ultrapure water and methanol

In the ESI-MS spectrum reported in *Figure 4.15*, registered in positive ion mode with a cone voltage of 30V, the presence of complex **4** is confirmed by the peaks of the pseudo-molecular ion $[M+H]^+$ at 617.3 m/z, of the adduct $[M+Na]^+$ at 639.3 m/z and of the fragment $[M\text{-}O_2C(CH_2)_2CONH(CH_2)_2CH_3]^+$ at 458.2 m/z.

^{1}H-NMR

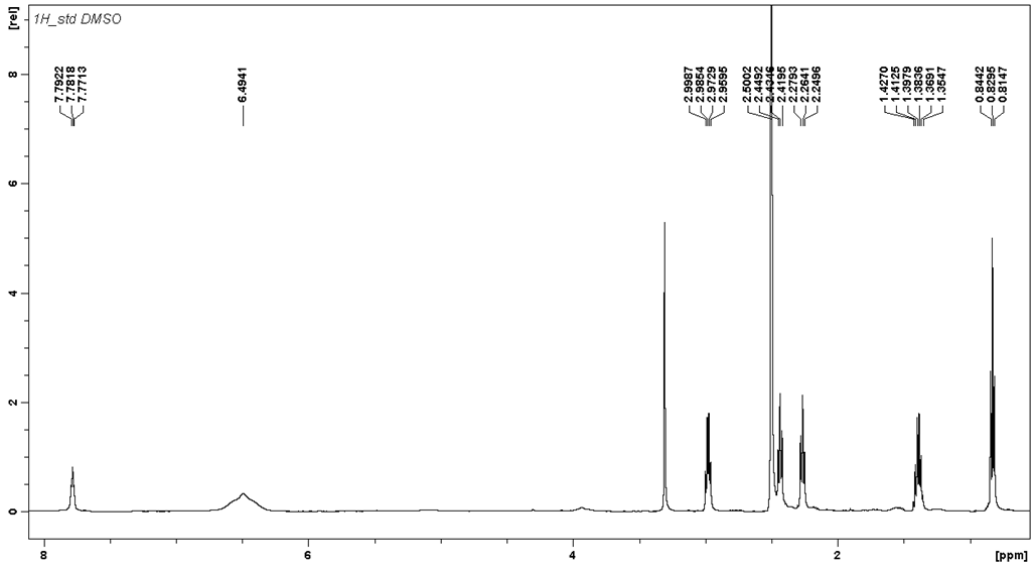

Figure 4.16: ^{1}H-NMR spectrum of complex **4**, registered in DMSO-d_6

The ^{1}H-NMR (500 MHz, DMSO-d_6) spectrum of complex **4** (*Figure 4.16*) shows the following signals, δ: 0.83 (t, 6H, -$CH_2CH_2CH_3$, ^{3}J = 7.12 Hz), 1.39 (sext, 4H, -$CH_2CH_2CH_3$, ^{3}J = 7.12 Hz), 2.26 (t, 4H, -CH_2CON, ^{3}J = 7.28 Hz), 2.43 (t, 4H, -CH_2CO_2, ^{3}J = 7.28 Hz), 2.98 (q, 4H, -$CH_2CH_2CH_3$, ^{3}J = 7.12 Hz), 6.49 (m, 6H, -NH_3), 7.78 (t, 2H, -NH, ^{3}J = 5.20 Hz) ppm.

^{13}C-NMR

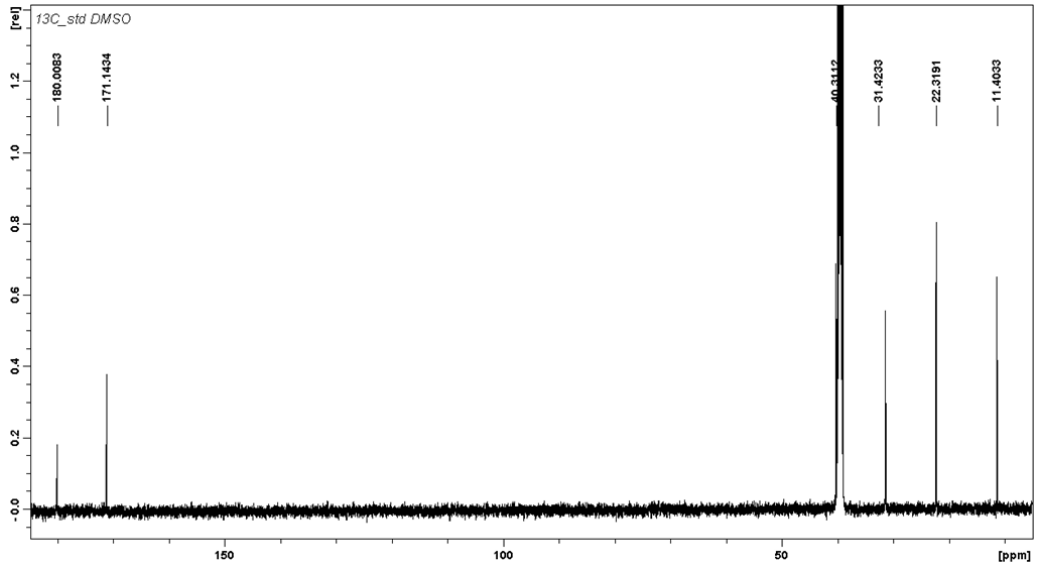

Figure 4.17: ^{13}C -NMR spectrum of complex **4**, registered in DMSO-d_6

The ^{13}C-NMR (125.7 MHz, DMSO-d_6) spectrum of complex **4** (*Figure 4.17*) shows the following signals, δ: 11.4 (-$CH_2CH_2\mathit{C}H_3$), 22.3 (-$CH_2\mathit{C}H_2CH_3$), 31.4 (-$\mathit{C}H_2CON$ and -$\mathit{C}H_2CO_2$), 40.3 (-$\mathit{C}H_2CH_2CH_3$), 171.1 (-$\mathit{C}ON$), 180.0 (-O$\mathit{C}O$) ppm.

Heteronuclear Single Quantum Correlation (HSQC)-NMR

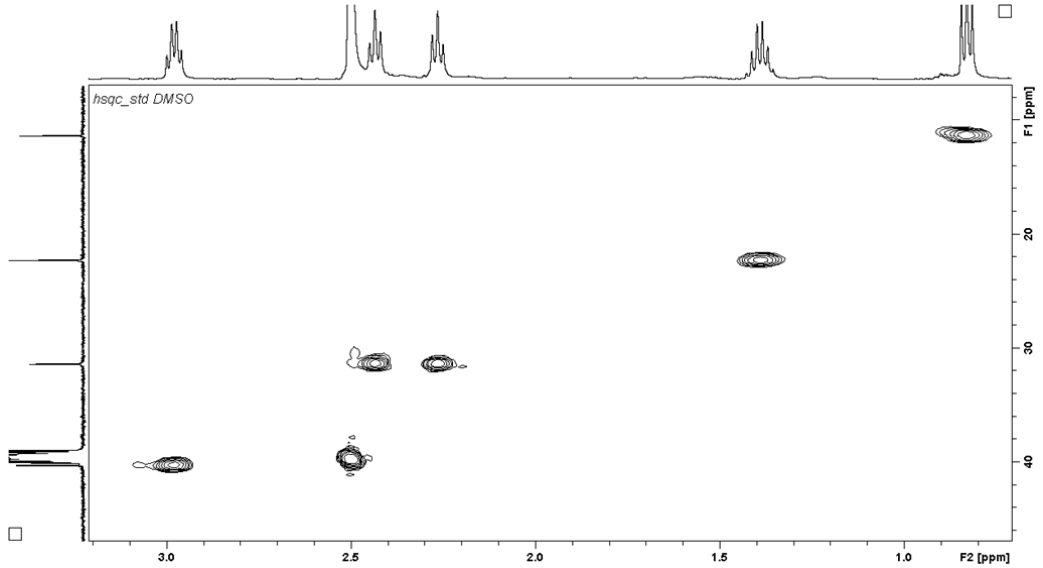

Figure 4.18: hsqc -NMR spectrum of complex **4**, registered in DMSO-d_6

The HSQC-NMR spectrum (*Figure 4.18*) allows to correctly assign the ^{13}C signals, in particular the one at 31.4 ppm: in fact, it is possible to verify that the two methylenic groups of the succinate have the same chemical shift, at 31.4 ppm.

^{195}Pt-NMR

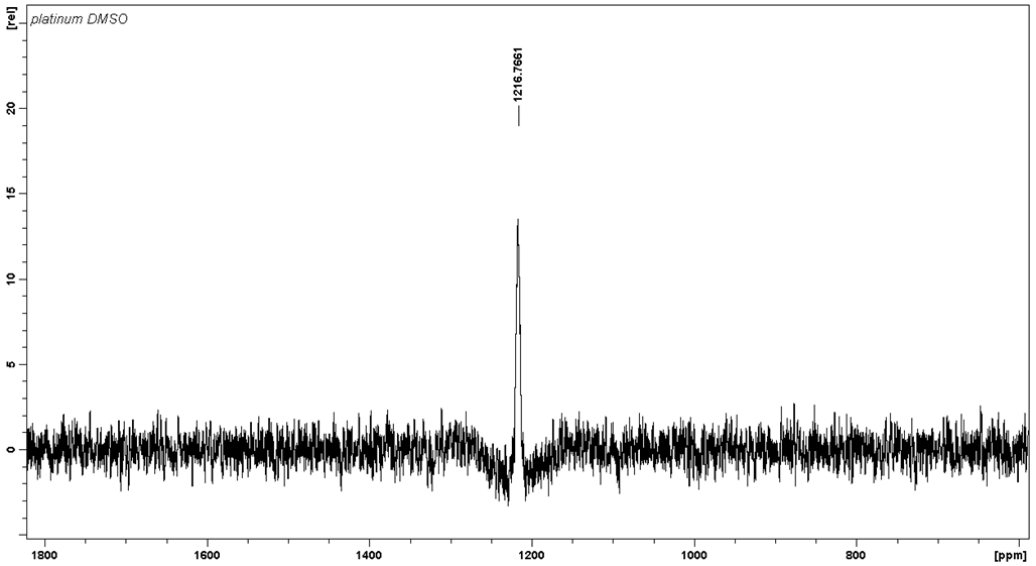

Figure 4.19: ^{195}Pt-NMR spectrum of complex **4**, registered in DMSO-d_6

In *Figure 4.19* the ^{195}Pt-NMR spectrum of complex **4** is reported. It was registered in DMSO-d_6 (at a 107.2 MHz NMR frequency) and shows a signal at 1217 ppm, which is consistent with a Pt(IV) complex containing two chlorides, two amines and two carboxylato ligands. In this case, the signal has a very similar chemical shift to that observed for complex **3**: in fact, the axial carboxylato of **3** and **4** show little differences in the chain but far from the platinum core, which results less affected.

4.9 Synthesis of Conjugate 5a

The synthesis of the conjugates was set up using NPs **a** because of its higher manageability and then the procedures were applied to the other NPs samples (**b**-**d**).

At first, the synthetic procedure was carried out using different reaction times (1, 2, 4 and 24 hours) in order to evaluate the best time necessary to reach the highest Pt loading on NPs. When the appropriate reaction time was found, it was fixed and applied to all the other conjugates syntheses (**5b**-**5d**).

In particular, 1 mL of an ethanol suspension of NPs **a** (35.0 mg) was centrifuged (10 minutes, 10000 rpm) in order to separate and remove ethanol. Then the NPs were washed with anhydrous DMF and, finally, resuspended in this solvent. This suspension was added to a solution of the activated intermediate **3** (10-fold molar excess with respect to NPs amino groups) and the reaction was carried out for different periods of time (1, 2, 4 and 24 hours) at room temperature.

After the established time, the suspension was centrifuged (10 minutes, 10000 rpm) in order to separate the solution (containing the unreacted Pt(IV) complex) from the NPs. These latter were washed several times with ethanol, in order to remove DMF and the residual coupling reagents. The reaction product was then divided into two aliquots: the former was kept as an ethanol suspension and the latter was washed with ultrapure water, frozen by means of liquid nitrogen and then lyophilized.

The suspension was used for SEM, DLS, and ζ potential analyses and for the biological tests.

The lyophilized sample, instead, was employed for the microwave mineralization, in order to quantify the amount of Pt loaded on the conjugates. Initially the lyophilization was employed also for dimensional analyses but, once lyophilized, the sample was impossible to be resuspended in solution: this result was confirmed also by SEM micrographs.

4.9.1 Characterization of Conjugate 5a

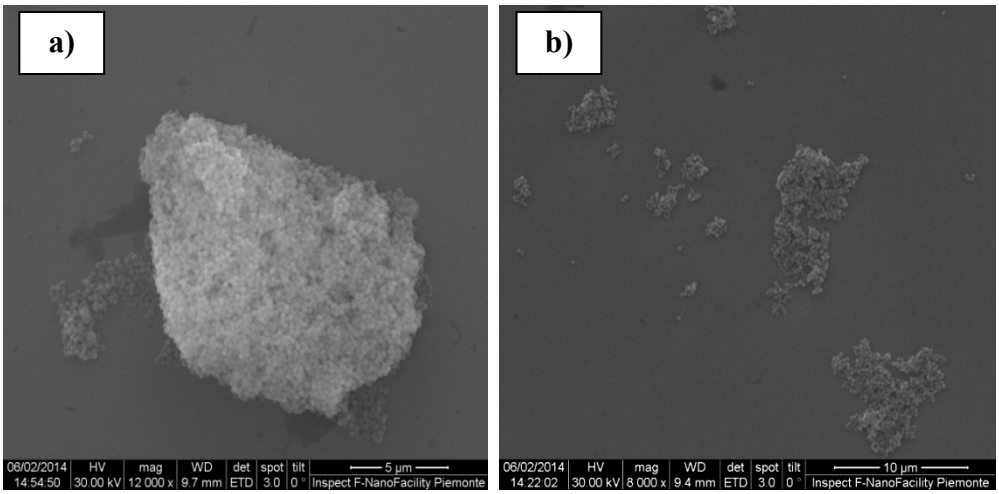

Figure 4.20: SEM micrographs of a) lyophilized and b) not lyophilized conjugate **5a**

SEM micrographs of conjugate **5a** allow to observe two main events. At first, the lyophilization, since it completely dries the sample, leads to irreversible aggregation of the NPs (*Figure 4.20a*): also the sonication does not allow to resuspend the conjugate. For this reason, this technique cannot be employed for size measurements and biological tests because they require stable suspensions. *Figure 4.20b* shows the cross-links between nearby NPs, due to the fact that a difunctional complex can exploit the first functionality for the coupling with an amino group of a nanoparticle and the second functionality for the reaction with a $-NH_2$ group of another nanoparticle. It results, therefore, in the formation of stable NPs aggregates.

4.9.2 Quantification of Pt Loading on Conjugate 5a

The Pt loading of the conjugates was determined by means of ICP-MS, after microwave mineralization. This method consisted in an acid digestion of each conjugate (2-3 mg) in quartz cuvettes that were then put into a closed vessel in the microwave oven. For the digestion, 800 µL of 70% w/w nitric acid and 200 µL of 35% w/w hydrogen peroxide in water were used. The microwaves (1200 W) were applied for 45 minutes, with the temperature set at 200 °C, using a temperature-controlled microwave heating.

When the mineralization was completed, the vessel was cooled down to room temperature and then opened to pull out the cuvettes, whose content was transferred into a marked flask using 1% v/v HNO_3 and sonicated for 1 hour at 60 °C. The samples were then centrifuged (10 minutes, 10000 rpm) in order to separate the silica residue from the solution, which was properly diluted with 1% v/v HNO_3 and analyzed by means of ICP-MS.

Table 4.5 summarizes the Pt loadings of **5a** (expressed as the percentage of Pt moles respect to the to the total available amino groups moles). The results point out that the highest loading was reached within 4 hours. This reaction time, therefore, was fixed and applied for the syntheses of conjugates **5b**-**5d**.

reaction time	conjugate	% Pt loading
1 h	**5a**	26.09 (± 1.78)
2 h		23.76 (± 0.72)
4 h		26.70 (± 1.64)
24 h		25.61 (± 2.98)

Table 4.5: Pt loadings of conjugate **5a** at different reaction time (at fixed Pt/amino groups ratio, 10:1)

4.10 Synthesis of Conjugates 5b-5d

Conjugates **5b**-**5d** were synthesized by using the same synthetic procedure previously described. In particular, an ethanol suspension of nanoparticles (NPs **b** 20.6 mg, NPs **c** 12.8 mg, NPs **d** 13.67 mg in 1 mL of solvent) was centrifuged (10 minutes, 10000 rpm) to remove the solvent. Then the solid residue was washed with anhydrous DMF and, finally, resuspended in this solvent. This suspension was added to a solution of complex **3** (10:1 Pt/amino groups ratio) and the reaction was performed for 4 hours at room temperature.

Each suspension was then centrifuged (10 minutes, 10000 rpm) to remove the solvent and the NPs were washed several times with ethanol. An aliquot of the synthesized conjugates was kept as an ethanol suspension and another one was washed with ultrapure water, frozen with liquid nitrogen and then lyophilized. After the mineralization (described in *paragraph 4.9.2*), each sample was analyzed by means of ICP-MS. The final results are the mean of at least three replicates.

In *Table 4.6* the Pt loadings of conjugates **5b**-**5d** (together with the one of **5a**, as a comparison) are reported: all the samples show values higher than 25%, with respect to the total amino groups, and, in particular, it seems that the smaller the employed NPs, the higher the Pt loading.

reaction time	conjugate	% Pt loading
4 h	**5a**	26.70 (± 1.64)
	5b	29.22 (± 2.10)
	5c	35.87 (± 3.28)
	5d	35.53 (± 4.65)

Table 4.6: Pt loadings of conjugates **5a**-**5d** at fixed reaction time (4 hours) and Pt/amino groups ratio (10:1)

4.10.1 Characterization of Conjugates 5b-5d

The SEM micrograph of the lyophilized conjugates showed large aggregates (a magnification of an area was reported in order to observe the NPs aggregation), whereas those of not lyophilized conjugates pointed out the cross-links formation between nearby NPs. *Figure 4.21* shows the SEM micrographs obtained from lyophilized (a) and not lyophilized (b) conjugate **5b**.

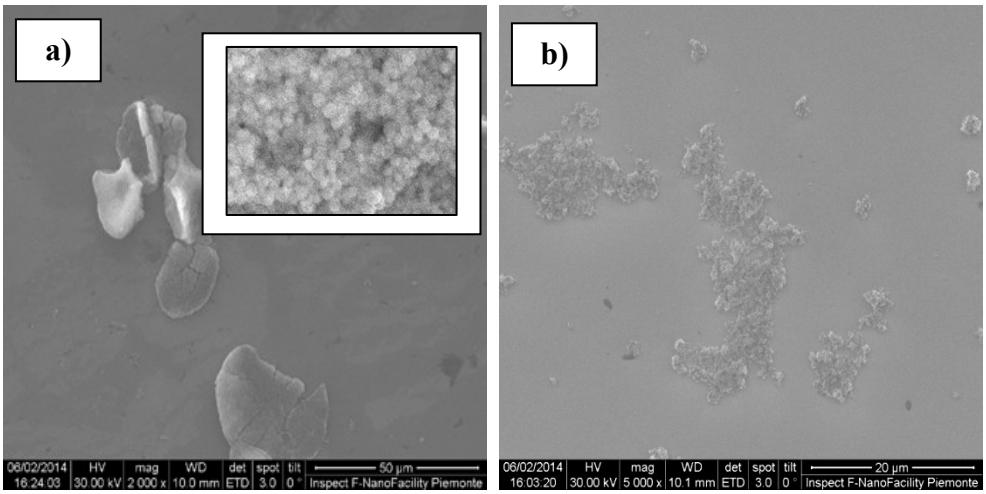

Figure 4.21: SEM micrographs of a) lyophilized and b) not lyophilized conjugate **5b**. In the first one, a magnification of an area is reported in order to point out the NPs aggregation

The use of difunctionalized complexes, therefore, results to be not suitable for the following biological tests because an unstable suspension can precipitate in the culture medium, giving no reliable and consistent results. Moreover, too large conjugates are not useful for the exploitation of the EPR effect, typical of the tumor tissues. Therefore, the following platinum syntheses were focused on Pt(IV) complexes, whose axial ligands show one inert functionality (in this case, an ethanolato) and one functionalizable group, which should avoid the formation of aggregates between NPs.

4.11 Synthesis of (OC-6-44)-diamminedichloridoethanolatohydroxidoplatinum(IV) (6)

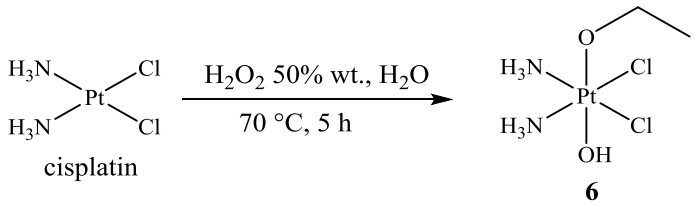

To a mixture of cisplatin (120 mg, 0.400 mmol) in 150 mL of absolute ethanol, an hydrogen peroxide solution (50% w/w in H_2O, 3 mL) was added dropwise. The solution was stirred at 70 °C for 5 hours and then cooled to room temperature. The unreacted cisplatin was removed by centrifugation and the solvent was eliminated under reduced pressure. The compound was precipitated with diethyl ether, yielding a yellow solid, which was washed with cool ethanol and diethyl ether and then dried *in vacuo*.

Yield: 116 mg, 0.320 mmol, 80.0%.

Elemental analysis calculated for $C_2H_{12}Cl_2N_2O_2Pt$: C 6.63, H 3.34, N 7.74, Pt 53.87%. Found: C 6.41, H 3.67, N 7.91, and Pt 53.78%.

4.11.1 Characterization of the Complex

RP-HPLC-ESI-MS

The analysis was performed by employing a stationary phase consisting of a C18 Phenosphere-NEXT column 5 μm, 250 × 4.60 mm ID, a mobile phase composed by a 70:30 mixture of a 15 mM aqueous solution of formic acid and pure methanol (by isocratic elution), a flow rate of 0.500 mL/min, a temperature of 37 °C and the UV-Visible detector set at 210 nm. Compound **6** showed a

retention time of 4.56 minutes and its identity was attributed by the corresponding ESI-MS spectrum (*Figure 4.22*).

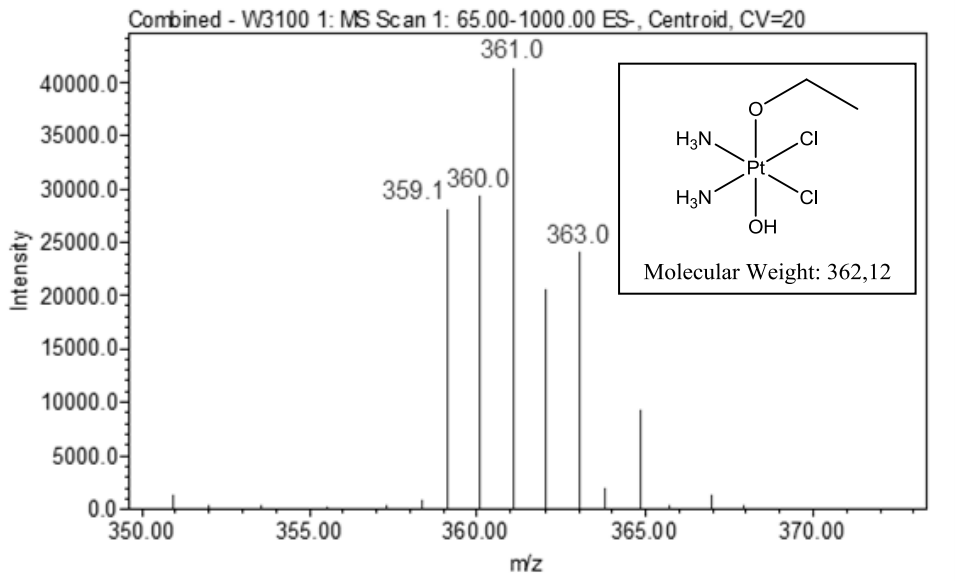

Figure 4.22: ESI-MS spectrum of complex **6**, prepared in ultrapure water

In *Figure 4.22* the ESI-MS spectrum, registered in negative ion mode with a cone voltage of 20V, confirms the presence of complex **6** with the pseudo-molecular ion $[M-H]^-$ peak at 361.0 m/z.

[1]H-NMR

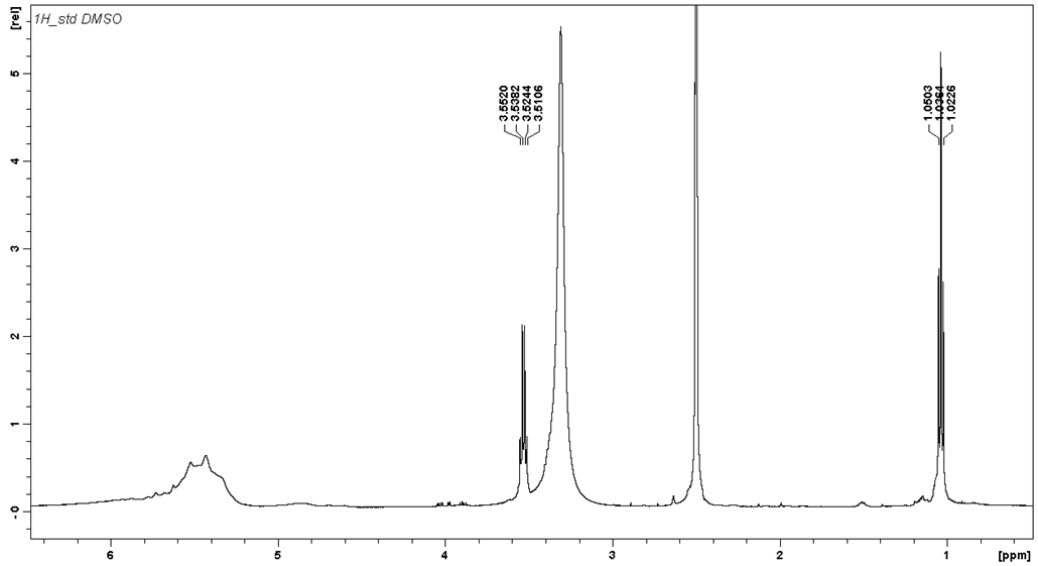

Figure 4.23: ^{1}H-NMR spectrum of complex **6**, registered in DMSO-d_6

The ^{1}H-NMR (500 MHz, DMSO-d_6) spectrum of complex **6** shows the following signals, δ: 1.04 (t, 3H, –CH_3, ^{3}J = 6.89 Hz), 3.53 (q, 2H, –CH_2, ^{3}J = 6.89 Hz), 5.43 (m, 6H, –NH_3) ppm.

^{13}C-NMR

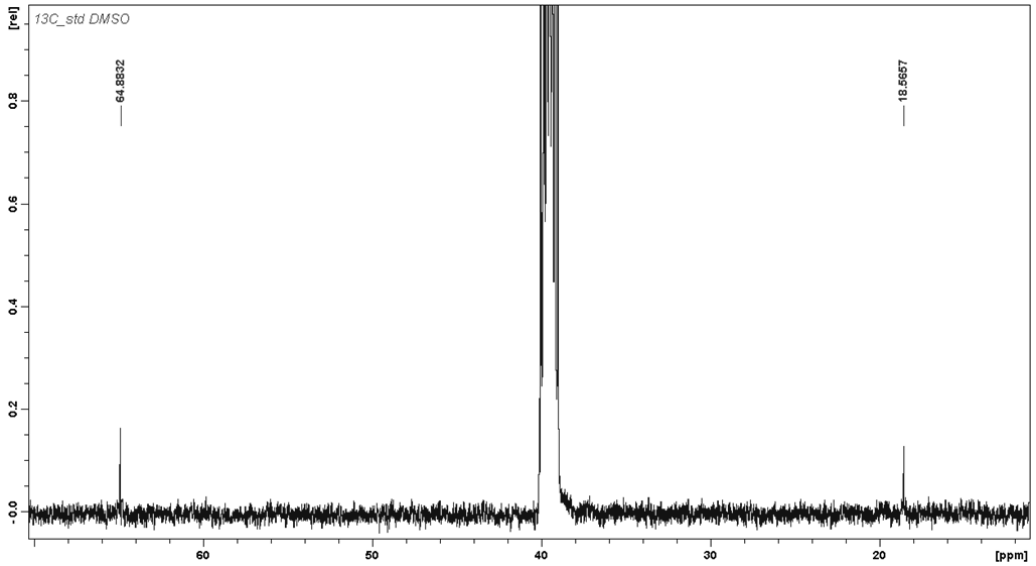

Figure 4.24: ^{13}C-NMR spectrum of complex **6**, registered in DMSO-d_6

The ^{13}C-NMR (125.7 MHz, DMSO-d_6) spectrum of complex **6** shows the following signals, δ: 18.6 (–*C*H_3), 64.9 (–*C*H_2) ppm.

^{195}Pt-NMR

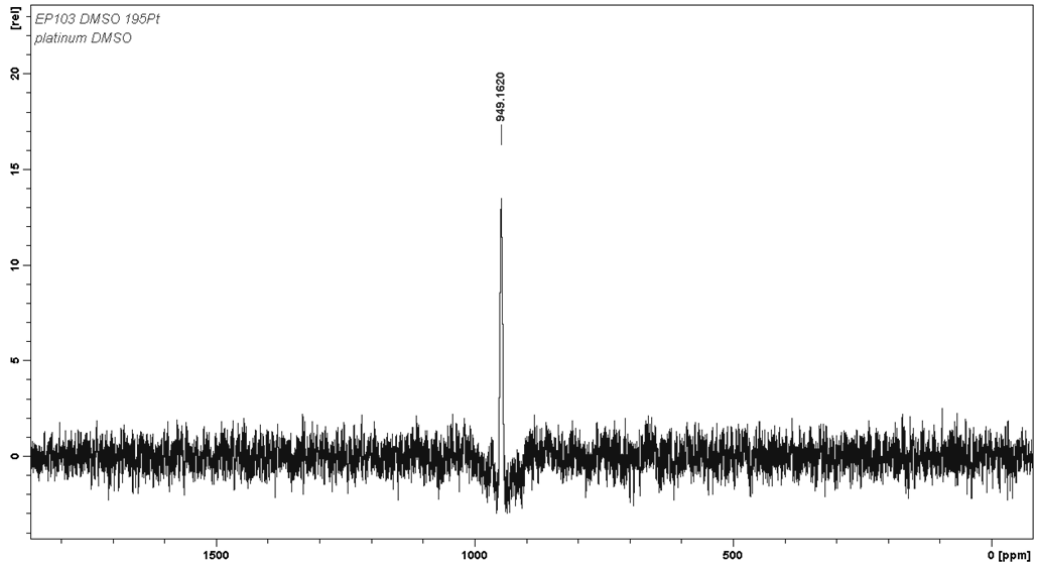

Figure 4.25: ^{195}Pt-NMR spectrum of complex **6**, registered in DMSO-d_6

The ^{195}Pt-NMR spectrum of complex **6** (*Figure 4.25*) was registered in DMSO-d_6 (at a 107.2 MHz NMR frequency) and shows a signal at 949 ppm, which is consistent with a Pt(IV) complex with an alcoxydo, two chlorides, two amines and a hydroxido ligand.

4.12 Synthesis of (OC-6-44)-diammine(4-carboxypropanoato)dichloridoethanolatoplatinum(IV) (7)

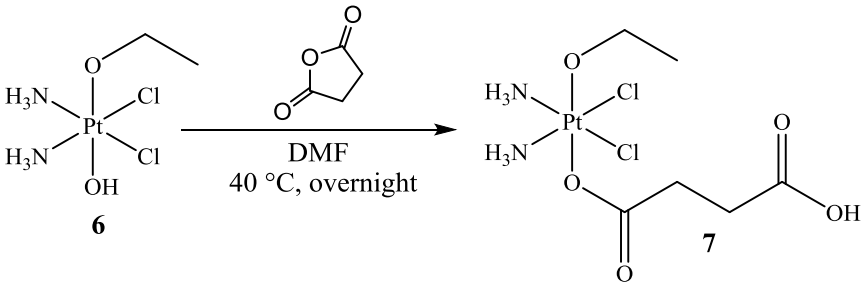

Complex **7** was synthesized according to slight modifications of a literature procedure [8]. In particular, succinic anhydride (66.3 mg, 0.663 mmol) was added dropwise to a solution of **6** (120 mg, 0.331 mmol) in anhydrous DMF. The reaction mixture was stirred at 40 °C overnight. The resulting yellow solution was filtered to remove possible unreacted starting material and then DMF was eliminated under reduced pressure. The subsequent addition of 1 mL of cool acetone led to the precipitation of a yellow solid, which was washed with diethyl ether and then dried *in vacuo*.

Yield: 93.4 mg, 0.202 mmol, 61.0%.

Elemental analysis calculated for $C_6H_{16}Cl_2N_2O_5Pt$: C 15.59, H 3.49, N 6.06, Pt 42.21%. Found: C 15.36, H 3.30, N 6.22, and Pt 42.10%.

4.12.1 Characterization of the Complex

RP-HPLC-ESI-MS

The analysis was performed by employing a stationary phase consisting of a C18 Phenosphere-NEXT column 5 μm, 250 × 4.60 mm ID, a mobile phase composed by a 70:30 mixture of a 15 mM aqueous solution of formic acid and pure methanol (by isocratic elution), a flow rate of 0.500 mL/min, a temperature of 37 °C and the UV-Visible detector set at 210 nm. Compound **7** showed a retention time of 7.91 minutes and its identity was attributed by the corresponding ESI-MS spectrum (*Figure 4.26*).

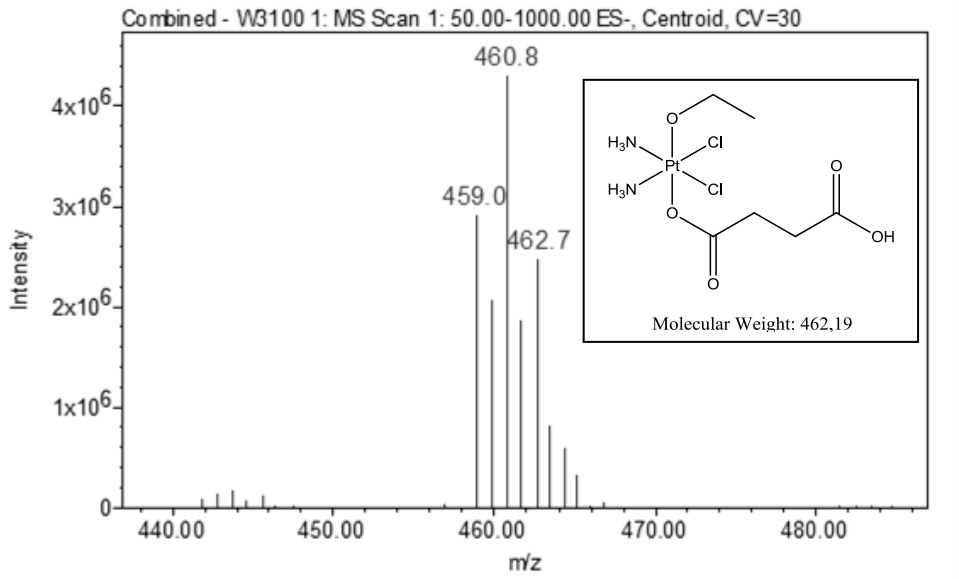

Figure 4.26: ESI-MS spectrum of complex **7**, prepared in ultrapure water

Figure 4.26 shows the ESI-MS spectrum of complex **7**, registered in negative ion mode with a CV of 30V, containing the pseudo-molecular ion $[M-H]^-$ peak at 460.8 m/z.

[1]H-NMR

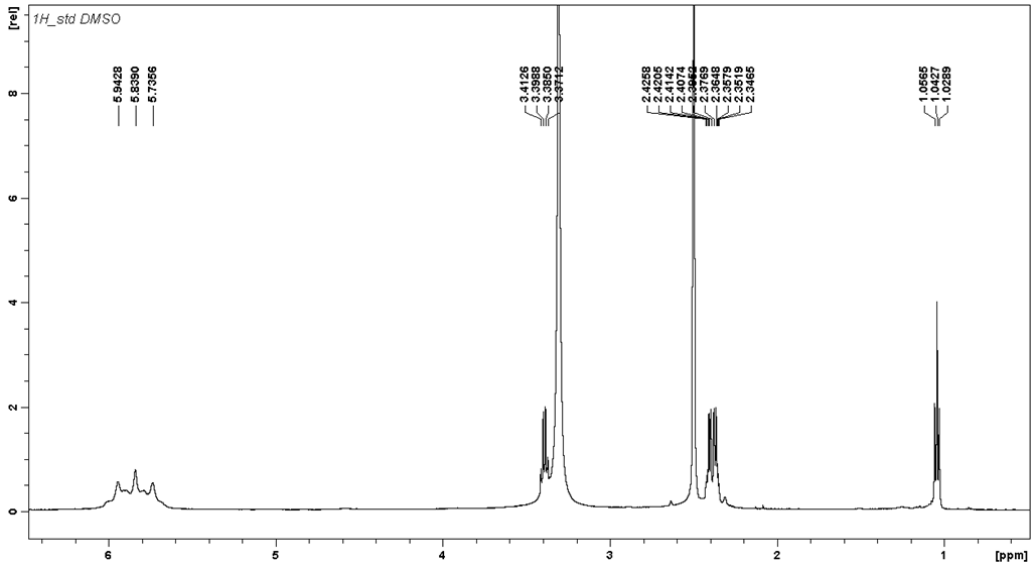

Figure 4.27: [1]H-NMR spectrum of complex **7**, registered in DMSO-d_6

The [1]H-NMR (500 MHz, DMSO-d_6) spectrum of complex **7** shows the following signals, δ: 1.04 (t, 3H, –C*H*$_3$, ^{3}J = 6.89 Hz), 2.37 (m, 2H, –C*H*$_2$CO$_2$H), 2.40 (m, 2H, –C*H*$_2$CO$_2$), 3.40 (q, 2H, –OC*H*$_2$, ^{3}J = 6.89 Hz), 5.84 (m, 6H, –N*H*$_3$) ppm.

^{13}C-NMR

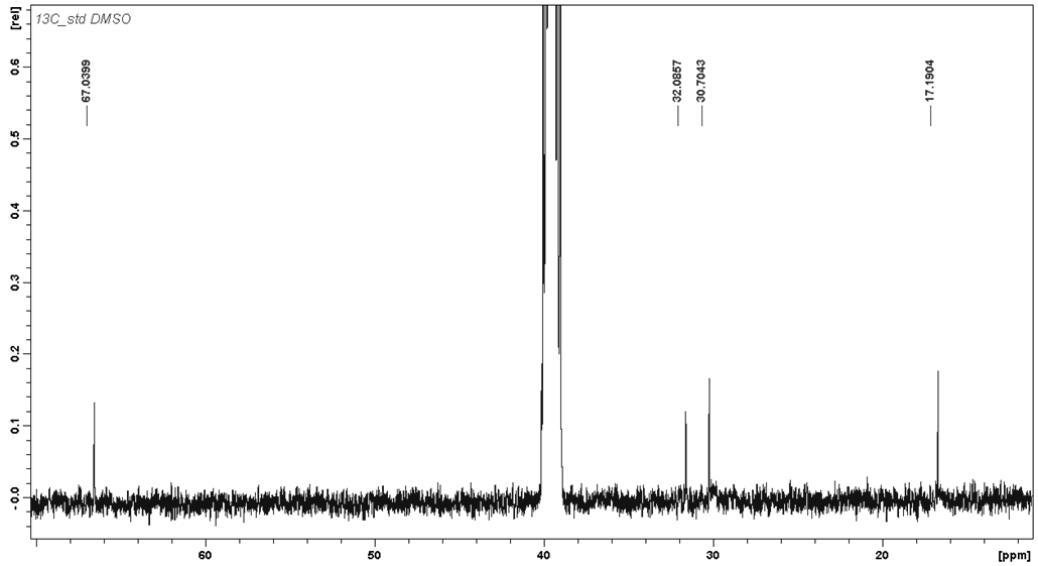

Figure 4.28: ^{13}C-NMR spectrum of complex **7**, registered in DMSO-d_6

The ^{13}C-NMR (125.7 MHz, DMSO-d_6) spectrum of complex **7** shows the following signals, δ: 17.2 (–*C*H_3), 30.7 (–*C*H_2CO_2H), 32.1 (–*C*H_2CO_2), 67.0 (–O*C*H_2), 174.5 (–*C*OOH), 180.5 (–O*C*O) ppm.

^{195}Pt-NMR

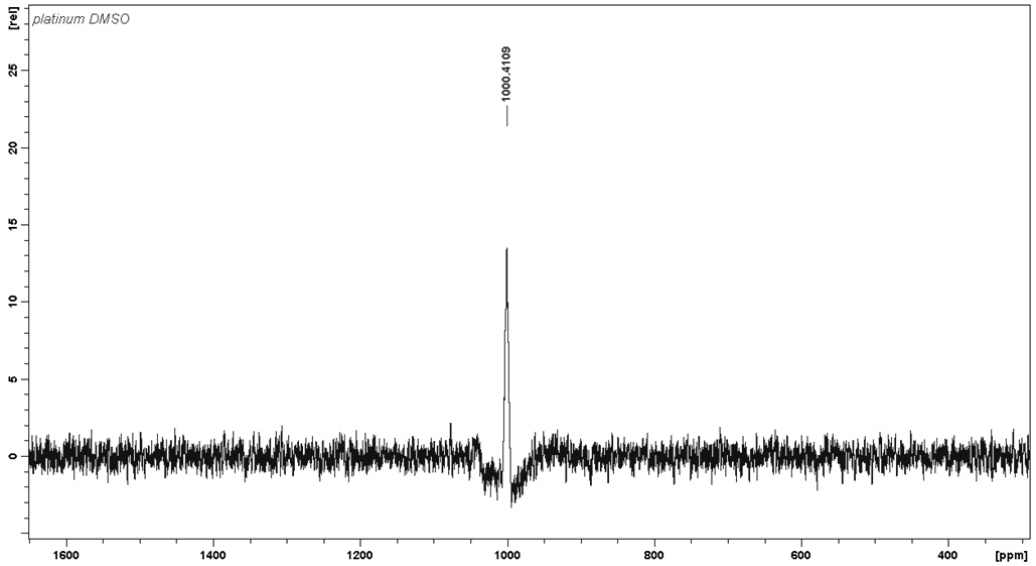

Figure 4.29: ^{195}Pt-NMR spectrum of complex **7**, registered in DMSO-d_6

Figure 4.29 shows the ^{195}Pt-NMR spectrum of complex **7** in DMSO-d_6 (at a 107.2 MHz NMR frequency). It is possible to observe a signal with a chemical shift value of 1000 ppm, consistent with a Pt(IV) complex with an alkoxydo, two chlorides, two amines and a succinato ligand.

4.13 Synthesis of the Activated N-hydroxysuccinimidyl Ester of 7 (8)

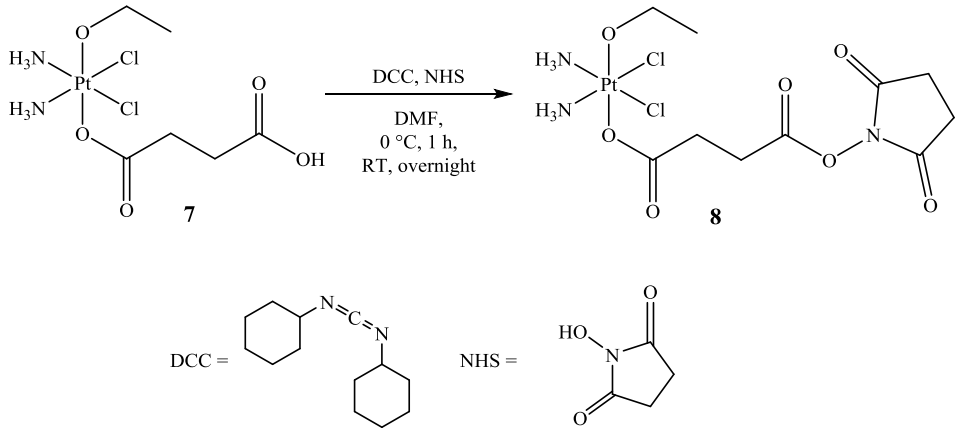

A mixture of **7** (90.0 mg, 0.195 mmol), DCC (48.2 mg, 0.234 mmol) and NHS (26.9 mg, 0.234 mmol) in anhydrous DMF was stirred at 0 °C for 1 hour and then at room temperature overnight. To remove dicyclohexylurea, the solution was cooled to -18 °C and, subsequently, filtered. DMF was eliminated under reduced pressure to form a brown oil. The compound was then precipitated with diethyl ether, yielding a pale yellow solid.

Yield: 73.9 mg, 0.132 mmol, 67.9%.

Elemental analysis calculated for $C_{10}H_{19}Cl_2N_3O_7Pt$: C 21.48, H 3.42, N 7.51, Pt 34.88%. Found: C 21.26, H 3.31, N 7.72, and Pt 35.01%.

4.13.1 Characterization of the Complex

RP-HPLC-ESI-MS

The analysis was performed by employing a stationary phase consisting of a C18 Phenosphere-NEXT column 5 μm, 250 × 4.60 mm ID, a mobile phase

composed by a 50:50 mixture of a 15 mM aqueous solution of formic acid and pure methanol (by isocratic elution), a flow rate of 0.500 mL/min, a temperature of 37 °C and the UV-Visible detector set at 210 nm. Compound **8** showed a retention time of 6.26 minutes and its identity was attributed by the corresponding ESI-MS spectrum (*Figure 4.30*).

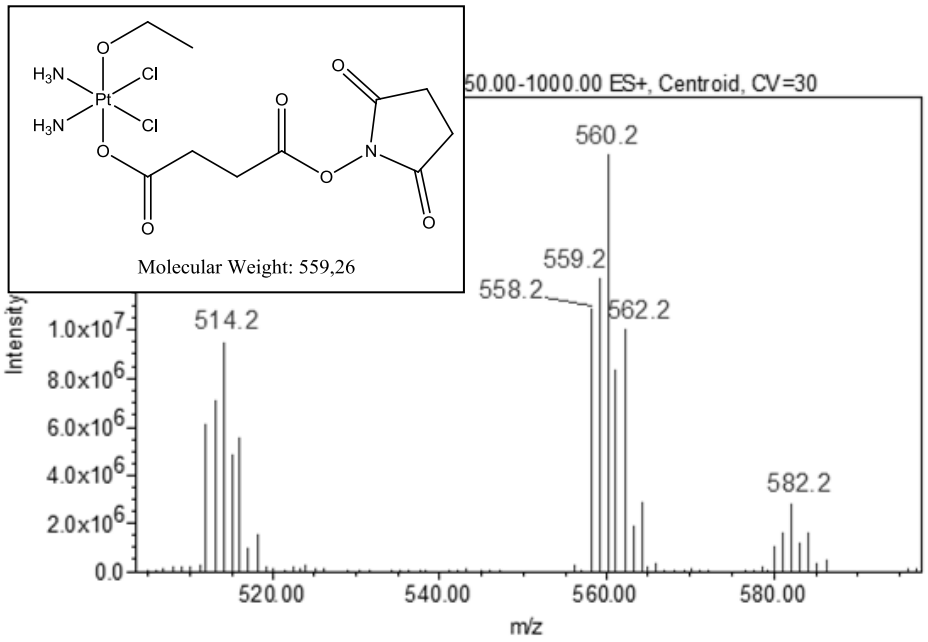

Figure 4.30: ESI-MS spectrum of complex **8**, prepared in a 50:50 mixture of ultrapure water and methanol

In the ESI-MS spectrum reported in *Figure 4.30*, registered in positive ion mode with a cone voltage of 30V, the presence of complex **8** is confirmed by the pseudo-molecular ion $[M+H]^+$ peak at 560.2 m/z and by the peaks of the adduct $[M+Na]^+$ at 582.2 m/z and the fragment $[M-OCH_2CH_3]^+$ at 514.2 m/z.

^{1}H-NMR

The ^{1}H-NMR (500 MHz, DMSO-d_6) spectrum of complex **8** shows the following signals, δ: 1.04 (t, 3H, –C*H*$_3$, ^{3}J = 6.59 Hz), 2.55 (t, 2H, –C*H*$_2$CO$_2$N, ^{3}J = 6.96 Hz), 2.76 (t, 2H, –C*H*$_2$CO$_2$, ^{3}J = 6.96 Hz), 2.80 (s, 4H, –C*H*$_2$CON), 3.40 (q, 2H, –OC*H*$_2$, ^{3}J = 6.59 Hz), 5.85 (m, 6H, –N*H*$_3$) ppm.

^{13}C-NMR

The ^{13}C-NMR (125.7 MHz, DMSO-d_6) spectrum of complex **8** shows the following signals, δ: 17.2 (–*C*H$_3$), 25.9 (–*C*H$_2$CON), 27.6 (–*C*H$_2$CO$_2$N), 31.2 (–*C*H$_2$CO$_2$), 67.1 (–O*C*H$_2$), 170.7 (–*C*ON), 174.4 (–*C*OON), 179.0 (–O*C*O) ppm.

^{195}Pt-NMR

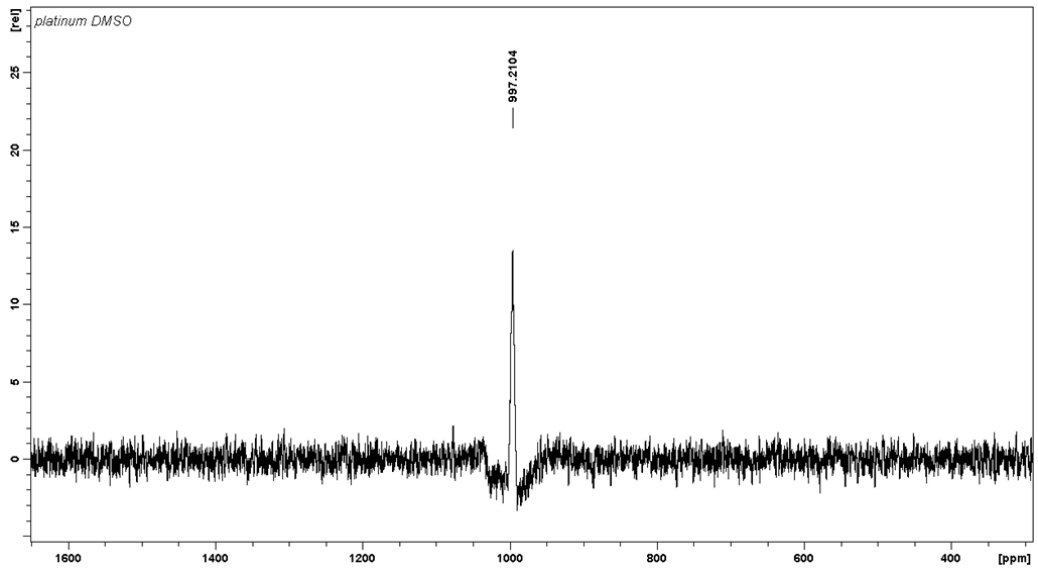

Figure 4.31: ^{195}Pt-NMR spectrum of complex **8**, registered in DMSO-d_6

The ^{195}Pt-NMR spectrum of complex **8** (*Figure 4.31*) was registered in DMSO-d_6 (at a 107.2 MHz NMR frequency) and shows a signal with a chemical shift value of 997 ppm, which is consistent with a Pt(IV) complex with an alkoxydo, two chlorides, two amines and a carboxylato ligand.

4.14 Synthesis of (OC-6-44)-diamminedichloridoethanolato(4-oxo-4-(propylamino)butanoato)platinum(IV) (9)

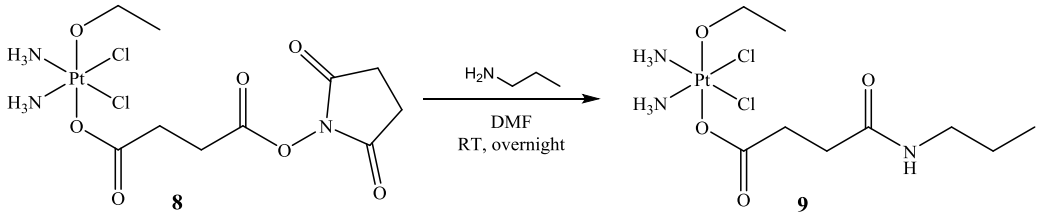

To a solution of **8** (50.0 mg, 0.0894 mmol) in anhydrous DMF, propylamine (36.9 µL, 0.447 mmol) was added and the mixture was stirred at room temperature overnight. The solution was filtered and then the solvent was removed under reduced pressure to form a yellow-brown oil. The subsequent recrystallization of the product with ethanol/diethyl ether led to the precipitation of a pale-yellow solid. The product was dried *in vacuo*.

Yield: 36.1 mg, 0.0717 mmol, 80.2%.

Elemental analysis calculated for $C_9H_{23}Cl_2N_3O_4Pt$: C 21.48, H 4.61, N 8.35, Pt 38.76 %. Found: C 21.26, H 4.45, N 8.74, and Pt 38.88 %.

4.14.1 Characterization of the Complex

RP-HPLC-ESI-MS

The analysis was performed by employing a stationary phase consisting of a C18 Phenosphere-NEXT column 5 μm, 250 × 4.60 mm ID, a mobile phase composed by a 50:50 mixture of a 15 mM aqueous solution of formic acid and pure methanol (by isocratic elution), a flow rate of 0.500 mL/min, a temperature of 37 °C and the UV-Visible detector set at 210 nm. Compound **9** showed a retention time of 9.71 minutes and its identity was attributed by the corresponding ESI-MS spectrum (*Figure 4.32*).

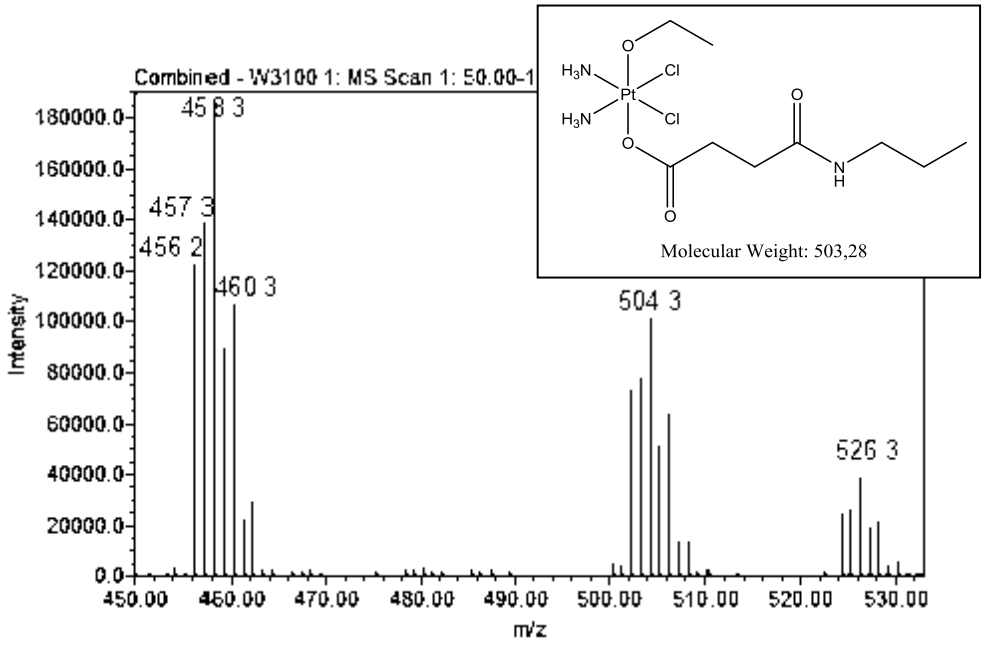

Figure 4.32: ESI-MS spectrum of complex **9**, prepared in a 50:50 mixture of ultrapure water and methanol

In the ESI-MS spectrum reported in *Figure 4.32*, registered in positive ion mode with a cone voltage of 30V, the presence of complex **9** is confirmed by the

pseudo-molecular ion $[M+H]^+$ peak at 504.3 m/z and the peaks of the adduct $[M+Na]^+$ at 526.3 m/z and the fragment $[M-OCH_2CH_3]^+$ at 458.3 m/z.

^{1}H-NMR

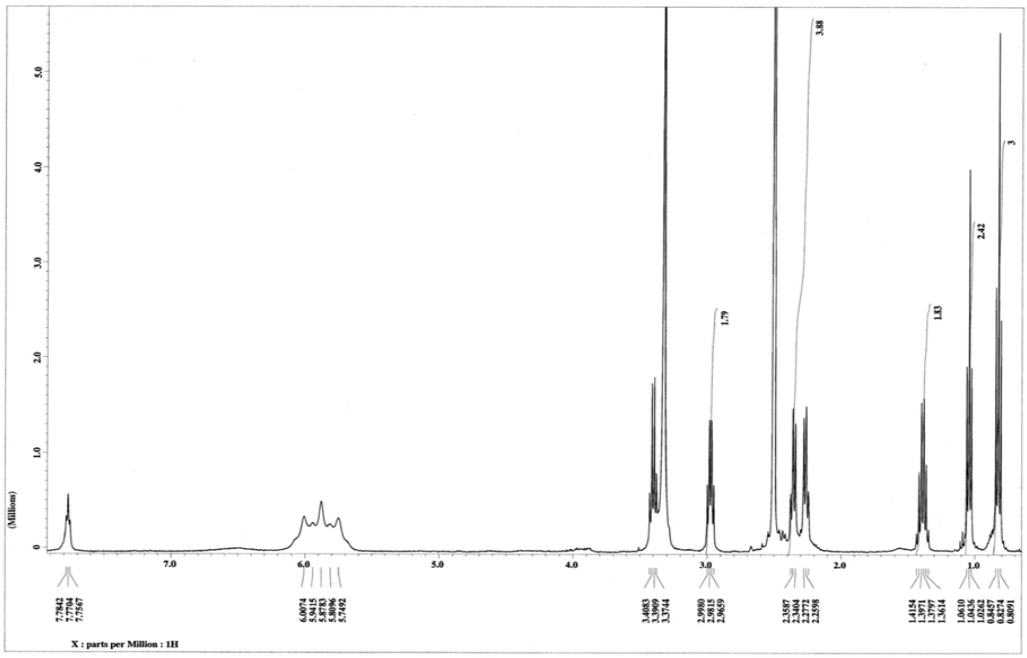

Figure 4.33: ^{1}H-NMR spectrum of complex **9**, registered in DMSO-d_6

The ^{1}H-NMR (400 MHz, DMSO-d_6) spectrum of complex **9** shows the following signals, δ: 0.83 (t, 3H, -$CH_2CH_2CH_3$, ^{3}J = 7.08 Hz), 1.04 (t, 3H, -CH_3, ^{3}J = 6.96 Hz), 1.39 (sext, 2H, -$CH_2CH_2CH_3$, ^{3}J = 7.08 Hz), 2.26 (t, 2H, -CH_2CON, ^{3}J = 6.96 Hz), 2.36 (t, 2H, -CH_2CO_2, ^{3}J = 6.96 Hz), 2.98 (q, 2H, -$CH_2CH_2CH_3$, ^{3}J = 7.08 Hz), 3.40 (q, 2H, -OCH_2, ^{3}J = 6.96 Hz), 5.88 (m, 6H, -NH_3), 7.77 (t, 1H, -N*H*, ^{3}J = 5.49 Hz) ppm.

^{13}C-NMR

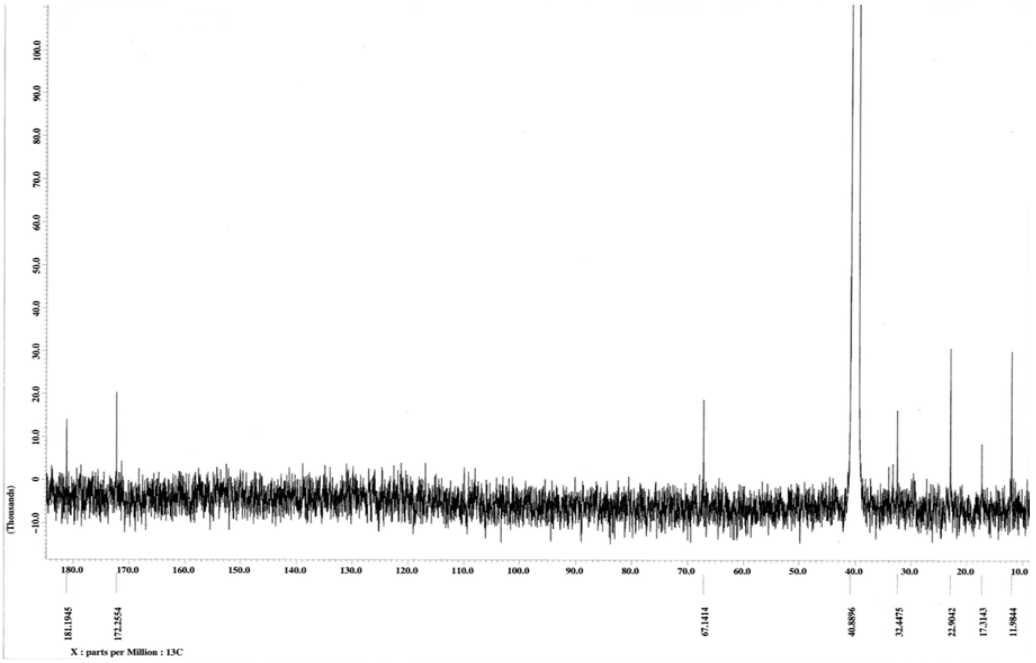

Figure 4.34: ^{13}C-NMR spectrum of complex **9**, registered in DMSO-d_6

The ^{13}C-NMR (100.6 MHz, DMSO-d_6) spectrum of complex **9** shows the following signals, δ: 12.0 (-$CH_2CH_2CH_3$), 17.3 (-CH_3), 22.9 (-$CH_2CH_2CH_3$), 32.4 (-CH_2CON and -CH_2CO_2), 40.9 (-$CH_2CH_2CH_3$), 67.1 (-OCH_2), 172.3 (-CON), 181.2 (-OCO) ppm.

^{195}Pt-NMR

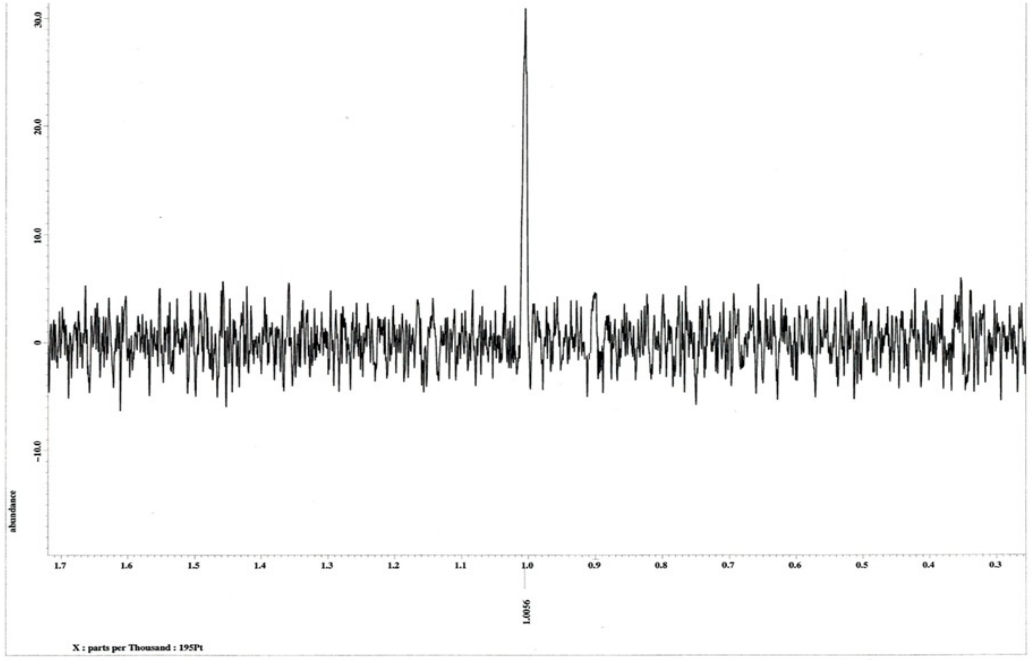

Figure 4.35: ^{195}Pt-NMR spectrum of complex **9**, registered in DMSO-d_6

In *Figure 4.35* the ^{195}Pt-NMR spectrum of complex **9**, registered in DMSO-d_6 (at a 86.0 MHz NMR frequency), is reported. It showed a signal at 1006 ppm, which is consistent with a Pt(IV) complex with an alkoxydo, two chlorides, two amines and a carboxylato ligand.

4.15 Synthesis of Conjugates 10a-10d

As previously described for the synthesis of conjugates **5a**-**5d**, an ethanol suspension of each kind of nanoparticles (NPs **a** 35.0 mg, NPs **b** 20.6 mg, NPs **c** 12.8 mg, NPs **d** 13.67 mg in 1 mL of solvent) was centrifuged (10 minutes, 10000 rpm), then washed with anhydrous DMF and, finally, resuspended in this solvent. After changing the reaction time (1, 2, 4 and 24 hours) for the coupling of NPs **a** with the Pt(IV) complex to find the best condition, the suspension of

NPs **b-d** was added to a solution of the activated intermediate **8**. At first, the Pt/NPs amino groups ratio and the reaction time was fixed at 10:1 and at 4 hours (at room temperature) respectively. Then, the Pt/NPs ratio was fixed at 5:1 in order to reduce the amount of Pt(IV) complex used in the coupling reaction, whereas the time was fixed at 4 hours.

After the established time, the suspension was centrifuged (10 minutes, 10000 rpm) in order to separate the supernatant (containing the unreacted Pt(IV) complex) from the NPs. These latter were washed several times with ethanol. The reaction product was then divided into two aliquots: the former was kept as an ethanol suspension and the latter was washed with ultrapure water, frozen with liquid nitrogen and then lyophilized.

4.15.1 Characterization of Conjugates 10a-10d

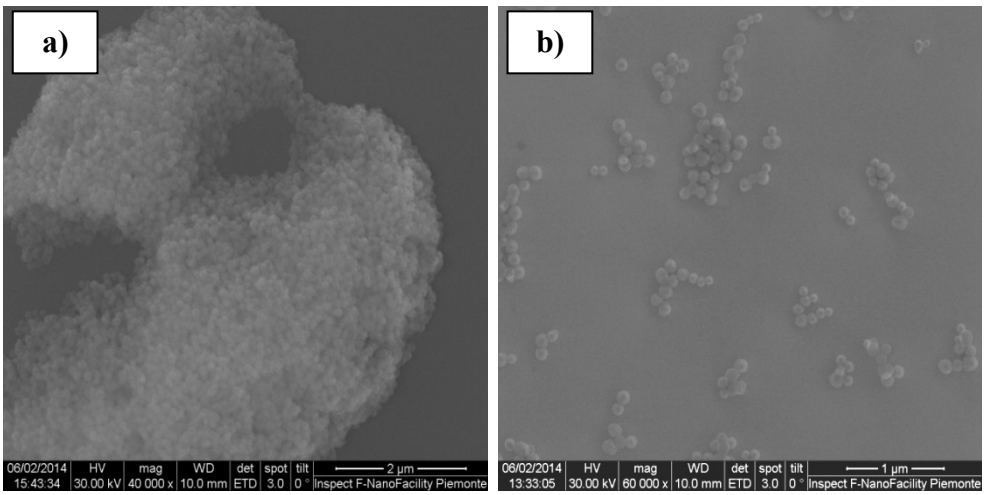

Figure 4.36: SEM micrographs of a) lyophilized and not lyophilized conjugate **10b**

The SEM micrographs of conjugates **10a-10d** show large aggregates (*Figure 4.36a*), due to the lyophilization process (the lyophilized conjugates cannot be resuspended). On the contrary, without lyophilization aggregates are not formed

(*Figure 4.36b*): in fact, the presence of only one available functionality avoids the formation of cross-links between NPs and made the suspension more stable. For this reason, the monofunctionalizable complexes were chosen for further studies, whereas the difunctionalizable ones were abandoned.

4.15.2 Quantification of Pt Loading on 10a-10d

After the mineralization of the lyophilized conjugates (described in *paragraph 4.9.2*), each sample was analyzed by means of ICP-MS to determine the Pt loading. The data were the results of at least three replicates, were expressed as % respect to the total available amino groups) and are shown in *Table 4.7*. In particular, on the left side it is possible to observe the Pt loading of **10a** at different reaction times: as in the case of conjugate **5a**, the highest percentage of loading was reached within 4 hours. The right side of the table, instead, reports the Pt loadings get after fixed coupling time (4 hours) with two different Pt/NPs amino groups ratio: in the left column the usual 10:1 ratio is indicated, whereas the right column refers to the 5:1 ratio. From the analysis of these data, it is evident that there are no significant differences between the two sets of results and, therefore, the 10:1 ratio does not lead to a considerable loading increase. Moreover, as conjugates **5a**-**5d** (*paragraph 4.10*), the smaller the NPs the higher the Pt loading.

conjugate	10:1 Pt/NH_2 ratio		conjugate		10:1 Pt/NH_2 ratio	5:1 Pt/NH_2 ratio
	reaction time	% Pt loading		reaction time	% Pt loading	% Pt loading
10a	1 h	16.51 (± 1.22)	**10a**	4 h	24.71 (± 3.61)	19.96 (± 0.11)
	2 h	15.91 (± 0.94)	**10b**		21.65 (± 2.06)	21.62 (± 2.17)
	4 h	24.71 (± 3.61)	**10c**		24.27 (± 1.88)	28.15 (± 1.06)
	24 h	23.77 (± 1.12)	**10d**		32.38 (± 1.45)	33.37 (± 2.17)

Table 4.7: Pt loadings (respect to the total amino groups) of conjugate **10a** at different reaction time (left) and Pt loadings of conjugates **10a**-**10d** at fixed reaction time and with different Pt/NH_2 ratio (right)

4.16 Spontaneous Release of Platinum from Conjugates

In order to verify the drug release from the NPs, in particular, 2-3 mg of each lyophilized conjugate were suspended in 3 mL of ultrapure water and the suspension was magnetically stirred for 4 hours (it corresponded to the time employed for cellular accumulation experiments). The suspension was then centrifuged (10 minutes, 10000 rpm) to separate the solution from the NPs and the platinum released in the solution was measured by means of ICP-MS.

The test showed that, within 4 hours, the 15% of the Pt loaded on NPs (percentage calculated with respect to the total Pt loaded on the conjugate) was released. Moreover, the RP-HPLC-ESI-MS analysis allowed to identify the main species released from the NPs surface: it corresponds to complex **7** linked, via amidic bond, to the 3-aminopropylsilane (APS) arm (defined as **7-APS**, *Figure 4.37*), detached from the NPs due to the hydrolysis of Si-O-Si bonds.

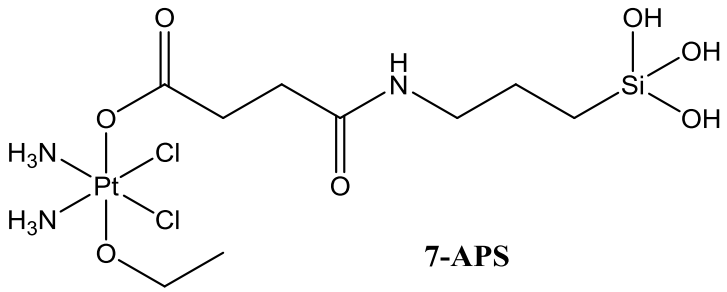

Figure 4.37: Structural formula of the main species released from the NPs surface

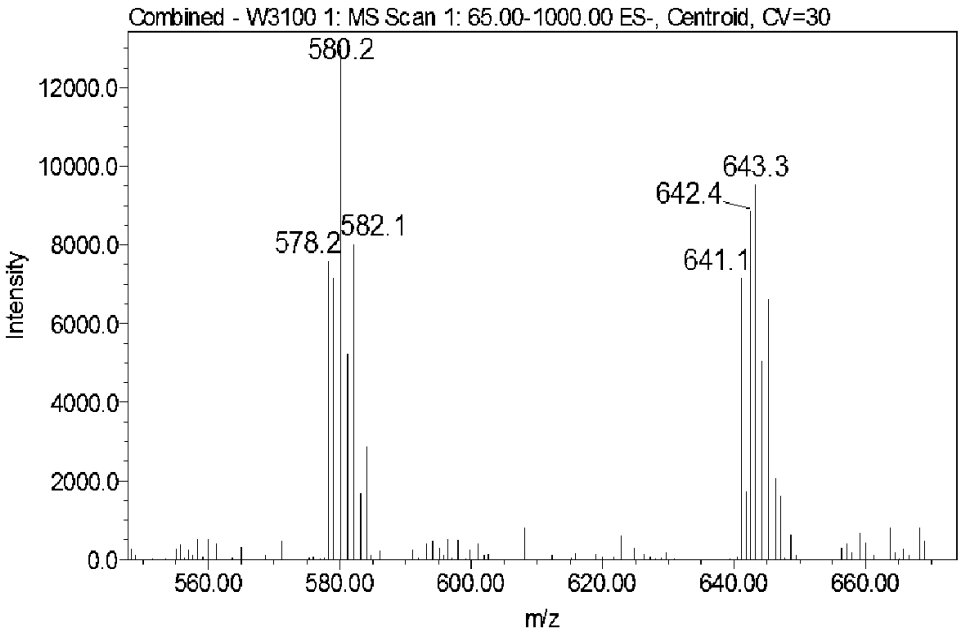

Figure 4.38: ESI-MS spectrum which allowed to identify the main released species **7-APS**

The structure of **7-APS** is confirmed by its ESI-MS spectrum (*Figure 4.38*), registered in negative ion mode with a cone voltage of 30V. It shows two peaks with the platinum pattern at 580.2 m/z and 643.3 m/z, which can be attributed to the pseudo-molecular ion $[M\text{-}H]^-$ and the adduct $[M+NO_3]^-$, respectively, of **7-APS** (*Figure 4.37*). The correct attribution of the two peaks is confirmed by their simulations, reported in *Figures 4.39* and *4.40*.

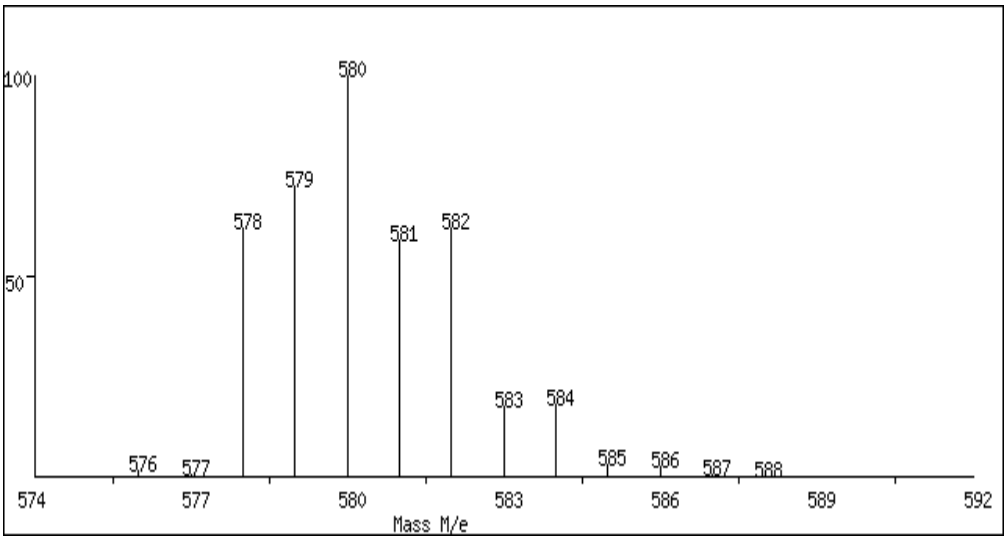

Figure 4.39: MS simulation of the pseudo-molecular ion $[M-H]^-$

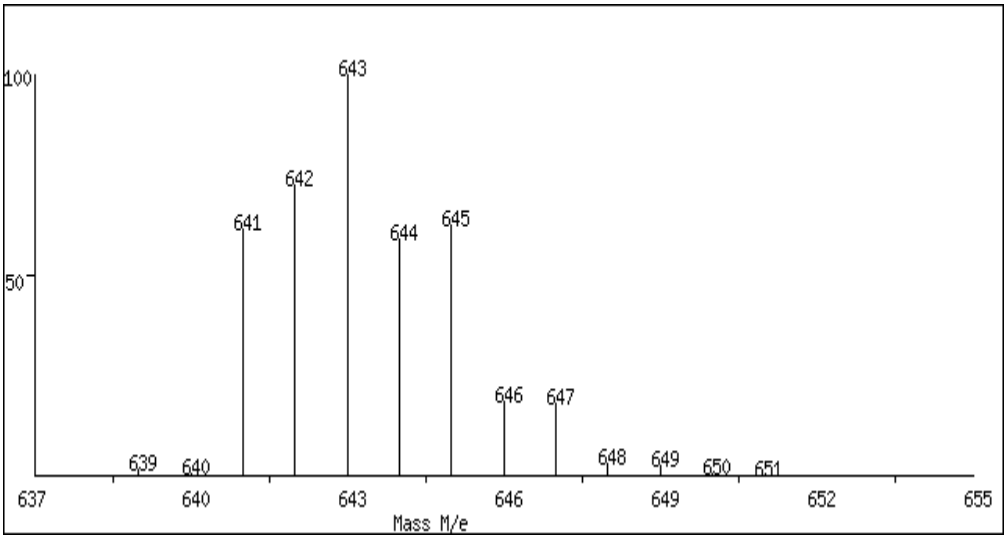

Figure 4.40: MS simulation of the adduct $[M+NO_3]^-$

The observed behavior is justified by the detachment of the amino groups from the NPs surface, due to the hydrolysis of Si-O-Si bonds [9, 10, 11, 12]. This hydrolysis seems to depend on the chain length of the organic linker: APTMS,

in fact, have a primary amine at the end of a propyl chain, which can catalyze the hydrolysis of siloxane bonds both intra- and intermolecularly (*Figure 4.41*). In particular, intramolecular catalysis is achieved via the formation of stable five-membered cyclic intermediates [13], causing the loss of the APS. Moreover, the detachment can be induced by nearby amino groups (intermolecular catalysis) and, for this reason, the loss of not coupled APS arms or **7-APS** may occur: in this latter case, this justifies the observed release in aqueous solution.

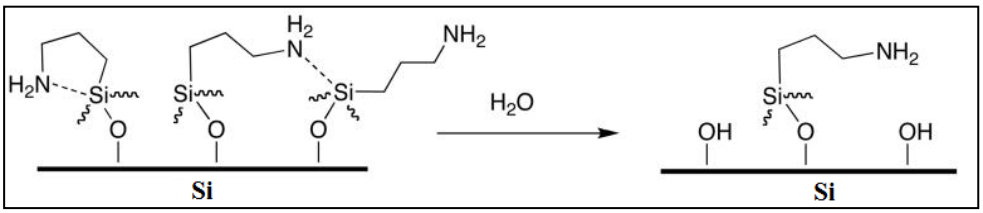

Figure 4.41: Representation of the intra- and intermolecularly catalyzed hydrolysis of siloxane bonds. The picture was slightly modified by literature [13]

The subsequent target was to evaluate the behavior of the conjugates in the presence of reducing agents (such as ascorbic acid, glutathione, etc.): in fact, to the spontaneous detachment, the Pt release due to the so-called "activation by reduction" must be added. In this latter case, however, the released complex should be cisplatin.

4.17 The Mechanism of Action of the Pt(IV) Complexes: the Activation by Reduction

The most accredited intracellular mechanism by which Pt(IV) complexes exert their antitumor effects, as described in *paragraph 2.5*, is the activation by reduction (*Figure 4.42*).

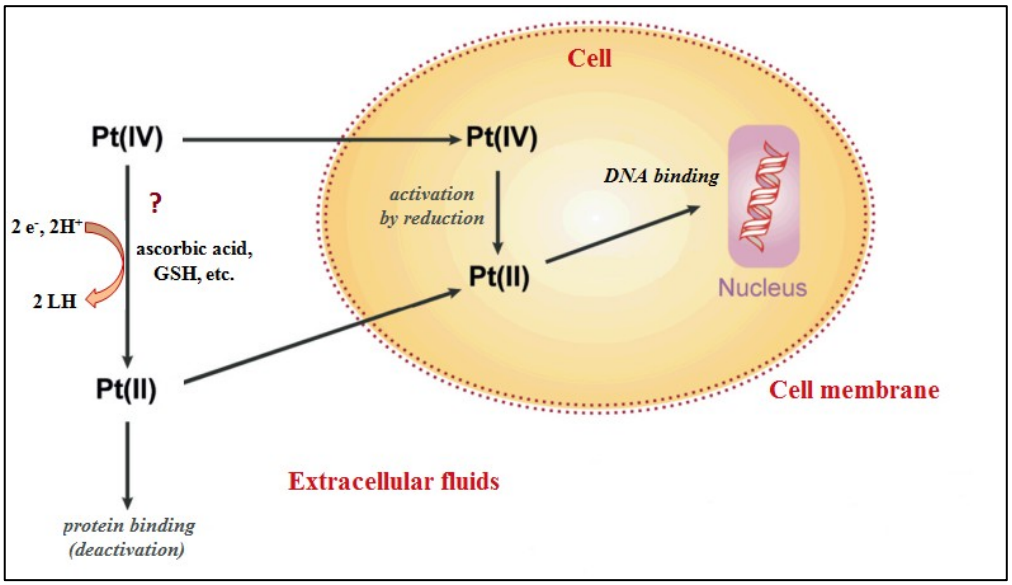

Figure 4.42: Schematic representation of the "activation by reduction". The picture is adapted from literature [14]

The selective reduction can be justified by the fact that the tumor is hypoxic (i.e. oxygen deficient) because of its continuous and uncontrolled growth and, therefore, there is not a sufficient supply of nutrients and the tumor site is more reducing than a healthy one.

Into a neoplastic cell, several reducing agents (which show a higher concentration with respect to extracellular fluids) can activate a Pt(IV) complex and, among them, ascorbic acid and reduced glutathione (GSH) can be mentioned (*Figure 4.43*).

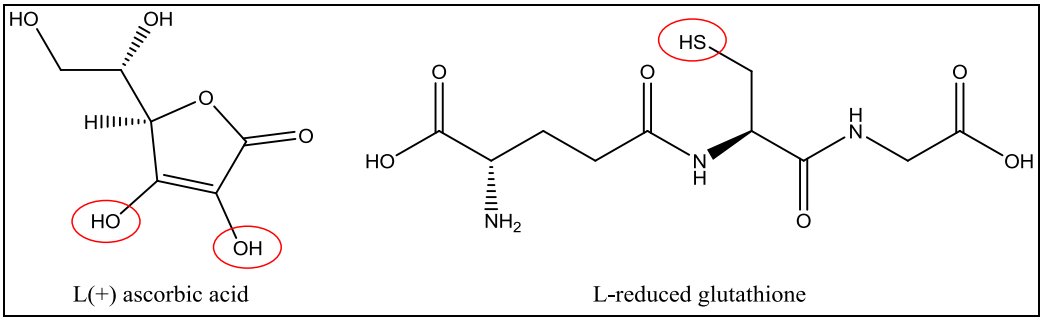

Figure 4.43: Structural formulas of the two main reducing agents present in a tumor cell (i.e. ascorbic acid and GSH). The groups involved in the activation reaction of a Pt(IV) complex are highlighted

The reduction mechanism of Pt(IV) complexes has been the subject of many studies and it is still not completely clear. Both mechanisms of "outer sphere" and "inner sphere" were invoked. In particular, the latter is based on the formation of bonds between an equatorial chloride ligand of the Pt complex and a specific functionality of the reducing agent: -OH for the ascorbic acid and -SH for glutathione (*Figure 4.43*).

Other researchers have proposed a reductive process, divided into two stages: during the first phase a reduction which involves an electron occurs leading to a Pt(III) species and an ascorbate radical, whereas in the second step a further reduction occurs, by using a single electron, to give rise to a Pt(II) compound.

Other studies showed that the Pt(IV) complexes that present equatorial chloride ligands in *trans* each other, by reacting with ascorbic acid, favor the mechanism involving the inner sphere forming Pt(II) compounds in which the chloride ligands have been replaced by those which were previously the axial ligands. The presence of chlorides in *cis* position, however, provides the outer sphere mechanism, with the formation of a product with equatorial chloride ligands [15].

A similar behavior can be observed for GSH.

It is not possible to define a precise mechanism for the reduction of each complex and, for this reason, it is possible only to make assumptions. What is

certain is that, if the reduction process involves the inner sphere, the ease of bonds rupture and formation is essential to allow a reaction to occur and the reagents steric hindrance plays an important role. The reduction potential gives only a thermodynamics information but the reaction kinetics is very important. It was experimentally verified that complexes containing hydroxido or chloride groups are faster reduced than those containing amines and carboxylates. This seems to be related to their ability to form bonds with the reductants. Moreover, when a good leaving ligand is in *trans* position to this "bridge" the reduction is faster.

4.17.1 Study of the Reduction Process of the Synthesized Pt(IV) Complexes

The reduction kinetics was studied for (OC-6-44)-diammine(4-carboxypropanoato)dichloridoethanolatoplatinum(IV) (**7**) and (OC-6-44)-diamminedichloridoethanolato(4-oxo-4-(propylamino)butanoato)platinum(IV) (**9**).

The former is the complex coupled on the NPs, whereas the latter was chosen as a model of the conjugate itself.

Among the possible bioreductants, L(+) ascorbic acid and L-reduced glutathione (GSH) were chosen to perform the reduction studies.

4.17.1.1 Reduction Kinetics of Complex 7

4.17.1.2 Study of the Behavior with L(+) Ascorbic Acid

A 1 mM solution of complex **7**, in a 2 mM aqueous solution of HEPES buffer (pH 7.5), was prepared and then diluted with methanol to obtain a final 0.5 mM Pt concentration.

L(+) ascorbic acid, in a molar ratio 10:1 with respect to **7**, was then added. This addition must be rapid and immediately followed by the HPLC-MS analysis, which allowed to study the reduction process for about 16 hours, with a measurement every 30 minutes, at 37 °C and employing a mobile phase consisting of a 50/50 methanol/15 mM formic acid mixture. The stationary phase was, in this case, a C18 Phenomenex Gemini® column 5 μm, 250 × 3.00 mm ID.

The chromatograms (*Figure 4.44*) show that the reducing agent peak has a retention time of 2.90 minutes and, therefore, does not interfere with the peak of the complex, which has a retention time of 3.78 minutes.

After all the measurements, the chromatograms were analyzed to get the peak area of the complex signal: its decrease over time is indicative of the progressive reduction by ascorbic acid (*Figure 4.44*).

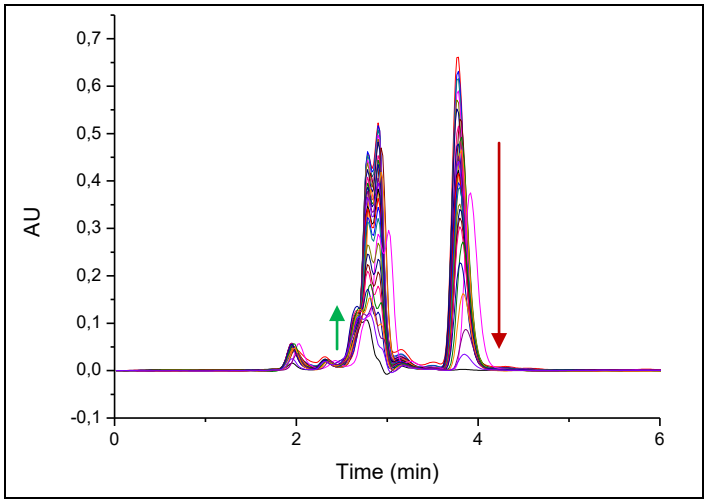

Figure 4.44: Chromatograms of complex **7** in presence of ascorbic acid, registered during the reduction process

In addition, it is possible to observe the increase of an additional peak, near the one of the reducing agent (at 2.67 minutes). By examining the ESI-MS spectra registered during the reduction process, it is possible to observe the formation of a series of reduction products: cisplatin derivatives (all Pt(II) compounds), including some Pt(II) species in which the axial ligands have been coordinated instead of the equatorial ligands, as already reported by Gibson for other complexes [15].

Then the data analysis was carried out, by calculating the normalized areas and the corresponding natural logarithm values for a pseudo-first order kinetic analysis.

The graph reported in *Figure 4.45* shows the natural logarithm of the peak normalized area as a function of time.

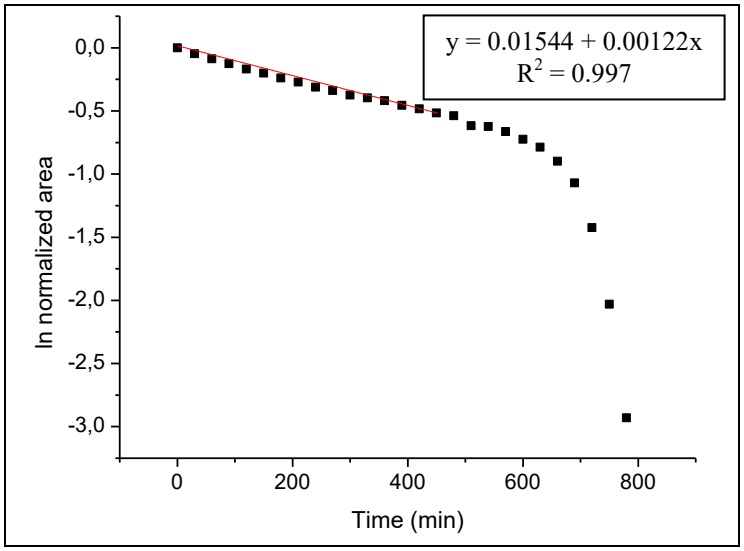

Figure 4.45: Decrease of the chromatographic peak area of **7** during the reduction with ascorbic acid. In particular, the results of one of the three independent replicates are reported

The data were processed with the initial rate method: the first 420 minutes were considered and the values in this range were fitted by a line of generic equation y = A + Bx (in *Figure 4.45*, A = 0.01544 and B = 0.00122), the slope of which represents the kinetic constant, k.

Then it was possible to proceed with the determination of the half-life time t½ by using the following equation:

$$t_{1/2} = \frac{ln2}{k}$$

Three independent samples of the same complex **7** were analyzed in triplicate. After the processing of the results, it was verified that the reduction of complex **7** had an average half-life time of 9.36 (± 0.57) hours.

4.17.1.3 Study of the Behavior with L-Reduced Glutathione (GSH)

The sample of complex **7** was prepared according to the same procedure applied in the case of ascorbic acid (see *paragraph 4.17.1.2*).

The reducing agent was eluted at 3.08 minutes giving no interferences to the complex, which had, instead, a retention time of 3.78 minutes.

The recorded chromatograms (*Figure 4.46*) show that complex **7** was not reduced by GSH: the peak area of the complex signal, in fact, remained unchanged during the analysis time (16 hours). This behavior reflected the one reported by Gibson *et al.* for satraplatin [15].

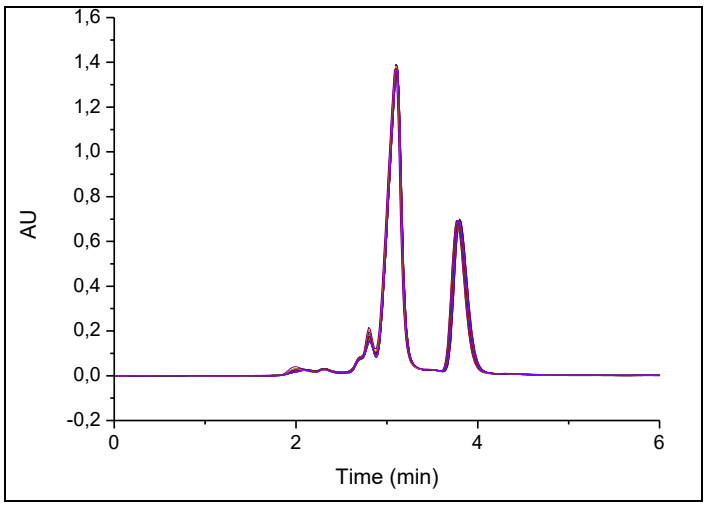

Figure 4.46: Chromatograms of complex **7** in presence of GSH, registered during the reduction process

4.17.2.1 Reduction Kinetics of Complex 9

4.17.2.2 Study of the Behavior with L(+) Ascorbic Acid

Complex **9** was dissolved in methanol in order to prepare a 1 mM solution. Subsequently, this latter was diluted with a 2 mM HEPES buffer aqueous solution (pH 7.5) to obtain a final complex concentration of 0.5 mM. Then L(+) ascorbic acid was added to the mixture, in a 10:1 molar ratio with respect to the Pt(IV) complex.

The reduction process was followed by HPLC-MS, with a measurements every 50 minutes, at 37 °C and by using a mobile phase consisting of a 60:40 methanol/15 mM formic acid mixture. The chromatograms are reported in *Figure 4.47*.

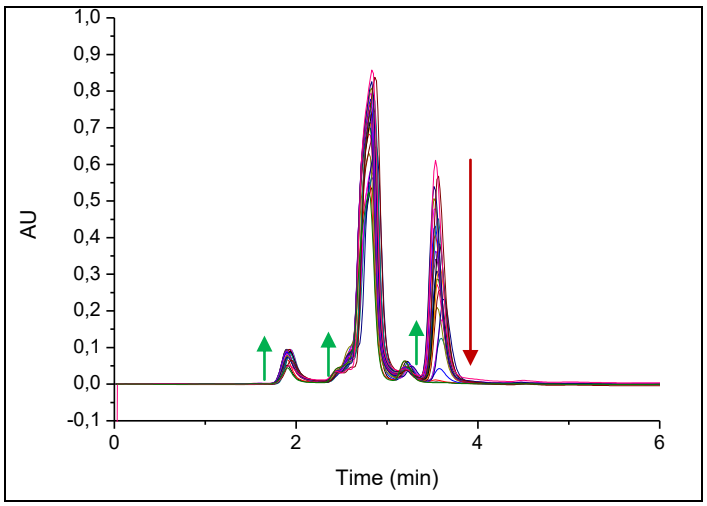

Figure 4.47: Chromatograms of complex **9** in the presence of ascorbic acid

Also in this case, ascorbic acid was found to be a suitable reducing agent: a decrease in the complex signal area (corresponding to a retention time of 3.53 minutes) was observed, whereas no changes were found as regards the peak of ascorbic acid (eluted at 2.83 minutes).

Moreover, it was possible to observe the progressive formation of a new peak at 3.23 minutes, attributed to the axial ligand detached from the complex. At the same time, an increase in intensity (and, therefore, in area) of the signals at 1.92 and 2.45 minutes was verified: it was not possible to make correct attributions for the first species, whereas the second one was identified as the aquated form of cisplatin.

After the complete reduction of the complex, the data (expressed as a mean of three independent analyses) were processed according to the procedure employed for complex **7** (see *paragraph 4.17.1.2*).

Figure 4.48 shows the natural logarithms of the normalized areas in function of time for one of the three replicates, together with the interpolation of the data.

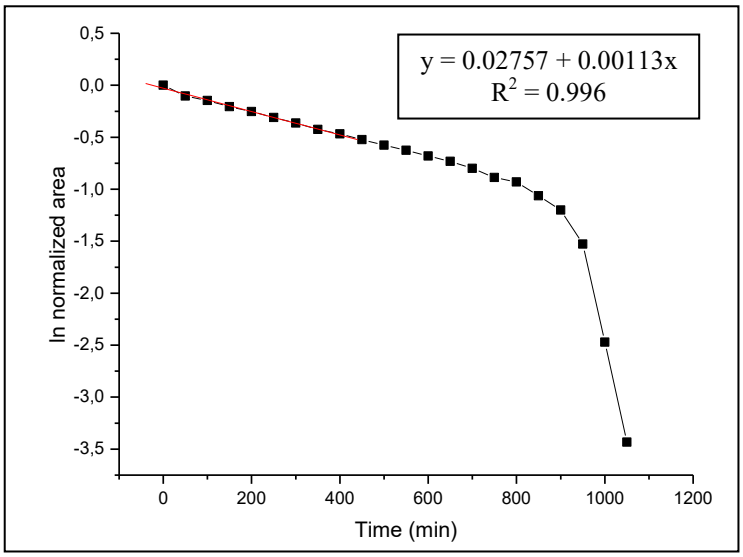

Figure 4.48: Decrease of the peak area of **9** in the presence of ascorbic acid. In particular, the results of one of the three independent replicates are reported

The data processing allowed to determine an average half-life time t½ of 10.38 (± 0.20) hours.

4.17.2.3 Study of the Behavior with L-Reduced Glutathione (GSH)

The activation by reduction of complex **9** with GSH did not occur: in fact, this reducing agent resulted to be ineffective in reducing the Pt(IV) complex, which remained unchanged during the whole analysis time (as well as complex **7**).

4.17.3 Conclusions of the Reduction Kinetics of Pt(IV) Complexes

The studies carried out allow to verify that complexes **7** and **9** are reduced and activated to cisplatin and its derivatives by using ascorbic acid. Reduced glutathione, instead, results to be ineffective and this is consistent with the behavior of other studied Pt(IV) complexes [15]. Over the years, in fact, the reduction processes of numerous symmetrical compounds has been studied but almost all of them did not undergo reduction by GSH. Therefore, the results obtained can be considered useful in confirming this behavior even for this kind of asymmetrical complexes here presented, although it is not possible to say with certainty that this occurs for all the Pt(IV) compounds.
The following target was the evaluation of the Pt release from conjugate **10b** in the presence of reducing agents, in particular ascorbic acid.

4.18 Platinum Release from Conjugates in Reducing Conditions

Conjugate **10b** (2-3 mg) was suspended in 3 mL of ultrapure water in the presence of ascorbic acid (10-fold molar excess respect to the platinum amount). The release test allows to observe that more than 90% of the Pt loaded is released in 24 hours (a time shorter than the one employed in the cellular viability experiments, i.e. 72 hours). Moreover, the ESI-MS analysis allowed to

identify the presence of the aquation products of cisplatin: therefore, in reducing conditions, cisplatin is released from conjugates, thus exploiting the activation by reduction mechanism.

4.19 Biological In Vitro Studies

After the phase of chemical characterization, it was necessary to evaluate the biological behavior in *in vitro* experiments. In particular, it was important to verify their ability in inhibiting cell growth and proliferation, their accumulation into the tumoral cells and their mechanisms of internalization.

4.19.1 The Antiproliferative Activity (IC_{50})

The IC_{50} (Half-Inhibiting Concentration) is a parameter employed for the evaluation of the efficacy of a drug: in particular, it represents the drug concentration able to inhibit the 50% of the tumoral cells growth. In this assay, the cells (seeded in 96-well plates the day before the treatment) are treated with increasing concentrations of the drug and the results are shown in a dose-response graph (*Figure 4.49*), in which the cell viability is reported as a function of the logarithm of the drug concentration and the data are fitted by a sigmoidal curve. The IC_{50} is the concentration at which the 50% of the activity corresponds and the lower the value the more effective the drug (high efficacy is achieved with low drug concentrations).

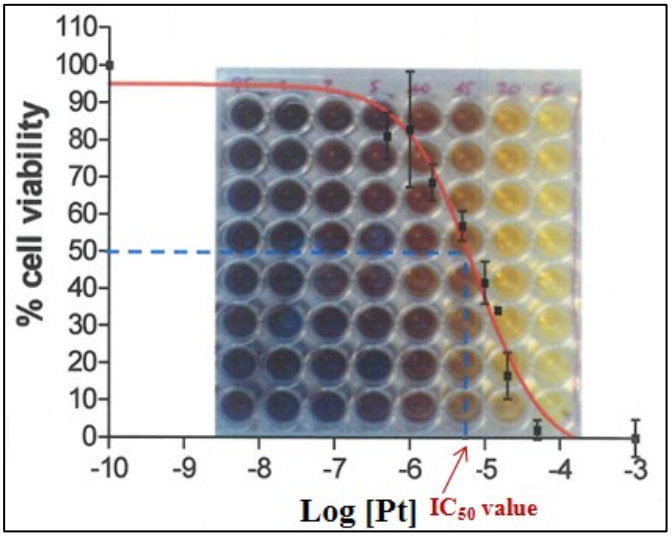

Figure 4.49: Dose-response sigmoid from which the complex IC_{50} value is obtained

In this work, compound **7**, conjugates **10b-10d** and cisplatin (as a comparison) were tested on A2780 human ovarian carcinoma cell line (European Collection of Cell Cultures, UK), which was grown in RPMI 1640 medium (GIBCO, Invitrogen Life Science, San Giuliano Milanese, Italy). This latter was supplemented with L-glutamine (2 mM), penicillin (100 IU/mL), streptomycin (100 mg/L) and 10% fetal bovine serum (FBS).

The samples were prepared as described below: cisplatin was dissolved in 0.9% w/v NaCl aqueous solution brought to pH 3 (by using HCl), obtaining a 1 mM concentration, complex **7** was dissolved in ultrapure water and the concentration was 5 mM, and conjugates **10b-10d** were provided as ethanol suspensions.

In order to evaluate also the antiproliferative activity of the released species **7-APS**, conjugate **10b** was suspended and magnetically stirred for 7 hours (in order to allow a higher complex amount to be released) in 7 mL of RPMI 1640 medium (supplemented with penicillin and streptomycin) at room temperature. The suspension was centrifuged and, after the removal of the NPs pellet, an aliquot of the solution was employed for the viability test, after the

quantification of the Pt content of the released species present in the solution by means of ICP-OES. Before the use, **7-APS** was sterilized by filtration (porosity 0.45 μm).

The treatments were performed at 37 °C in a 5% CO_2 humidified chamber and cells were continuously treated for 72 hours. Then, in order to evaluate the remaining cellular viability, after the treatment with the previously mentioned compounds, the resazurin reduction assay was employed [16]. When a cell damage occurs, the intracellular enzyme Lactate Dehydrogenase (LDH) is rapidly released in the extracellular medium and the cell viability is inversely proportional to the LDH concentration. It can be quantified by means of a coupled enzymatic reaction, which is based on the reduction of the resazurin to the fluorescent resorufin, which emits at 590 nm (*Figure 4.50*), due to the Diaphorase enzyme. The process is accompanied by the oxidation of NADH to NAD^+ and the reduction of pyruvate to lactate.

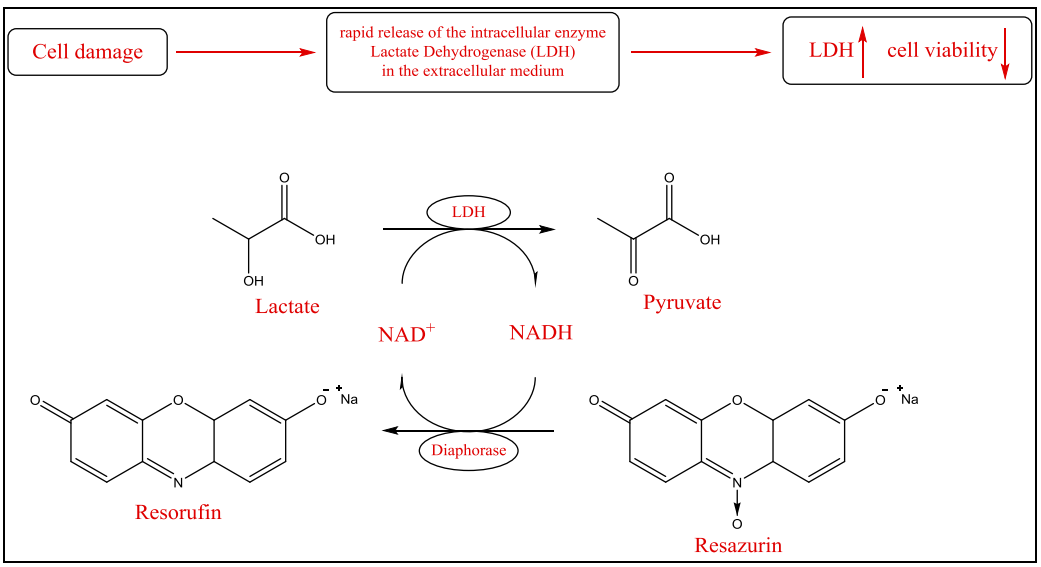

Figure 4.50: Schematic reduction reaction of resazurin in the fluorescent resorufin, which is the assay employed for the measurement of the remaining cell viability. This reaction is accompanied by the reduction of lactate in pyruvate and the oxidation of NADH to NAD^+

In particular, at the end of the treatment, the viability was assayed by 100 μg/mL resazurin in fresh medium for 1 hour at 37 °C: the live cells with an active metabolism are able to reduce resazurin in resorufin and, then, this latter was measured by means of its fluorescence with a Tecan Infinite F200Pro plate reader. Fluorescence (excitation λ at 535 nm, emission λ at 595 nm) is directly proportional to the cell viability.

However, conjugate **10c** contained rhodamine B as fluorophore and, therefore, it could interfere with the resazurin assay results. For this reason, all the IC_{50} values were confirmed with the colorimetric assay based on methylene blue staining [17], which can be quantified by means of absorbance at 620 nm, thus being not affected by the presence of the fluorophore.

Before carrying out the assay, pictures of cells were taken with an inverted microscope Leica DM IL LED, coupled with a camera to observe NPs aggregation.

Each IC_{50} value, derived from the dose-response sigmoids shown in *Figure 4.51*, was obtained as a mean of at least three independent replicates. The data were normalized to 100% of viability for not-treated cells and the fluorescence/absorbance of the medium without cells was used as a blank.

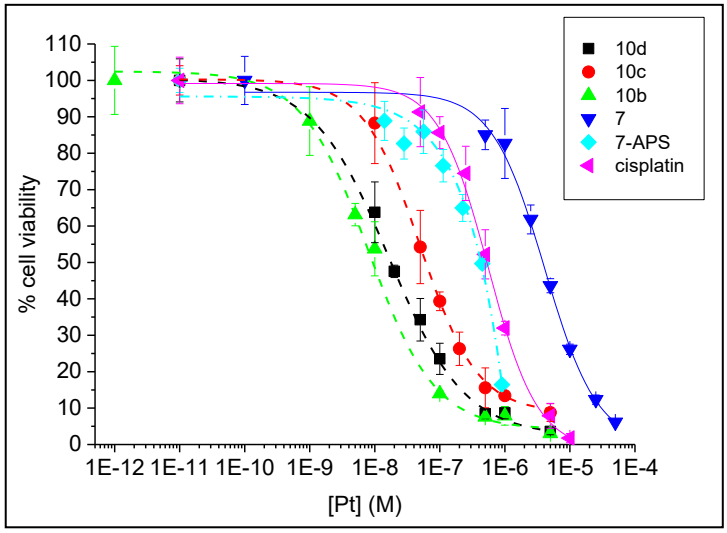

Figure 4.51: Dose-response curves of conjugates **10b-10d**, compared to cisplatin, complex **7** and the released specie **7-APS**. The compounds were tested for 72 hours on A2780 human ovarian carcinoma cell line

The dose-response sigmoid of each sample allows to determine the corresponding IC_{50}; the results are reported in *Table 4.8* and *Figure 4.52*.

Compound	**IC_{50} (nm)**
cisplatin	460 ± 110
7	5070 ± 380
b, c, d	>> 20000
10b	11 ± 3
10c	70 ± 12
10d	40 ± 14
7-APS	960 ± 60

Table 4.8: IC_{50} numerical values of conjugates **10b-10d**, compared to cisplatin, **7**, the released species and free NPs

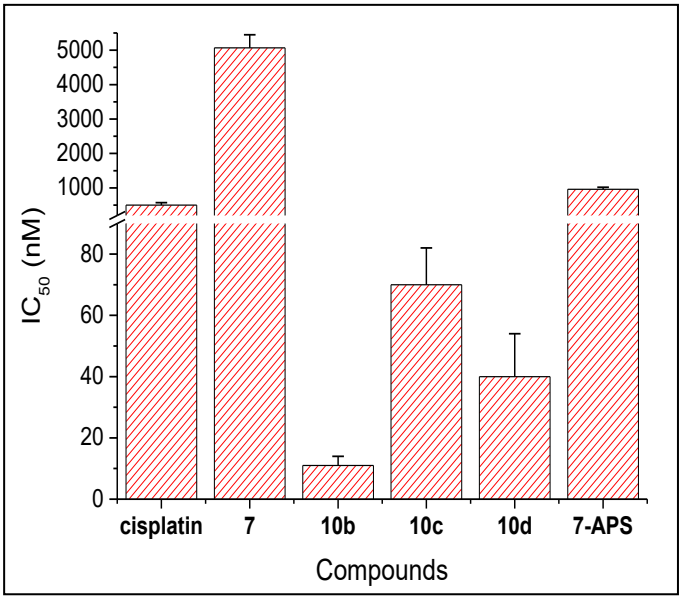

Figure 4.52: Representation by bars graphs of the obtained IC_{50} values

The data indicate that the conjugates, on A2780 cell line, are more effective than cisplatin. A higher efficacy is observed also respect to free complex **7** and, in particular, respect to the free NPs **b-d**, which do not show any activity. An important result is the IC_{50} of **7-APS**: its lower activity with respect to **10b-10d** (about two orders of magnitude) demonstrates that, even though a detachment of the complex from the NPs surface occurred, the activity of free conjugates is, in any case, elevated and thus not dependent on the species released by hydrolysis.

After the determination of the antiproliferative activity, each sample was tested in order to evaluate its accumulation into the cells and, therefore, its ability to cross cell membrane.

4.19.2 The Cellular Accumulation

The cytotoxic activity of a drug results from the combination of several factors, such as its diffusion through the cell membrane, its intracellular accumulation, its activation to obtain the active metabolite and its reactivity towards the DNA. The accumulation into the cells, in particular, can occur by mechanisms of passive diffusion, transport mediated by membrane proteins, endocytosis, etc. and depends on the drug concentration, the treatment time and the cell line.

The so-called accumulation, defined also as uptake or influx and abbreviated as A, represents the amount of drug that, after crossing the cell membrane, accumulates into the cell. This value is normalized upon the cells number (expressed as 10^6 of cells) and depends on the extracellular drug concentration (in fact, it considers the actually intracellular concentration without taking into account the extracellular one): this makes the accumulation a little comparable parameter from a system to another one.

$$A = \frac{ng_{Pt}}{10^6\ of\ cells}$$

A more correct way to indicate an effective accumulation result is to consider the Accumulation Ratio (AR) [18]: this value represents the ratio between the intracellular compound concentration ($[Pt]_{IC}$) and the extracellular one ($[Pt]_{EC}$), i.e. that of the culture medium, and is comparable between different systems, since it does not depend on the initial concentration of the administered drug.

$$AR = \frac{[Pt]_{IC}}{[Pt]_{EC}}$$

In particular, in this work, cisplatin, complex **7**, conjugates **10b**-**10d** and the released species **7-APS** were tested on A2780 human ovarian carcinoma cell line with a 4 hours treatment. The concentrations were 10 μM cisplatin and **7**, 0.1 μM conjugates **10b**-**10d** and the release sample was tenfold diluted in

complete medium. Immediately after the treatment, 100 µL of culture medium were harvested to measure the neat extracellular platinum concentration following adsorption to sterile plasticware. After the treatment, cells were washed three times in phosphate buffer saline (PBS), detached from the 25 cm^2 flasks using 1 mL of 0.05% Trypsin EDTA (HyClone, Thermo Fisher Scientific) and harvested in fresh complete medium. An automatic cell counting device (Countess®, Life Technologies) was used to measure the cells number and the mean diameter from every cell count. About 5×10^6 cells were transferred into a glass tube and spun at 1100 rpm for 5 minutes at room temperature. The supernatant was carefully removed by aspiration and, in order to limit the cellular loss, about 200 µL of the supernatant were left. Cell pellet was stored at -20 °C. After defrosting, 350 µL of 70% w/w HNO_3 were added and left 1 hour at 60 °C in an ultrasonic bath. Then the sample was diluted with a 1% aqueous solution of HNO_3 (by adding 5650 µL) to a final 3% of acid concentration and the platinum content was quantified by means of ICP-MS.

The ICP-MS results were expressed as µg/L (ppb) of Pt and, then, they were divided by Pt atomic weight (195 u) to determine the Pt concentration (µM) of that sample. The intracellular platinum quantity, even though Pt(IV) complexes undergo reduction and aquation processes, corresponds to the initially entered drug amount.

The data processing, after the normalization of the Pt amount found into the cells upon the cells number and volume (calculated from the actual mean cell diameter measured for every sample) allowed to obtain the intracellular platinum concentration. The ratio between the intra- and extracellular concentration of Pt allowed to obtain the AR value of each studied sample. The obtained AR data are shown in *Table 4.9* and as *Figure 4.53*.

Compound	AR
cisplatin	1.39 ± 0.52
7	0.38 ± 0.09
10b	64.56 ± 19.02
10c	76.07 ± 12.94
10d	41.28 ± 10.08
7-APS	0.60 ± 0.20

Table 4.9: AR data for conjugates **10b-10d**, compared with cisplatin, **7** and the released species

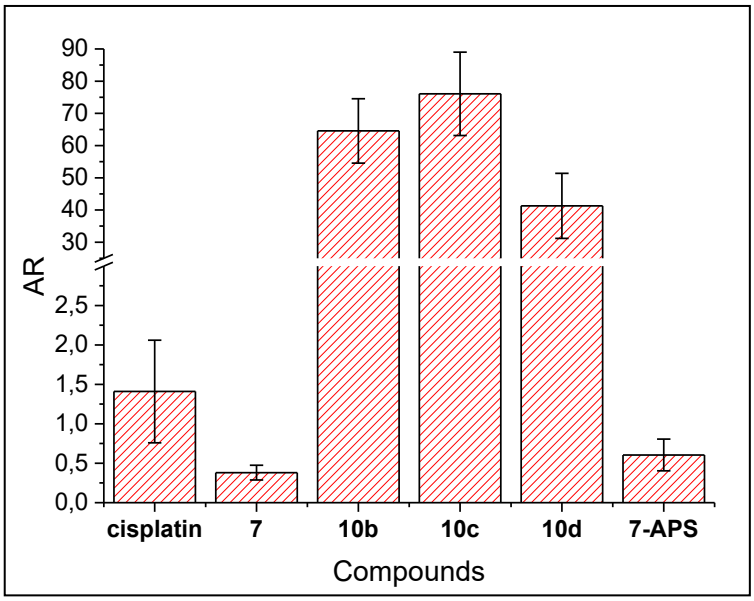

Figure 4.53: Bars graphs of the AR data

The results indicate that the conjugates present high accumulation ratio values (higher than cisplatin, complex **7** and the released species **7-APS** of more than one order of magnitude). These results demonstrate that there is a correlation between IC_{50} and AR: conjugates **10b-10d** show a high antiproliferative activity

due to the fact that they enter cells in large quantity and accumulate inside them, allowing the drug to exert its cytotoxic activity.

4.19.3 Confocal Microscopy

The effective cellular accumulation can be verified by the use of the Confocal Microscopy (*Figure 4.54*). This technique is based on the fact that the resulting picture and the observed object have the same focal plane: in fact, it is able to filter out the out-of-focus light by the employment of two pinholes, spatially located immediately after the source of light and immediately before the detector. This results in an improvement in the image resolution because the confocal microscope removes the light above and below the focal plane (unlike Fluorescence Microscopy), allowing to obtain an in focus image.

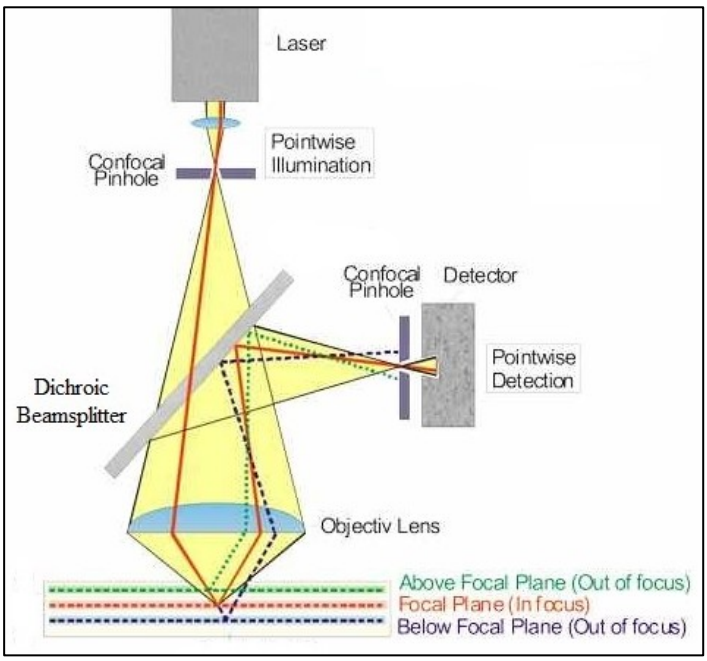

Figure 4.54: Scheme of a confocal microscope [19]

In the specific case of NPs, this technique allowed to focus on the nanoparticles accumulated into the cells, by employing appropriate filters: in particular, excitation λ at 488 nm and emission λ at 505-550 nm for fluorescein (*Figures 4.55, 4.56, 4.59, 4.60*), and excitation λ at 550 nm and emission λ at 570 nm for rhodamine B (*Figures 4.57* and *4.58*).

The instrument employed was a Zeiss LSM 510 confocal system, Carl Zeiss Microscopy GmbH, Germany.

In particular, the day before the tests, the A2780 cells were seeded in 4 wells-chambered slides (Nunc™ Lab-Tek™ II Chamber Slide™ System, Thermo Fisher Scientific). They were treated with free NPs **b**-**d** and the corresponding conjugates (**10b**-**10d**) for 4 hours (by employing the same treatment protocol described for AR experiments). The cells were then washed with phosphate-buffered saline (PBS), rinsed in Ringer's solution (140 mM NaCl, 5 mM KCl, 2 mM $CaCl_2$, 1 mM $MgCl_2$, 10 mM HEPES, 5.2 mM sucrose, pH = 7.4), and fixed 30 minutes at 4 °C in fixing solution (3% w/v paraformaldehyde in PBS, pH = 7.5) for the confocal analyses.

For each sample, the pictures of the fluorescent channel (top, left), the contrast phase image (top, right) and the merged one (bottom) of the same microscope field at 20× magnification are reported (*Figures 4.55-4.60*). The results showed the efficacy of the NPs as vectors that were internalized by the cells.

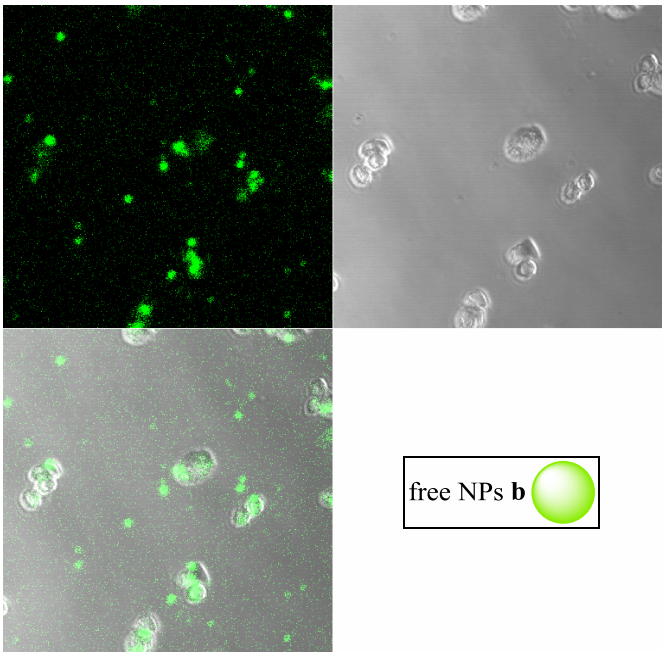

Figure 4.55: Confocal microscopy images for free NPs **b**

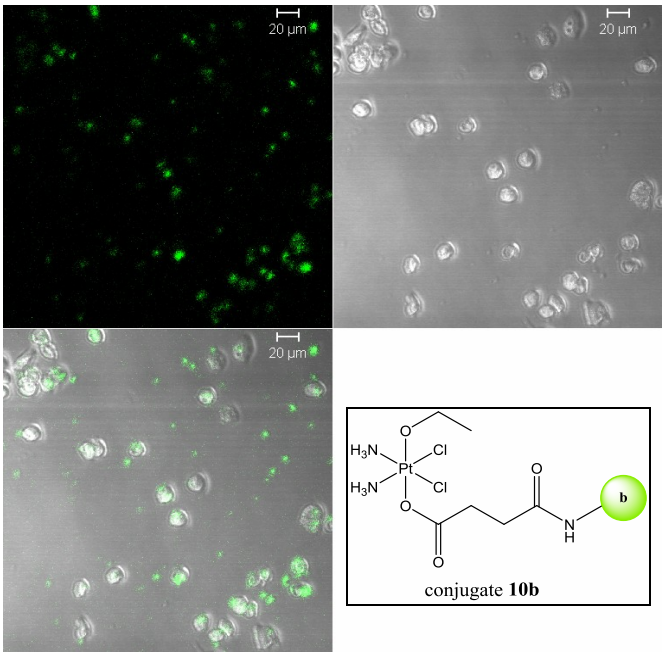

Figure 4.56: Confocal microscopy images for conjugate **10b**

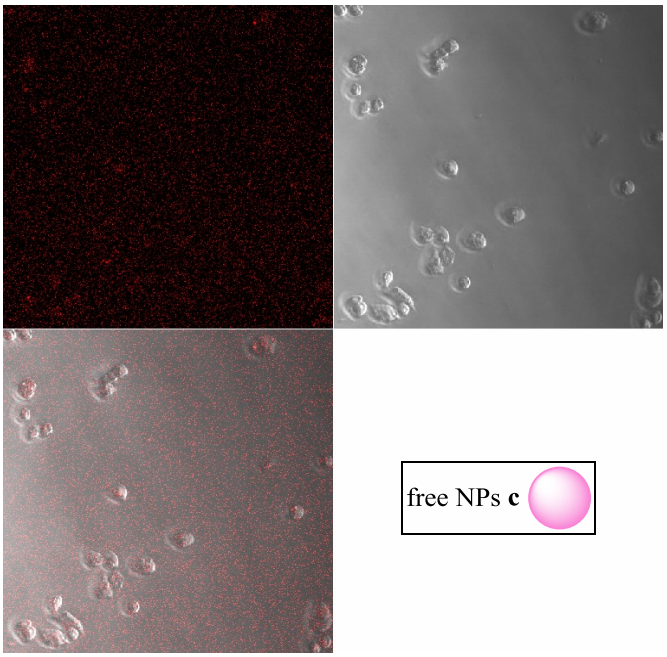

Figure 4.57: Confocal microscopy images for free NPs **c**

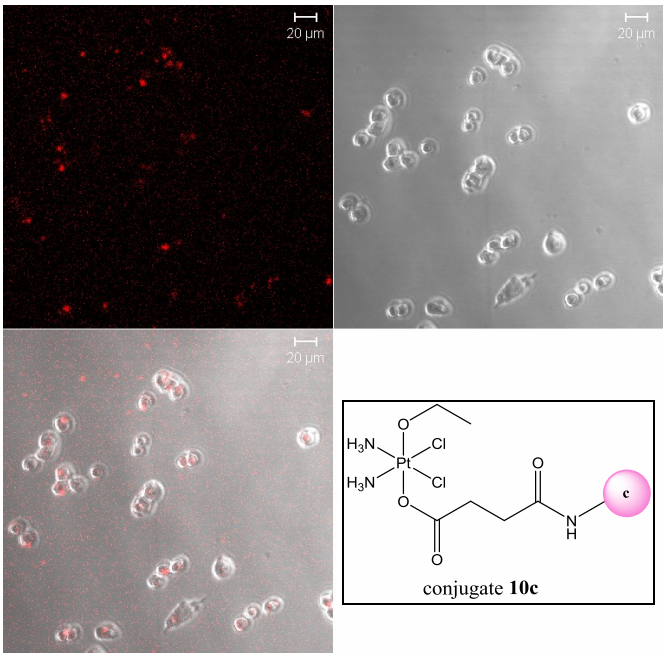

Figure 4.58: Confocal microscopy images for conjugate **10c**

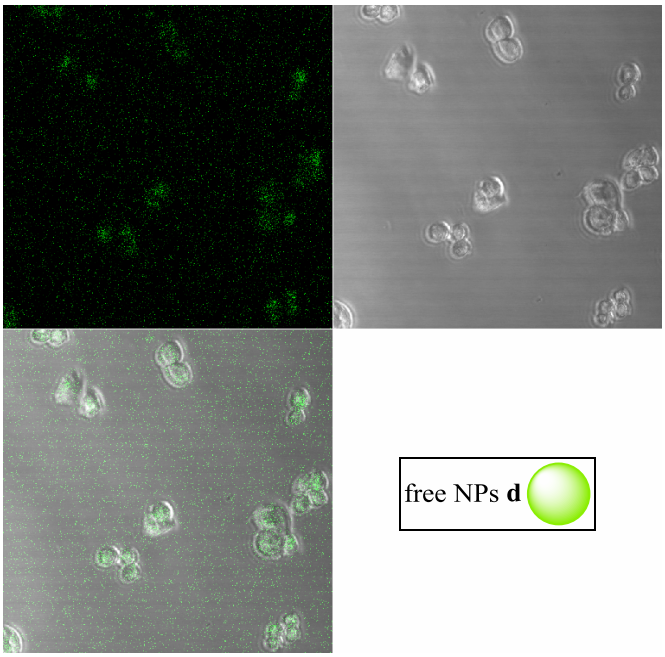

Figure 4.59: Confocal microscopy images for free NPs **d**

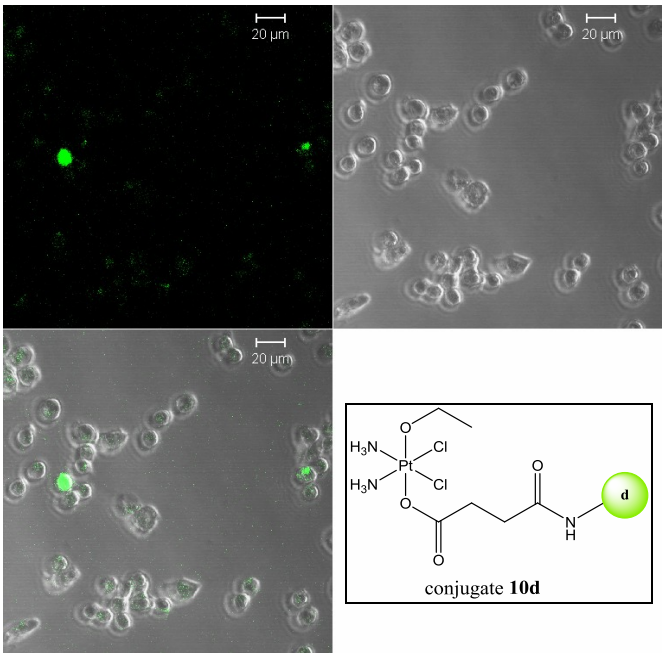

Figure 4.60: Confocal microscopy images for conjugate **10d**

4.19.4 Studies on the NPs Internalization Mechanisms

The endocytosis is a mechanism of active transport that allows macromolecules to enter cells. In particular, a substance is wound through a portion of the cell plasmatic membrane, which invaginates inside the cell and then is detached giving rise to an endocytic vesicle containing the species.
Since this is an active mechanism, the cell requires energy to maintain it. For this reason, the endocytosis is inhibited by low temperatures (4 °C) and by agents that block the cell metabolism (such as sodium azide). This latter decouples the cell respiration and, therefore, depletes the cellular ATP. Usually the electron flow in the transport chain to reach the final acceptor (that is the oxygen) is closely related to the phosphorylation of ADP in ATP. NaN_3 is able to inhibit the electron transport chain, since it reacts with the ferric form of heme group and, thus, leads to the inhibition of the ATP synthesis, because the proton-motive force can no longer be generated [20].

In order to verify if an inhibition of the NPs internalization occurred at 4 °C, some experiments were performed at this temperature. The results were the same obtained for the control cells, suggesting that an active transport mechanism is involved; this was confirmed by the use of sodium azide (*Figure 4.61*).

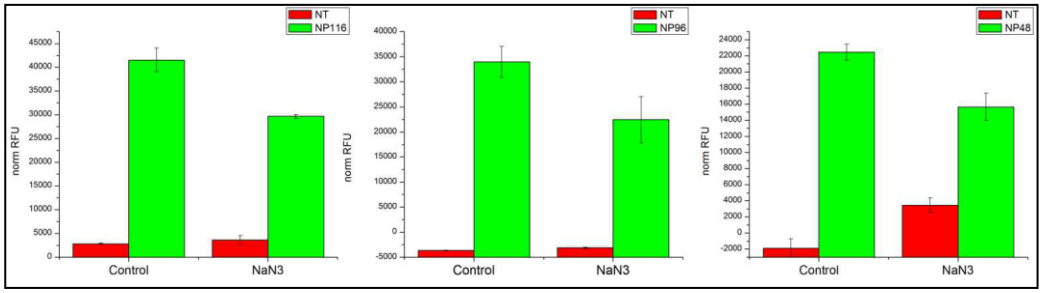

Figure 4.61: Study of the inhibition of the NPs active transport mechanism, in the presence of NaN_3.
norm RFU = fluorescence normalized to the viability, *control NP* = cells not treated with NaN_3, *NT* = cells not treated with both NPs and NaN_3

The endocytosis mechanisms (*Figure 4.62*) can be classified in: proper endocytosis, performed by all the cells, which consists of the ingestion of fluid or solid materials of small size, and phatocytosis, i.e. the ingestion of big particles, carried out by professional phagocytes (such as neutrophils, eosinophils, etc.) or rarely by optional phagocytic cells (fibroblasts, endothelial cells, etc.).

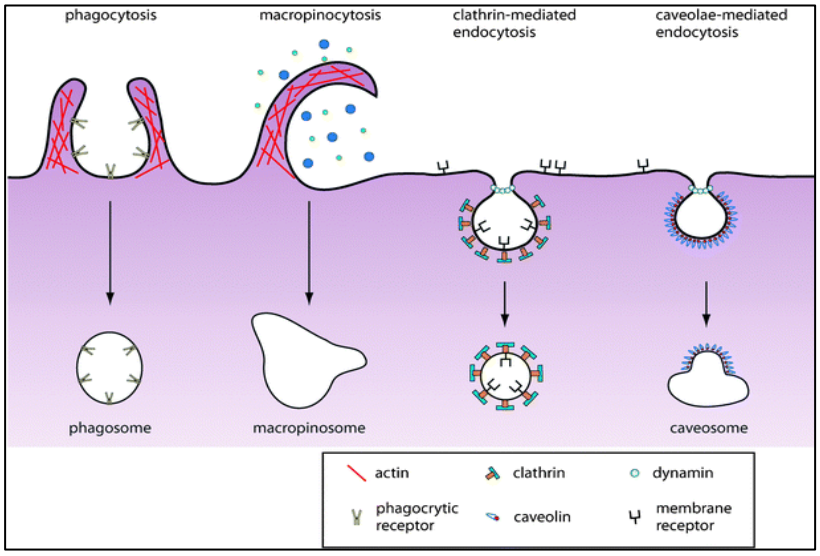

Figure 4.62: Possible mechanisms of endocytosis [21]

The proper endocytosis, depending on the mechanism with which the endocytic vesicle are formed, can be distinguished in macropinocytosis, clathrin- or caveolae-mediated endocytosis.

The macropinocytosis begins with the formation of extended protrusions of the plasma membrane, sustained by actin cytoskeletal elements. These protrusions are then merged with the membrane itself to form large endocytic vesicles containing extracellular material.

The clathrin-mediated endocytosis is a highly selective process that begins with the recognition between ligands and specific plasma membrane receptors, followed by the accumulation of ligand-receptor adduct in specific points of the membrane, known as clathrin coated pits. The formation of clathrin coated endocytic vesicle is mediated by actin cytoskeletal elements. The just formed vesicle loses the clathrin coating and the not-coated vesicle will subsequently merge with an endosome to form a premature endosome.

Another mechanism based on the formation of endocytotic vesicles is the caveolae-mediated one. The caveolae are formed in those areas of the membrane constituted by the so-called "lipid rafts", which are areas rich in cholesterol, glycosphingolipids and membrane proteins.

In order to verify the mechanism responsible for the internalization of the studied vectors, species able to inhibit these specific mechanisms are employed: a decrease of the biological response (and, therefore, of the internalized vector amount) indicates that the inhibitor fulfills its role and that this particular endocytic process is involved.

One of the macropinocytosis inhibitors is amiloride: it inhibits the reabsorption of sodium through the sodium channels (sodium-hydrogen antiporter or exchanger). The mechanism by which it inhibits macropinocytosis is unknown [22].

The mechanism mediated by clathrin is inhibited by various species, among which chlorpromazine [23], the mechanism of action of which is not yet clear.
As regards the endocytosis mediated by caveolae, genistein can be mentioned. It is an inhibitor of the receptor associated tyrosine kinases, proteins involved in the "lipid raft" structure. Moreover, in previous studies on A549 human lung carcinoma cell line, genistein was effective in inhibiting the endocytosis of 200 nm size NPs, with a 50% decrease of uptake with respect to control cells [23].

In order to verify the mechanisms of endocytosis (phagocytosis, macropinocytosis, clathrin-dependent endocytosis, caveolae-mediated endocytosis, etc.) involved in the internalization of the studied NPs, specific inhibitors of the various endocytosis mechanisms were employed. Only the free NPs were tested but the same behavior was expected for the conjugates.
For this purpose, another cell line (A549, human lung carcinoma) was employed because A2780 cells showed problems during their use. In particular, after being washed with PBS, the number of A2780 cells was markedly lower than the number of initially treated cells: in fact, PBS (without Ca^{2+} and Mg^{2+} ions) caused a massive cellular detachment from the plastics support. For this reason, it was initially substituted by the buffer EBSS (Earle's Balanced Salt Solution, a saline solution of glucose and sodium bicarbonate containing calcium and magnesium cations, which are crucial for cellular adhesion) resulting in a decreased but still significant detachment of the cells. On the contrary, A549 cells were less affected by the washing step and, therefore, were chosen for the following experiments. In particular, the cells were treated with 100 µL of a 50 µg/mL suspension of NPs and the experiments were carried out for 4 hours at 37 °C in the presence of chlorpromazine (CPZ), genistein (G) or amiloride (AM), as endocytosis inhibitors. After the established 4 hours, each well was washed with 100 µL of EBSS in order to remove the NPs excess. Furthermore, Trypan

Blue was added to switch off the fluorescent signal of the NPs remained on the cells surface. Then, a microplate reader allowed to observe the results (*Figure 4.63*).

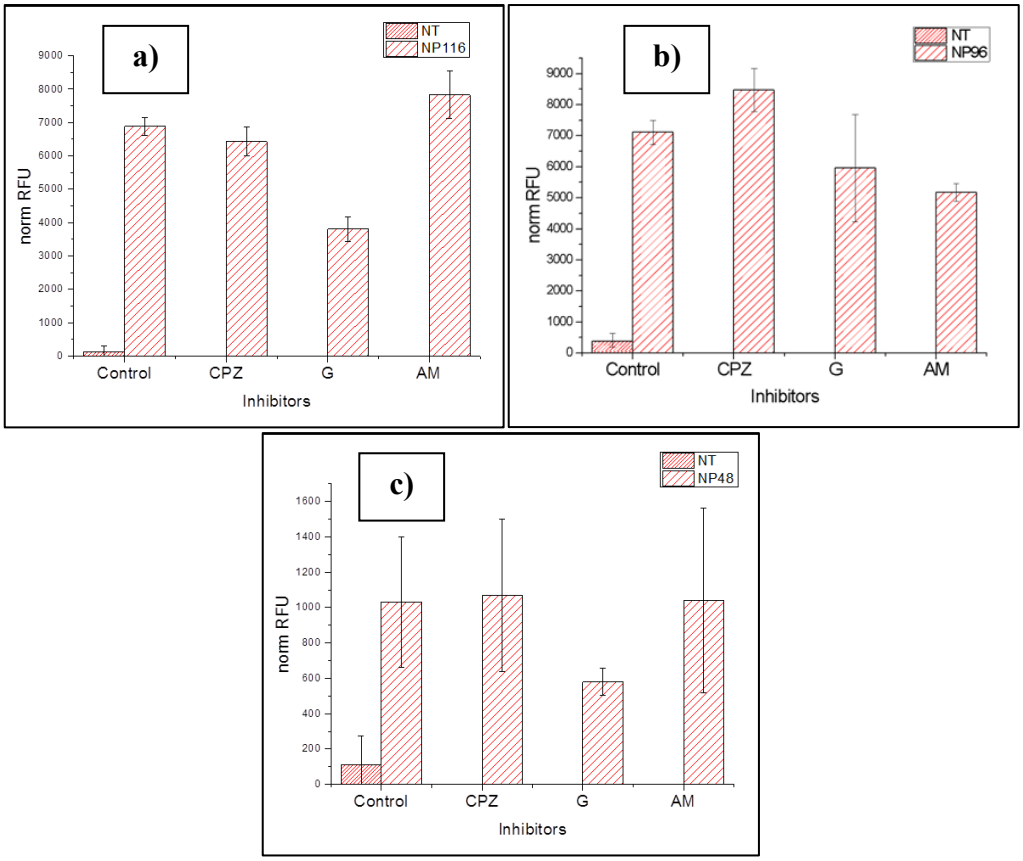

Figure 4.63: a) Uptake of NPs **b** (116 nm), b) NPs **c** (96 nm) and c) NPs **d** (48 nm), in the presence of inhibitors.
norm RFU = fluorescence normalized to the viability, *control NP* = cells not treated with inhibitors, *NT* = cells not treated with both NPs and inhibitors

The bars graphs in *Figures 4.63a* and 4.*63c* show that NPs **b** and **d** are internalized into the cells mostly by caveolae-mediated endocytosis: in fact, the genistein is the most effective inhibitor. The NPs **c** (*Figure 4.63b*), instead, give no clear results: amiloride seems to be the most effective but genistein result is

not much different from amiloride. Therefore, NPs **c** are probably internalized by both macropinocytosis and caveolae-mediated endocytosis.

4.20 Conclusions

In this chapter, two different Pt(IV) complexes, containing one (**7**) or two (**2**) free carboxylic groups, were synthesized, activated and coupled to amino-functionalized fluorescent silica NPs of different sizes (**a**-**d**). Conjugates **5a**-**5d** showed irreversible aggregation, due to the formation of cross-links between nearby NPs. On the contrary, stable suspensions of conjugates **10a**-**10d** were obtained: this aspect confirmed that the use of monofunctionalizable Pt(IV) compounds avoids the formation of large aggregates.

The release studies in aqueous solutions allowed to observe the spontaneous detachment of the complex bound to the aminopropylsilane (**7-APS**), due to the hydrolysis of the Si-O bond on the NPs surface: this can represent a decrease of the therapeutic potential of the conjugate because of an aspecific loss before the drug arrival to the cells. However, the released amount resulted to be about the 15% within 4 hours: therefore, in the case of *in vivo* tests, the detachment in the extracellular fluids should be limited. Then, once inside the cells, the activation by reduction can occur, due to the presence of reducing agents, and the active species, i.e. cisplatin, can be released (as suggested by the release tests of conjugate **10b** in reducing conditions).

Furthermore, conjugates **10b**-**10d** were tested on A2780 human ovarian carcinoma cell line in order to evaluate their antiproliferative activity, which resulted to be higher than that of cisplatin, **7**, free NPs and **7-APS**. This increased efficacy was ascribed to the high cellular accumulation of the conjugates, verified by means of ICP-MS measurements of the Pt uptake and observed by confocal microscopy. Moreover, the mechanism of internalization

was evaluated by means of the use of specific inhibitors, which allowed to verify that caveolae-mediated endocytosis was the main mechanism involved.

References

[1] T. Yu, A. Malugin, H. Ghandehari, Impact of Silica Nanoparticle Design on Cellular Toxicity and Hemolytic Activity, *ACS Nano*, 5 (2011), 5717-5728.

[2] H. Giesche, Synthesis of monodispersed silica powders I. Particle properties and reaction kinetics, *J. Eur. Ceram. Soc.*, 14 (1994) 189-204.

[3] W. Stöber, A. Fink, E. Bohn, Controlled growth of monodisperse silica spheres in the micron size range, *J. Colloid Interface Sci.*, 26 (1968) 62–69.

[4] D. Grojo, L. Boarino, N. De Leo, R. Rocci, G. Panzarasa, P. Delaporte, M. Laus, K. Sparnacci, Size scaling of mesoporous silica membranes produced by nanosphere mediated laser ablation, *Nanotechnology*, 23 (2012).

[5] M. Ravera, E. Perin, E. Gabano, I. Zanellato, G. Panzarasa, K. Sparnacci, M. Laus, D. Osella, Functional fluorescent nonporous silica nanoparticles as carrier for Pt(IV) anticancer prodrugs, *J. Inorg. Biochem.*, 151 (2015) 132-142.

[6] R. H. Müller, Zetapotential und Partikelladung in der Laborpraxis – Einführung in die Theorie, praktische Meßdurchführung, Dateninterpretation, Wissenschaftliche Verlagsgesellschaft Stuttgart, 254 S., 1996.

[7] S. C. Dhara, *Indian J. Chem.*, 8 (1970), 193-194.

[8] R.P. Feazell, N. Nakayama-Ratchford, H. Dai, S.J. Lippard, Soluble Single-Walled Carbon Nanotubes as Longboat Delivery Systems for Platinum(IV) Anticancer Drug Design, *J. Am. Chem. Soc.*, 129 (2007), 8438–8439.

[9] M. Etienne, A. Walcarius, Analytical Investigation of the Chemical Reactivity and Stability of Aminopropyl-Grafted Silica in Aqueous Medium, *Talanta*, 59 (2003), 1173-1188.

[10] E. A. Smith, W. Chen, How to prevent the loss of surface functionality derived from aminosilanes, *Langmuir*, 24 (2008), 12405-12409.

[11] C. Graf, Q, Gao, I. Schütz, C. N. Noufele, W. T. Ruan, U. Posselt, E. Korotianskiy, D. Nordmeyer, F. Rancan, S, Hadam, A. Vogt, J. Lademann, V. Haucke, E. Rühl, Surface functionalization of silica nanoparticles supports colloidal stability in physiological media and facilitates internalization in cells, *Langmuir*, 28 (2012), 7598-7613.

[12] F. Rancan, Q. Gao, C. Graf, S. Troppens, S. Hadam, S. Hackbarth, C. Kembuan, U. Blume-Peytavi, E. Rühl, J. Lademann, A. Vogt, Skin penetration and cellular uptake of amorphous silica nanoparticles with variable size, surface functionalization, and colloidal stability, *ACS Nano*, 6 (2012), 6829-6842.

[13] M. Zhu, M.Z. Lerum, W. Chen, How To Prepare Reproducible, Homogeneous, and Hydrolytically Stable Aminosilane-Derived Layers on Silica, *Langmuir*, 28 (2012) 416–423.

[14] N. Graf, S. J. Lippard, Redox activation of metal-based prodrugs as a strategy for drug delivery, *Adv. Drug Deliv. Rev.*, 64 (2012), 993–1004.

[15] E. Wexselblatt, D. Gibson, What do we know about the reduction of Pt(IV) pro-drugs?, *J. Inorg. Biochem.*, 117 (2012), 220-229.

[16] E. Magnani, E. Bettini, Resazurin detection of energy metabolism changes in serum-starved PC12 cells and of neuroprotective agent effect, *Brain Res. Protocol.*, 5 (2000), 266–272.

[17] M. H. Oliver, N. K. Harrison, J. E. Bishop, P. J. Cole, G. J. Laurent, A rapid and convenient assay for counting cells cultured in microwell plates: application for assessment of growth factors, *J. Cell Sci.*, 92 (1989) 513-518.

[18] A. Ghezzi, M. Aceto, C. Cassino, E. Gabano, D. Osella, Uptake of antitumor platinum(II)-complexes by cancer cells, assayed by inductively coupled plasma mass spectrometry (ICP-MS), *J. Inorg. Biochem.*, 98 (2004), 73–78.

[19] Withfriendship.com website, confocal microscopy.

[20] F. Palmieri, M. Klingenberg, Inhibition of respiration under the control of azide uptake by mitochondria, *Eur. J. Biochem.*, 1 (1967) 439–446).

[21] L. Y. T. Chou, K. Ming, W. C. W. Chan, Strategies for the intracellular delivery of nanoparticles, *Chem. Soc. Rev.*, 40 (2011), 233–245.

[22] M. Koivusalo, C. Welch, H. Hayashi, C. C. Scott, M. Kim, T. Alexander, N. Touret, K. M. Hahn, S. Grinstein, Amiloride inhibits macropinocytosis by lowering submembranous pH and preventing Rac1 and Cdc42 signaling, *J. Cell Biol.*, 188 (2010), 547-563.

[23] T. dos Santos, J. Varela, I. Lynch, A. Salvati, K. A. Dawson, Effects of Transport Inhibitors on the Cellular Uptake of Carboxylated Polystyrene Nanoparticles in Different Cell Lines, *PLoS One*, 6 (2011), e24438, 1-10.

Chapter V

Synthesis, Characterization of Platinum Complexes and Coupling Reactions with New Amino-Functionalized Silica Nanoparticles

5.1 Introduction

The NPs described in *Chapter IV* were decorated with a prone-to-hydrolysis amino arm and this caused a partial loss of the loaded complex. Therefore, in order to avoid this detachment, new types of silica nanoparticles were prepared. At first, NPs similar to the previous ones (i.e. the same amino arm was exposed) were synthesized but their structure did not include any fluorophore, in order to verify if, even in the absence of the fluorescent dye, the Si-O-Si bonds hydrolysis may occur. Then, another type of NPs was prepared: also in this case, the structure did not include any fluorophore and, moreover, a new amino arm decorated the surface of the nanoparticles. In fact, in this case, the *N*-(6-aminohexyl)aminomethyltriethoxysilane (AHAMTES) was employed since it was reported that its use allowed to obtain hydrolytically stable amino-functionalized silica substrates [1].

The (3-aminopropyl)trimethoxysilane (APTMS) and (3-aminopropyl)triethoxysilane (APTES) have a primary amino group in the propyl position and it can catalyze the formation and hydrolysis of siloxane bonds both intra- and intermolecularly (as described in *paragraph 3.16*). In particular, intramolecular catalysis is achieved via the formation of stable five-membered cyclic intermediates (or a six-membered cyclic intermediate in the case of amine in butyl position). The same behavior can be observed with species containing a secondary amino group in propyl/butyl position but not with AHAMTES [1].

The hydrolytic stability derived from the use of AHAMTES indicates that the intramolecularly catalyzed detachment can be minimized by controlling the length of the alkyl linker in aminosilanes [2].

Based on the results reported in *Chapter IV*, the two mentioned types of NPs were coupled only to mono-functionalizable complexes to avoid the formation of irreversible aggregates [3]. For this reason, the NPs were coupled to the

activated *N*-hydroxysuccinimidyl ester of (OC-6-44)-diammine(4-carboxypropanoato)dichloridoethanolatoplatinum(IV) (**8**), in order to study the behavior with these NPs types and to make a comparison with the conjugates described in *Chapter IV*, and to the activated *N*-hydroxysuccinimidyl ester of (OC-6-44)-(acetylamido-*N*)diammine(4-carboxypropanoato)dichloridoplatinum (IV). Its precursor, the (OC-6-44)-(acetylamido-*N*)diamminedichloridohydroxidoplatinum(IV), represents the only case in which a *N*-donor ligand is directly coordinated to the platinum core during the oxidation process. Other Pt(IV) compounds contain coordinated nitriles (therefore, a *N*-donor ligand), such as the iminol- or imino ester-Pt(IV) series, but in equatorial position [4, 5].

For the synthesis of (OC-6-44)-(acetylamido-*N*)diamminedichloridohydroxidoplatinum(IV), the Radziszewski reaction between acetonitrile and hydrogen peroxide was exploited: in fact, it proceeds through the formation of the highly reactive intermediate peroxyacetimidic acid (PAIA) [6, 7, 8]. Its subsequent reaction with cisplatin allows to obtain a Pt(IV) compound, whose axial ligands are provided by PAIA itself. In particular, the acetylamido represents the inert functionality, whereas the hydroxido can react with succinic anhydride in order to introduce a further functionalizable group.

The synthesized Pt(IV) complexes are listed in order of discussion:

- (OC-6-44)-(acetylamido-*N*)diamminedichloridohydroxidoplatinum(IV) (**11**),
- (OC-6-44)-(acetylamido-*N*)diammine(4-carboxypropanoato)dichlorido platinum(IV) (**12**),
- Activated *N*-hydroxysuccinimidyl ester of **12** (**13**).

5.2 Synthesis of (OC-6-44)-(acetylamido-N)diamminedichloridohydroxidoplatinum(IV) (11)

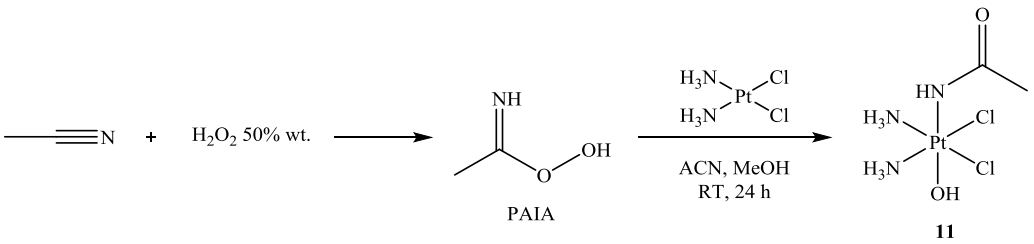

The employed synthetic procedure was reported in the literature [9]. In particular, a mixture of acetonitrile (ACN, 10 mL) and a 50% w/w aqueous solution of hydrogen peroxide (1 mL) was stirred at room temperature for 30 minutes. Then cisplatin (100 mg, 0.333 mmol) was added and the resulting suspension was stirred for 5 minutes. Methanol (5 mL) was added and the reaction was carried out at room temperature for 24 hours. The resulting pale yellow solid was separated by centrifugation, washed with acetonitrile and dried *in vacuo*.

Yield: 95.0 mg, 0.253 mmol, 76.0%.

Elemental analysis calculated for $C_2H_{11}Cl_2N_3O_2Pt$: C 6.40, H 2.96, N 11.20. Found: C 6.20, H 2.71, N 10.98.

5.2.1 Characterization of the Complex

RP-HPLC-ESI-MS

The analysis was performed by employing a stationary phase consisting of a C18 Phenosphere-NEXT column 5 µm, 250 × 4.60 mm ID, a mobile phase composed by a 90:10 mixture of a 15 mM aqueous solution of formic acid and pure methanol (by isocratic elution), a flow rate of 0.500 mL/min, a temperature

of 37 °C and the UV-Visible detector set at 210 nm. Compound **11** showed a retention time of 4.77 minutes and its identity was attributed by the corresponding ESI-MS spectrum (*Figure 5.1*).

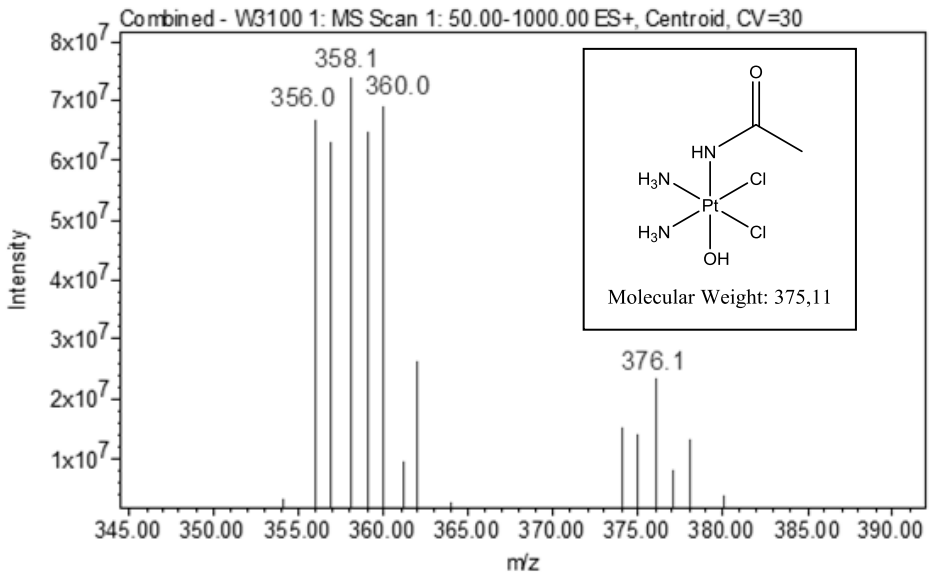

Figure 5.1: ESI-MS spectrum of complex **11**, prepared in ultrapure water

The ESI-MS spectrum of complex **11** (*Figure 5.1*), registered in positive ion mode with a 30V cone voltage, shows the pseudo-molecular ion $[M+H]^+$ peak at 376.1 m/z and the peak of the fragment $[M-OH]^+$ at 358.1 m/z.

[1]H-NMR

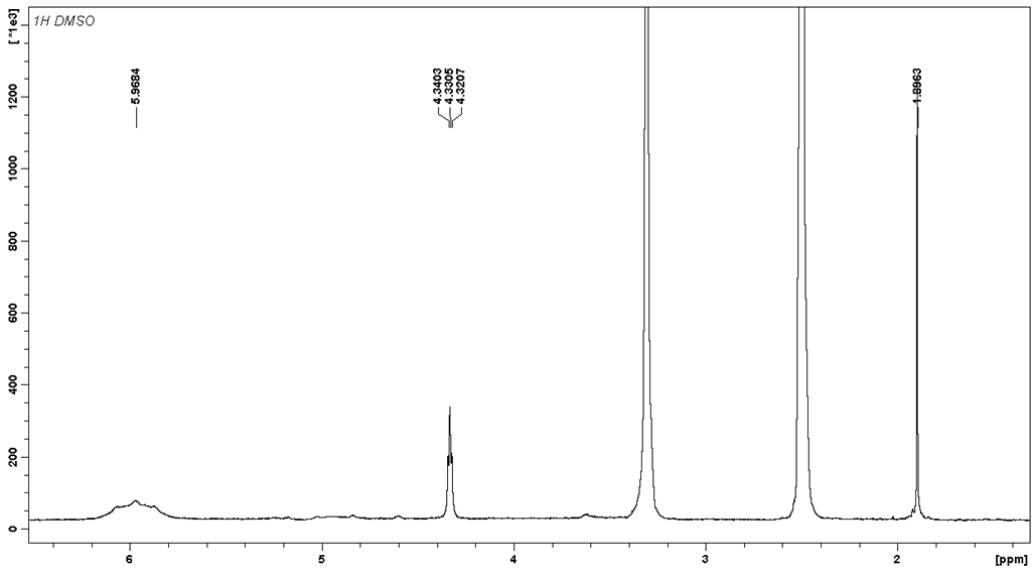

Figure 5.2: ^{1}H-NMR spectrum of complex **11**, registered in DMSO-d_6

The ^{1}H-NMR (500 MHz, DMSO-d_6) spectrum of complex **11** shows the following signals, δ: 1.90 (s, 3H,-C*H*$_3$), 4.33 (t, 1H, -N*H*-, ^{3}J = 4.9 Hz), 5.97 (m, 6H, -N*H*$_3$) ppm.

^{13}C-NMR

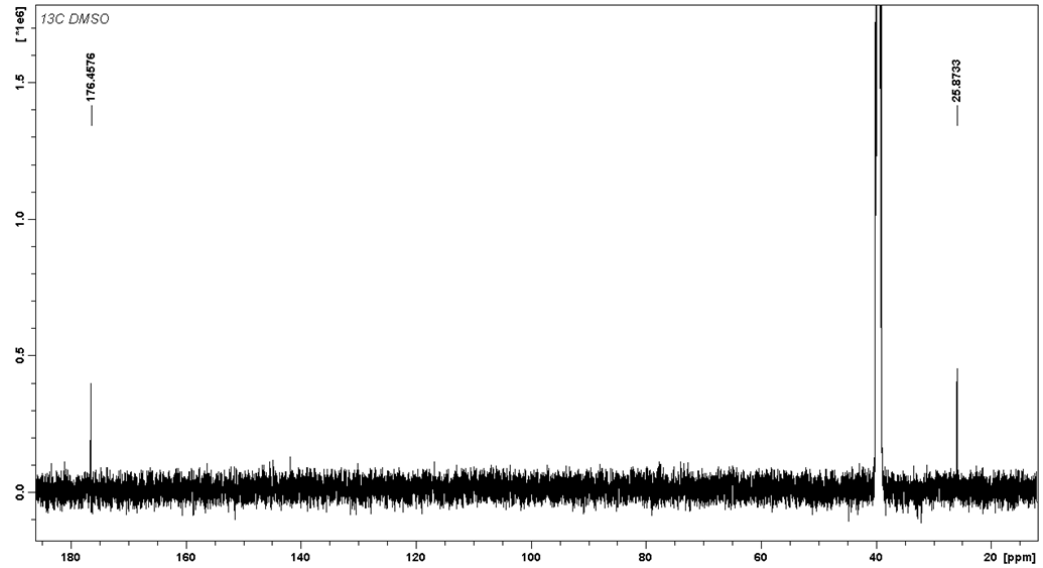

Figure 5.3: ^{13}C-NMR spectrum of complex **11**, registered in DMSO-d_6

The ^{13}C-NMR (125.7 MHz, DMSO-d_6) spectrum of complex **11** shows the following signals, δ: 25.9 (-*C*H_3), 176.5 (-*C*O) ppm.

^{195}Pt-NMR

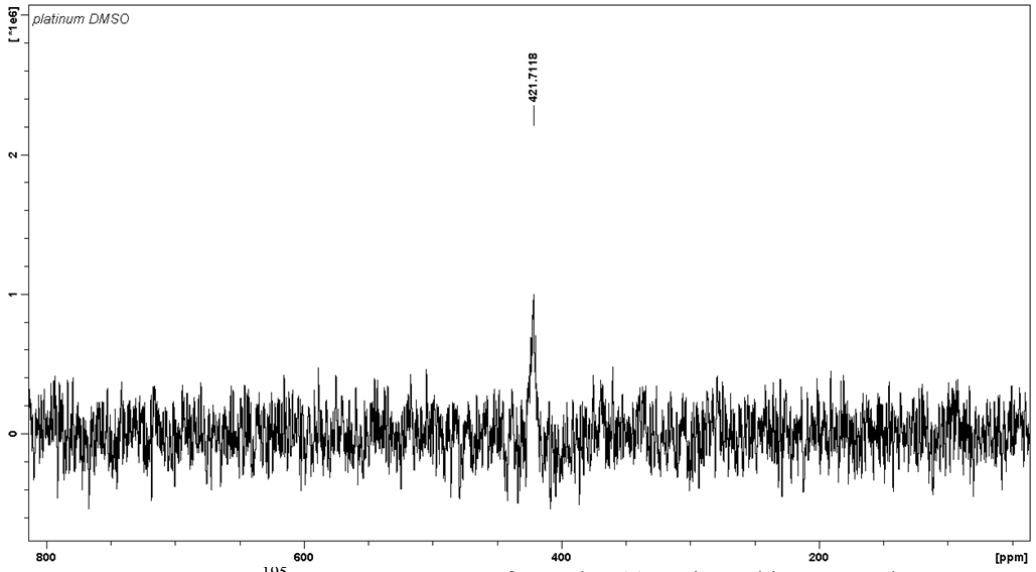

Figure 5.4: ^{195}Pt-NMR spectrum of complex **11**, registered in DMSO-d_6

The ^{195}Pt-NMR spectrum of complex **11** (*Figure 5.4*) was registered in DMSO-d_6 (at a 107.2 MHz NMR frequency) and shows a signal at 422 ppm (qt, ^{1}J = 128.04 Hz). The chemical shift is consistent with a Pt(IV) complex with two chlorides, three *N*-coordinated ligands and a hydroxido. The signal multiplicity is typical of the coupling of ^{195}Pt (spin quantum number I = ½) with two ^{14}N atoms (I = 1) and the signal is quite broad, due to the coupling with the quadrupolar nucleus ^{14}N.

5.3 Synthesis of (OC-6-44)-(acetylamido-N)diammine(4-carboxypropanoato)dichloridoplatinum(IV) (12)

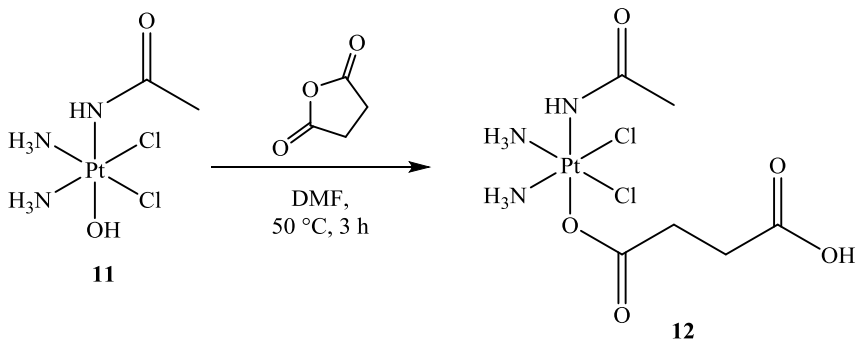

The synthetic procedure was reported in the literature [9]. In particular, succinic anhydride (266 mg, 2.66 mmol) was added dropwise to a mixture of **11** (100 mg, 0.266 mmol) in 5 mL of DMF and the reaction was carried out at 50 °C until the yellow solution became completely clear (about 3 hours). Then it was filtered and the DMF was removed under reduced pressure. A pale yellow powder was precipitated with acetone/diethyl ether, then washed with diethyl ether and dried *in vacuo*.

Yield: 91.0 mg, 0.192 mmol, 71.8%.

5.3.1 Characterization of the Complex

RP-HPLC-ESI-MS

The analysis was performed by employing a stationary phase consisting of a C18 Phenosphere-NEXT column 5 μm, 250 × 4.60 mm ID, a mobile phase composed by a 70:30 mixture of a 15 mM aqueous solution of formic acid and pure methanol (by isocratic elution), a flow rate of 0.500 mL/min, a temperature of 37 °C and the UV-Visible detector set at 210 nm. Compound **12** showed a

retention time of 6.24 minutes and its identity was attributed by the corresponding ESI-MS spectrum (*Figure 5.5*).

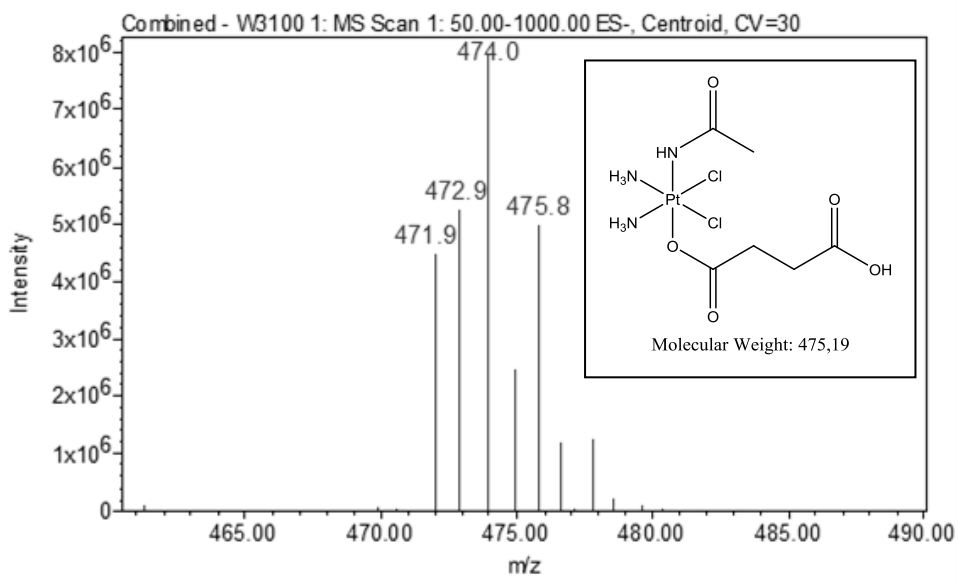

Figure 5.5: ESI-MS spectrum of complex **12**, prepared in ultrapure water

The ESI-MS spectrum of complex **12**, registered in negative ion mode with a cone voltage of 30V (*Figure 5.5*), confirms the success of the synthesis showing the pseudo-molecular ion $[M-H]^-$ peak at 474.0 m/z.

^{1}H-NMR

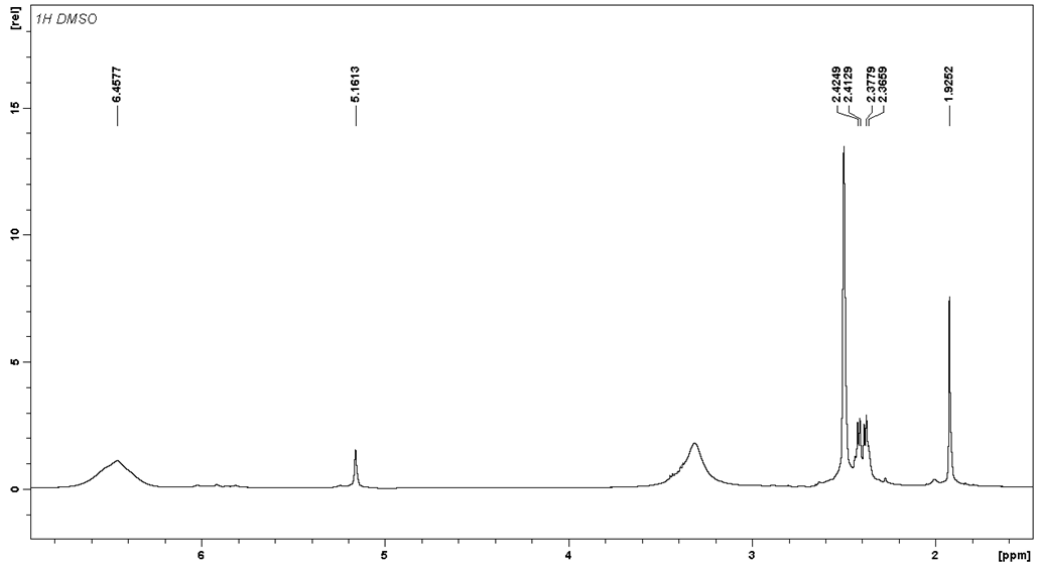

Figure 5.6: ^{1}H-NMR spectrum of complex **12**, registered in DMSO-d_6

The ^{1}H-NMR (500 MHz, DMSO-d_6) spectrum of complex **12** shows the following signals, δ: 1.93 (s, 3H, -C*H*$_3$), 2.38 (m, 2H, -C*H*$_2$-CO_2H), 2.42 (m, 2H, -C*H*$_2$-CO_2), 5.16 (s, 1H, -N*H*-), 6.46 (m, 6H, -N*H*$_3$) ppm.

^{13}C-NMR

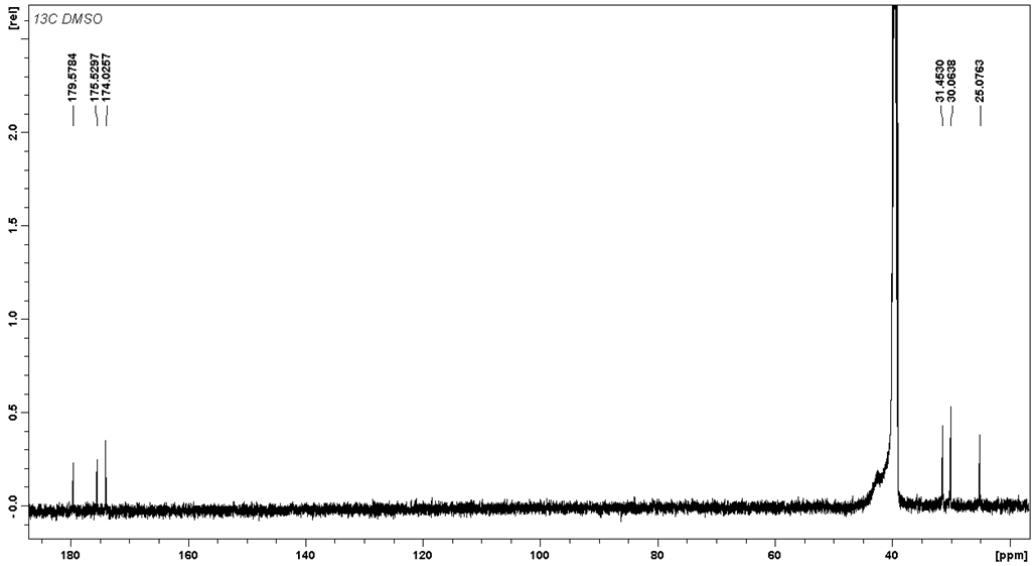

Figure 5.7: ^{13}C-NMR spectrum of complex **12**, registered in DMSO-d_6

The ^{13}C-NMR (125.7 MHz, DMSO-d_6) spectrum of complex **12** shows the following signals, δ: 25.1 (-*C*H_3), 30.1 (-*C*H_2-CO_2H), 31.4 (-*C*H_2-CO_2), 174.0 (-CH_2-*C*O_2H), 175.5 (-*C*O-CH_3), 179.5 (-CH_2-*C*O_2) ppm.

^{195}Pt-NMR

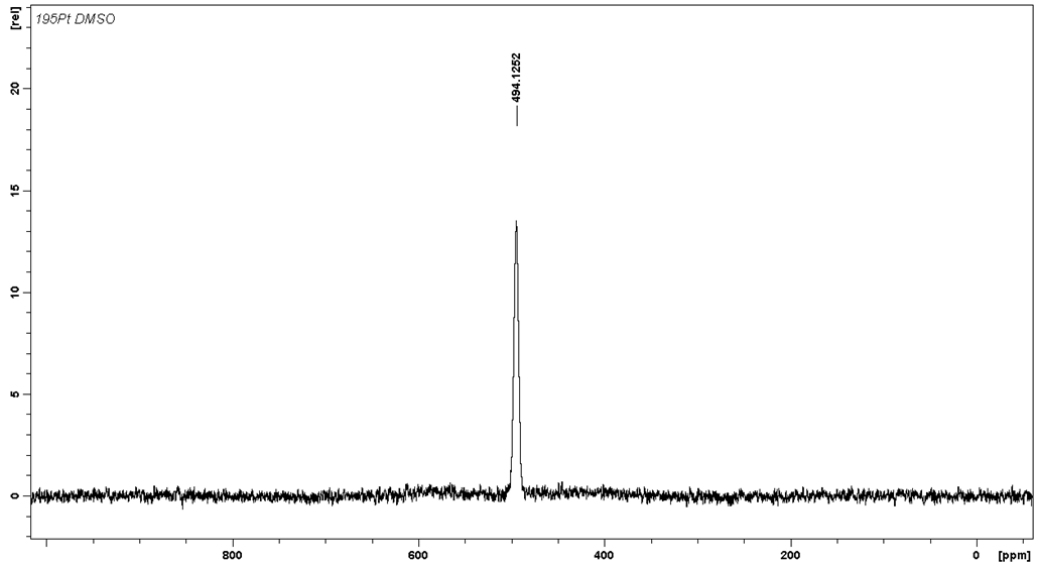

Figure 5.8: ^{195}Pt-NMR spectrum of complex **12**, registered in DMSO-d_6

The ^{195}Pt-NMR spectrum of complex **12** (*Figure 5.8*) was registered in DMSO-d_6 (at a 107.2 MHz NMR frequency) and shows a signal at 494 ppm, which is consistent with a Pt(IV) complex containing two chlorides, three *N*-coordinated ligands and a carboxylato.

5.4 Synthesis of the Activated N-hydroxysuccinimidyl Ester of 12 (13)

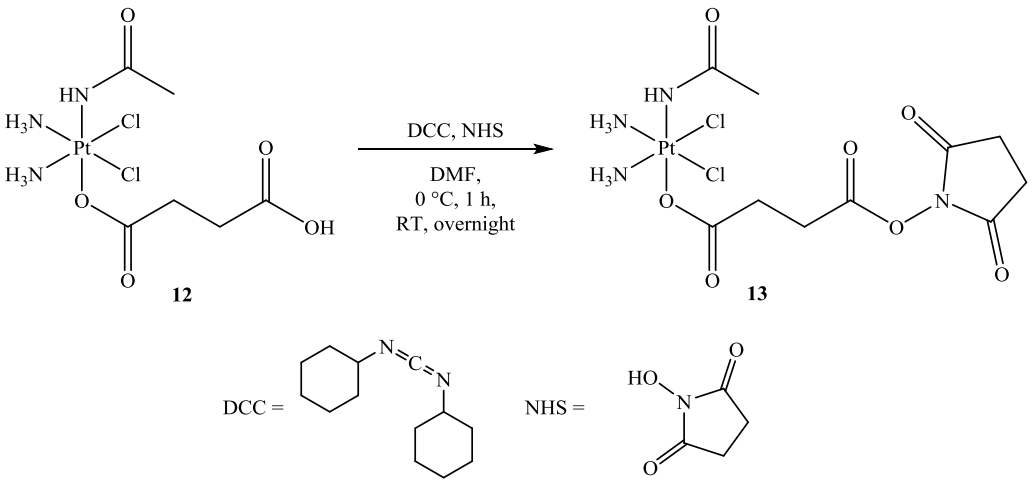

A mixture of **12** (50.0 mg, 0.105 mmol), DCC (26.1 mg, 0.126 mmol) and NHS (14.5 mg, 0.126 mmol) in 2 mL of anhydrous DMF was stirred at 0 °C for 1 hour and at room temperature overnight. Then the solution was cooled to -18 °C and filtered in order to remove dicyclohexylurea. The DMF was removed under reduced pressure and a pale yellow powder was precipitated by the addition of a mixture of acetone/diethyl ether. It was washed with diethyl ether and then dried *in vacuo*.

Yield: 41.8 mg, 0.0730 mmol, 69.4%.

5.4.1 Characterization of the Complex

RP-HPLC-ESI-MS

The analysis was performed by employing a stationary phase consisting of a C18 Phenosphere-NEXT column 5 µm, 250 × 4.60 mm ID, a mobile phase composed by a 70:30 mixture of a 15 mM aqueous solution of formic acid and pure methanol (by isocratic elution), a flow rate of 0.500 mL/min, a temperature of 37 °C and the UV-Visible detector set at 210 nm. Compound **13** showed a retention time of 6.54 minutes and its identity was attributed by the corresponding ESI-MS spectrum (*Figure 5.9*).

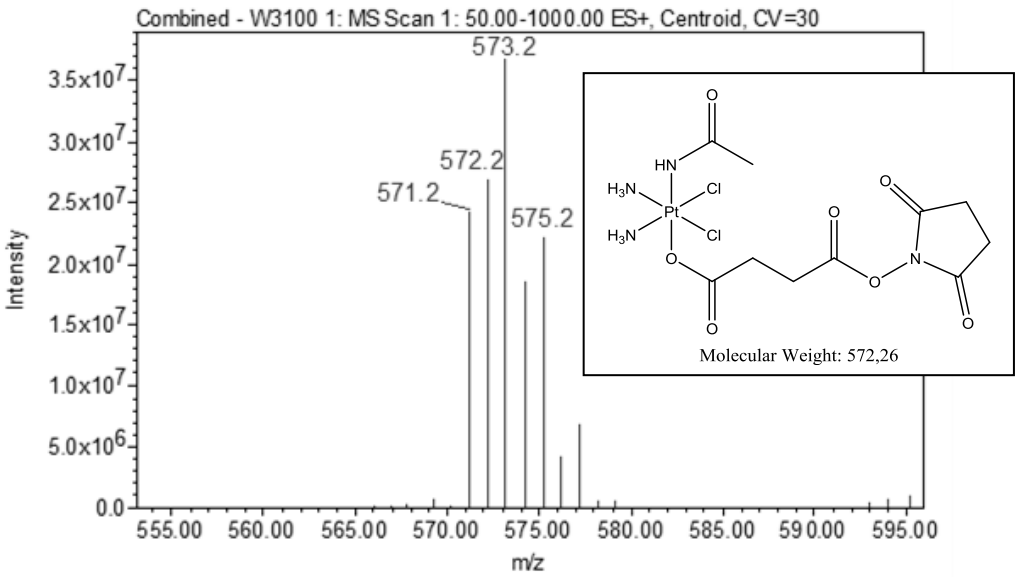

Figure 5.9: ESI-MS spectrum of complex **13**, prepared in a 50:50 mixture of ultrapure water and methanol

The ESI-MS spectrum of complex **13** (*Figure 5.9*), registered in positive ion mode with a 30V cone voltage, shows the pseudo-molecular ion $[M+H]^+$ peak at 573.2 m/z: it confirms the success of the synthesis.

^{1}H-NMR

The ^{1}H-NMR (500 MHz, DMSO-d_6) spectrum of complex **13** shows the following signals, δ: 1.93 (s, 3H, -C*H*$_3$), 2.38 (m, 2H, -C*H*$_2$-CO$_2$N), 2.42 (m, 2H, -C*H*$_2$-CO$_2$), 2.81 (s, 4H, –C*H*$_2$CON), 5.16 (s, 1H, -N*H*-), 6.45 (m, 6H, -N*H*$_3$) ppm.

^{13}C-NMR

The ^{13}C-NMR (125.7 MHz, DMSO-d_6) spectrum of complex **13** shows the following signals, δ: 25.1 (-*C*H$_3$), 25.4 (–*C*H$_2$CON), 30.0 (-*C*H$_2$-CO$_2$N), 31.4 (-*C*H$_2$-CO$_2$), 170.2 (–*C*ON), 174.0 (-CH$_2$-*C*O$_2$N), 175.5 (-*C*O-CH$_3$), 179.5 (-CH$_2$-*C*O$_2$) ppm.

^{195}Pt-NMR

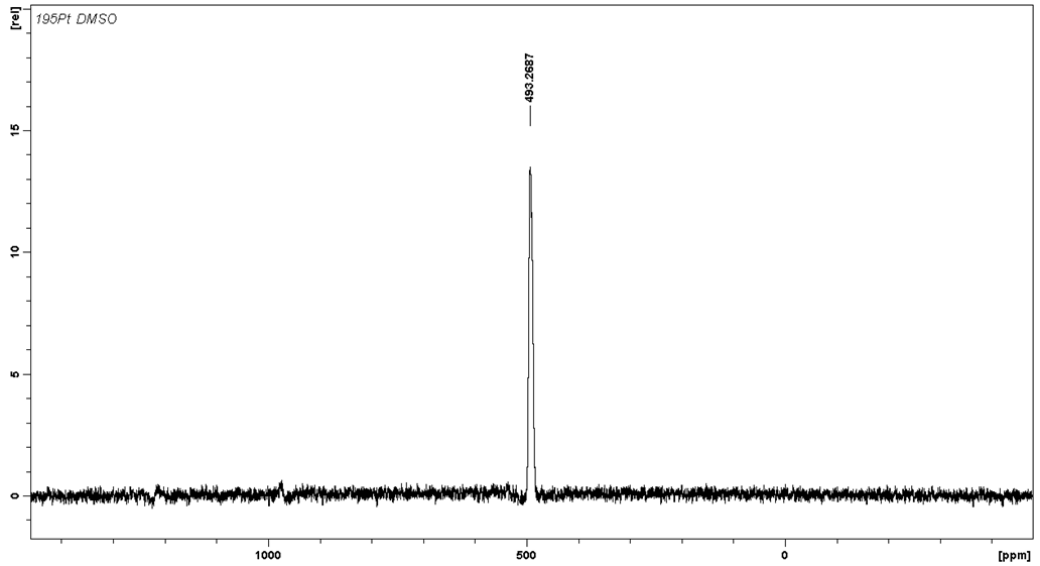

Figure 5.10: ^{195}Pt-NMR spectrum of complex **13**, registered in DMSO-d_6

Figure 5.10 shows the ^{195}Pt-NMR spectrum of complex **13**, registered in DMSO-d_6 (at a 107.2 MHz NMR frequency), containing a signal at 493 ppm, consistent with a Pt(IV) complex with two chlorides, three *N*-coordinated ligands and a carboxylato.

5.5 Synthesis of NPs Decorated with APTES (e)

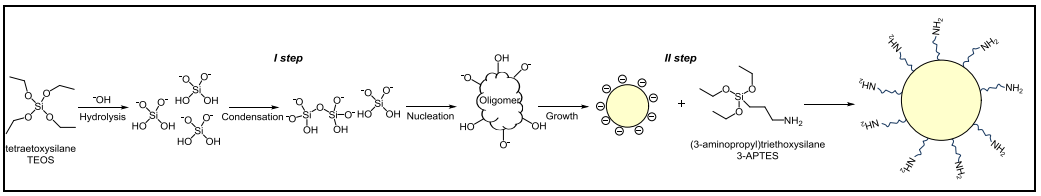

Figure 5.11: Synthetic scheme for the preparation of NPs **e**

The silica nanoparticles were synthesized by using a similar procedure (*Figure 5.11*) to the one described in *Chapter IV* [3]. In particular, in a three-necked

flask equipped with a reflux condenser, 20 mL of a 28% w/w ammonia solution were added to 25 mL of ultrapure water, they were diluted with methanol to the final volume of 320 mL and magnetically stirred at 830 rpm, with a temperature set to 30 °C. Subsequently, TEOS (20 mL, 90 mmol) was added to the mixture and the reaction was carried out for 2.5 hours. Then the silica nanoparticles were collected by centrifugation (8500 rpm, 35 minutes), resuspended in ethanol by means of ultrasonic tip (power 117 W, 5 minutes) and these two steps were repeated three times.

The ethanol suspension was added to a mixture of 35 mL of ultrapure water, 6 mL of a 28% w/w ammonia solution and methanol to the final volume of 320 mL, and then (3-aminopropyl)triethoxysilane (APTES, 536 µL, 2.29 mmol) was added. The suspension was magnetically stirred at 830 rpm, at 30 °C and the reaction was carried out for 16 hours. The NPs were collected by centrifugation (8500 rpm, 35 minutes) and washed with ethanol by means of five cycles of resuspension (by ultrasonic tip) and centrifugation. The synthesized NPs were stored in ethanol at 4 °C.

5.5.1 Quantification of the Amino Functionalities

In order to proceed with the quantification of the exposed amino groups, 1 mL of the ethanol suspension was dried in an oven (20 minutes at 100 °C) and, then, the dried product was weighed to calculate the content of the suspension (0.0630 g NPs / mL ethanol suspension).

The amino groups present on the NPs surface were quantified by employing the same procedure described in *paragraph 4.3.2*. In particular, 7.94 mL of ethanol suspension were centrifuged to get 0.500 g of NPs that were suspended in 20 mL of a 0.2 M HCl and 0.5 M NaCl aqueous solution, in order to protonate all the available amino groups. After the centrifugation, they were suspended in 20

mL of ultrapure water, in order to remove the HCl and NaCl excess, and then centrifuged. They were suspended in 20 mL of a 1 M aqueous solution of KNO_3 and the suspension was mechanically shaken overnight, in order to exchange chloride with nitrate anions. Then the suspension was centrifuged and the chlorides, present in the solution, were titrated with a 0.01 M $AgNO_3$ aqueous solution by means of an Ag^+ selective electrode (the titration is based on the AgCl precipitation). The potential of the solution was registered, at 25 °C, after each addition of $AgNO_3$ and is reported in a graph as a function of the titrant volume (*Figure 5.12*). Then the data were processed and expressed as amino group density: 0.283 mmol NH_2 / g NPs.

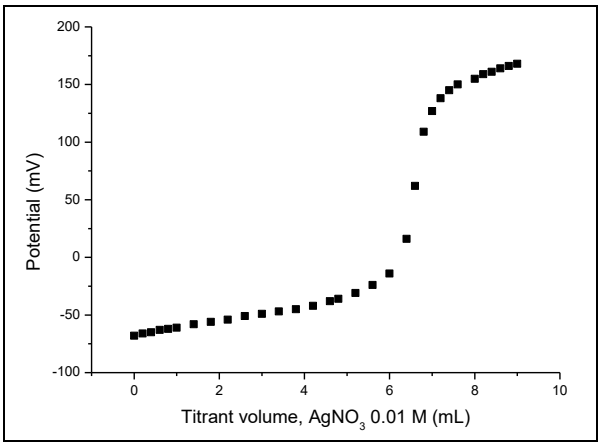

Figure 5.12: Titration curve of silica NPs **e**

5.5.2 Size and Stability Investigations

Dynamic Light Scattering (DLS) and ζ potential analyses were carried out in order to study the NPs size and the suspension stability, respectively. These measurements were performed in a 10 mM KNO_3 aqueous solution (after being treated with a 0.2 M HCl aqueous solution and then centrifuged) at 25 °C with a

Malvern Zetasizer Nano ZS (see *paragraph 4.2* for the instrumental information). The nanoparticles diameter was also verified by Transmission Electron Microscope (TEM) analysis. In particular, for the TEM investigation of particle shape, small amounts of the synthesized products (free NPs and conjugates), dispersed in ethanol, were transferred onto 200-mesh Cu TEM grids with formvar support film. Grids were observed through a Philips CM 10 (Eindhoven, Netherland) Transmission Electron Microscope operating at 100 kV (*Figure 5.13*).

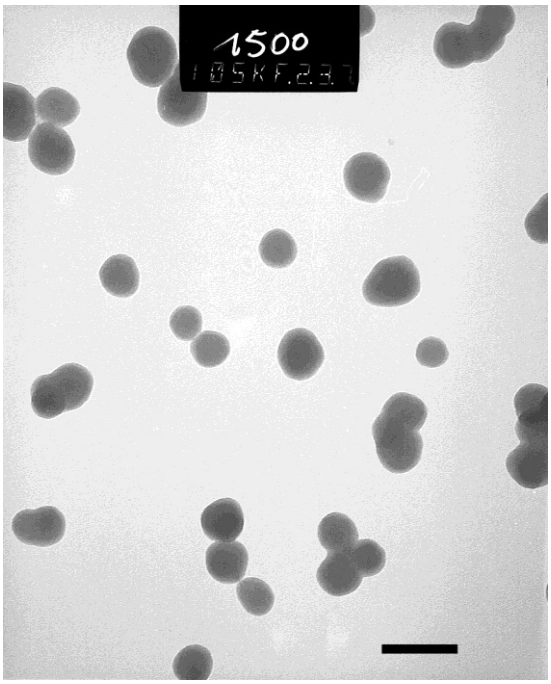

Figure 5.13: TEM micrograph of NPs **e** (the bar represents 100 nm)

The ζ potential is a measure of the stability of a suspension (as described in *paragraph 4.3.3*) and a value ≥ |30| mV indicates a stable suspension. NPs **e** result to be very stable, since they exceed the threshold of stability (in fact, their ζ potential was 53 ± 2 mV) and the possibility of aggregation is avoided.

As regards the size, as observed in *paragraph 4.3.3*, the same NPs analyzed by means of DLS (125 ± 2 nm) result to be bigger than the one analyzed by TEM (51 ± 1 nm) since the hydrodynamic radius have to be considered and, therefore, the NPs appear larger.

5.5.3 Solid-State NMR Characterization

^{29}Si solid-state NMR applied to silica NPs allows to verify the types of covalent bonds present on their surface.

Usually, the Si sites are indicated by the formula $(SiO)_n\underline{Si}R_mX_{4-n-m}$, in which *X* represents -OCH_3, -OCH_2CH_3, -OH or -Cl groups, *R* can be a methyl or a group different from *X* (in this work, *R* = 3-aminopropylic arm) [10]. Furthermore, the Si sites are defined with a specific nomenclature, which indicates mono- (M), di- (D), tri- (T) and quaternary (Q) coordination of oxygen (or, in some cases, Cl) atoms to Si (*Figure 5.14*).

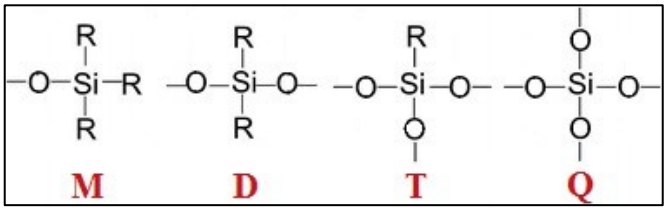

Figure 5.14: Coordinated groups to a Si atom on a silica material surface.
The picture was adapted from literature [11]

Such abbreviations are indicated as M^n, D^n, T^n and Q^n (where *n* is the number of linked "SiO"). In particular, the silica core of the employed NPs is composed of tetrafunctional units (i.e. silicon bound to four "SiO" units, i.e. $[(SiO)_4Si]$), corresponding to Q^4.

Free silanols are indicated as Q^3 ($[(SiO)_3Si(OH)]$): in fact, Si is bound to four oxygen atoms (three from "SiO" units and one from -OH group (i.e. X = 1, R = 0, m = 0).

A Si atom bound to three oxygens (SiO) and one R group (such as a 3-aminopropyl), $[(SiO)_3SiR]$, showed m = 1 and X = 0: therefore, it was defined as T^3. On the contrary, when silicon is bound to three oxygen atoms, one from -OH (X = 1), and to a 3-aminopropyl group (m = 1), the attribution is T^2 ($[(SiO)_2SiR(OH)]$).

A silicon bound to two R (m = 2) and two oxygen groups from "SiO" (n = 2) is considered difunctional and is indicated as $[(SiO)_2SiR_2]$ (D^2).

If the Si atom is bound to three R groups (m = 3) and only one oxygen (from "SiO"), it is defined monofunctional and is described as $[(SiO)SiR_3]$ (M^1).

All the possible combinations, corresponding to precise ranges of ^{29}Si chemical shift, are reported in *Tables 5.1* and *5.2*.

	$(SiO)_nSiR_mX_{4-n-m}$			
Si site	**n**	**m**	**R**	**X**
Q^n	0, 1, 2, 3, 4	0	groups different from X	$-OCH_3$, $-OCH_2CH_3$, -OH, -Cl
T^n	0, 1, 2, 3	1		
D^n	0, 1, 2	2		
M^n	0, 1	3		

Table 5.1: Symbols of the functional groups present on silica materials

m \ n	0	1	2	3	4
0	$Si(X)_4$ (Q^0)	$(SiO)Si(X)_3$ (Q^1)	$(SiO)_2Si(X)_2$ (Q^2)	$(SiO)_3Si(X)$ (Q^3)	$(SiO)_4Si$ (Q^4)
1	$SiR(X)_3$ (T^0)	$(SiO)SiR(X)_2$ (T^1)	$(SiO)_2SiR(X)$ (T^2)	$(SiO)_3SiR$ (T^3)	-
2	$SiR_2(X)_2$ (D^0)	$(SiO)SiR_2(X)$ (D^1)	$(SiO)_2SiR_2$ (D^2)	-	-
3	$SiR_3(X)$ (M^0)	$(SiO)SiR_3$ (M^1)	-	-	-

Table 5.2: All the possible combinations of *n* and *m* in the general formula $[(SiO)_nSiR_mX_{4-n-m}]$ and their symbols are indicated below, in brackets

In particular, the solid state ^{29}Si-NMR spectra were acquired on a Bruker Avance III 500 spectrometer and a wide bore 11.7 T magnet with operational frequencies for ^{1}H and ^{29}Si of 500.13 and 99.35 MHz, respectively. A 4 mm triple resonance probe with Magic Angle Spinning (MAS) was employed in all the experiments. NPs **e** (previously lyophilized) were packed on a Zirconia rotor and spun at a MAS rate of 10 kHz. The relaxation delays (d1) between accumulations were 2.5 seconds. For the ^{29}Si{^{1}H} CPMAS experiments, the radio frequency (RF) fields (υ_{rfH}) of 55 and 28 kHz were used for the initial excitation and the decoupling, respectively. During the Cross-Polarization (CP) period, the ^{1}H RF field υ_{rfH} was ramped using 100 increments, whereas the ^{29}Si RF field (υ_{rfSi}) was maintained at a constant level. During the acquisition, the protons were decoupled from the silicons by using a TPPM (Two Pulse Phase Modulation) decoupling scheme. A moderate ramped RF field υ_{rfH} of 62 kHz was used for spin locking, while the carbon RF field υ_{rfSi} was matched to obtain

optimal signal and the CP contact time of 2000 μseconds was used. The chemical shifts were externally referenced to TMS at 0 ppm.
The results of the analysis were shown in *Figure 5.15*.

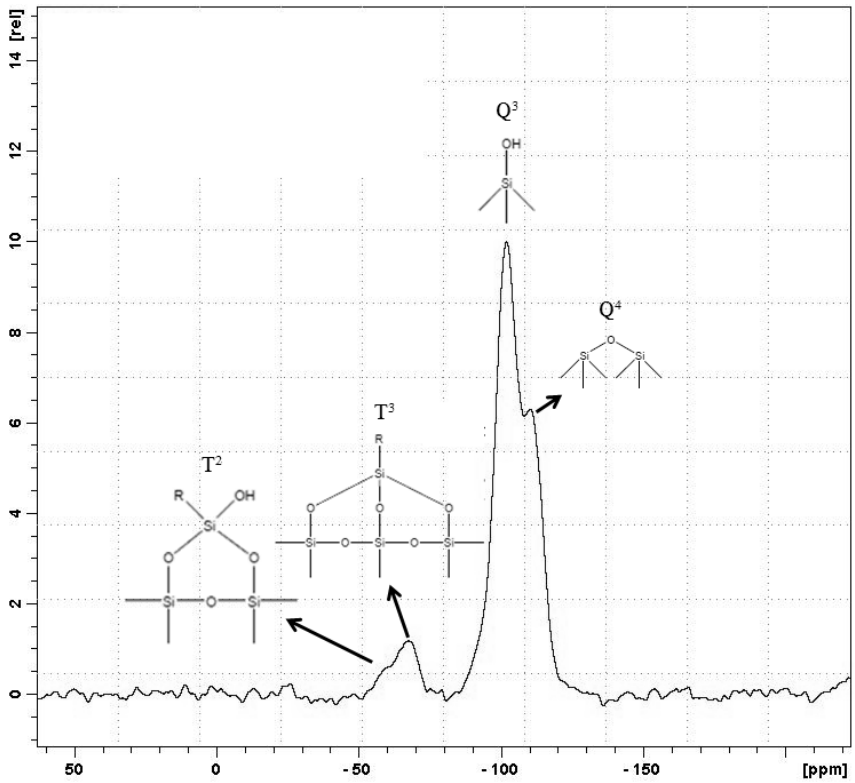

Figure 5.15: $^{29}Si\{^{1}H\}$ CPMAS NMR spectrum of NPs **e**

The spectrum reported in *Figure 5.15* confirmed the functionalization of NPs **e** and gave information on the NPs surface. In particular, the peak at about -100 ppm was ascribed to isolated silanol groups $[(SiO)_3Si(OH)]$ (Q^3) and the one at -110 ppm indicated surface siloxane bridges $[(SiO)_4Si]$ (Q^4). The two peaks at -60 and -68 ppm, instead, allowed to verify the decoration with the amino silane (in this case, APTES): they were attributed to $[(SiO)_2SiR(OH)]$ (T^2) and $[(SiO)_3SiR]$ (T^3), respectively, in which R was $-CH_2CH_2CH_2NH_2$.

5.6 Synthesis of Conjugates 14e and 15e

The ethanol suspension **e** (1 mL, 63.0 mg NPs, 0.0178 mmol amino groups) was centrifuged, washed once with anhydrous DMF and then suspended in anhydrous DMF. This suspension was added to a solution of **8** (10.0 mg, 0.0178 mmol), prepared in 1 mL of DMF, and the mixture was magnetically stirred for 4 hours at room temperature. The suspension was centrifuged (9000 rpm, 15 minutes) and the conjugate (**14e**) was washed with ultrapure water and ethanol, in order to completely remove not coupled **8**, NHS and DMF.
The same procedure was employed for the synthesis of conjugate **15e**: in particular, 1 mL of the anhydrous DMF suspension **e** was added to a solution of **13** (10.2 mg, 0.0178 mmol), prepared in 1 mL of anhydrous DMF.

5.6.1 Quantification of the Pt Content in 14e and 15e

An aliquot of the ethanol suspensions **14e** and **15e** was centrifuged and the pellet was dried in order to be mineralized by means of microwaves. Each mineralization was carried out at least in triplicate by following the same procedure employed for conjugates **5a-5d** and **10a-10d** (see *paragraph 4.9.2*). Each mineralized sample was transferred into a marked flask by means of 1% v/v nitric acid and sonicated for 1 hour at 60 °C. After that, the samples were centrifuged (9000 rpm, 15 minutes) in order to separate the silica residue from the solution. The Pt content of the supernatants was quantified by means of ICP-OES analysis and the results are reported in *Table 5.3*.

Conjugate	% Pt loading (respect to the total available amino groups)	mol Pt/g NPs
14e	30.8 ± 1.1	7.89 (± 0.28) × 10^{-5}
15e	22.5 ± 1.5	5.77 (± 0.38) × 10^{-5}

Table 5.3: Pt loading of conjugates **14e** and **15e**. Each result was obtained from at least three independent coupling reactions

The data showed that conjugate **14e** had a higher Pt content with respect to **15e**: probably, complex **8** resulted to be more reactive than **13**.

5.6.2 Characterization of Conjugates 14e and 15e

Conjugates **14e** and **15e** were characterized by DLS and TEM, in order to verify their size, and by ζ potential to evaluate the stability of their suspensions. *Table 5.4* and *Figure 5.16* show the results.

Conjugate	TEM diameter	DLS diameter	ζ potential
e	51 ± 1 nm	125 ± 2 nm	53 ± 2 mV
14e	59 ± 5 nm	124 ± 2 nm	40 ± 3 mV
15e	57 ± 4 nm	120 ± 2 nm	38 ± 2 mV

Table 5.4: Diameter and ζ potential of conjugates **14e** and **15e**, compared with **e**

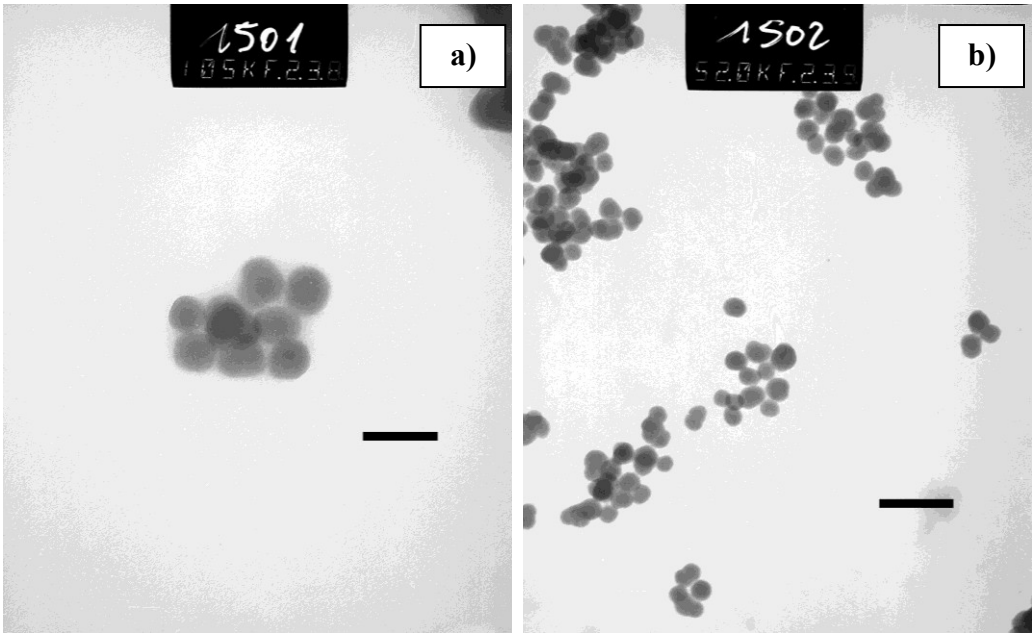

Figure 5.16: TEM micrographs of conjugates a) **14e** and b) **15e** (the bars represent 100 nm and 200 nm, respectively)

As regards the size, the new conjugates showed the same behavior in solution (i.e. the increased dimensions, due to the hydrodynamic radius) observed for the previous NPs. Furthermore, a preservation of the size, after the coupling reaction, was observed: in fact, **14e** and **15e** nano-systems resulted only slightly grown with respect to **e**.

Moreover, the suspensions were stable, since the ζ potential values were higher than +30 mV (*Table 5.4*), even though there was a decrease in the ζ potential data from **e** to **14e** and **15e** (from about +53 mV to about +40 mV). It is known that the value observed for free NPs is due to the protonated amino groups exposed from the nanoparticles surface and, therefore, the coupling of the Pt(IV) complex to the amino functionalities leads to a loss of positive charge, since an amount of these amines is occupied in an amidic bond: this justified the lower ζ potential values with respect to the one of free **e**.

5.6.3 Platinum Release from Conjugates 14e and 15e in Reducing Conditions

Conjugates **14e** and **15e** were centrifuged, the ethanol solutions were removed and the pellets were suspended in 1 mM HEPES buffer solution (pH 7.4) and ascorbic acid (10-fold molar excess respect to the Pt content) was added. The mixtures were mechanically shaken both for 8 and 24 hours and then the suspensions were centrifuged (9000 rpm, 15 minutes). The solutions were analyzed by means of ICP-MS, in order to quantify the Pt released: the 62% (± 8) of the total platinum loaded on **14e** was released within 8 hours and after 24 hours almost all the platinum was released.

For conjugate **15e**, instead, the ascorbic acid reduced only a little amount of complex and this behavior was in agreement with the one observed in the reduction kinetics studies of other acetylamido derivatives [12] that were, however, reduced by cell extracts.

5.6.4 Spontaneous Platinum Release from Conjugates 14e and 15e

The spontaneous release of Pt complex from **14e** and **15e,** in the absence of any reducing agents, was studied in order to evaluate the behavior of NPs **e** and to compare it with the previously synthesized NPs **a**-**d** (see *Chapter IV* and, in particular, *paragraph 4.16*).

As reported in *paragraph 5.6.3*, the conjugates were centrifuged, the ethanol solution was removed and the pellet was suspended in 1 mM HEPES buffer solution (pH 7.4) and mechanically shaken for 4 hours. Then the suspension was centrifuged (9000 rpm, 15 minutes) and the solution was analyzed by means of ICP-MS, in order to quantify the Pt released. Furthermore, the pellet was

suspended again in HEPES solution and the suspension was mechanically shaken for further 4 hours, in order to verify if, after the replacement of the solution, a further detachment still occurred. Also in this case, the suspension was centrifuged and the Pt content in the solution was determined by ICP-MS.
The results indicated that, for both **14e** and **15e**, the 15% of the total loaded complex was detached within 4 hours: the released amount was similar to the one obtained for conjugate **10b** in water in *Chapter IV* (*paragraph 4.16*). Moreover, the complex continued to be released after the renewal of the buffer solution: in fact, after further 4 hours, the Pt detached represented the 20% and it was cumulative with the first 15%. These data suggested that, without the replacement of the solution, an equilibrium between conjugate and released species was established but the renewal destabilized the equilibrium and favored a further detachment. The species detached was the same identified in *paragraph 4.16* and defined as **7-APS**. Therefore, even though the type of NPs was slightly different from the previous ones (**a**-**d**), in fact there were no fluorophores and core-shell structure and the amino silane arm was different (APTES, instead of APTMS), a loss of Pt was observed. It was attributed to the previously mentioned formation of stable five-membered cyclic intermediates and to the detachment induced by nearby amino groups [1]. The detachment results to be, therefore, independent from the nature of the alkoxy group of the silane arm (methoxy for APTMS and ethoxy for APTES) but is closely related to the presence of amino groups (primary in both cases, but also in the case of secondary amines) in propyl position, which are very suitable for the formation of cyclic intermediates.
For this reason, it was necessary to synthesize NPs with a longer chain amino silane, i.e. *N*-(6-aminohexyl)aminomethyltriethoxysilane (AHAMTES), the hydrolytic stability of which was demonstrated to be higher, due to the absence of intramolecularly catalyzed detachments [2] (*Figure 5.17*).

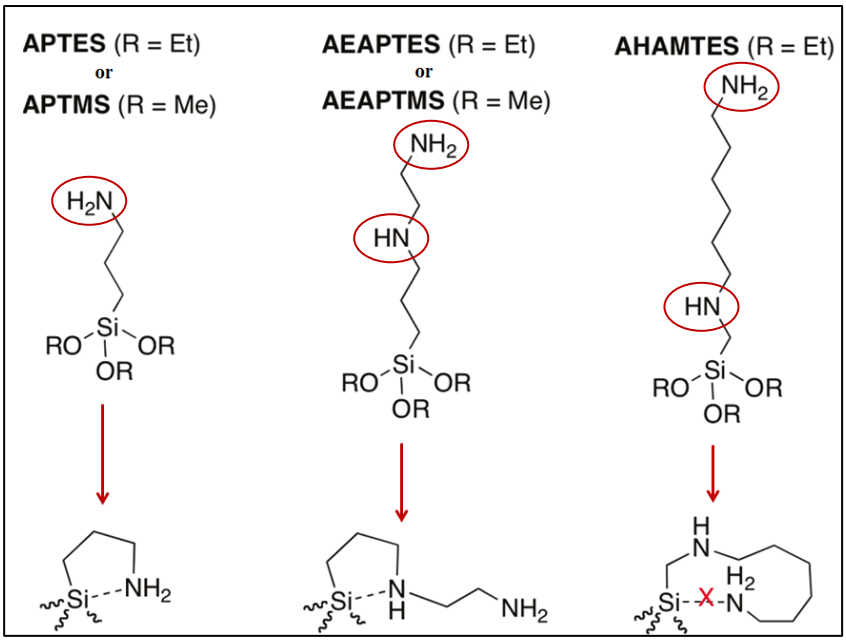

Figure 5.17: The correlation between the position of the amino group in the alkylic chain of different amino silanes and the intra-molecularly catalyzed detachment from the NPs surface. The picture is a modification of that in literature [1]

5.7 Synthesis of NPs Decorated with AHAMTES (f - i)

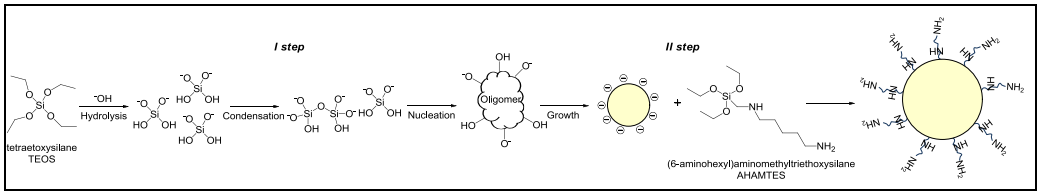

Figure 5.18: Schematic synthesis of NPs **f-i**

The synthetic procedure to prepare these types of NPs (*Figure 5.18*) was the same employed for the synthesis of NPs **e** (*paragraph 5.5*) but differed in the reaction time used to decorate the silica core. In particular, in a three-necked flask equipped with a reflux condenser, 20 mL of a 28% w/w ammonia solution

were added to 25 mL of ultrapure water, they were diluted with methanol to the final volume of 320 mL, magnetically stirred at 830 rpm and the temperature was set to 30 °C. Subsequently, TEOS (20 mL, 90 mmol) was added to the mixture and the reaction was carried out for 2.5 hours. Then the silica nanoparticles were collected by centrifugation (8500 rpm, 35 minutes), resuspended in ethanol by means of ultrasonic tip (power 117 W, 5 minutes) and these two steps were repeated three times.

The ethanol suspension was added to a mixture of 35 mL of ultrapure water, 6 mL of a 28% w/w ammonia solution and methanol to the final volume of 320 mL, and then AHAMTES (2.89 mL, 9.17 mmol) was added. The suspension was magnetically stirred at 830 rpm, the temperature was set to 30 °C and the reaction was carried out for different times (in particular for 16 (**f**), 27 (**g**), 38 (**h**), 62 hours (**i**)), in order to study the kinetics of AHAMTES loading on the silica surface. Subsequently, the NPs were collected by centrifugation (8500 rpm, 35 minutes) and washed with ethanol by means of five cycles of resuspension (by ultrasonic tip) and centrifugation. The synthesized NPs were stored in ethanol at 4 °C.

5.7.1 Quantification of the Amino Functionalities

For the quantification of the amino groups, 0.5 g of NPs **f-i** were washed several times with ethanol, in order to completely remove not reacted ammonia and AHAMTES. Then, they were suspended twice in 20 mL of a 0.2 M HCl and 0.5 M NaCl aqueous solution. After the centrifugation, they were suspended in 20 mL of ultrapure water and then centrifuged. They were suspended in 20 mL of 1 M KNO_3 and the suspension was mechanically shaken overnight, in order to allow the exchange of chloride anions with nitrates. Then the suspension was centrifuged and the solution containing chloride anions was titrated with a 0.01

M $AgNO_3$ aqueous solution by means of a Ag^+-selective electrode. The results were expressed as total amino groups density, mmol/g NPs (*Table 5.5*) and the titration curve of NPs **h** is reported as an example in *Figure 5.19*.

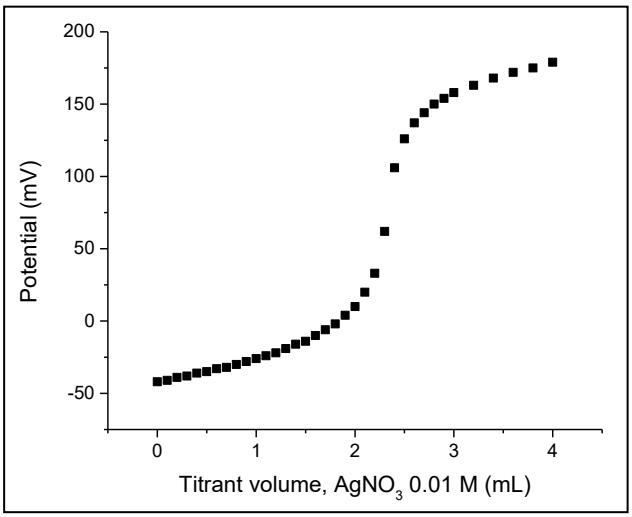

Figure 5.19: Titration curve of NPs **h** (in this case the nanoparticles amount employed for the quantification of the amino functionalities was 0.4 g, instead of 0.5 g)

NPs	total amino groups density (mmol/gNPs)
f	0.057 ± 0.006
g	0.079 ± 0.008
h	0.131 ± 0.013
i	0.129 ± 0.013

Table 5.5: NPs **f-i** total amino groups density

The results, compared to the $-NH_2$ density of NPs **e** (i.e. 0.283 mmol/g), indicate a lower amino silane loading in the case of AHAMTES (i.e. NPs **f-i**). In fact, the hydrolysis (and, therefore, the reactivity) of the amino silane arm, process necessary for the functionalization of the NPs surface, depends on the length of

the arm chain: a longer amino silane (such as AHAMTES) hydrolyzes more slowly than a shorter chain silane (such as APTES or APTMS) [13]. For this reason, being AHAMTES less reactive than APTES and being its hydrolysis fundamental for the NPs functionalization, a lower number of amino groups is present on the NPs surface.

The total amino groups densities are reported in *Figure 5.20* as a function of the reaction time with AHAMTES, to set the experimental conditions in order to get the highest silane loading.

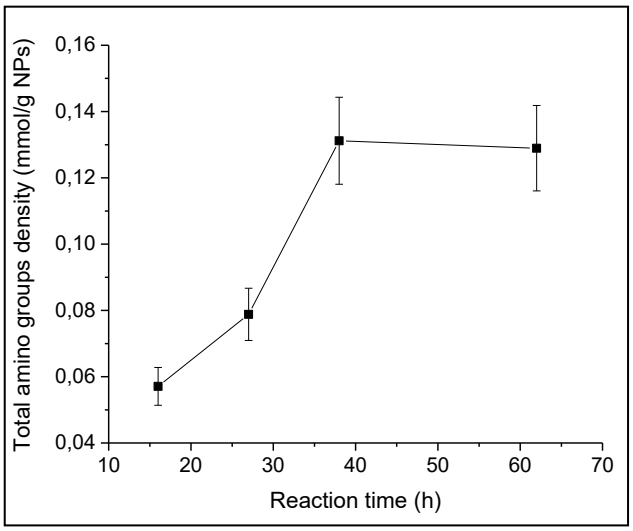

Figure 5.20: AHAMTES loading on NPs surface as a function of the reaction time. Each data point is the mean of three independent samples

The results indicate that the maximum amount of AHAMTES loaded on the NPs surface was reached within 38 hours of reaction. For this reason, the reaction time was set at 38 hours and NPs **h** were employed for the coupling procedures.

5.7.2 Size and Stability Investigations of NPs f - i

DLS and ζ potential analyses of NPs **f-i** were performed in order to the verify their size and suspension stability (see *paragraph 5.5.2*). The results are reported in *Table 5.6*.

NPs	DLS diameter	ζ potential
f	135 ± 6 nm	23 ± 2 mV
g	151 ± 6 nm	26 ± 1 mV
h	131 ± 5 nm	26 ± 2 mV
i	188 ± 1 nm	25 ± 2 mV

Table 5.6: DLS and ζ potential data of NPs **f-i**

The DLS data show that all the NPs samples have similar dimensions, except for NPs **i** which result to be larger than the others: this is probably due to the fact that the decoration reaction lasts more than two days and a half (i.e. 62 hours). This could be explained by considering the fact that the size of the NPs as such increased or numerous multilayers of the amino silane were formed [2] and, therefore, the NPs result to be larger.

The ζ potential results point out that, even though all the four NPs types do not exceed the threshold of stability (i.e. values ≥ |30| mV), they show values very close to the required one. Therefore, they are considered reasonably stable.

As regards TEM analysis, only NPs **h** (i.e. the most relevant sample) were analyzed. *Figure 5.21* shows the micrographs of the silica core (without amino groups) and the protonated NPs **h** (silica core with amino groups, after their protonation). The protonated sample was obtained by centrifugation of the ethanol suspension, subsequent resuspension in 0.2 M HCl (in order to create a

repulsion among the amino arms), centrifugation and resuspension in ethanol. The TEM and DLS diameters and ζ potential of these two samples are reported in the *Table 5.7*.

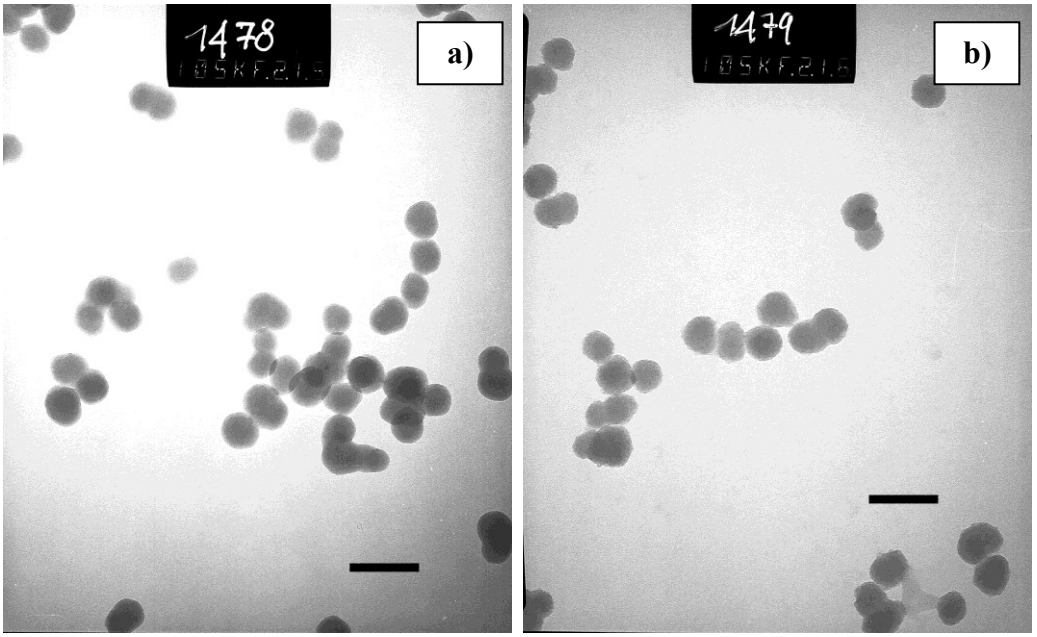

Figure 5.21: TEM micrographs of NPs **h** a) without amino functionalities and b) with protonated amino groups. The bars represents 100 nm

NPs h	DLS diameter	ζ potential	TEM diameter
without amino groups	112 ± 4 nm	-13 ± 1 mV	45 ± 4 nm
with protonated amino groups	131 ± 5 nm	26 ± 2 mV	50 ± 5 nm

Table 5.7: Size and suspension stability of NPs **h** without amino groups and with protonated amino groups

The comparison between DLS and TEM analyses of the silica core and the protonated NPs **h** indicate that a size increase occurred after the functionalization of the nanoparticles surface.

As far as ζ potential is concerned, the final NPs show a positive value, typical of the amino functionalities (exposed from the NPs surface) in their protonated form. The silica core, instead, has a negative ζ potential: it is due to the free hydroxyl groups of silica, present before the surface functionalization (*Figure 5.18*, before the II synthetic step of the NPs).

5.7.3 Solid-State NMR Characterization

In order to evaluate the functionalization of NPs **h**, an aliquot of the NPs was lyophilized and then analyzed by means of Solid-State NMR technique: in *Figure 5.22*, the CPMAS NMR spectrum is shown.

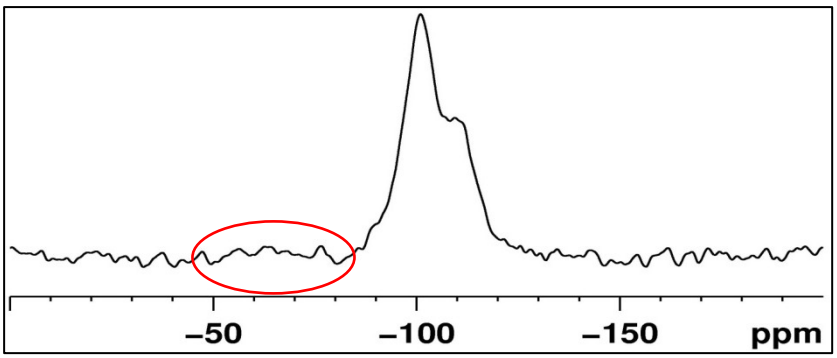

Figure 5.22: CPMAS NMR spectrum of NPs **h**

The spectrum reported in *Figure 5.22* confirms the functionalization of NPs **h** and gives information as regards the NPs surface. Similarly to the previous NPs, the peak at about -100 ppm is ascribed to isolated silanol groups $[(SiO)_3Si(OH)]$ (Q^3) and the one at -110 ppm indicates surface siloxane bridges $[(SiO)_4Si]$ (Q^4).

In this case, T^2 and T^3 (indicated by a red oval) result to be very weaker than Q^3 and Q^4: this suggests the presence of a lower number of amino silane arms on the NPs surface, with respect to the previous NPs, in agreement with the measured amino groups density of NPs **h** (*Table 5.5*) and NPs **e** (i.e. 0.283 mmol NH_2 / g NPs).
Although the available amino functionalities number was lower, this type of NPs was coupled to the complexes **8** and **13** and compared with the previous NPs (i.e. **a**-**d** and **e**).

5.8 Synthesis of Conjugate 14h at Different Reaction Times

The coupling procedure was slightly different from the one employed for the synthesis of conjugates **14e** and **15e** (*paragraph 5.6*): in fact, it was necessary to create a repulsion among the amino arms in order to avoid the aggregation of nearby NPs, favored by the longer chains of AHAMTES. In this case, the aggregation was reversible: in fact, the use of an acidic solution allowed the protonation of the amino groups, the repulsion among the arms and, therefore, the disaggregation of eventual agglomerates.
In particular, the ethanol suspension **h** (1 mL, 78.9 mg NPs, 0.0104 mmol amino groups) was centrifuged, washed once with 0.2 M HCl, once with ultrapure water (to remove HCl excess), once with ethanol and once with anhydrous DMF, then the NPs were suspended in anhydrous DMF. This suspension was added to a solution of **8** (5.8 mg, 0.0104 mmol) in 1 mL of DMF and, then, an appropriate amount of *N,N*-diisopropylethylamine (DIPEA) was added till the formation of a NPs agglomeration (visible to naked eye). The synthesis was carried out at room temperature for different reaction times (such as 1, 2, 4 and 8 hours).

The suspensions were centrifuged (9000 rpm, 15 minutes) and the conjugates were washed with ultrapure water and ethanol, in order to completely remove not coupled **8**, NHS and DMF.

5.8.1 Quantification of the Pt Content in Conjugates 14h (at 1, 2, 4 and 8 hours)

An aliquot of the ethanol suspensions **14h** (at 1, 2, 4 and 8 hours) was centrifuged and the pellet was dried in order to be mineralized by means of microwaves. For each sample, the results were expressed as the average of the Pt loading obtained after three independent couplings, according to the previously described procedure (*paragraph 4.9.2*). The couplings data at different reaction time are shown in *Table 5.8*.

conjugate	**reaction time**	**% Pt loading (respect to the total amino groups)**
14h	1 h	10.6 ± 0.1
	2 h	13.4 ± 0.7
	4 h	16.2 ± 0.8
	8 h	10.4 ± 0.4

Table 5.8: Pt loadings on conjugates **14h** obtained at different reaction times

The data show that the highest platinum loading is obtained within 4 hours, even though, by a comparison with the previously synthesized conjugates, the loaded amount is lower than the one observed for **10a**-**10d**, **14e** and **15e**.

5.9 Synthesis of Conjugate 14h and 15h at Fixed Reaction Time but with Different Pt/Total Amino Groups Ratios

After fixing the reaction time at 4 hours, the conjugates were synthesized by using different Pt/amino groups ratios (such as 0.5:1, 1:1, 2:1 and 5:1) in order to evaluate the loading capability of the NPs. Some aliquots of the ethanol suspension **h** (1 mL, 78.9 mg NPs, 0.0104 mmol amino groups) were centrifuged, washed with 0.2 M HCl, ultrapure water, ethanol, anhydrous DMF and then suspended in anhydrous DMF. These suspensions were added to 1 mL of anhydrous DMF containing **8**: 2.9 mg, 0.00518 mmol (Pt/N = **0.5:1**); 5.8 mg, 0.0104 mmol (**1:1**); 11.6 mg, 0.0207 mmol (**2:1**); 28.9 mg, 0.0518 mmol (**5:1**). After the addition of an appropriate quantity of DIPEA (till a NPs agglomeration was observed), the reaction was carried out at room temperature for 4 hours.
The same procedure was employed for the synthesis of conjugates **15h**, in which some NPs suspension aliquots (1 mL, 78.9 mg NPs, 0.0104 mmol amino groups) were added to 1 mL of anhydrous DMF containing **13**: 3.0 mg, 0.00518 mmol (**0.5:1**); 5.9 mg, 0.0104 mmol (**1:1**); 11.8 mg, 0.0207 mmol (**2:1**); 29.6 mg, 0.0518 mmol (**5:1**). Then DIPEA was added and the reaction was performed at room temperature for 4 hours.
The suspensions were centrifuged (9000 rpm, 15 minutes) and the conjugates were washed with ultrapure water and ethanol.

5.9.1 Quantification of the Pt Content in 14h and 15h (Different Pt/Amino Groups Ratios)

An aliquot of the ethanol suspensions of both **14h** and **15h** (with different Pt/amines ratio) was treated as previously described (*paragraph 4.9.2*) to

quantify the Pt loading. The results are shown in *Table 5.9* for conjugates **14h** and in *Table 5.10* for conjugates **15h**. Each coupling result was the average of at least three synthetic reactions.

Conjugate	Pt/total amino groups ratio	% Pt loading	mol Pt/g NPs
14h	0.5:1	13.3 ± 1.0	1.74 (± 0.13) × 10^{-5}
	1:1	16.2 ± 0.8	1.94 (± 0.10) × 10^{-5}
	2:1	15.8 ± 1.7	1.90 (± 0.21) × 10^{-5}
	5:1	18.2 ± 0.6	2.38 (± 0.08) × 10^{-5}

Table 5.9: Pt loadings on conjugates **14h** at different Pt/amines ratios but at fixed reaction time

The coupling results for **14h** show that there are no significant differences between the different ratios. Therefore, since the 2:1 and 5:1 ratios do not lead to a considerable loading increase, the 1:1 ratio was employed for the preparation of further conjugates.

Conjugate	Pt/total amino groups ratio	% Pt loading	mol Pt/g NPs
15h	0.5:1	9.4 ± 0.3	1.23 (± 0.04) × 10^{-5}
	1:1	12.1 ± 2.0	1.45 (± 0.24) × 10^{-5}
	2:1	14.9 ± 0.5	1.79 (± 0.06) × 10^{-5}
	5:1	17.3 ± 0.9	2.26 (± 0.11) × 10^{-5}

Table 5.10: Pt loadings on conjugates **15h** at different Pt/amines ratios but at fixed reaction time

In the case of **15h**, the results show that there is an increase of the Pt loading by increasing the amount of complex employed in the synthesis. However, since

the increase is not significant, the ratio was fixed at 1:1 in order to avoid the employment of large amount of Pt(IV) complex and to use the same procedure described for the conjugate **14h**.

5.9.2 Characterization of Conjugates 14h and 15h with 1:1 Pt/Total Amino Groups Ratio

The two conjugates were analyzed by means of DLS and TEM in order to verify their size and then the ζ potential values were determined to evaluate their suspensions stability. The results are shown in *Table 5.11* and *Figure 5.23*.

Conjugate	DLS diameter	ζ potential	TEM diameter
14h (1:1 ratio)	126 ± 3 nm	19 ± 1 mV	49 ± 3 nm
15h (1:1 ratio)	127 ± 4 nm	17 ± 1 mV	52 ± 5 nm

Table 5.11: Size and suspension stability results of conjugates **14h** (1:1 ratio) and **15h** (1:1 ratio)

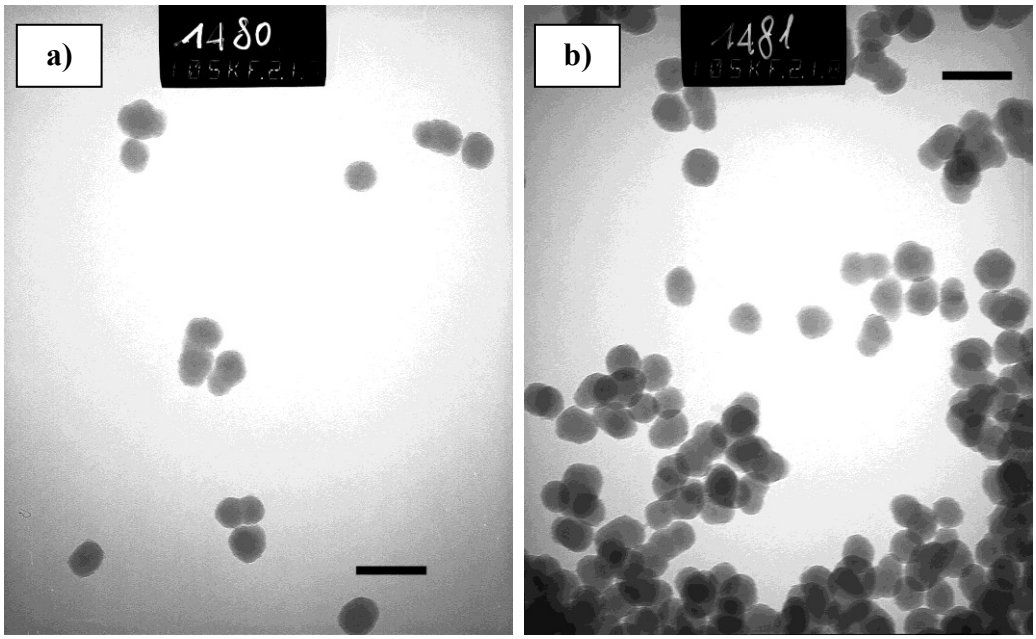

Figure 5.23: TEM micrographs of conjugates a) **14h** (1:1 ratio) and b) **15h** (1:1 ratio). The bars represents 100 nm

An increase in the NPs size by passing from TEM to DLS (*Table 5.11* and *Figure 5.23*) is observed also in this case, due to the hydrodynamic radius present in aqueous solutions. Moreover, the comparison between NPs **h** and conjugates **14h** (1:1 ratio) and **15h** (1:1 ratio) points out that, after the coupling with the Pt(IV) complexes, there is not a significant size increase: the dimensions are preserved.

As regards the ζ potential values (*Table 5.11*), they are lower than +30 mV, indicating a limited stability because the attractive forces begin to prevail over the repulsive ones. However, in the case of **14h** (1:1 ratio) and **15h** (1:1 ratio), no aggregation processes were observed. Moreover, ζ potential values result to be decreased with respect to the free NPs **h**: in fact, they turn from about +26 mV to about +20 mV. This fact can be attributed to the coupling of some amino groups, causing a decrease of the positive charge and, therefore, of the ζ potential values.

5.9.3 Releases from Conjugates 14h and 15h: Spontaneous and in Reducing Conditions

The spontaneous Pt release from **14h** and **15h**, in the absence of any reducing agents, was verified by mechanically stirring the conjugates (after being dried) in 1 mM HEPES buffer solution (pH 7.4). After 1, 4 or 8 hours, the suspensions were centrifuged (9000 rpm, 15 minutes) and the platinum content in the solutions was measured by ICP-MS.

The results indicate that only the 5 % (± 1) of the total loaded complex is detached, independently on the time and on the renewal of the buffer solution. These data show that the synthesized conjugates are hydrolytically stable (after the renewal of the solution no further release was observed, unlike conjugate **10b**) and the first amount detached could be attributed to possible multilayers, obtained due to the long silanization time [2].

In the presence of ascorbic acid (10-fold molar excess respect to Pt), the release test for **14h** gave the results reported in *Table 5.12*:

Conjugate	Test time	% released Pt (respect to the total Pt loaded on 14h)
14h	1 h	35 ± 1
	4 h	51 ± 3
	8 h	71 ± 2

Table 5.12: Pt release from conjugate **14h** in reducing conditions (i.e. in the presence of ascorbic acid)

The data show that the platinum complex is progressively released due to the action of the ascorbic acid, which allows the so-called activation by reduction, which can go to completion within 24 hours, ensuring a complete reduction into the cells during the viability assays (i.e. 72 hours).
For conjugate **15h**, instead, as observed in *paragraph 5.6.3*, this reducing agent does not show a significant effect: only the 10% (± 2) of the total Pt loaded was released within 24 hours.

5.10 Biological In Vitro Studies

After the phase of characterization of the synthesized nano-systems **14e**, **15e**, **14h** (1:1 ratio) and **15h** (1:1 ratio), their *in vitro* ability in the inhibition of the cell growth and proliferation (IC_{50}) and their cellular accumulation were verified.

5.10.1 The Antiproliferative Activity (IC_{50})

The conjugates **14e**, **15e**, **14h**, **15h**, and complexes **7** and **12** were tested on human ovarian carcinoma A2780 cell line, grown in RPMI 1640 medium. This latter was supplemented with L-glutamine (2 mM), penicillin (100 IU/mL), streptomycin (100 mg/L) and 10% fetal bovine serum (FBS).
The treatments were performed at 37 °C in a 5% CO_2 humidified chamber and cells were continuously treated for 72 hours. Then, in order to evaluate the remaining cellular viability, after the treatment with the previously mentioned compounds, the resazurin reduction assay was employed [14]. In particular, at the end of the treatment, the viability was assayed by 100 μg/mL resazurin in fresh medium for 1 hour at 37 °C: the live cells with an active metabolism are

able to reduce resazurin in resorufin and, then, this latter was measured by means of its fluorescence with a Tecan Infinite F200Pro plate reader. Fluorescence (excitation λ at 535 nm, emission λ at 595 nm) is directly proportional to the cell viability.

Each IC_{50} value (*Table 5.13* and *Figure 5.24*), derived from the dose-response sigmoids, was obtained as a mean of at least three independent replicates and the data were normalized to 100% of viability for not-treated cells and the fluorescence/absorbance of the medium without cells was used as blank.

Compound	**IC_{50} (μM)**
cisplatin	0.5 ± 0.1
7	5.02 ± 0.66
14e	0.015 ± 0.004
15e	0.020 ± 0.005
12	20.5 ± 1.7
14h	0.240 ± 0.071
15h	0.280 ± 0.037

Table 5.13: IC_{50} values of the conjugates, compared to the two free Pt(IV) complexes **7** and **12** and to cisplatin, on A2780 cells

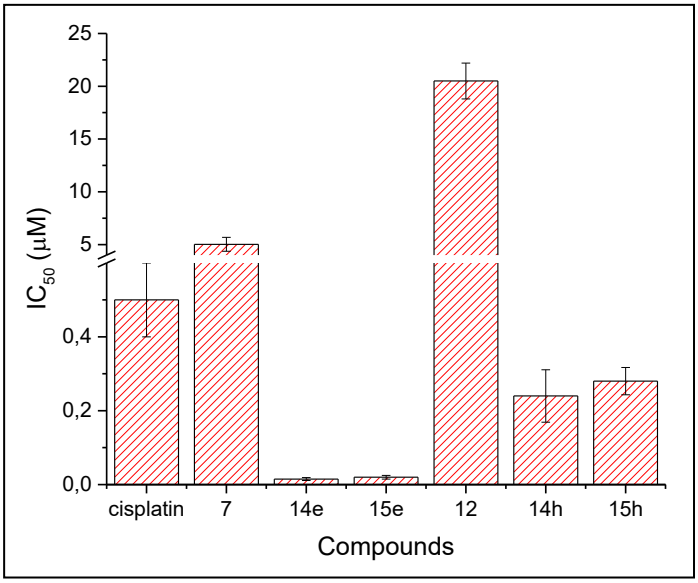

Figure 5.24: Bars graph of the IC_{50} values on A2780 cell line

The results allow to evaluate that all the conjugates are more effective than cisplatin and free Pt(IV) complexes. Moreover, these latter are less cytotoxic with respect to cisplatin itself (in particular, **12** is less active than **7**).

These data, compared to the results shown in *paragraph 4.19.1*, indicate that **14e** and **15e** have a very similar antiproliferative activity to the one observed for **10b-10d** (*Figure 5.25*). However, conjugates **14h** and **15h** are less effective (of about one order of magnitude) than **10b-10d**.

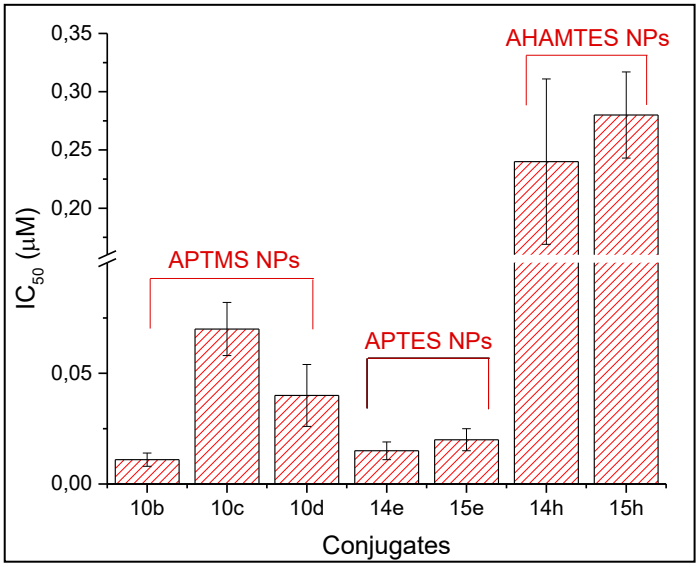

Figure 5.25: Bars graph of the IC_{50} values for all the conjugates (i.e. **10b-10d**, **14e** and **15e**, **14h** and **15h**)

5.10.2 The Cellular Accumulation

In order to find a possible reason of the lower cytotoxicity of **14h** and **15h**, their cellular accumulation was measured to evaluate the possible correlation between the IC_{50} value and the accumulation of the drug into the cells.

In particular, 10 μM suspensions of the conjugates **14e**, **15e**, **14h**, **15h** and 10 μM solutions of the platinum complexes (i.e. cisplatin, **7** and **12**) were tested on A2780 human ovarian carcinoma cell line. After 4 h treatment, 100 μL of culture medium were harvested to measure the neat extracellular platinum concentration (to take into account the adsorption on plasticware) and the cells were washed three times in PBS, detached from the 25 cm^2 flasks using 1 mL of 0.05% Trypsin EDTA and harvested in fresh complete medium. An automatic cell counting device was used to measure the cells number and the mean diameter from every cell count. About 5×10^6 cells were transferred into a glass tube and spun at 1100 rpm for 5 minutes at room temperature. The supernatant

was almost completely removed by aspiration (200 µL were left) and the cell pellet was stored at -20 °C. Before ICP-MS measurement, the pellet was defrosted and 350 µL of 70% w/w HNO_3 were added to each glass tube. The samples were mineralized for 1 hour at 60 °C in an ultrasonic bath and then diluted with a 1% v/v HNO_3 aqueous solution (by adding 5650 µL) to a final 3% v/v of acid concentration. The platinum content present in each solution was quantified by means of ICP-MS.

The results were expressed as µM Pt concentration.

The data processing, after the normalization of the Pt amount found into the cells upon the cells number and volume (calculated from the actual mean cell diameter of every sample) allowed to obtain the intracellular platinum concentration. The ratio between the intra- and extracellular concentration of Pt allowed to obtain the AR value of each sample. The obtained AR data are shown in *Table 5.14* and *Figure 5.26*.

Compound	**AR**
cisplatin	1.4 ± 0.6
7	0.38 ± 0.09
14e	68.44 ± 11.89
15e	55.00 ± 10.50
12	0.22 ± 0.01
14h	31.71 ± 2.27
15h	33.98 ± 5.94

Table 5.14: Accumulation Ratio values on A2780 cell line

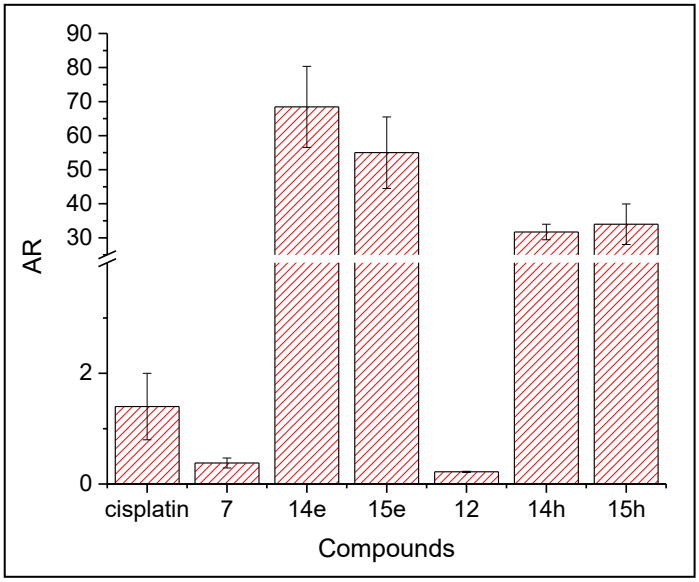

Figure 5.26: Bars graph of the AR values on A2780 cells

The results show that all the conjugates are accumulated into the cells more than cisplatin and the free platinum complexes: in particular, the order of magnitude of the AR value is the same observed for **10b-10d** (*Figure 5.27*).

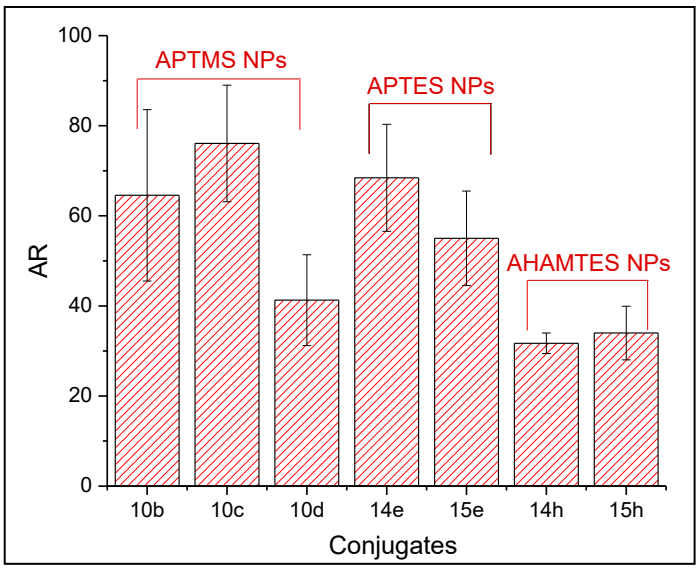

Figure 5.27: Comparison of the AR values of the three types of conjugates (i.e. **10b-10d**, **14e** and **15e**, **14h** and **15h**)

As regards the higher efficacy of **14e** and **15e** than the hydrolytically stable **14h** and **15h**, it can be justified by their higher cellular accumulation: the lower amino groups density on NPs **h** (functionalized with AHAMTES) than the NPs **e** (with APTES) leads to a lower amount of drug accumulated into the cells. The lower AR and, in turn, the antiproliferative activity can be explained also by considering the ζ potential: in fact, positively charged nanoparticles are accumulated by endocytosis mechanisms much more than the ones with negative charges [16, 17, 18] and a positive ζ potential value of the NPs favored the electrostatic interaction with the cell membrane. According to these considerations, conjugates **14e** and **15e** were more accumulated than conjugates **14h** and **15h** by virtue of their higher ζ potential.

5.11 Conclusions

In this chapter, two monofunctionalized Pt(IV) complexes were synthesized and coupled to two different types of amino-functionalized nonporous silica nanoparticles: the first was decorated with the aminopropyl arm APTES (**e**), whereas the second with the aminohexylaminomethyl arm AHAMTES (**h**). Spontaneous release tests of all the conjugates (**14e**, **15e**, **14h** and **15h**) were performed in buffer solution (pH 7.4) and showed that the NPs **h** were hydrolytically stable (unlike NPs **e**, which behaved like the nanoparticles described in *Chapter IV*). In the presence of ascorbic acid, the conjugates **14e** and **14h** showed an almost complete release due to the typical activation by reduction of Pt(IV) compounds, whereas **15e** and **15h** did not release a large amount of complex (this behavior was observed also for other acetylamido species). However, since many reducing agents are present into the tumor cells, the active metabolite is ensured to be formed.

Then, the four conjugates were tested on A2780 cell line: their antiproliferative activities and cellular accumulations resulted to be much higher than cisplatin and the free Pt(IV) complexes (**7** and **12**), due to the internalization mechanisms by endocytosis. However, the higher stability of conjugates **14h** and **15h** was not accompanied by an increase of the *in vitro* cytotoxic activity.

In any case, the results confirm that NPs are vectors able to ensure more enhanced *in vitro* cellular accumulation and antiproliferative activity than a free platinum complex. Moreover, thinking about *in vivo* application, it is important to have a delivery system with a more controlled release such as in the case of hydrolytically stable NPs.

5.12 Perspectives

Aiming at exploiting the previously prepared silica NPs with different kinds of Pt(IV) complexes functionalized with a 4-carboxypropanoato, another Pt(II) complex was synthesized: a tridentate aromatic ligand (i.e. a terpyridine) was used to prepare cationic monodentate Pt(II) complexes able to interact with DNA in a different manner with respect to cisplatin. Such complexes could intercalate DNA (apart from coordination) and could also interact with a particular structure of DNA: the quadruple helix DNA [19].

Only some regions of DNA show this unusual structure: in particular, the guanine rich sequences. If four of these DNA sequences occupy adjacent positions, a quadruple helix structure can be formed (through hydrogen bonds among four guanines) and it is called G-quadruplex (*Figure 5.28*). These conformations are stabilized by ions or charged molecules which are placed in the middle of the structure itself.

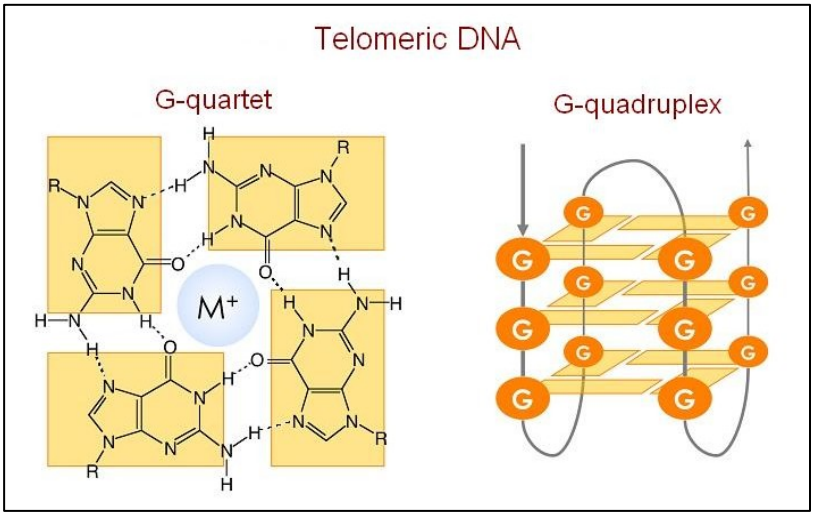

Figure 5.28: Schematic representation of G-quadruplex DNA structure. The picture is adapted from literature [20]

The G-quadruplex affects the activity of a particular enzyme, the telomerase (regulating the elongation process of telomeres, i.e. the end of chromosomes), which is involved in almost all the tumor processes. For this reason, the G-quadruplex structures are emerging as new distinctive targets for the development of new anticancer drugs. In this regard, in recent years, many studies are being carried out for the design and synthesis of new and efficient G-quadruplex ligands, which must show a higher affinity for the quadruple helix than for the double one.

The main requirements of these ligands for the stabilization of the quadruple helix are a large aromatic planar surface, the presence of positive charges and the stacking ability. These characteristics can be found in metal complexes with a positive charge that allows them to effectively bind to the negatively charged G-quadruplex DNA. In particular, square planar copper(II) and nickel(II) complexes are effective stabilizers of telomeres. Furthermore, porphyrins- and terpiridine-based ligands were tested and the Cu(II) and Pt(II) complexes resulted to be more selective for the G-quadruplex than for the double helix

[21]. This latter feature makes these compounds suitable for the use as anticancer drugs: in fact, their lower affinity for the double helix results in a reduction of side effects. To increase this affinity it is possible to employ ligands containing more than one planar polyaromatic interconnected structure (for example, anthracene). In this regard, a recent study was focused on the synthesis of platinum(II) and copper(II) complexes, coordinated to an anthracene-terpyridine ligand [22].

In the following paragraphs, the syntheses and characterizations of some platinum complexes containing terpyridine are described and they are exploitable for future coupling reactions with amino-functionalized vectors, suitable for passive Drug Targeting and Delivery (DTD) strategies.

The synthesized platinum complexes are here reported:

- (SP-4-3)-dichlorido((1*Z*,5*Z*)-cycloocta-1,5-diene)platinum(II) (**16**),
- (SP-4-3)-chlorido(2,2':6',2''-terpyridine)platinum(II) chloride (**17**),
- (OC-6-33)-chloridodihydroxido(2,2':6',2''-terpyridine)platinum(IV) chloride (**18**),
- (OC-6-33)-(4-carboxypropanoato)chloridohydroxidoplatinum(IV) (**19**).

5.12.1 Synthesis of the (SP-4-3)-dichlorido((1Z,5Z)-cycloocta-1,5-diene)platinum(II) (16)

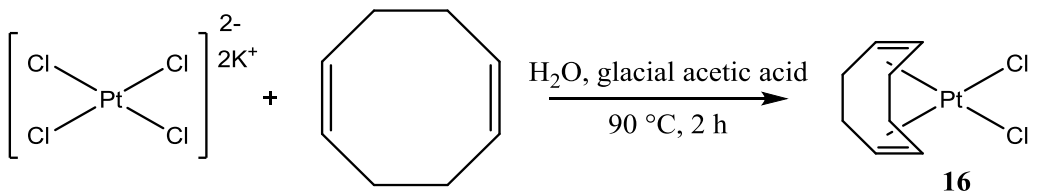

16

Potassium tetrachloroplatinate(II) (1.00 g, 2.41 mmol) was dissolved in 16 mL of ultrapure water and the red solution was filtered to remove possible solid

residues. Then, 24 mL of glacial acetic acid and (1*Z*,5*Z*)-cycloocta-1,5-diene (COD, 1.00 mL, 8.15 mmol) were added and the mixture was magnetically stirred for 2 hours in a steam bath at 90 °C, in the dark. During this time, the solution changed color (from red to pale yellow) and a white solid precipitated in the mixture. When significant changes were no more observed, ¾ of the volume were removed under reduced pressure. Subsequently, the solid was collected by centrifugation and was washed three times with ultrapure water, three times with ethanol and once with diethyl ether. The white reaction product was dried *in vacuo*.

Yield: 703 mg, 1.88 mmol, 78.0%.

5.12.2 Characterization of the Complex

^{1}H-NMR

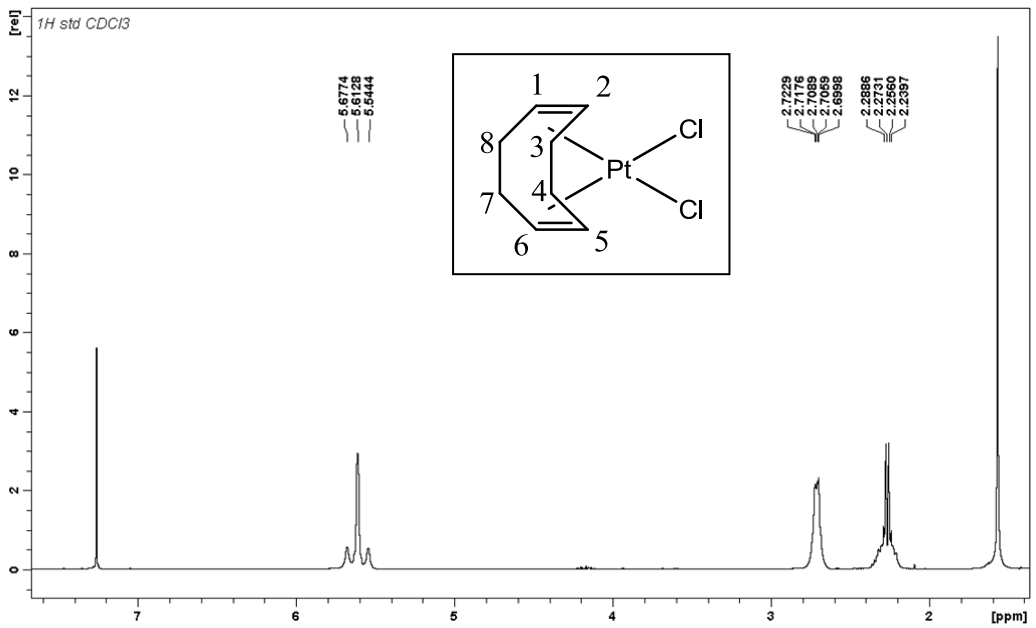

Figure 5.29: ^{1}H-NMR spectrum of complex **16**, registered in $CDCl_3$

The ^{1}H-NMR (500 MHz, $CDCl_3$) spectrum of complex **16** (*Figure 5.29*) shows the following signals, δ: 2.27 and 2.71 (m, H3, H4, H7, H8, 8H), 5.61 (m, H1, H2, H5, H6, 4H) ppm.

^{13}C-NMR

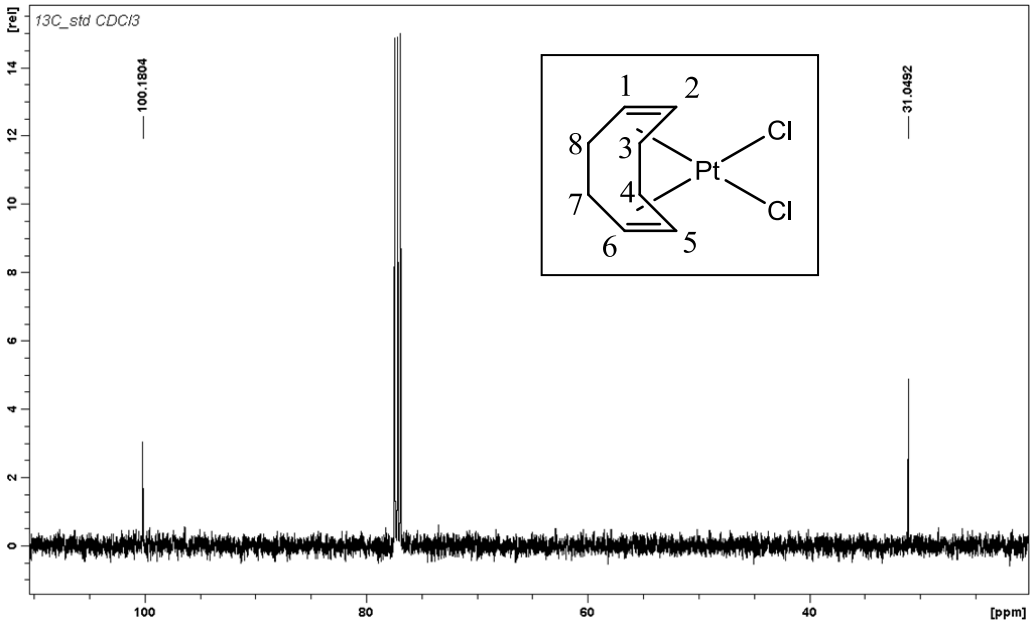

Figure 5.30: ^{13}C-NMR spectrum of complex **16**, registered in $CDCl_3$

The ^{13}C-NMR (125.7 MHz, $CDCl_3$) spectrum of complex **16** (*Figure 5.30*) shows the following signals, δ: 31.0 (C3, C4, C7, C8), 100.2 (C1, C2, C5, C6) ppm.

^{195}Pt-NMR

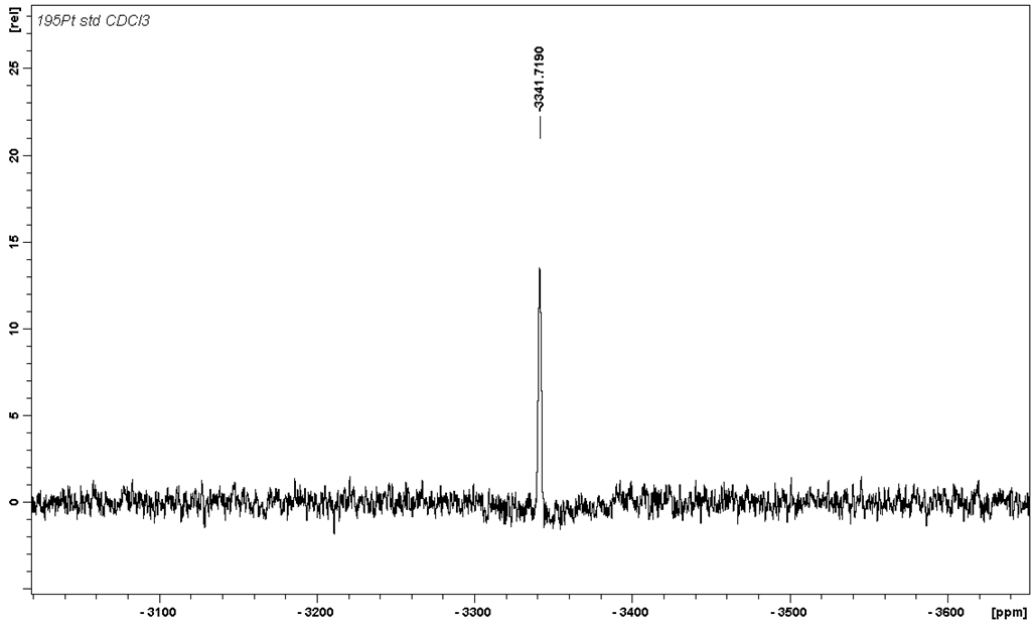

Figure 5.31: ^{195}Pt-NMR spectrum of complex **16**, registered in $CDCl_3$

The ^{195}Pt-NMR spectrum (*Figure 5.31*) of complex **16** (with a 107.2 MHz NMR frequency) shows a signal at -3342 ppm: it is consistent with a Pt(II) complex containing two chlorides and the (1Z,5Z)-cycloocta-1,5-diene ligand.

The preparation of the Pt(II)-terpyridine precursor successfully occurred and this complex was employed for the synthesis of the desired Pt(II) **17**.

5.13 Synthesis of the (SP-4-3)-chlorido(2,2':6',2''-terpyridine)platinum(II) Chloride (17)

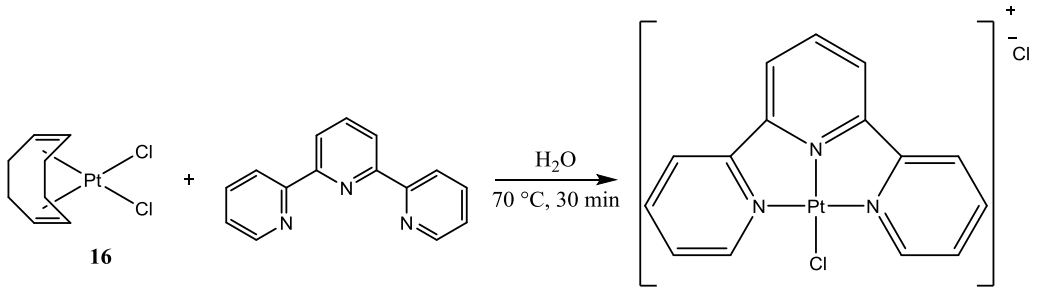

Complex **16** (154 mg, 0.412 mmol) was suspended in 10 mL of ultrapure water. Then, terpyridine (101 mg, 0.433 mmol) was added to the mixture, which was magnetically stirred for 30 minutes at 70 °C. After the established time, the water of the red solution was removed under reduced pressure and a red product was precipitated, washed with diethyl ether and then dried *in vacuo*.
Yield: 170 mg, 0.341 mmol, 82.7%.

5.13.1 Characterization of the Complex

RP-HPLC-ESI-MS

The analysis was performed by employing a stationary phase consisting of a C18 Phenosphere-NEXT column 5 μm, 250 × 4.60 mm ID, a mobile phase composed by a 70:30 mixture of a 15 mM aqueous solution of formic acid and pure methanol (by isocratic elution), a flow rate of 0.500 mL/min, a temperature of 37 °C and the UV-Visible detector set at 210 nm. In this case, the sample was prepared by dissolving it in a 20 mM NaCl aqueous solution in order to avoid

the complex hydrolysis, i.e. the loss of the chloride ligand and its replacement by a water molecule, typical of the Pt(II) species in water. Compound **17** showed a retention time of 10.91 minutes and its identity was attributed by the corresponding ESI-MS spectrum (*Figure 5.32*).

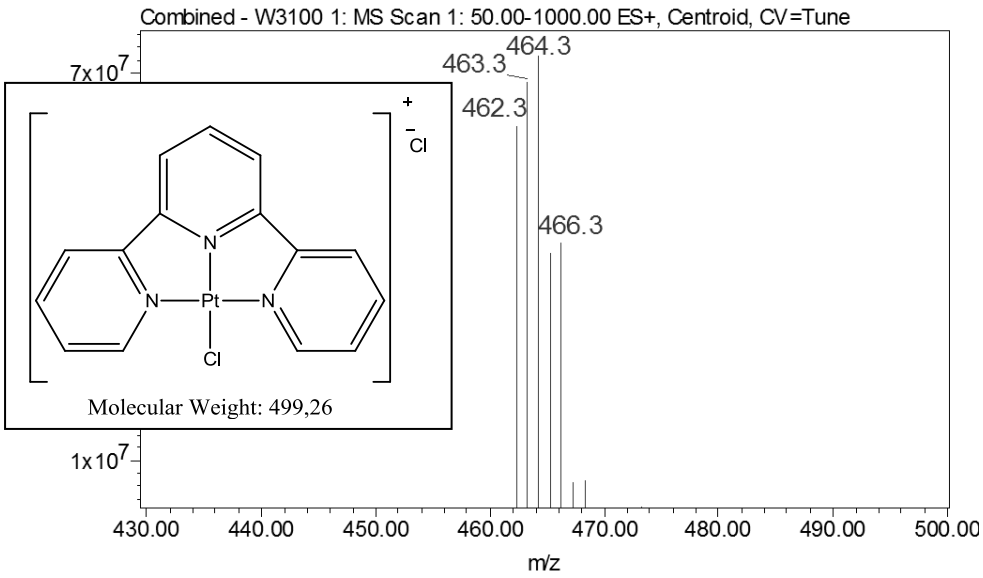

Figure 5.32: ESI-MS spectrum of complex **17**, prepared in a 20 mM NaCl solution

The ESI-MS spectrum (*Figure 5.32*), registered in positive ion mode with a cone voltage of 30V, shows a value at 464.3 m/z, corresponding to the species $[M\text{-}Cl]^+$ of complex **17** and this confirms the success of the reaction.

[1]H-NMR

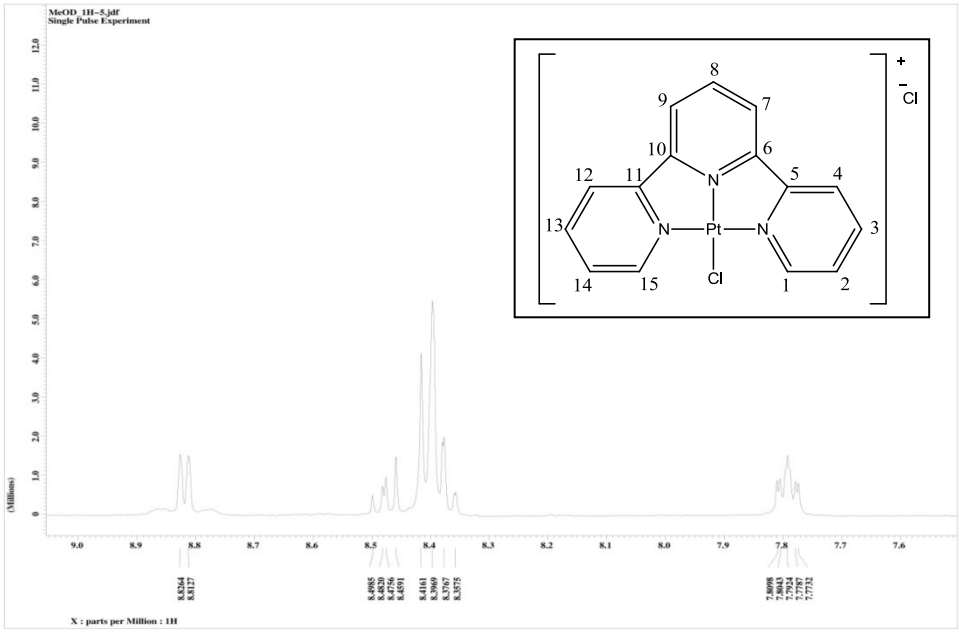

Figure 5.33: [1]H-NMR spectrum of complex **17**, registered in MeOD-d_4

The [1]H-NMR (400 MHz, MeOD-d_4) spectrum of complex **17** (*Figure 5.33*) shows the following signals, δ: 7.79 (m, H2, H14, 2H), 8.40 (m, H1, H15, H3, H13, H7, H9, 6H), 8.47 (m, H8, 1H), 8.82 (m, H4, H12, 2H) ppm.

^{13}C-NMR

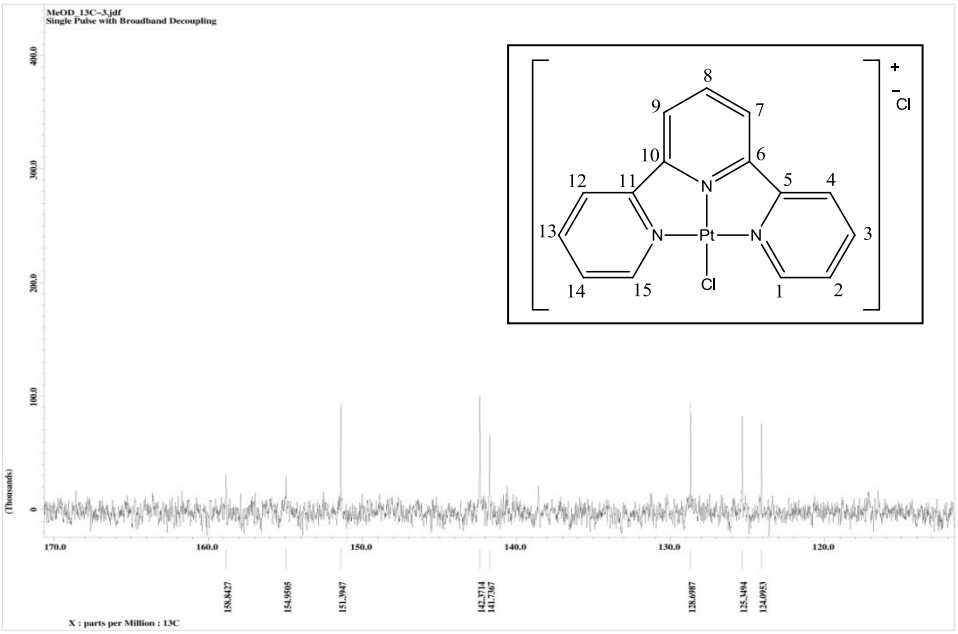

Figure 5.34: ^{13}C-NMR spectrum of complex **17**, registered in MeOD-d_4

The ^{13}C-NMR (100.6 MHz, MeOD-d_4) spectrum of complex **17** (*Figure 5.34*) shows the following signals, δ: 124.1 (C2, C14), 125.3 (C7, C9), 128.7 (C4, C12), 141.7 (C8), 142.4 (C3, C13), 151.4 (C1, C15), 154.9 (C6, C10), 158.8 (C5, C11) ppm.

^{195}Pt-NMR

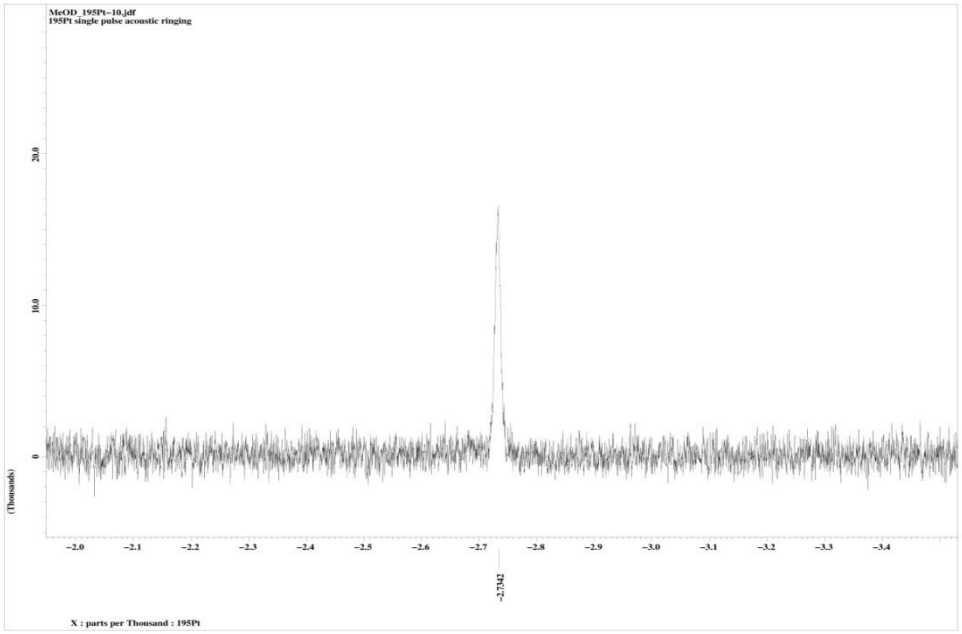

Figure 5.35: ^{195}Pt-NMR spectrum of complex **17**, registered in MeOD-d_4

The ^{195}Pt-NMR spectrum (*Figure 5.35*) of complex **17** (with a 86.0 MHz NMR frequency) shows a signal at -2734 ppm, consistent with a Pt(II) complex with one chloride and three amines.

This complex was successfully prepared and the subsequent phase consisted of its oxidation by the use of hydrogen peroxide, in order to synthesize a more stable and inert Pt(IV) compound.

5.14 Synthesis of the (OC-6-33)-chloridodihydroxido(2,2':6',2''-terpyridine)platinum(IV) Chloride (18)

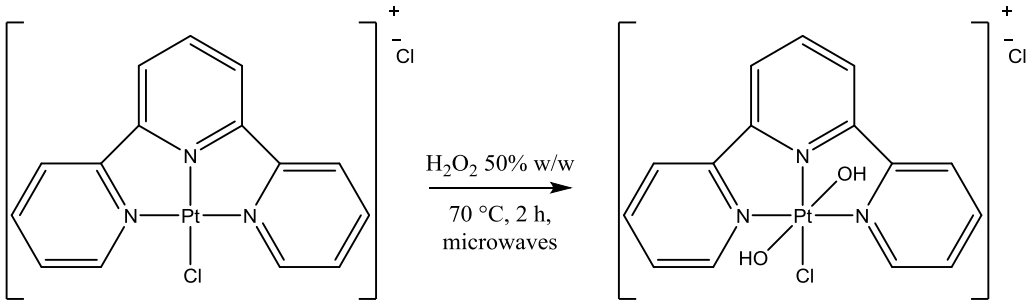

17 **18**

Complex **17** (40.0 mg, 0.0801 mmol) was dissolved in a 50% w/w aqueous solution of hydrogen peroxide (2.00 mL, 35.2 mmol) and the reaction was assisted by microwaves by using a CEM Discover® SP System, equipped with a focused single mode and self-tuning cavity, an air cooling system, an automated power control based on temperature feedback, and was performed for 2 hours at 70 °C. After the established time, the water of the yellow solution was removed under reduced pressure. The yellow compound was collected by adding acetone/diethyl ether, washed with diethyl ether and then dried *in vacuo*.
Yield: 35.0 mg, 0.0656 mmol, 81.9%.

5.14.1 Characterization of the Complex

RP-HPLC-ESI-MS

The analysis was performed by employing a stationary phase consisting of a C18 Phenosphere-NEXT column 5 μm, 250 × 4.60 mm ID, a mobile phase composed by a 70:30 mixture of a 15 mM aqueous solution of formic acid and

pure methanol (by isocratic elution), a flow rate of 0.500 mL/min, a temperature of 37 °C and the UV-Visible detector set at 210 nm. Compound **18** showed a retention time of 3.95 minutes and its identity was attributed by the corresponding ESI-MS spectrum (*Figure 5.36*).

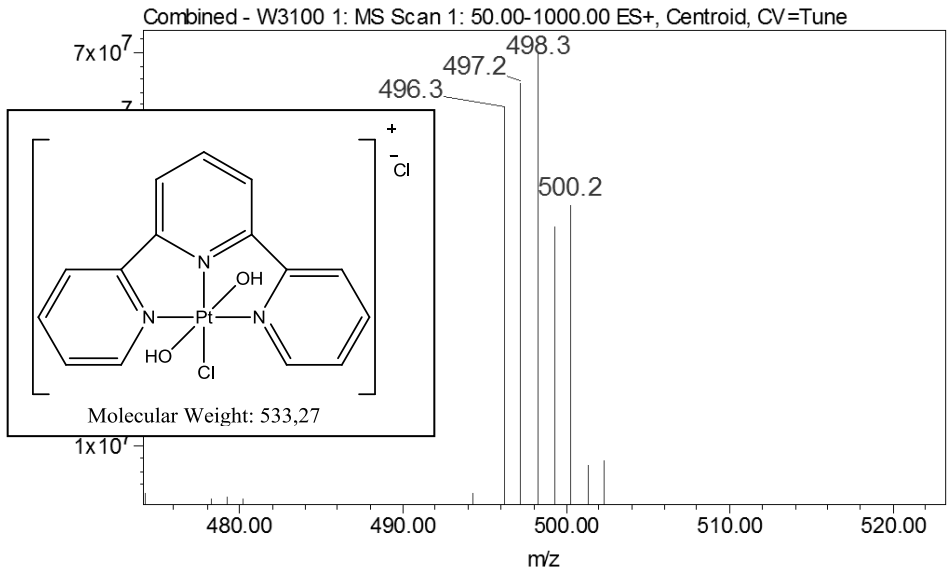

Figure 5.36: ESI-MS spectrum of complex **18**, prepared in ultrapure water

The ESI-MS spectrum (*Figure 5.36*), registered in positive ion mode with a cone voltage of 30V, confirms the presence of the desired product: in fact, a value at 498.3 m/z, corresponding to the species $[M\text{-}Cl]^+$ of complex **18**, is observed.

[1]H-NMR

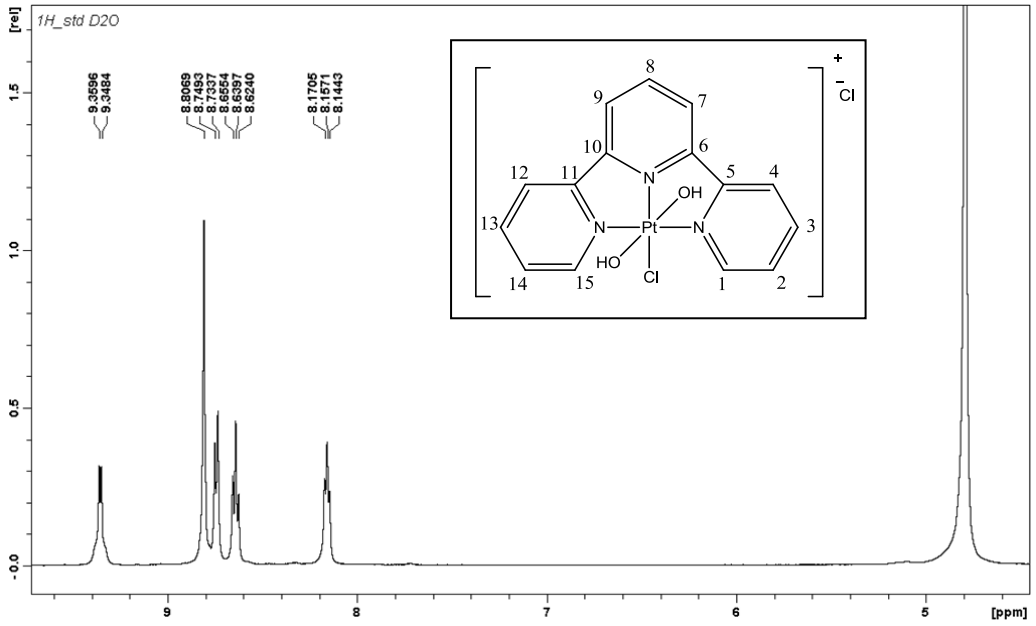

Figure 5.37: [1]H-NMR spectrum of complex **18**, registered in D_2O

The [1]H-NMR (500 MHz, D_2O) spectrum of complex **18** (*Figure 5.37*) shows the following signals, δ: 8.16 (t, H2, H14, 2H, ^3J = 6.7 Hz), 8.64 (t, H7, H9, 2H, ^3J = 7.8 Hz), 8.73 (d, H1, H15, 2H, ^3J = 7.8 Hz), 8.81 (s, H3, H8, H13, 3H), 9.35 (d, H4, H12, 2H, ^3J = 5.6 Hz) ppm.

^{13}C-NMR

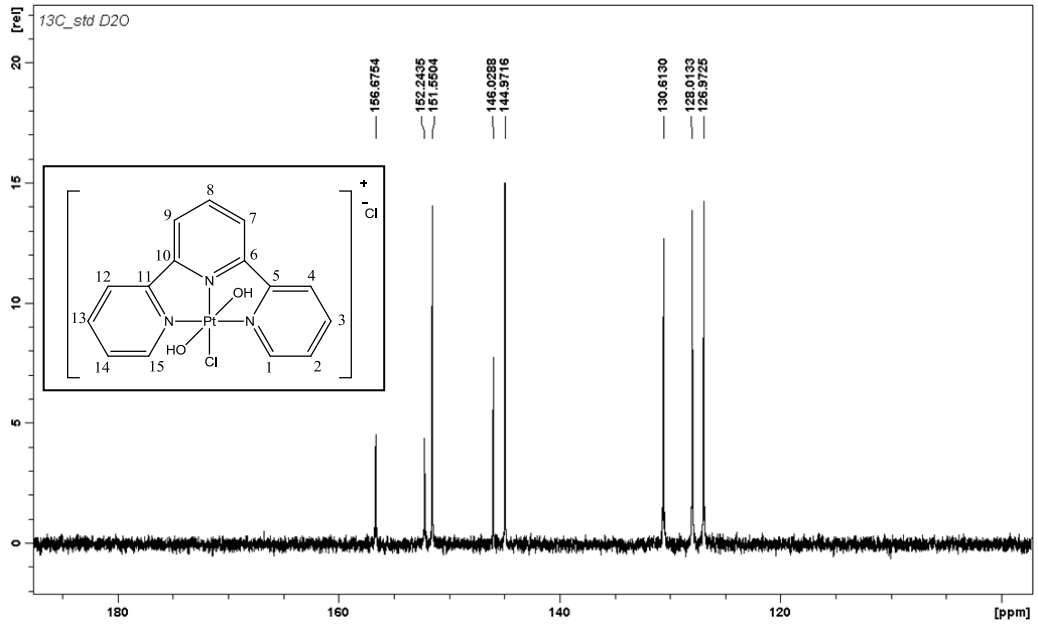

Figure 5.38: ^{13}C-NMR spectrum of complex **18**, registered in D_2O

The ^{13}C-NMR (125.7 MHz, D_2O) spectrum of complex **18** (*Figure 5.38*) shows the following signals, δ: 126.9 (C2, C14), 128.0 (C7, C9), 130.6 (C4, C12), 144.9 (C3, C13), 146.0 (C8), 151.6 (C1, C15), 152.2 (C6, C10), 156.7 (C5, C11) ppm.

^{195}Pt-NMR

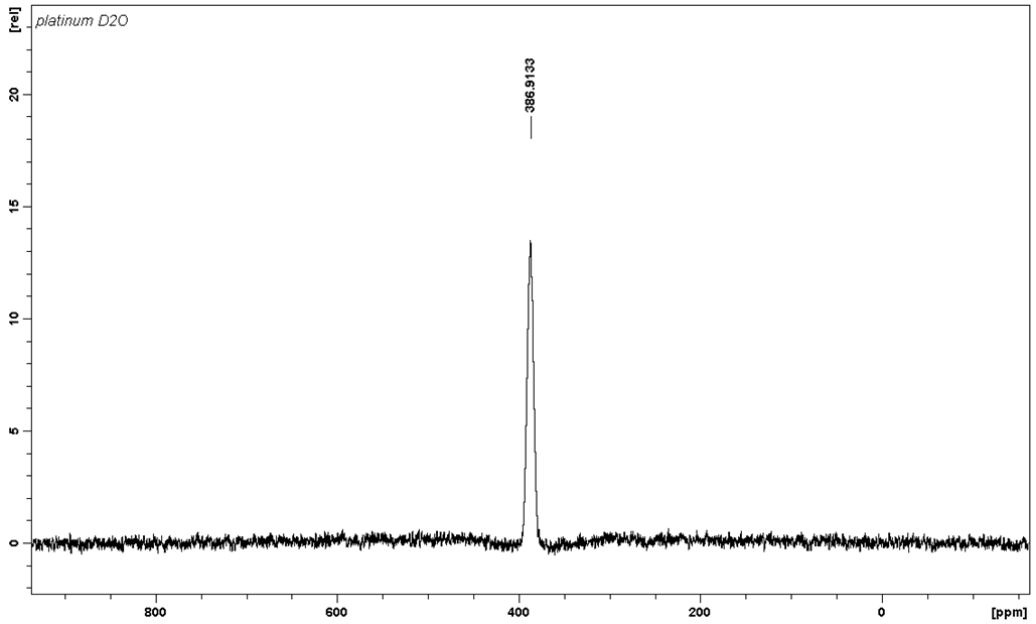

Figure 5.39: ^{195}Pt-NMR spectrum of complex **18**, registered in D_2O

The ^{195}Pt-NMR spectrum (*Figure 5.39*) of complex **18** (with a 107.2 MHz NMR frequency) shows a signal at 387 ppm, consistent with a Pt(IV) complex containing a chloride, three amines and two hydroxido ligands.

The Pt(II) oxidation occurred giving rise to a completely pure complex. However, the conditions reaction were very strict: in fact, no additional water was employed and microwaves resulted to be necessary. The prepared compound was further functionalized in order to expose a 4-carboxypropanoato group.

5.15 Synthesis of the (OC-6-33)-(4-carboxypropanoato)chloridohydroxidoplatinum(IV) (19)

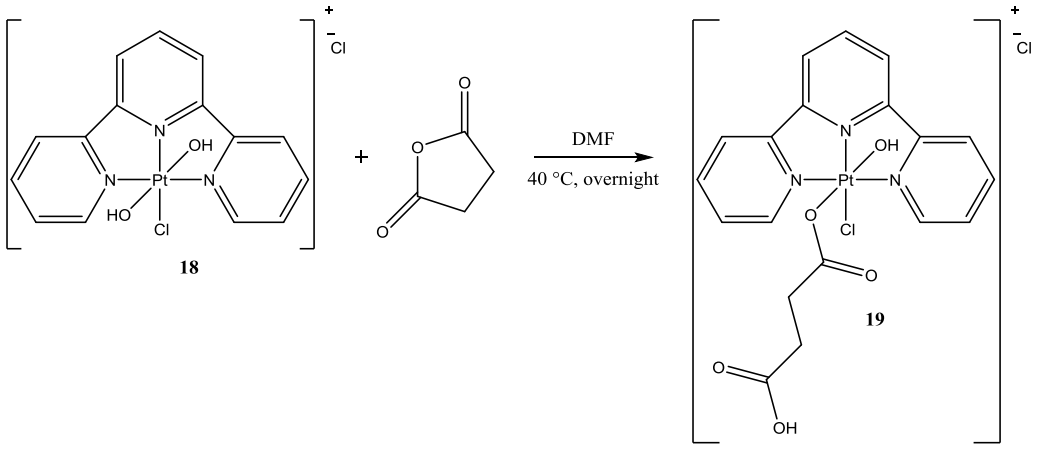

A solution of succinic anhydride (46.9 mg, 0.469 mmol) in 1 mL of DMF was added to a suspension of complex **18** (50.0 mg, 0.0938 mmol) in 2 mL of DMF and the reaction was carried out at 40 °C overnight. The solvent was then removed from the suspension under reduced pressure and an orange solid was collected by the addition of acetone/diethyl ether. It was purified with an anionic exchange resin (Amberlite® IRA-400(OH) Supelco), in which the hydroxido groups were replaced by chloride anions, and then dried *in vacuo*.
Yield: 44.8 mg, 0.0707 mmol, 75.4%.

5.15.1 Characterization of the Complex

RP-HPLC-ESI-MS

The analysis was performed by employing a stationary phase consisting of a C18 Phenosphere-NEXT column 5 μm, 250 × 4.60 mm ID, a mobile phase composed by a 90:10 mixture of a 15 mM aqueous solution of formic acid and

pure methanol (by isocratic elution), a flow rate of 0.500 mL/min, a temperature of 37 °C and the UV-Visible detector set at 210 nm. Compound **19** showed a retention time of 9.06 minutes and its identity was attributed by the corresponding ESI-MS spectrum (*Figure 5.40*).

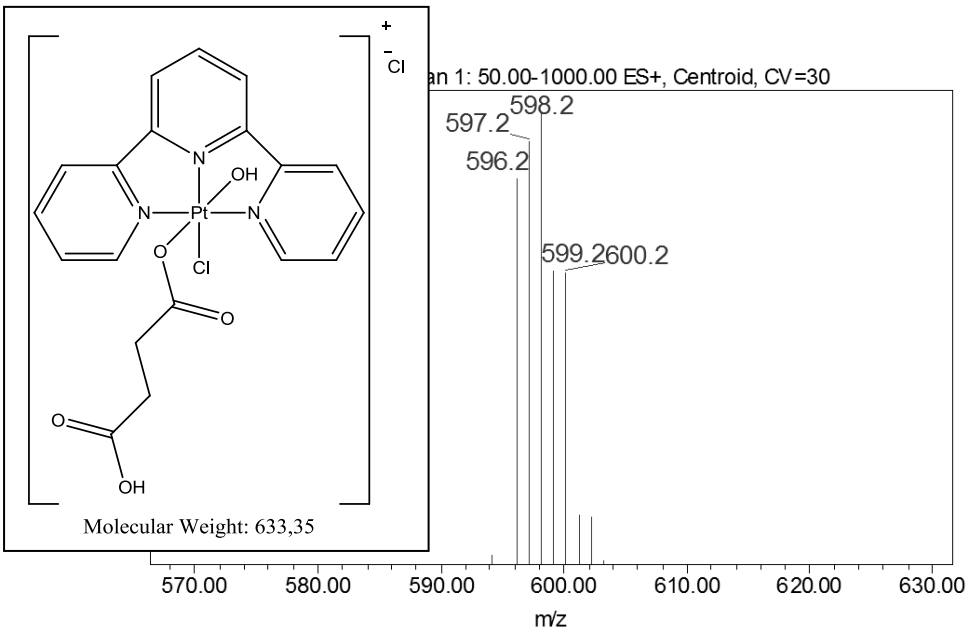

Figure 5.40: ESI-MS spectrum of complex **19**, prepared in ultrapure water

The ESI-MS spectrum (*Figure 5.40*), registered in positive ion mode with a cone voltage of 30V, shows a value at 598.2 m/z, corresponding to the species $[M\text{-}Cl]^+$ of complex **19** and this confirms that the complex was successfully synthesized.

[1]H-NMR

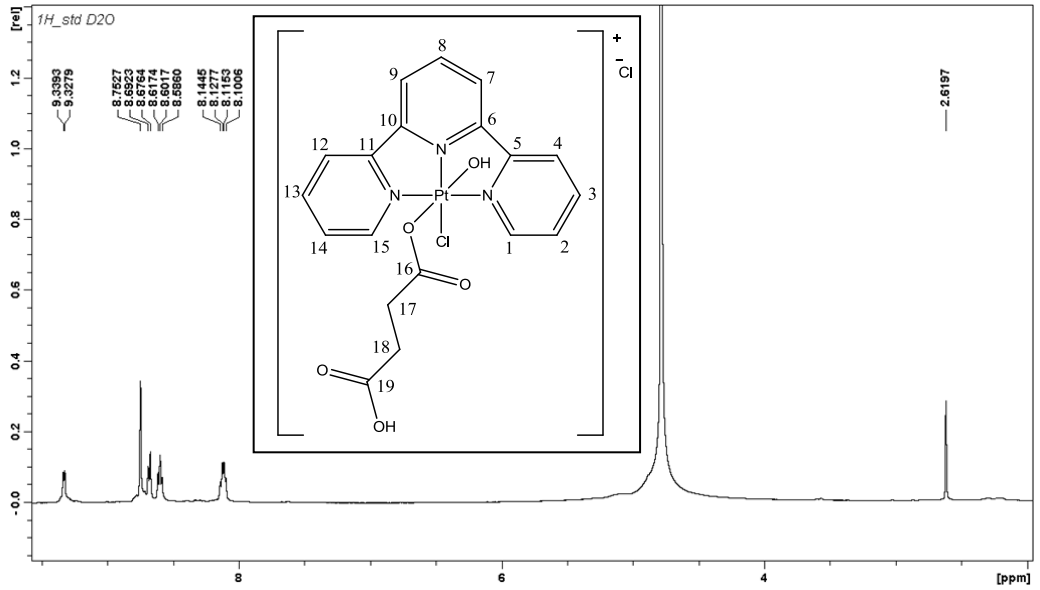

Figure 5.41: [1]H-NMR spectrum of complex **19**, registered in D_2O

The [1]H-NMR (500 MHz, D_2O) spectrum of complex **19** (*Figure 5.41*) shows the following signals, δ: 2.62 (s, H17, H18, 4H), 8.13 (m, H2, H14, 2H), 8.60 (t, H7, H9, 2H, ^3J = 7.9 Hz), 8.69 (d, H1, H15, 2H, ^3J = 7.9 Hz), 8.75 (s, H3, H8, H13, 3H), 9.34 (d, H4, H12, 2H, ^3J = 5.7 Hz) ppm.

^{13}C-NMR

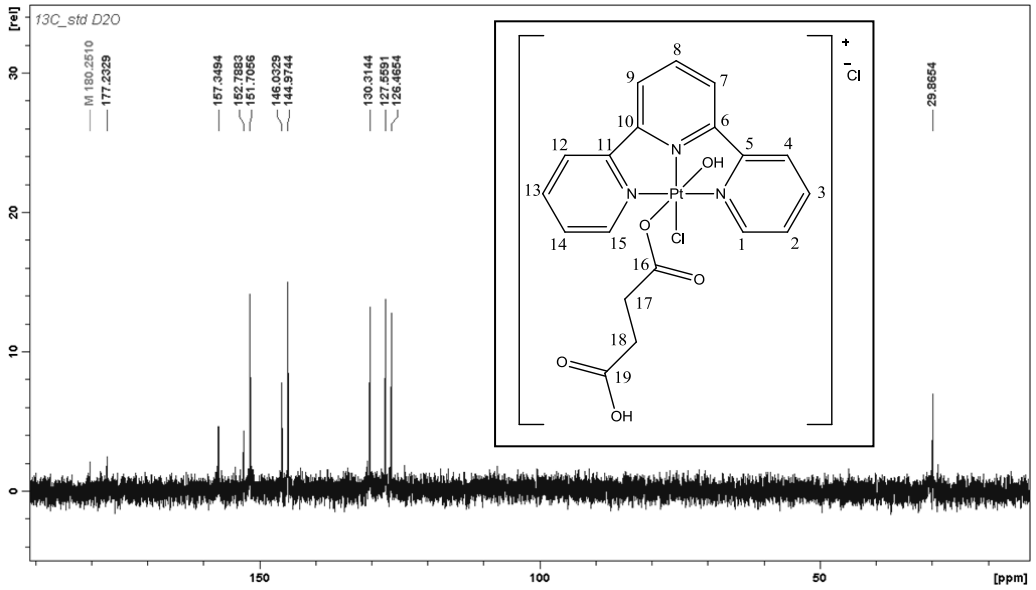

Figure 5.42: ^{13}C-NMR spectrum of complex **19**, registered in D_2O

The ^{13}C-NMR (125.7 MHz, D_2O) spectrum of complex **19** (*Figure 5.42*) shows the following signals, δ: 29.9 (C17, C18), 126.5 (C2, C14), 127.6 (C7, C9), 130.3 (C4, C12), 144.9 (C3, C13), 146.0 (C8), 151.7 (C1, C15), 152.8 (C6, C10), 157.3 (C5, C11), 177.2 (C19), 180.3 (C16) ppm.

^{195}Pt-NMR

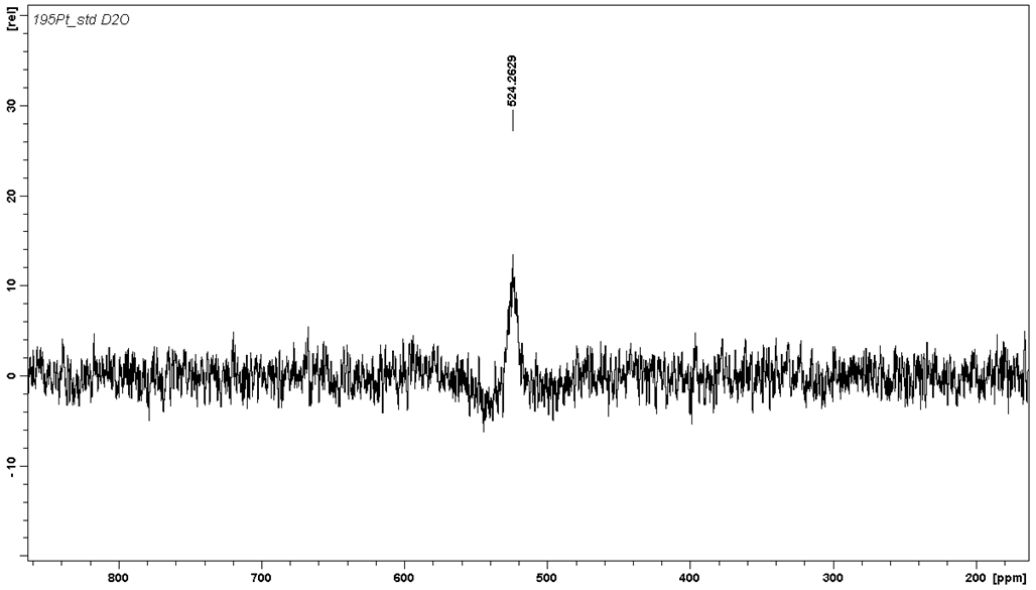

Figure 5.43: ^{195}Pt-NMR spectrum of complex **19**, registered in D_2O

The ^{195}Pt-NMR spectrum (*Figure 5.43*) of complex **19** (with a 107.2 MHz NMR frequency) shows a signal at 524 ppm: it is consistent with a Pt(IV) complex containing a chloride, three amines, a hydroxido and a succinato ligand.

The successfully synthesized complex can be exploited for further coupling reactions with amino-functionalized vectors, suitable for passive DTD strategies: this is the purpose of future projects.

References

[1] M. Zhu, M.Z. Lerum, W. Chen, How To Prepare Reproducible, Homogeneous, and Hydrolytically Stable Aminosilane-Derived Layers on Silica, *Langmuir*, 28 (2012), 416–423.

[2] E.A. Smith, W. Chen, How to Prevent the Loss of Surface Functionality Derived from Aminosilanes, *Langmuir*, 24 (2008), 12405–12409.

[3] M. Ravera, E. Perin, E. Gabano, I. Zanellato, G. Panzarasa, K. Sparnacci, M. Laus, D. Osella, Functional fluorescent nonporous silica nanoparticles as carrier for Pt(IV) anticancer prodrugs, *J. Inorg. Biochem.*, 151 (2015), 132-142.

[4] K. V. Luzyanin, M. Haukka, N. A. Bokach, M. L. Kuznetsov, V. Y. Kukushkin, A. J. L. Pombeiro, Platinum(IV)-mediated hydrolysis of nitriles giving metal-bound iminols, *J. Chem. Soc., Dalton Trans.*, (2002), 1882-1887.

[5] N. A. Bokach, V. Y. Kukushkin, M. L. Kuznetsov, D. A. Garnovskii, G. Natile, A. J. L. Pombeiro, Direct Addition of Alcohols to Organonitriles Activated by Ligation to a Platinum(IV) Center, *Inorg. Chem.*, 41 (2002), 2041-2053.

[6] B. Radziszewski, *Ber. Dtsch. Chem. Ges.*, 18 (1885), 355-356.

[7] G. Laus, Kinetics of acetonitrile-assisted oxidation of tertiary amines by hydrogen peroxide, *J. Chem. Soc., Perkin Trans. 2* (2001), 864-868.

[8] H. D. Brauer, B. Eylers, A. Lange, Formation of singlet molecular oxygen by the Radziszewski reaction between acetonitrile and hydrogen peroxide in the absence and presence of ketones, *J. Chem. Soc., Perkin Trans. 2* (2002), 1288-1295.

[9] G. Pelosi, M. Ravera, E. Gabano, F. Fregonese, D. Osella, Unprecedented one-pot synthesis of an unsymmetrical cisplatin-based Pt(IV)–acetamidato complex, *Chem. Commun.*, 51 (2015), 8051-8053.

[10] J. W. Wiench, Y. S. Avadhut, N. Maity, S. Bhaduri, G. K. Lahiri, M. Pruski, S. Ganapathy, Characterization of Covalent Linkages in Organically Functionalized MCM-41 Mesoporous Materials by Solid-State NMR and Theoretical Calculations, *J. Phys. Chem. B*, 111 (2007), 3877-3885.

[11] S. G. Vasil'ev, V. I. Volkov, E. A. Tatarinova, A. M. Muzafarov, A Solid-State NMR Investigations of MQ Silicone Copolymers, *Appl. Magn. Reson.*, 44 (2013), 1015–1025.

[12] M. Ravera, E. Gabano, I. Zanellato, F. Fregonese, G. Pelosi, J. A. Platts, D. Osella, *Dalton Trans.*, 45 (2016), 5300-5309.

[13] Y. Xie, C. A. S. Hill, Z. Xiao, H. Militz, C. Mai, Silane coupling agents used for natural fiber/polymer composites: A review, *Composites: Part A*, 41 (2010), 806–819.

[14] E. Magnani, E. Bettini, Resazurin detection of energy metabolism changes in serum-starved PC12 cells and of neuroprotective agent effect, *Brain Res. Protocol.*, 5 (2000), 266–272.

[15] A. Ghezzi, M. Aceto, C. Cassino, E. Gabano, D. Osella, Uptake of antitumor platinum(II)-complexes by cancer cells, assayed by inductively coupled plasma mass spectrometry (ICP-MS), *J. Inorg. Biochem.*, 98 (2004), 73–78.

[16] C. He, Y. Hua, L. Yin, C. Tang, C. Yin, Effects of particle size and surface charge on cellular uptake and biodistribution of polymeric nanoparticles, *Biomaterials*, 31 (2010), 3657–3666.

[17] V. Forest, M. Cottier, J. Pourchez, Electrostatic interactions favor the binding of positive nanoparticles on cells: A reductive theory, *Nano Today*, 10 (2015), 677-680.

[18] S. Salatin, S. M. Dizaj, A. Y. Khosroushahi, Effect of the surface modification, size, and shape on cellular uptake of nanoparticles, *Cell. Biol. Int.*, 39 (2015), 881-890.

[19] G. Biffi, D. Tannahill, J. McCafferty, S. Balasubramanian, Quantitative visualization of DNA G-quadruplex structures in human cells, *Nat. Chem.*, 5 (2013), 182–186.

[20] The cancer chemotherapy center of JFCR website.

[21] H. Bertrand, D. Monchaud, A. De Cian, R. Guillot, J. L. Mergny, M. P. Teulade-Fichou, The importance of metal geometry in the recognition of G-quadruplex-DNA by metal-terpyridine complexes, *Org. Biomol. Chem.*, 5 (2007), 2555-2559.
[22] S. Gama, I. Rodrigues, F. Mendes, I. C. Santos, E. Gabano, B. Klejevskaja, J. Gonzalez-Garcia, M. Ravera, R. Vilar, A. Paulo, Anthracene-terpyridine metal complexes as new G-quadruplex DNA binders, *J. Inorg. Biochem.*, 160 (2016), 275-286.

Chapter VI

Coupling Reactions with Chitosan and Chitosan Derivatives

6.1 Introduction

Chitosan is a linear polysaccharide composed of randomly distributed β-(1-4)-linked D-glucosamine and *N*-acetyl-D-glucosamine (*Figure 6.1*).

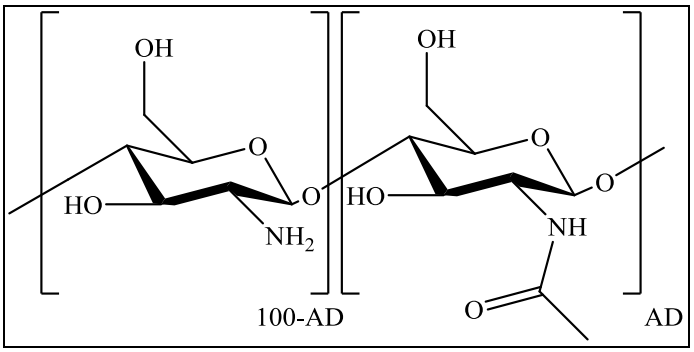

Figure 6.1: Chitosan structure with deacetylated and acetylated units (AD = acetylation degree)

This biopolymer shows several advantages that allow it to be widely employed in many fields (such as pharmaceutical, cosmetic and food industries, agriculture, etc.): in fact, it is nontoxic, biodegradable, biocompatible and it has many other biological properties [1].

Chitosan is not widely present in nature (only in some fungi, such as Mucoraceae) but it is a chitin derivative, which is the second most abundant polysaccharide in nature after cellulose and one of the main components of the exoskeleton of crustaceans and insects. In particular, it is produced by crustaceans shells [2].

Chitin is a chitosan in which there are no amines but only *N*-acetyl groups. Therefore, chitosan is obtained by means of the deacetylation of chitin, occurring by the hydrolysis under alkali conditions at high temperature (110-140 °C) for 4-6 hours: these strict conditions are necessary because the *N*-acetyl group is stable against hydrolysis due to the presence of hydrogen bonds

between C=O and N-H groups of nearby units. However, the deacetylation process is not complete and the number of *N*-acetyl groups, expressed as molar percentage, is defined acetylation degree (AD). If AD is lower than 60%, chitin is considered chitosan. Another characteristic that allows to evaluate the nature of the polysaccharide is the solubility in aqueous solution of organic acids (such as acetic acid), which is verified for AD lower than 50-60%: in fact, chitin is insoluble in such aqueous solutions (as well as in the most of the solvents), whereas chitosan in soluble [2].

Chitosan is a polycation and its charge density depends on the acetylation degree and pH [3], therefore, on the content of protonated amino groups. These latter (pKa from 6.2 to 7.0) are totally protonated in acids whose pKa is lower than 6.2: only in this conditions chitosan in soluble, whereas it cannot be dissolved in water, aqueous solutions at alkaline or physiological pH and organic solvents [4].

In order to improve the solubility in water of chitosan, it is possible to employ the much expensive chitosan oligomers or to make chemical modifications (e.g. the grafting of small cationic molecules or polymers (such as PEG [5]) on the chitosan structure or to carry out the quaternarization of the amines) [3]. In particular, in the past, many chitosan derivatives were synthesized, such as *N*-carboxymethylated chitosan (CMC) and *N*-trimethyl chitosan chloride (TMC), and this latter was highly studied because of its well-defined structure, improved solubility and easy preparation [6]. However, its synthesis requires the use of methyl iodide which is classified as a potential carcinogen. It can damage lung, liver, kidneys and, in particular, the central nervous system. Its toxicity is due to its methylating action: the enzymes that contain thiols are particularly affected and, therefore, inhibited. The lack of these enzymes in the central nervous system causes serious damages.

In order to avoid the employment of methyl iodide, another possibility was considered: the reaction of chitosan with a quaternized species [7]. This latter can overcome the solubility limits of chitosan by the exposure of a positively charged group.

Furthermore, the quaternarization allows chitosan to be soluble in water, regardless of pH, only if the quaternarization degree represents at least the 25% of the total available groups [8] and the maximum limit is about 64%.

In this chapter, chitosan from shrimp shell (low viscosity and estimated molecular weight of 60-120 kDa) was employed. Several studies were carried out to perform modifications in order to make it more soluble in aqueous solutions, independently of the pH: in particular, the (3-carboxypropyl)trimethylammonium chloride was used. Then the modified chitosan was coupled to the complex **8**, the activated form of (OC-6-44)-diammine(4-carboxypropanoato)dichloridoethanolatoplatinum(IV) (**7**) (*Figure 6.2*).

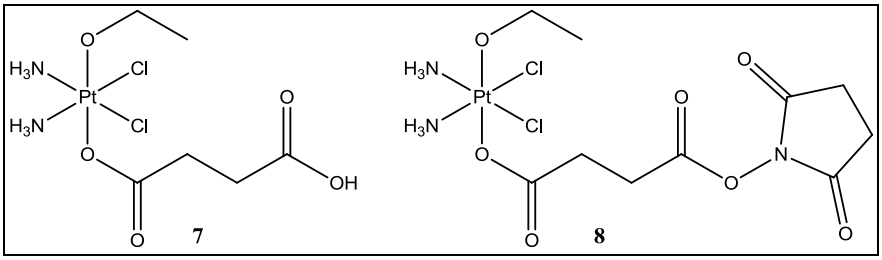

Figure 6.2: Structure of the complex **7** and its activated form (**8**), which was coupled to chitosan

Subsequently, the conjugate was coupled to other species (characterized by the presence of a carboxylic group) in order to evaluate the possibility to further functionalize chitosan: in particular, the main purpose was to load a tridentate ligand (i.e. 4-(bis(quinolin-2-ylmethyl)amino)butanoic acid), able to chelate Re and ^{99m}Tc compounds. This latter, being a γ-rays emitter, is commonly exploited

for imaging techniques for the diagnosis of some tumors. Therefore, technetium, in combination with the Pt complex, could make chitosan a useful vehicle for "theranostics", which is based on the use of vectors that can be employed both from a therapeutic and a diagnostic point of view (*Figure 6.3*).

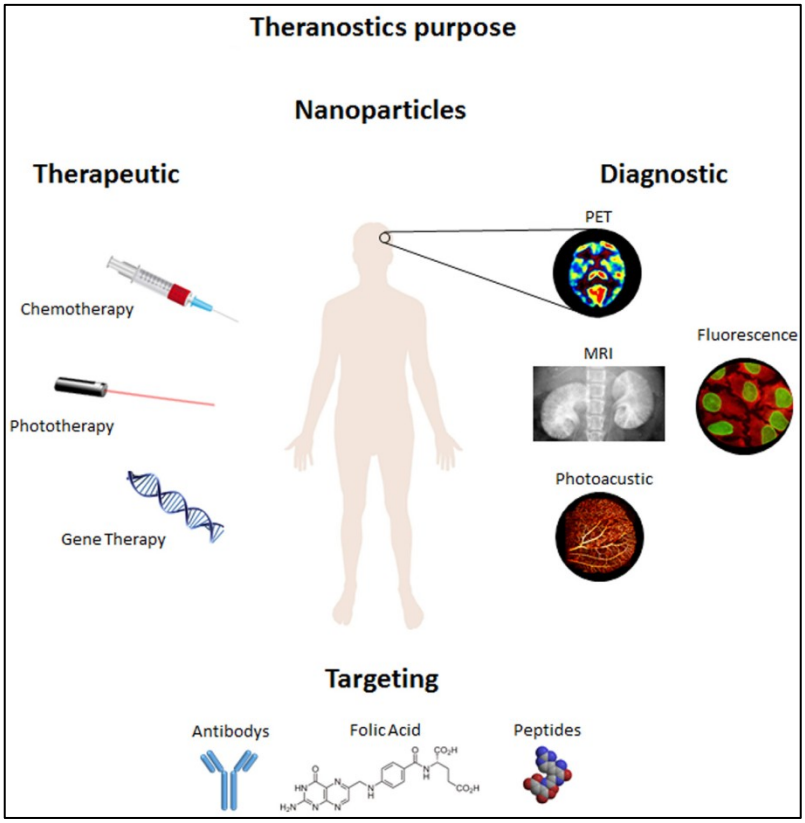

Figure 6.3: Theranostics purposes in the diseases treatment.
The picture is a modification of that reported in literature [9]

In particular, the therapy is ensured by DTD strategies which, by the use of vectors, reduce dosages because one particle binds a high number of complexes (if the complex is effective, the conjugate is more effective and, therefore, a lower dosage is required) and minimize side-effects because the drug is selectively led to the tumor site (in which it is activated) and accumulated by EPR effect. The diagnosis (which provides for the localization and

characterization of the disease), instead, is made possible by non-invasive techniques, which exploit the presence of magnetic fields, fluorophores or radiopharmaceutical compounds (such as ^{99m}Tc derivatives).

Furthermore, it is important to note that the use of passive DTD vectors, such as nanoparticles or macromolecules, containing several functional groups allows to load the vectors with different amount of therapeutic and diagnostic agents. This is very important since a Pt complex acts at μM level and a ^{99m}Tc derivative works in the nM range.

The studies of the chitosan couplings with complex **8** were preceded by the evaluation of the reaction of the platinum compound with glucosamine, which represents a chitosan unit.

The synthesized conjugates are reported in order of discussion:

- (OC-6-44)-diamminedichloridoethanolato(4-oxo-4-(((3*S*,4*S*,5*S*)-2,4,5-trihydroxy-6-(hydroxymethyl)tetrahydro-2*H*-pyran-3-yl)amino) butanoato)platinum(IV) (**20**),
- Protonated chitosan - Pt(IV) complex conjugates (**21a**-**21f**),
- Chitosan modified with (3-carboxypropyl)trimethylammonium chloride (**22**),
- Modified chitosan - Pt(IV) complex conjugates at different reaction time and with different amounts of platinum compound (**22a**-**22h**),
- Activated *N*-hydroxysuccinimidyl ester of 4-(methylsulphonyl)benzoic acid (**23**),
- Modified chitosan **22b** - complex **23** conjugate (**24**),
- Modified chitosan **22b** - 4-(bis(quinolin-2-ylmethyl)amino)butanoic acid conjugate (**25**),
- Rhenium(I) complex - diethylenetriamine chelate (**26**),
- Rhenium(I) complex - 4-(bis(quinolin-2-ylmethyl)amino)butanoic acid chelate (**27**),

- Conjugate **25** - rhenium(I) complex chelate (**28**).

6.2 Synthesis of the (OC-6-44)-diamminedichloridoethanolato(4-oxo-4-(((3S,4S,5S)-2,4,5-trihydroxy-6-(hydroxymethyl)tetrahydro-2H-pyran-3-yl)amino)butanoato)platinum(IV) (20)

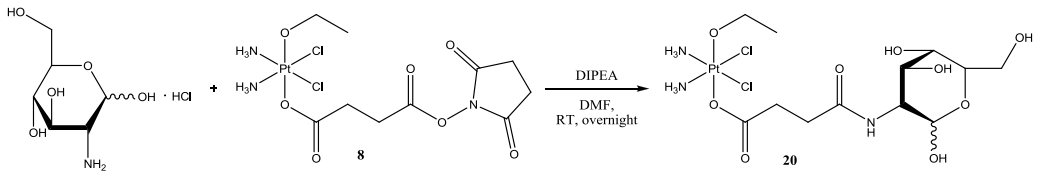

Glucosamine hydrochloride (8.40 mg, 0.0390 mmol) was added to a solution of **8** (21.8 mg, 0.0390 mmol) in 2.5 mL of anhydrous DMF. Then *N,N*-diisopropylethylamine (DIPEA, 13.6 µL, 0.0780 mmol) was added in order to deprotonate the amino group of glucosamine and the reaction was carried out at room temperature overnight. The solution was filtered (porosity 0.45 µm) and the DMF was removed under reduced pressure to obtain a yellow oil. A yellow powder was precipitated by the addition of some drops of acetone and then diethyl ether and was dried *in vacuo*.
Yield: 29.9 mg.

6.2.1 Characterization of the Complex

RP-HPLC-ESI-MS

The analysis was performed by employing a stationary phase consisting of a C18 Phenosphere-NEXT column 5 µm, 250 × 4.60 mm ID, a mobile phase composed by a 70:30 mixture of a 15 mM aqueous solution of formic acid and

methanol (isocratic elution), a flow rate of 0.500 mL/min, a temperature of 37 °C and the UV-Visible detector set at 210 nm.

In particular, in *Figure 6.4* is reported the chromatogram of the synthesized species.

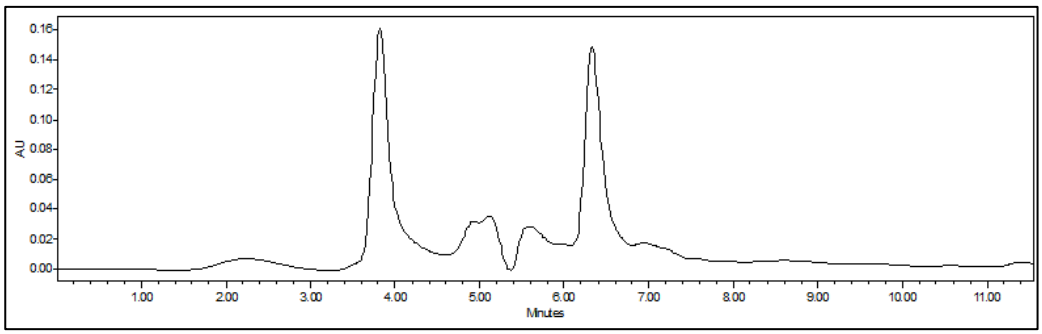

Figure 6.4: Chromatogram of the product obtained after the coupling of glucosamine with complex **8**

The *Figure 6.4* shows the presence of two main species (eluted at 3.82 and 6.33 minutes, respectively), identified by their ESI-MS spectra (*Figures 6.5a* and *6.5b*).

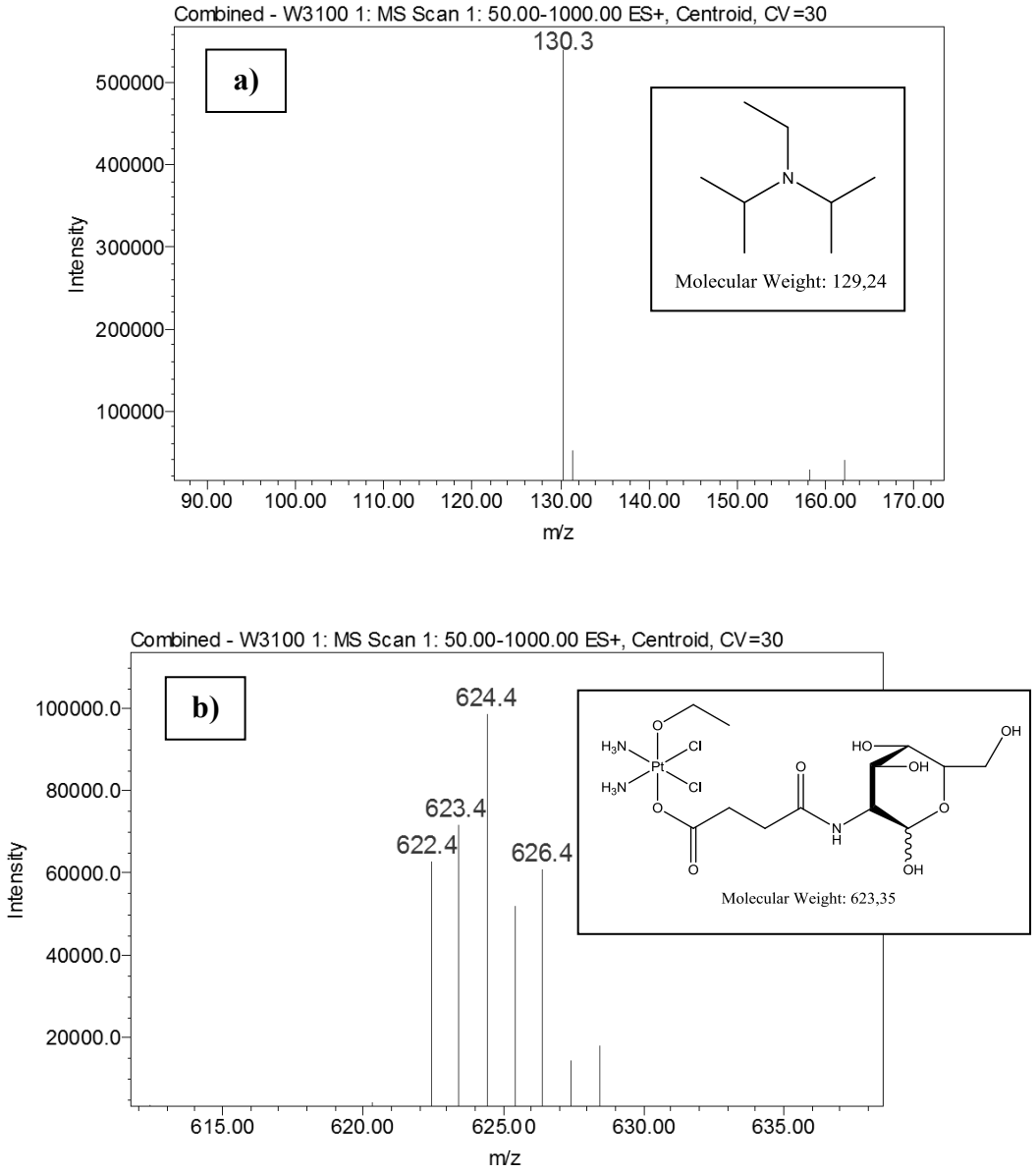

Figures 6.5: ESI-MS spectra of the two main species observed in *Figure 6.4*, eluted at a) 3.82 and b) 6.33 minutes

The ESI-MS spectrum in *Figure 6.5a*, registered in positive ion mode with a cone voltage of 30V, allows to verify the presence of DIPEA (probably in the form of a chloride salt), corresponding to the peak eluted at 3.82 minutes: in

fact, it is possible to observe the value at 130.3 m/z which can be attributed to the pseudo-molecular ion $[M+H]^+$ (M = DIPEA). The peak eluted at 6.33 minutes is identified by the ESI-MS spectrum reported in *Figure 6.5b*, registered in positive ion mode with a cone voltage of 30V: it represents the pseudo-molecular ion of the desired product (**20**), corresponding to 624.4 m/z ($[M+H]^+$, where M = complex **20**).

Other peaks are observed in the chromatogram (*Figure 6.4*), between 5 and 6 minutes: they are attributed to platinum complexes, basing on their isotopic pattern, but there is not a precise identification.

In order to remove all the organic residues, the compound was purified by means of Cl-loaded anionic (Amberlite® IRA-400(OH)) and K-loaded cationic (Amberlite® IR-120(H)) exchange resins.

After the purification process, complex **20** resulted to be purer (*Figure 6.6*) because the diisopropylethylamine/diisopropylethylammonium were almost completely removed by the use of the cationic resin.

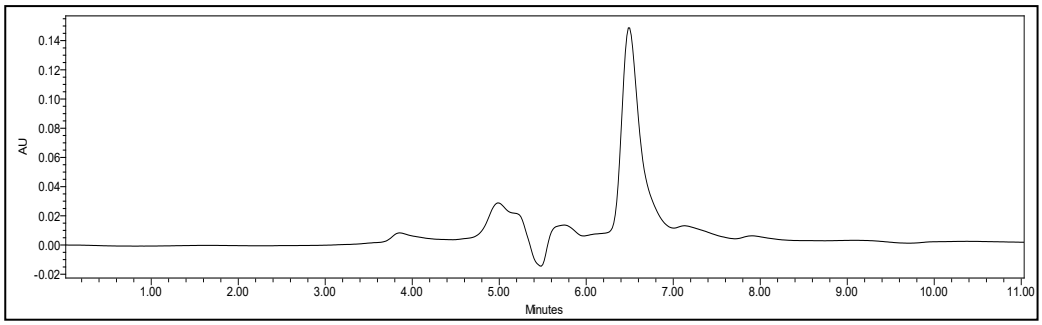

Figure 6.6: Chromatogram of complex **20**, after purification with ionic exchangers

However, the resins were not useful in the removal of the Pt complexes, eluted between 5 and 6 minutes: in fact, they have a similar behavior to complex **20** and, therefore, it is not possible to effectively separate them.

Although the desired product seemed to be not completely purifiable, a similar synthetic procedure was applied to chitosan because it has an advantage with respect to glucosamine: in fact, its estimated molecular mass is 60-120 kDa and this feature allows to perform the purification by dialysis in ultrapure water.

6.3 Conductometric Titration of Chitosan

Several methods can be employed for the determination of the deacetylation degree (DD) and, therefore, the quantification of the chitosan amino groups (such as some types of titration, elemental analysis, IR, NMR, solid-state NMR, etc.). In this work, the chosen procedure was the conductometric titration and it was reported in literature [4]. In particular, 93.3 mg of chitosan were dissolved in 20 mL of 0.0540 M HCl and then the solution was titrated with 0.158 M NaOH, by using a conductivitymeter: the conductivity of the solution (expressed in mS/cm), due to H^+ and OH^- ions, was registered after each titrant addition and the titration curve is reported in *Figure 6.7*.

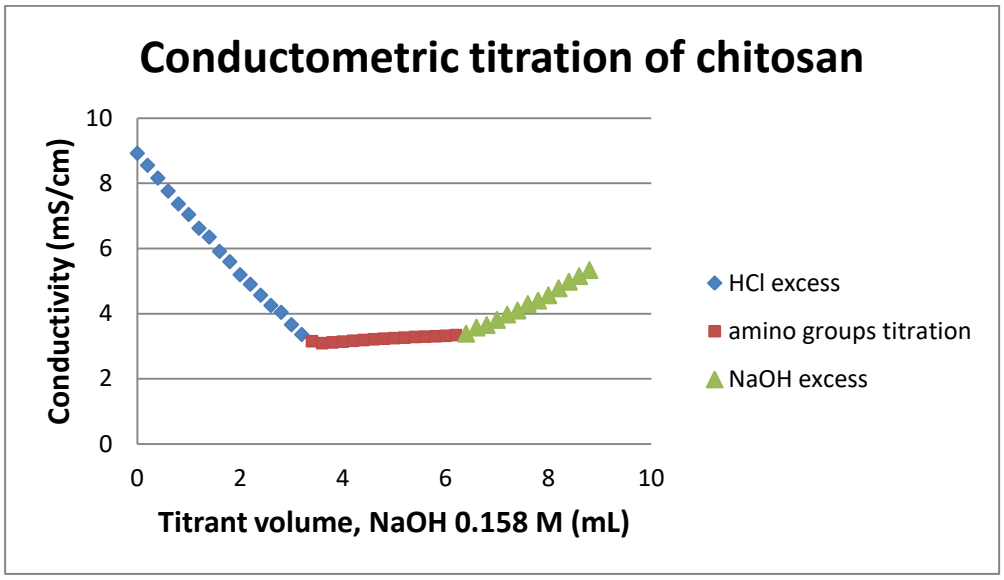

Figure 6.7: Conductometric titration of chitosan, dissolved in 0.0540 M HCl, using 0.158 M NaOH as a titrant

The titration curve shows three trends: the first (blue diamonds) represents the HCl excess neutralization by NaOH, the second (red square) indicates the progressive titration (i.e. neutralization) of the amino groups exposed from the chitosan surface, whereas the third (green triangle) corresponds to the excess of titrant. The elaboration of the titration results allowed to determine 5.16 mmol - NH_2 groups/g chitosan, with a deacetylation degree (DD) of 83.1 mol% and, therefore, a degree of acetylation (AD) of 16.9 mol%.

6.4 Acid-Base Titration of Chitosan

The same titration described in *paragraph 6.3* was repeated using a pHmeter in order to verify the pH range at which the chitosan was in its protonated form and, therefore, soluble in aqueous solutions. In particular, 93.3 mg of chitosan were dissolved in 20 mL of 0.0540 M HCl, then the solution was titrated with

0.158 M NaOH and the pH was measured after each titrant addition. In *Figure 6.8* the titration results are reported: the pH values as a function of the titrant volume.

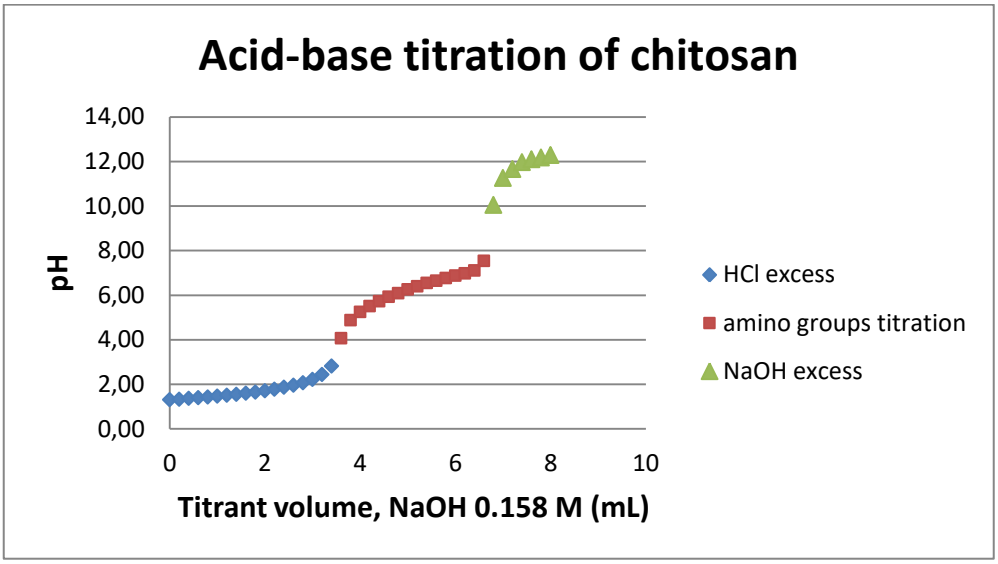

Figure 6.8: Acid-base titration of chitosan, dissolved in 0.0540 M HCl, using 0.158 M NaOH as a titrant

The titration curve shows three main trends: the first (blue diamonds) represents the pH values corresponding to the HCl excess, the second (red square) indicates the progressive titration of the amino groups exposed from the chitosan surface, whereas the third (green triangle) reports the pH values of the titrant excess. When the NH_2 groups are titrated, are deprotonated and begin to cause a loss in solubility of chitosan. The pH range of deprotonation is from 4 to about 7: at about 4 almost all the amino functionalities are still protonated and no particular behaviors are observed in solution. However, when the deprotonation proceeds (pH around 4.5-5), chitosan precipitation occurs and at almost neutral pH it is completely precipitated. Therefore, in order to obtain a stable chitosan solution, acidic pH values (about 4) must be ensured.

6.5 Synthesis of the Chitosan Conjugates (21a-21f)

The chitosan employed showed no solubility in all the solvents, except for acidic aqueous solutions. Therefore, in order to overcome this problem and to make chitosan more soluble, its amino groups were appropriately protonated: in particular, 100 mg were dissolved in 0.0540 M HCl (21.5 mL), then the aqueous solution was removed under reduced pressure and the product was dried *in vacuo* in order to obtain a beige powder.

Moreover, in order to verify the loading capacity on chitosan, six different conjugates (**21a**-**21f**) were synthesized using different amounts of Pt(IV) complex (percentage of theoretically coupled amino groups ranging from 1 to 15%). In particular, after the protonation treatment, a suitable quantity of complex **8** (*Table 6.1*) was dissolved in 3 mL of anhydrous DMF. Then, the protonated chitosan (100 mg, 0.516 mmol of -NH_2 groups) and a 2:1 molar excess (respect to **8**) of *N,N*-diisopropylethylamine (DIPEA) were added to each previously prepared solution.

Conjugate	**Theoretical coupling % (respect to the total amino groups mmol)**	**Employed amount of complex 8**
21a	1	2.9 mg, 0.00516 mmol
21b	2	5.8 mg, 0.0103 mmol
21c	3	8.7 mg, 0.0155 mmol
21d	5	14.4 mg, 0.0258 mmol
21e	10	28.9 mg, 0.0516 mmol
21f	15	43.3 mg, 0.0774 mmol

Table 6.1: Amounts of complex **8** employed for each conjugate (**21a**-**21f**)

Each suspension was stirred at room temperature for 24 hours. Then, the solvent was removed under reduced pressure and the products were dialyzed in ultrapure water for 2 days, by using a dialysis tubing cellulose membrane (molecular mass cut-off of 14 kDa). After the dialysis, each conjugate was not completely dissolved. The compounds were then frozen by means of liquid nitrogen and lyophilized to obtain a beige powder. The lyophilization process, as observed for the silica NPs in *Chapter IV*, did not allow the conjugates to be resuspended, due to the formation of large irreversible aggregates, but it was employed for the preparation of the samples to be mineralized.

Each product (4-5 mg) was mineralized by means of an acid digestion, according to which 800 μL of 70% w/w HNO_3 were added to each sample that was left 1 hour at 60 °C in an ultrasonic bath. Then they were diluted with 1% v/v HNO_3 and analyzed by means of ICP-OES. The results (expressed as means ± standard deviation of at least three independent replicates) are reported in *Table 6.2*.

Conjugate	Theoretical % Pt loading	Effective % Pt loading	mmol Pt complex/g chitosan	% coupling efficiency
21a	1	0.76 ± 0.12	0.00391 ± 0.00061	75.8 ± 11.8
21b	2	1.42 ± 0.22	0.00733 ± 0.00112	71.1 ± 10.8
21c	3	2.03 ± 0.25	0.0105 ± 0.0013	67.7 ± 8.5
21d	5	2.83 ± 0.90	0.0146 ± 0.0046	56.6 ± 18.0
21e	10	5.85 ± 0.14	0.0302 ± 0.0007	58.5 ± 1.4
21f	15	8.34 ± 0.29	0.0430 ± 0.0015	55.6 ± 2.0

Table 6.2: Pt loadings of conjugates **21a-21f** and corresponding coupling efficiency. The results are expressed as percentage respect to the amino groups density (5.16 mmol/g chitosan)

The data shown in *Table 6.2* allows to evaluate that the coupling efficiency is higher (about 70%) in the case of low values of theoretical loading (i.e. 1-3% respect to the total amino groups in **21a**-**21c**), whereas if the theoretical loading is higher (i.e. 5-15% for **21d**-**21f**) the effectively coupled amount of complex is about 60% of the desired one. Furthermore, the effective and the theoretical loadings are reported in a graph (*Figure 6.9*), showing an almost linear correlation (R_{adj}^2 = 0.999), which indicates that the yield of coupling is about 55%.

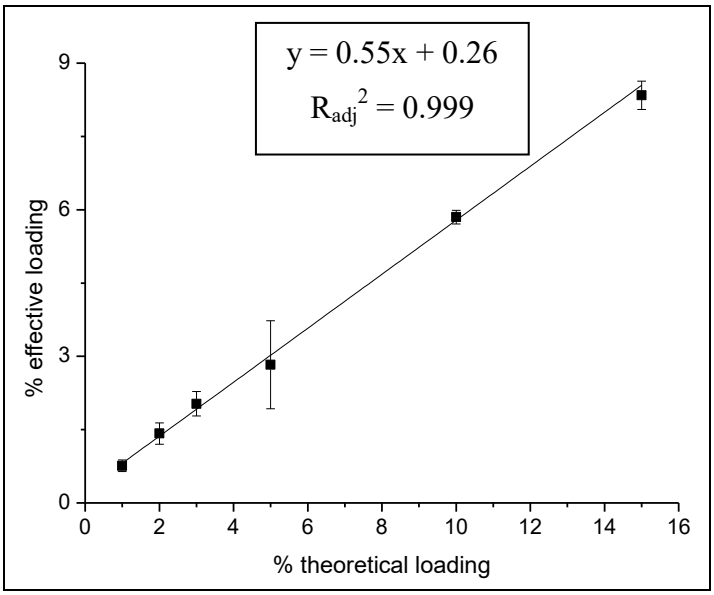

Figure 6.9: Effective vs. theoretical loadings of conjugates **21a**-**21f**

Moreover, in spite of the protonation, the chitosan conjugates were not completely soluble in aqueous solutions: part of the amines lost its positive charge, causing a solubility decrease, and, probably, other amino groups were deprotonated by DIPEA (not only the ones involved in the amidic bonds). The conjugates, therefore, resulted to be only partially soluble in aqueous solutions and this was observed after the dialysis process. For this reason, it was necessary

to couple a charged species to the chitosan in order to ensure a permanent positive charge on its surface and, therefore, to make it more soluble. In particular, a derivative of the ammonium chloride, the (3-carboxypropyl)trimethylammonium chloride, was employed.

6.6 Synthesis of the Chitosan Modified with (3-carboxypropyl)trimethylammonium Chloride (22)

The (3-carboxypropyl)trimethylammonium chloride needs to be opportunely activated, since the carboxylic group cannot be directly bound to the amino groups exposed on the chitosan surface. The ammonium derivative, therefore, was activated by the use of the coupling agent HBTU (*N,N,N′,N′*-tetramethyl-*O*-(1*H*-benzotriazol-1-yl)uronium hexafluorophosphate, belonging to the uronium salt family), in the presence of a tertiary amine (i.e. DIPEA, *N,N*-diisopropylethylamine). The synthesized activated intermediate was not isolated but was reacted with the nucleophilic species (i.e. the $-NH_2$ group of chitosan) in order to carry out a coupling by exploiting the formation of an amidic bond. The mechanism of this reaction is shown in *Figure 6.10*.

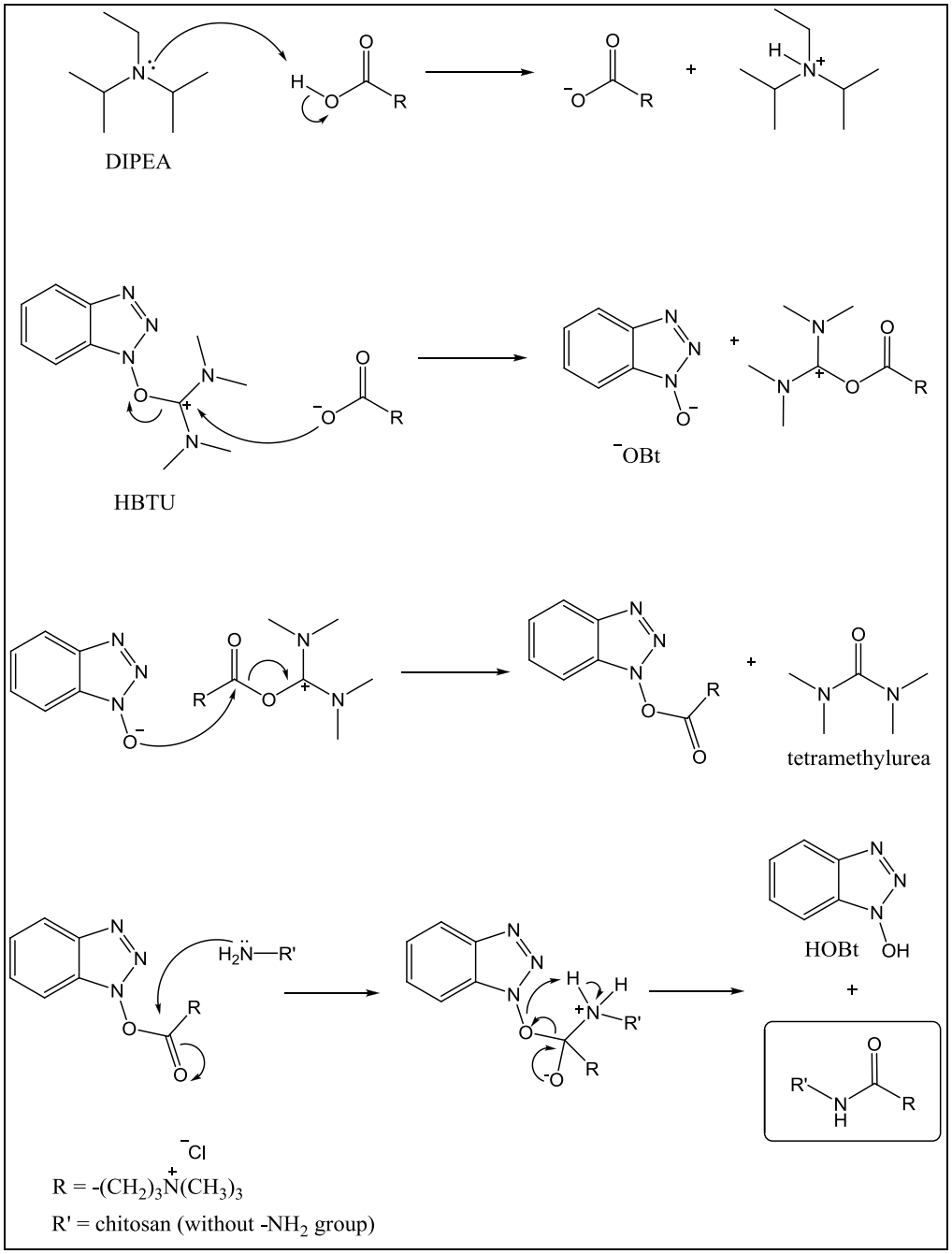

Figure 6.10: Activation mechanism of the (3-carboxypropyl)trimethylammonium chloride by means of the coupling agent HBTU and subsequent nucleophilic attack by the chitosan amino group

A mixture of ammonium derivative (256 mg, 1.41 mmol), HBTU (803 mg, 2.12 mmol) and DIPEA (738 μL, 4.24 mmol) in 4 mL of anhydrous DMF was magnetically stirred for 30 minutes. Then the protonated chitosan (228 mg, 1.18 mmol) and DIPEA (615 μL, 3.53 mmol) were added and the resulting mixture was stirred at room temperature for 24 hours. Subsequently, the suspension followed two different paths: an aliquot was processed for the quantification of the loaded species, whereas the remaining amount was employed for the further functionalizations. In particular, in the first case, the DMF was removed under reduced pressure and the product was dialyzed (also in this case, the dialysis tubing cellulose membrane molecular weight cut-off was 14 kDa) in ultrapure water for 2 days. After the dialysis, the chitosan was completely dissolved: the ammonium derivative was successful in increasing the chitosan solubility. Then the sample was frozen by means of liquid nitrogen and lyophilized to obtain a beige powder, which was used for the quantification of the charged species.

In order to determine the amount of the ammonium derivative loaded on chitosan, the same procedure employed to quantify the amino functionalities of chitosan was performed (*paragraph 6.2*). In particular, 21.0 mg of the sample were dissolved in 10 mL of 0.054 M HCl and titrated with 0.2 M NaOH by using a conductivitymeter. The titration results allowed to evaluate the number of remaining free amino groups, which were then subtracted from the initially available ones to obtain the amount of amino groups involved in the amidic bonds with the ammonium derivative. After the data processing, it was verified that the amount loaded was 29.5% respect to the total amino groups present in 21.0 mg (i.e. 0.108 mmol $-NH_2$) and corresponded to 1.52 mmol/g chitosan: the quantity loaded was about a quarter of the theoretical loading of ammonium derivative (6.18 mmol/g chitosan).

6.6.1 Size and Stability Investigations

The DLS technique was employed in order to evaluate the size of chitosan **22**. In particular, being **22** completely dissolved in water, the analysis was performed in this solvent, not adding any salts to modify the ionic strength. About 1 mL of the solution was transferred into a plastic disposable cuvette which was introduced into the instrument, a Malvern Zetasizer Nano ZS (Malvern Instruments Ltd., Malvern, UK) at a fixed scattering angle of 173°, using a He-Ne laser and DLS software for Windows (version 6.11, Malvern, UK) and setting the temperature at 25 °C.

The same solution, transferred into a suitable cuvette, was employed for the ζ potential measurements, which were carried out in order to evaluate the stability of the suspension.

The ζ potential data (41.5 ± 3.1 mV) allows to verify that the system exceeds the threshold of stability because its ζ potential value is higher than +30 mV: in particular, the positive charge is ensured by the presence of the ammonium derivative.

As regards the size (DLS diameter = 180 ± 10 nm), it is important to point out that, in water, each particle is surrounded by water molecules and, therefore, the result takes into account the hydrodynamic radius. Moreover, in this case, the analysis was carried out in the absence of any modifications of the ionic strength: the hydrodynamic radius, therefore, results the largest possible.

After the decoration of the chitosan surface with the (3-carboxypropyl)trimethylammonium chloride, the subsequent phase consisted of the coupling of this chitosan derivative with the platinum complex **8**. At first, it was necessary to evaluate the effect of the reaction time on the loading on

chitosan and then, after fixing this parameter, the loading efficiency by using different amounts of the platinum prodrug was studied.

6.7 Synthesis of the Modified Chitosan Conjugates at Different Reaction Times (22a-22e)

To the previously prepared chitosan suspension (**22**, i.e. the not dialyzed aliquot), complex **8** (13.2 mg, 0.0236 mmol, corresponding to 2% respect to the initial amino groups, i.e. 1.18 mmol) was added and the mixture was stirred for different reaction times: 2 hours (**22a**), 4 hours (**22b**), 6 hours (**22c**), 8 hours (**22d**), and 24 hours (**22e**). After the established times, a small aliquot of the suspensions was processed: DMF was removed under reduced pressure and each conjugate was dialyzed in ultrapure water for 2 days, obtaining completely water soluble conjugates. Then they were frozen by means of liquid nitrogen and lyophilized.

All the conjugates (4-5 mg) were mineralized by using the previously described procedure (*paragraph 6.5*), diluted with 1% v/v HNO_3 and analyzed by means of ICP-OES. The coupling results, expressed as means ± standard deviation of at least three independent replicates, are reported in *Table 6.3*.

Conjugate	Reaction time	Theoretical % Pt loading	Effective % Pt loading	mmol Pt complex/g chitosan
18a	2 h	2	0.78 ± 0.02	0.0400 ± 0.0009
18b	4 h		0.68 ± 0.19	0.0348 ± 0.0098
18c	6 h		0.86 ± 0.03	0.0441 ± 0.0015
18d	8 h		0.61 ± 0.08	0.0314 ± 0.0039
18e	24 h		0.99 ± 0.22	0.0513 ± 0.0112

Table 6.3: Pt loadings on chitosan at different reaction times but by the use of a fixed complex **8** amount. The results are expressed as percentage respect to the amino groups density (5.16 mmol/g chitosan)

Since no significant differences among the obtained Pt loadings were observed, the reaction time was fixed at 4 hours as a suitable compromise between reaction time and Pt loading.
The subsequent phase consisted in the evaluation of the Pt loading on chitosan at fixed coupling time but employing different quantities of complex, in order to verify the coupling efficiency in the presence of the (3-carboxypropyl)trimethylammonium chloride.

6.7.1 Synthesis of the Modified Chitosan Conjugates at Fixed Reaction Time but by using Different Prodrug Amounts (22b, 22f-22h)

To the previously prepared chitosan suspension (**22**, i.e. the not dialyzed aliquot), complex **8** was added and the mixture was stirred for 24 hours. Four different conjugates (**22b**, **22f-22h**) were synthesized using different amounts of Pt(IV) complex: these latter were expressed as percentage (from 1 to 10%) with respect to the total mmol of chitosan amino groups (*Table 6.4*).

Conjugate	Theoretical coupling % (respect to the total amino groups mmol)	Employed amount of complex 8
22f	1	6.6 mg, 0.0118 mmol
22b	2	13.2 mg, 0.0235 mmol
22g	5	32.9 mg, 0.0588 mmol
22h	10	65.8 mg, 0.118 mmol

Table 6.4: Amounts of complex **8**, expressed as percentage with respect to the total available amino groups mmol, employed to synthesize conjugates **22b**, **22f-22h**

After the established coupling time, a small aliquot of each suspension was processed: DMF was removed under reduced pressure and the dialysis was carried out in ultrapure water for 2 days, obtaining completely water soluble conjugates. Then they were frozen by means of liquid nitrogen and lyophilized.
Each conjugate (4-5 mg) was mineralized by using the previously described procedure (*paragraph 6.5*), diluted with 1% v/v HNO_3 and analyzed by means of ICP-OES. The coupling results, expressed as a mean of at least three independent replicates, are reported in *Table 6.5*.

Conjugate	Reaction time	Theoretical % Pt loading	Effective % Pt loading	mmol Pt complex/g chitosan
22f	24 h	1	0.45 ± 0.03	0.0232 ± 0.0015
22b		2	0.68 ± 0.19	0.0348 ± 0.0098
22g		5	1.38 ± 0.12	0.0710 ± 0.0062
22h		10	2.63 ± 0.05	0.135 ± 0.003

Table 6.5: Pt loadings on chitosan at fixed reaction time but by using different amounts of complex **8**. The results are expressed as percentage respect to the amino groups density

The results allows to evaluate that the loadings on chitosan are much lower than those reported in *Table 6.2* for conjugates **21a-21f** without the ammonium groups. Probably, the presence of a large quantity of another species (i.e. the (3-carboxypropyl)trimethylammonium functionality) influenced the subsequent loading, decreasing the number of available and accessible amino groups. For this reason, the Pt loading on conjugates **22b**, **22f-22h** resulted to be lower with respect to **21a-21f**.
The effective vs. theoretical loadings reported in a graph (*Figure 6.11*) shows a linear correlation ($R_{adj}^2 = 0.999$).

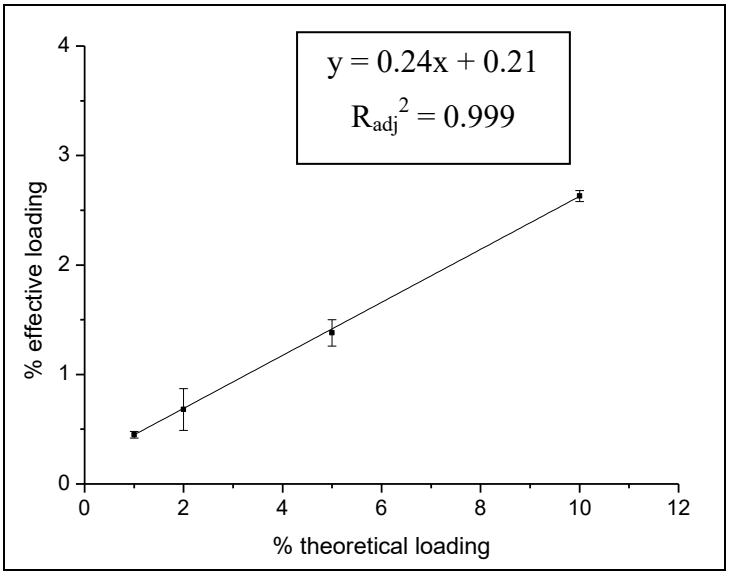

Figure 6.11: Effective vs. theoretical loadings of conjugates **22f-22i**

Table 6.5 and *Figure 6.11* point out that the higher the theoretical platinum loading the higher the effectively loaded. However, only a third of the theoretical amount was bound to chitosan. Therefore, the Pt/amino groups ratio was fixed at 2% in order to avoid any waste of complex (the unreacted platinum cannot be recovered): for this reason, the conjugate employed in the further coupling reactions was **22b**.

6.7.2 Size and Stability Investigations

The DLS and ζ potential analyses of **22b** were carried out in order to evaluate its dimension and the suspension stability in ultrapure water at 25 °C.

Also in this case, the conjugate exceeds the threshold of stability: the ζ potential value (37.5 ± 0.6 mV) is higher than +30 mV.

The dimensional analysis (DLS diameter = 215 ± 12 nm) demonstrates that the presence of another species on the chitosan surface causes an increase in size: in

fact, it passes from about 180 nm, when only the (3-carboxypopyl)trimethylammonium functionality decorates the surface, to about 215 nm after the coupling with also the Pt(IV) complex. Also in this case, the presence of a solvation shell must be considered.

6.8 Synthesis of the Activated N-hydroxysuccinimidyl Ester of 4-(methylsulphonyl)benzoic Acid (23)

After establishing the "reaction time" (4 hours) and the "Pt/-NH_2 groups ratio" (2% of complex respect to the total available amino groups mmol), the remaining suspension aliquot of conjugate **22b** was further functionalized with other compounds containing a carboxylic group in order to evaluate the possibility of loading several species on chitosan. At first, the conjugate was coupled with the 4-(methylsulphonyl)benzoic acid: it was chosen because sulfur can be detected (by selecting the S 180.731 nm line) and quantified by ICP-OES.

As seen for other compounds having free carboxylic groups, the activation by DCC (*N,N'*-dicyclohexylcarbodiimmide) and NHS (*N*-hydroxysuccinimide) was necessary.

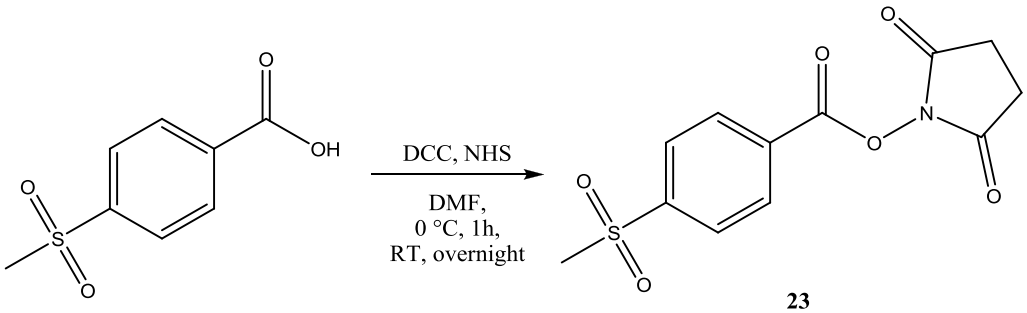

4-(methylsulphonyl)benzoic acid

23

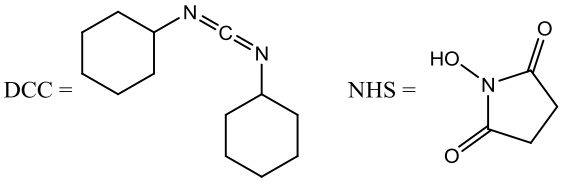

In particular, 4-(methylsulphonyl)benzoic acid (100 mg, 0.499 mmol) was dissolved in 2 mL of anhydrous DMF and, to the solution, DCC (124 mg, 0.599 mmol) and NHS (69.0 mg, 0.599 mmol) were added and the mixture was stirred at 0 °C for 1 hour and at room temperature overnight. After the established time, the solution was cooled to -18 °C and dicyclohexylurea was removed by filtration (porosity 0.45 μm). DMF was removed under reduced pressure to obtain a colorless oil. A white powder was precipitated by acetone/diethyl ether, washed with diethyl ether and then dried *in vacuo*.

Yield: 111 mg, 0.372 mmol, 74.5%.

6.8.1 Characterization of the Compound

RP-HPLC-ESI-MS

The analysis was performed by employing a stationary phase consisting of a C18 Phenosphere-NEXT column 5 μm, 250 × 4.60 mm ID, a mobile phase

composed by a 50:50 mixture of a 15 mM aqueous solution of formic acid and methanol (by isocratic elution), a flow rate of 0.500 mL/min, a temperature of 37 °C and the UV-Visible detector set at 210 nm. Complex **23** showed a retention time of 7.17 minutes and its identity was attributed by the corresponding ESI-MS spectrum (*Figure 6.12*).

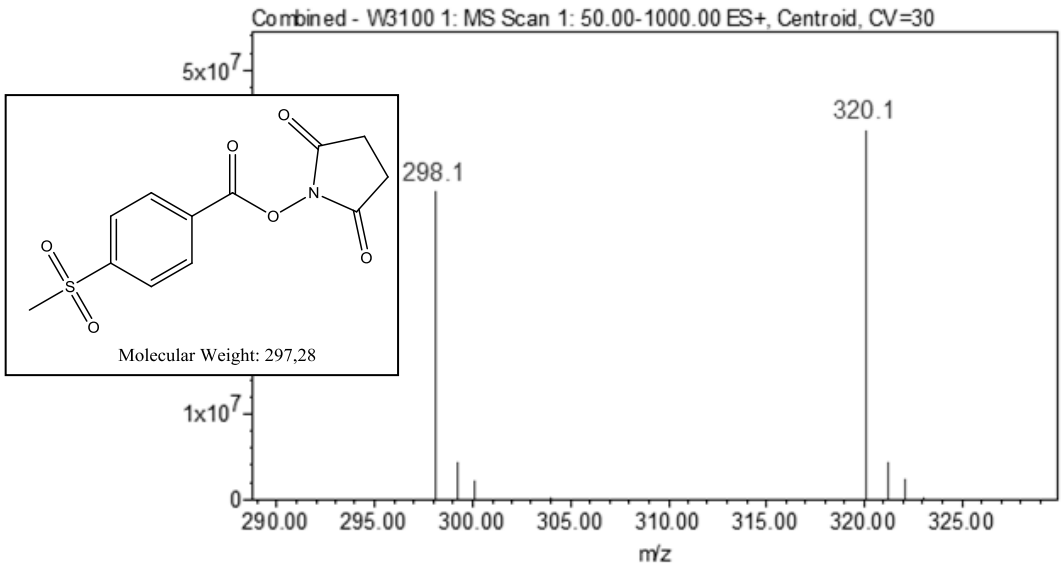

Figure 6.12: ESI-MS spectrum of complex **23**, prepared in a 50:50 ultrapure water and methanol mixture

The ESI-MS spectrum, registered in positive ion mode with a cone voltage of 30V, shows a value at 298.1 m/z, corresponding to the pseudo-molecular ion $[M+H]^+$ peak, and another one at 320.1 m/z which represents the adduct with sodium ion $[M+Na]^+$. Moreover, it is possible to observe the typical isotopic pattern of sulfur compounds: the m/z values are confirmed by the comparison with the simulated ESI-MS spectra (*Figure 6.13*).

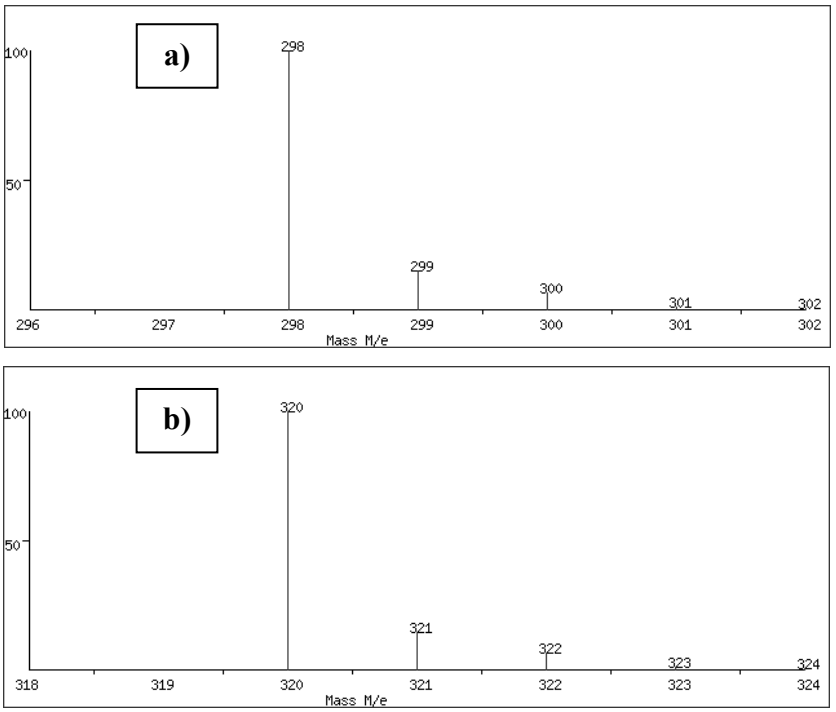

Figure 6.13: Simulated ESI-MS spectra of a) the pseudo-molecular ion $[M+H]^+$ and b) the sodium adduct $[M+Na]^+$ peaks of the compound **23**

^{1}H-NMR

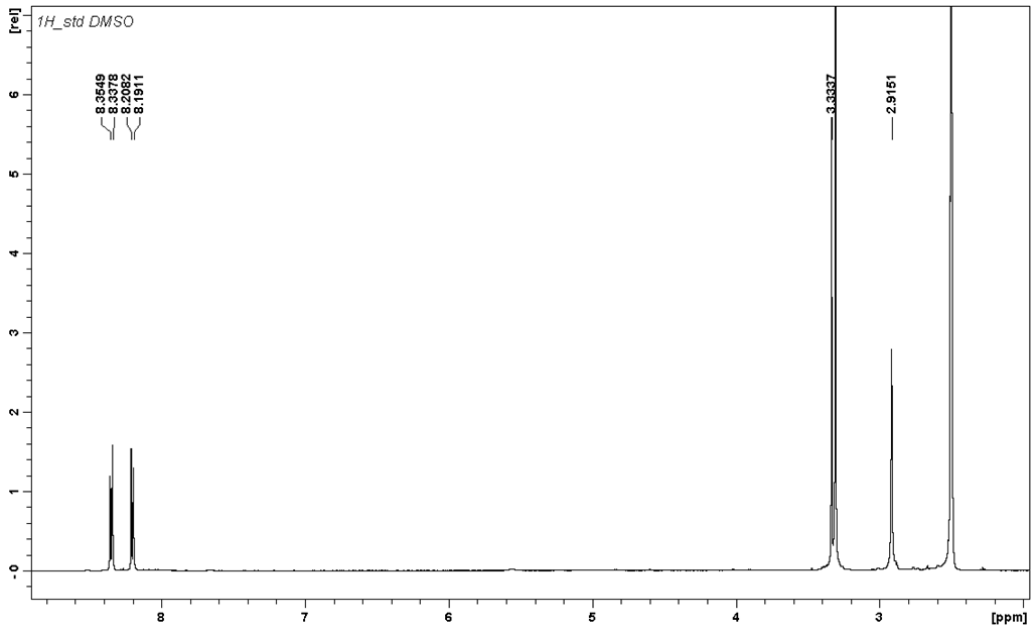

Figure 6.14: ^{1}H-NMR spectrum of complex **23**, registered in DMSO-d_6

The ^{1}H-NMR (500 MHz, DMSO-d_6) spectrum of compound **23** (*Figure 6.14*) shows the following signals, δ: 2.92 (s, 4H, -C*H*$_2$CON), 3.33 (s, 3H, -C*H*$_3$), 8.21 (d, 2H, -C*H*=CS, ^{3}J = 8.55 Hz), 8.35 (d, 2H, -C*H*=CCO, ^{3}J = 8.55 Hz) ppm.

^{13}C-NMR

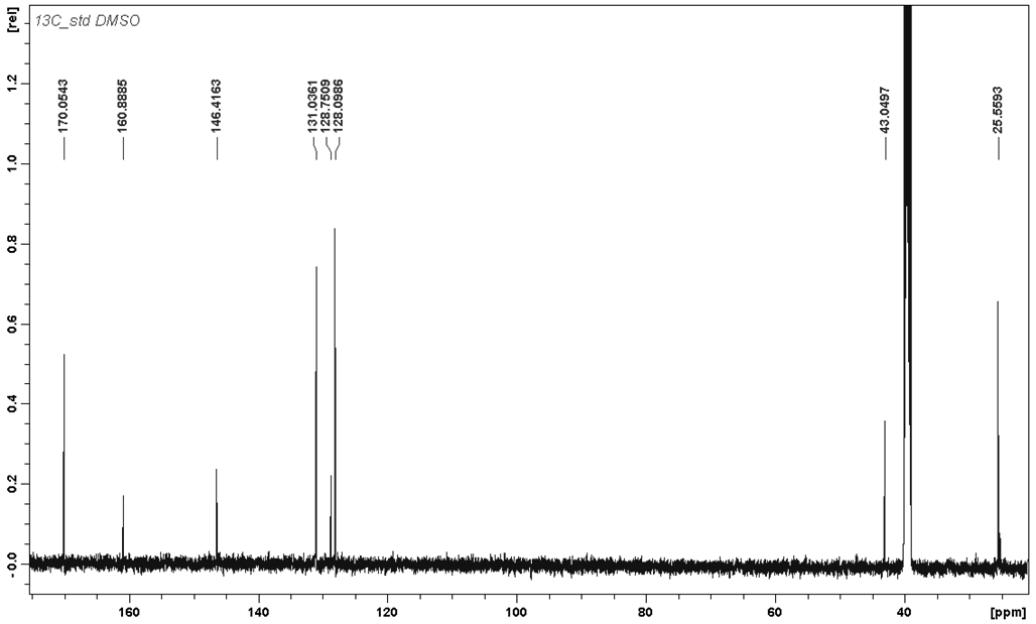

Figure 6.15: ^{13}C-NMR spectrum of complex **23**, registered in DMSO-d_6

The ^{13}C-NMR (125.7 MHz, DMSO-d_6) spectrum of complex **23** (*Figure 6.15*) shows the following signals, δ: 25.6 (-*C*H$_2$CON), 43.0 (-*C*H$_3$), 128.1 (-*C*H=CS), 128.8 (-CH=*C*CO), 131.0 (-*C*H=CCO), 146.4 (-CH=*C*S), 160.9 (-CH=C*C*O), 170.1 (-CH$_2$*C*ON) ppm.

After the characterization, complex **23** was coupled to the chitosan previously functionalized with the ammonium derivative and the Pt(IV) complex (**22b**).

6.9 Further Coupling of the Modified Chitosan Conjugate 22b with Compound 23 (24)

To the DMF suspension **22b**, containing chitosan coupled with both the ammonium derivative and complex **8**, compound **23** (14.0 mg, 0.0471 mmol, 4% respect to the total chitosan amino groups mmol) was added and the mixture was stirred at room temperature for 24 hours (to allow a large quantity to be coupled). DMF was then removed under reduced pressure and the conjugate was dialyzed in ultrapure water for 2 days, obtaining completely water soluble conjugates. An aliquot was frozen by means of liquid nitrogen and lyophilized.
The lyophilized samples (4-5 mg) were mineralized by using the previously described procedure (*paragraph 6.5*), diluted with 1% v/v HNO_3 and analyzed by ICP-OES.
The data (effective percentage of S loading = 0.40 ± 0.15 %, corresponding to 0.0207 ± 0.0075 mmol S complex/g chitosan) allows to evaluate that the loaded amount is about a tenth of the desired loading: probably, the activated species (**23**) is not very reactive and its coupling with the chitosan amino groups results to be difficult.

6.9.1 Size and Stability Investigations

The DLS and ζ potential analyses were carried out in order to evaluate the dimensions and the suspension stability of conjugate **24** in ultrapure water at 25 °C.
The ζ potential data (36.9 ± 1.0 mV) are higher than +30 mV: the threshold value is exceeded also in this case and, therefore, a high suspension stability is ensured.

The dimensional analysis (DLS diameter = 202 ± 22 nm) demonstrates that, after the coupling with a third species (**23**), the size is not much larger than the one of conjugate **22b**: by considering the standard deviations, the results obtained for **22b** (215 ± 12 nm) are very similar to the **24** data. Probably, it is due to the fact that **23** does not give a high hindrance to chitosan and, moreover, the loaded amount is quite low.

After having studied the size and ζ potential parameters, the subsequent phase consisted of verifying the behavior of another species: the 4-(bis(quinolin-2-ylmethyl)amino)butanoic acid (*Figure 6.16*). The tricarbonyl Re and Tc compounds are stabilized by many kinds of ligand and this allows to modulate the physicochemical features of the drug. As regards the nature of the ligand, some studies focused the attention on the importance of the choice of mono- bi- and tridentate ones [10] and a tridentate chelator resulted to be the most efficient [10, 11]: in fact, it occupies the three free coordination sites of the tricarbonyl metal (Re or Tc).

6.10 Coupling of the Modified Chitosan Conjugate 22b with the 4-(bis(quinolin-2-ylmethyl)amino)butanoic Acid (25)

The conjugate **25** was prepared by employing the same procedure described to synthesize the system **24** but, in this case, chitosan was decorated with the ammonium derivative, the Pt(IV) complex and the ligand reported in *Figure 6.16*.

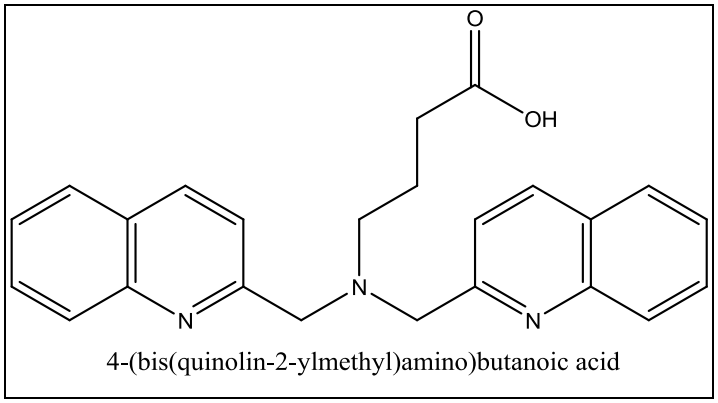

4-(bis(quinolin-2-ylmethyl)amino)butanoic acid

Figure 6.16: Tridentate ligand useful to chelate Re and Tc

In particular, a solution of ammonium derivative (256 mg, 1.41 mmol), HBTU (803 mg, 2.12 mmol) and DIPEA (738 μL, 4.24 mmol) in 4 mL of anhydrous DMF were magnetically stirred for 30 minutes. Then the protonated chitosan (228 mg, 1.18 mmol) and DIPEA (615 μL, 3.53 mmol) were added to the mixture and the reaction was carried out at room temperature for 24 hours. After this time, a small aliquot was processed (removal of the DMF, dialysis and lyophilization) in order to quantify the content of the (3-carboxypropyl)trimethylammonium chloride, by means of a conductometric titration: 29.5% respect to the total amino groups mmol, 1.52 mmol/g chitosan.
Then, complex **8** (13.2 mg, 0.0235 mmol, corresponding to 2% respect to the total amino groups mmol) was added to the mixture, which was stirred for 4 hours. An anhydrous DMF solution (1 mL) of tridentate ligand (9.1 mg, 0.0235 mmol), HBTU (13.4 mg, 0.0353 mmol) and DIPEA (8.20 μL, 0.0471 mmol) was stirred for 30 minutes and then it was added to the previously prepared mixture and the reaction was carried out at room temperature for 24 hours. Then, DMF was removed under reduced pressure and the sample was recovered with ultrapure water, in order to be dialyzed. However, by adding water, a dark brown powder precipitated: it was the tridentate ligand which, being very

lipophilic, was not soluble in water. For this reason, dichloromethane (DCM) was added to the obtained water suspension because it can dissolve the ligand (in fact, it became brown): the result was a biphasic solution in which a powder was still present. The brown organic fraction was separated by means of a separating funnel and this procedure was repeated several times till the excludable dichloromethane fraction resulted to be colorless. Then, the eventual remained DCM was removed under reduced pressure and the light brown solution was dialyzed (MW cut-off membrane of 14 kDa) in ultrapure water for 2 days: the conjugate resulted to be completely soluble in water.

The water solution (about 20 mL) was divided into two aliquots: the first was maintained with the free chelator (in order to further react with a ^{99m}Tc derivative), whereas the other one was employed to chelate a rhenium(I) complex. This latter, the *fac*-$[ReBr_3(CO)_3][Net_4]_2$, was used as a model of the technetium species because they had the same structure: in fact, they showed three hydrolizable groups (Br) and three carbonyls. The Re(I) compound was not synthesized in this work (its synthetic procedure was reported by Alberto *et al.* [12]) but it was used as such and its structure and characterization are shown in *paragraph 6.11.1*.

6.10.1 Size and Stability Investigations

The DLS and ζ potential analyses, performed in ultrapure water at 25 °C, were carried out in order to evaluate the dimension and the suspension stability of conjugate **25**.

Also in this case, the threshold of stability is exceeded since the ζ potential value is higher than +30 mV: 45.9 ± 1.1 mV.

From a dimensional point of view, it is possible to observe that the size (DLS diameter = 298 ± 21 nm) results to be increased respect to the previous cases (in

which the DLS diameters were about 200 nm): probably, this is due to the fact that the ligand is sterically hindered and this may cause an increase in size. Moreover, the analysis is performed in ultrapure water and, therefore, the solvation sphere must be considered. Although the size is about 300 nm, the conjugates can be used for passive DTD strategies by exploiting the EPR effect because the fenestrations of the vascular system still have compatible dimensions.

6.11 Chelation Reaction of the Re(I) Complex with Diethylenetriamine (26)

In order to set up the reaction condition for the coordination of a ^{99m}Tc complex to chitosan derivatives, the "cold" Re complex *fac*-$[ReBr_3(CO)_3][NEt_4]_2$, synthesized by Alberto [12], was used with the model triamine DIEN (diethylenetriamine).

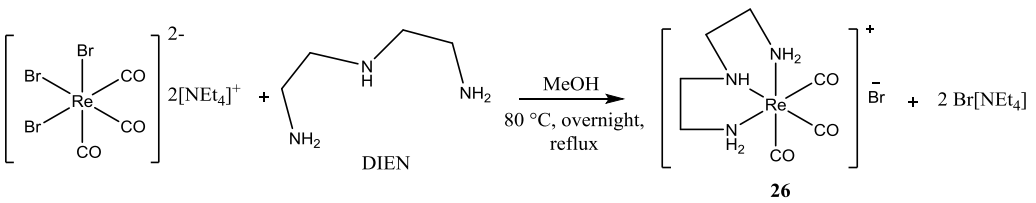

26

In particular, the *fac*-$[ReBr_3(CO)_3][NEt_4]_2$ (100 mg, 0.130 mmol) and diethylenetriamine (DIEN, 14.0 μL, 0.130 mmol) were dissolved in 12 mL of methanol and the mixture was heated at reflux (about 70 °C) overnight. The solvent was then removed under reduced pressure and the product was dried *in vacuo*.

Yield: 56.0 mg, 0.124 mmol, 95.2%.

6.11.1 Characterization of the Complex

RP-HPLC-ESI-MS

The analysis was performed by employing a stationary phase consisting of a C18 Phenosphere-NEXT column 5 μm, 250 × 4.60 mm ID, a mobile phase composed by a 50:50 mixture of a 15 mM aqueous solution of formic acid and methanol (isocratic elution), a flow rate of 0.500 mL/min, a temperature of 37 °C and the UV-Visible detector set at 210 nm. Complex **26** showed a retention time of 4.08 minutes and its identity was attributed by the corresponding ESI-MS spectrum (*Figure 6.17a*).

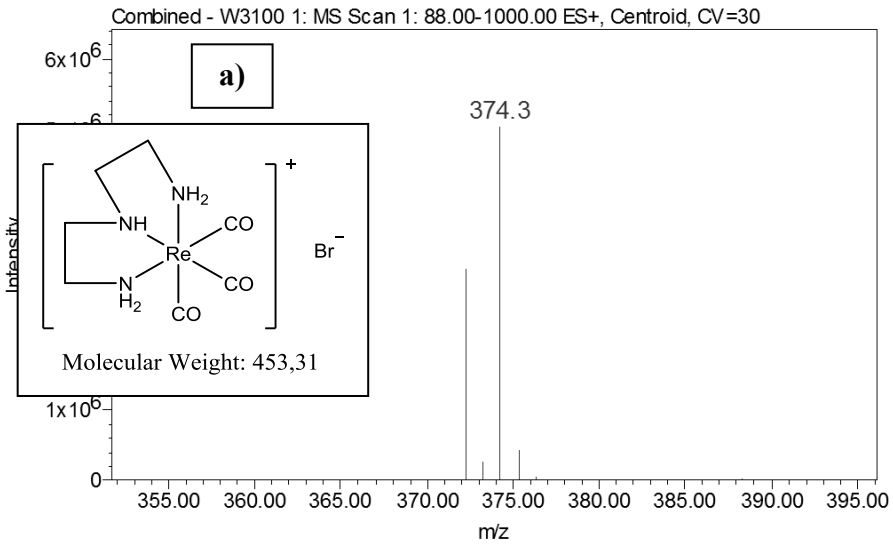

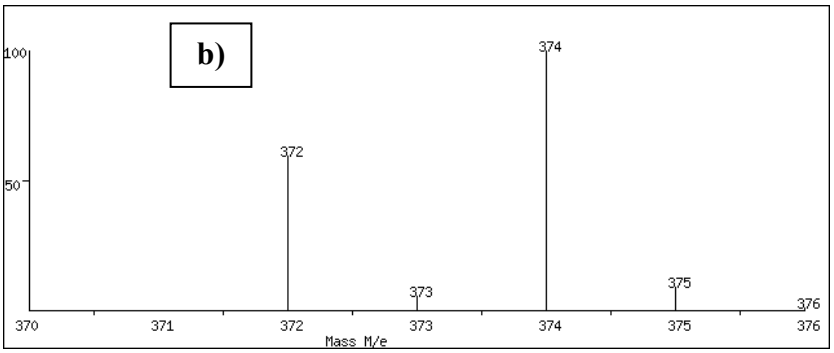

Figures 6.17: a) ESI-MS spectrum of the complex **26**, prepared in a 50:50 mixture of ultrapure water and methanol, b) simulated ESI-MS spectrum of the molecular ion $[M\text{-}Br]^+$ of complex **26**

The ESI-MS spectrum (*Figure 6.17a*), registered in positive ion mode with a cone voltage of 30V, allows to observe a value at 374.3 m/z which verifies the presence of the species $[M\text{-}Br]^+$ as confirmed by the simulation of this spectrum (*Figure 6.17b*).

Infrared Spectroscopy

Complex **26** and its precursor were analyzed by IR spectroscopy.

A dry KBr plate of the sample was prepared and the spectrum (*Figure 6.18*), with a 2 cm^{-1} resolution, was registered on a Bruker FTIR Equinox 55 spectrometer in the range 4000-400 cm^{-1}.

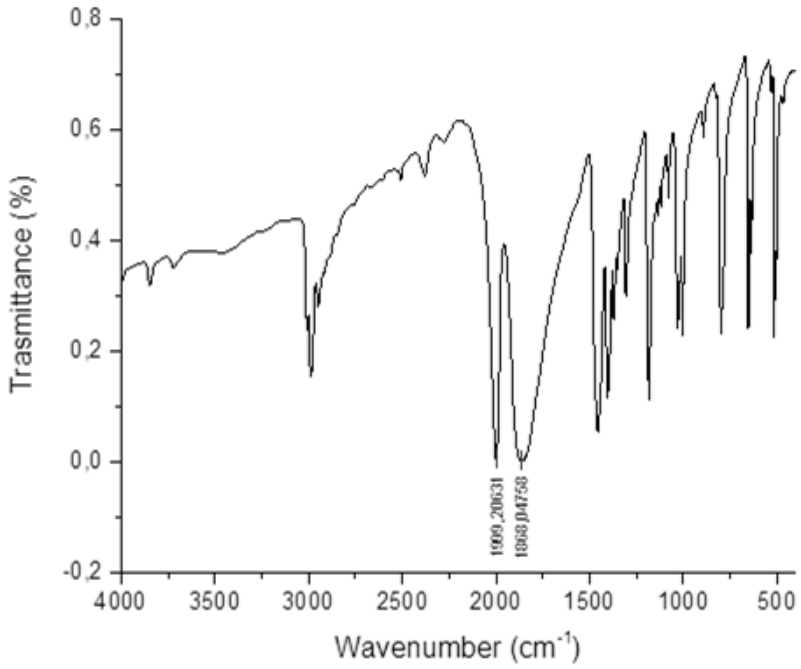

Figure 6.18: IR spectrum of the rhenium(I) complex, synthesized by Alberto *et al.* [12], prepared in KBr

The IR spectrum of *fac*-$[ReBr_3(CO)_3][NEt_4]_2$ shows several signals corresponding to the vibrational modes (i.e. stretching, bending, etc.) of the functional groups present on the considered compound. In particular, the attention is focused on the two signals at 1868 and 1999 cm^{-1} which represent the typical pattern of tricarbonyl compound and the values are consistent with the ones reported by Alberto *et al.* [12] (i.e. 1870 and 2001 cm^{-1}).

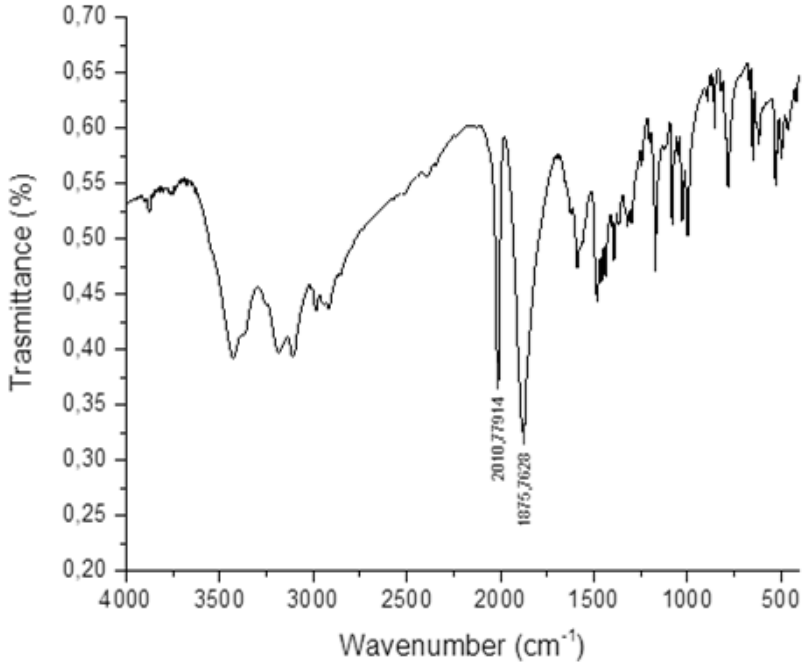

Figure 6.19: IR spectrum of the complex **26**, prepared in KBr

The IR spectrum of complex **26** (*Figure 6.19*) shows, in particular, two signals (typical of the presence of three carbonyl groups) at 1876 and 2011 cm^{-1} which result to be shifted respect to the values reported in *Figure 6.18* (i.e. 1868 and 1999 cm^{-1}), probably due to the coordination of the diethylenetriamine.

The reaction occurred successfully and, therefore, this method was applied to the ligand chosen to be bound to the chitosan surface.

6.12 Chelation Reaction of the Re(I) Complex with the 4-(bis(quinolin-2-ylmethyl)amino)butanoic Acid (27)

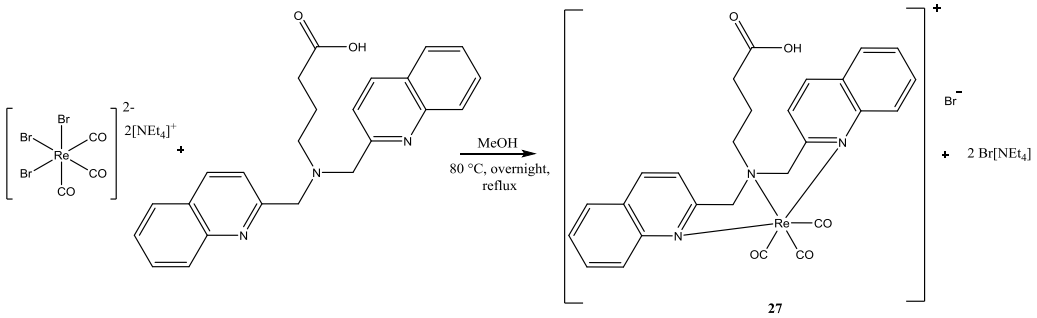

27

fac-$[ReBr_3(CO)_3][NEt_4]_2$ (25.0 mg, 0.0324 mmol) was reacted with 4-(bis(quinolin-2-ylmethyl)amino)butanoic acid (12.5 mg, 0.0324 mmol) in 4 mL of methanol, by using a reflux condenser, at 70 °C overnight. The solvent was then removed under reduced pressure and then the product obtained was dried *in vacuo*.

Yield: 22.8 mg, 0.0310 mmol, 95.5%.

6.12.1 Characterization of the Complex

RP-HPLC-ESI-MS

The analysis was performed by employing a stationary phase consisting of a C18 Phenosphere-NEXT column 5 μm, 250 × 4.60 mm ID, a mobile phase composed by a 50:50 mixture of a 15 mM aqueous solution of formic acid and pure methanol (by isocratic elution), a flow rate of 0.500 mL/min, a temperature of 37 °C and the UV-Visible detector set at 210 nm. Complex **27**, identified by

the corresponding ESI-MS spectrum (*Figure 6.20*), showed a retention time of 13.3 minutes.

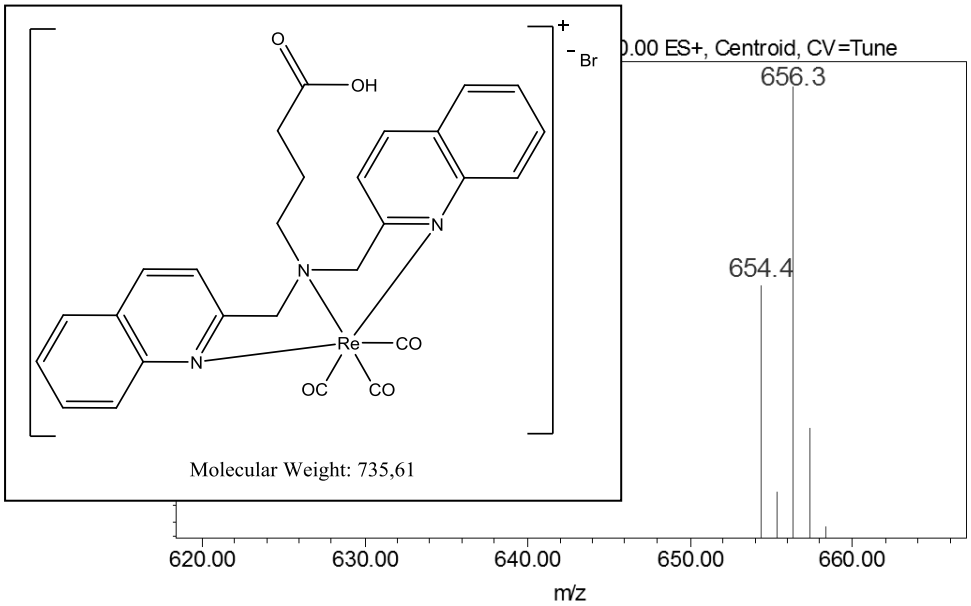

Figure 6.20: ESI-MS spectrum of the complex **27**, prepared in a 50:50 mixture of ultrapure water and methanol

In the ESI-MS spectrum, registered in positive ion mode with a cone voltage of 30V, it is possible to observe a m/z value at 656.3 which corresponds to the species $[M\text{-}Br]^+$ and it is confirmed also by the simulated ESI-MS spectrum (*Figure 6.21*).

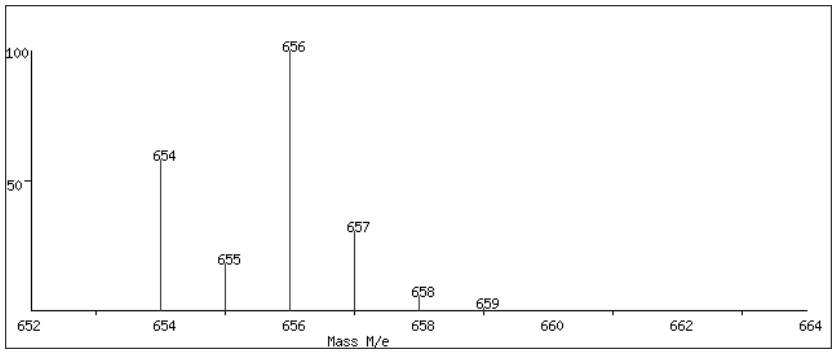

Figure 6.21: Simulated ESI-MS spectrum of the species $[M\text{-}Br]^+$ of complex **27**

Infrared Spectroscopy

The sample was prepared as described in *paragraph 6.11.1* and the corresponding IR spectrum shows, in particular, two signals at 1902 and 2016 cm^{-1} which result to be shifted respect to the values reported for the free Re(I) complex (i.e. 1868 and 1999 cm^{-1}) and for the complex chelated by DIEN (i.e. 1876 and 2011 cm^{-1}): this is probably due to the coordination of the hindered ligand.

Also this chelation reaction successfully occurred and, for this reason, the procedure was applied to the case of conjugate **25** with the rhenium(I) species.

6.13 Chelation Reaction of Conjugate 25 with the Re(I) Complex (28)

One of the two aliquots of the previously prepared conjugate **25** (about 10 mL, containing half of the tridentate ligand mmol, i.e. 0.0118 mmol) was reacted with the rhenium(I) complex. In particular, the *fac*-$[ReBr_3(CO)_3][NEt_4]_2$ (18.1 mg, 0.0235 mmol) was added to the water solution of **25** and the reaction was performed at 70 °C overnight. The solution was then dialyzed in ultrapure water for 2 days and an aliquot of the final solution was frozen by liquid nitrogen and lyophilized.

Conjugate **28** (4-5 mg) was mineralized by using the previously described procedure (*paragraph 6.5*), diluted with 1% v/v HNO_3 and analyzed by means of ICP-OES in order to quantify the Pt and Re contents.

The coupling results (effective percentage of Pt loading = 0.68 ± 0.19 %, corresponding to 0.0348 ± 0.0098 mmol Pt/g chitosan, effective percentage of

Re loading = 1.28 ± 0.62 %, corresponding to 0.0659 ± 0.0321 mmol Re (= ligand)/g chitosan) are expressed as a mean of at least three independent replicates and allow to evaluate that the Re content is higher than the Pt one. Moreover, it is possible to determine the ligand amount bound to the chitosan from the Re content: in fact, 1 mmol of ligand = 1 mmol of rhenium(I) complex. The radiopharmaceutical drugs are generally used at very low concentrations. In this case, the ligand concentration is much higher: this can allow to modulate the ^{99m}Tc complex quantity to be chelated, depending on the requirements.

6.13.1 Size and Stability Investigations

The DLS and ζ potential analyses of conjugate **28** were performed in ultrapure water at 25 °C and the results are shown and compared to the previous conjugates data in *Table 6.6*.

Conjugate	DLS diameter	ζ potential
22	180 ± 10 nm	41.5 ± 3.1 mV
22b	215 ± 12 nm	37.5 ± 0.6 mV
25	298 ± 21 nm	45.9 ± 1.1 mV
28	300 ± 24 nm	39.0 ± 2.4 mV

Table 6.6: Size and suspension stability results of conjugate **28** in ultrapure water

The ζ potential value of conjugate **28** is higher than +30 mV and this indicates that the suspension is highly stable.
As regards the size, also in this case (as described for conjugate **25**), it results to be increased with respect to the cases in which the chitosan surface was functionalized with (3-carboxypropyl)trimethylammonium derivative and the Pt(IV) complex.

6.13.2 Characterization of Conjugate 28

Infrared Spectroscopy

The sample was prepared as described in *paragraph 6.11.1* and the corresponding IR spectrum is reported in *Figure 6.22*.

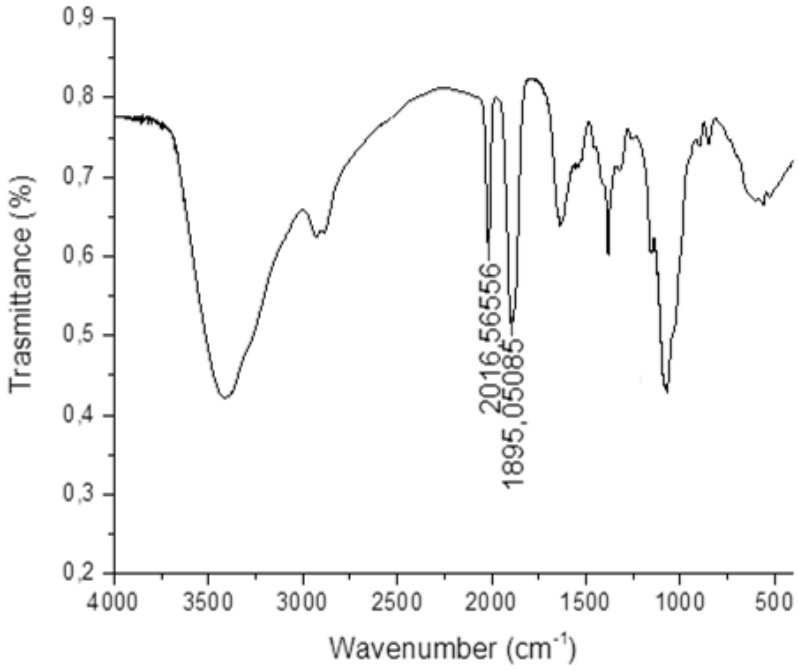

Figure 6.22: IR spectrum of the conjugate **28**, prepared in KBr

Two signals (typical of the presence of three carbonyl groups) can be observed at 1895 and 2017 cm^{-1} and they are similar to those obtained for complex **27** (i.e. 1902 and 2016 cm^{-1}): in fact, the species involved in the chelation are the same of the previous case.

The analysis of all the results allows to verify the occurred chelation and, therefore, that the system can be effectively used for chelating a technetium compound, exploitable for diagnostic purposes.

6.14 Conclusions

In this chapter, the very low soluble chitosan from shrimp shell was coupled to the activated form of (OC-6-44)-diammine(4-carboxypropanoato)dichloridoethanolatoplatinum(IV) (**8**). A protonation procedure was carried out before each coupling in order to allow the polysaccharide to be soluble in aqueous solutions. However, during the dialysis of the conjugates (to remove the unreacted species), portions of them precipitated and could not be resuspended again. Therefore, a chemical modification was performed in order to make chitosan soluble in aqueous solutions independently of the pH: in particular, the (3-carboxypropyl)trimethylammonium chloride was used.

The modified chitosan was coupled to the platinum complex at different coupling times and by using different amounts of the prodrug, in order to choose the best reaction conditions. These new conjugates were completely soluble in water.

The subsequent phase consisted of the introduction of a ligand able to chelate the ^{99m}Tc(I) species, i.e. (4-(bis(quinolin-2-ylmethyl)amino)butanoic acid). Before the reactions with the radioactive ^{99m}Tc, the cold Re analogous compound was used. In particular, the ability in the chelation of the rhenium(I) compound (*fac*-$[ReBr_3(CO)_3][NEt_4]_2$) was verified by using a tridentate ligand as a model (diethylenetriamine), the free quinolin ligand and then the complete conjugate containing the charged species, the platinum complex and the ligand itself.

The final conjugate was soluble independently of the pH, was functionalized with a Pt(IV) prodrug and contained a ligand able to chelate a Tc derivative with a similar structure to the *fac*-$[ReBr_3(CO)_3][NEt_4]_2$ one: it can represent a system suitable for theranostics purposes.

The perspectives of this work are the further reaction with a ^{99m}Tc complex in collaboration with Dr. A. Paulo (Centro de Ciências e Tecnologias Nucleares (C^2TN), Instituto Superior Técnico, Universidade de Lisboa, Portugal) and the *in vivo* evaluation of the conjugate.

References

[1] I. Aranaz, R. Harris, A. Heras, Chitosan Amphiphilic Derivatives. Chemistry and Applications, *Curr. Org. Chem.*, 14 (2010), 308-330.

[2] O. E. Philippova, E. V. Korchagina, Chitosan and Its Hydrophobic Derivatives: Preparation and Aggregation in Dilute Aqueous Solutions, *Polymer Science*, 54 (2012), 552-572.

[3] R. Riva, H. Ragelle, A. des Rieux, N. Duhem, C. Jérôme, V. Préat, Chitosan and Chitosan Derivatives in Drug Delivery and Tissue Engineering, *Adv. Polym. Sci*, 244 (2011), 19-44.

[4] E. S. de Alvarenga, Cristiane Pereira de Oliveira, C. R. Bellato, An approach to understanding the deacetylation degree of chitosan, *Carbohydr. Polym.*, 80 (2010), 1155-1160.

[5] L. Casettari, D. Vllasaliu, E. Castagnino, S. Stolnik, S. Howdle, L. Illum, PEGylated chitosan derivatives: Synthesis, characterizations and pharmaceutical applications, *Prog. Polym. Sci.*, 37 (2012), 659-685.

[6] A. B. Sieval, M. Thanou, A. F. Kotzé, J. C. Verhoef, J. Brussee, H. E. Junginger, Preparation and NMR characterization of highly substituted *N*-trimethyl chitosan chloride, *Carbohydr. Polym.*, 36 (1998), 157-165.

[7] N. A. Mohamed, M. W. Sabaa, A. H. El-Ghandour, M. M. Abdel-Aziz, O. F. Abdel-Gawad, Quaternized N-substituted carboxymethyl chitosan derivatives as antimicrobial agents, *Int. J. Biol. Macromol.*, 60 (2013), 156-164.

[8] A. Domard, M. Rinaudo, C. Terrassin, New method for the quaternarization of chitosan, *Int. J. Biol. Macromol.*, 8 (1986), 105-107.

[9] P. Pedrosa, R. Vinhas, A. Fernandes, P. V. Baptista, Gold Nanotheranostics: Proof-of-Concept or Clinical Tool?, *Nanomaterials*, 5 (2015), 1853-1879.

[10] R. Alberto, J. K. Pak, D. van Staveren, S. Mundwiler, P. Benny, Mono-, bi-, or tridentate ligands? The labeling of peptides with ^{99m}Tc-carbonyls, *Pept. Sci.*, 76 (2004), 324–333.

[11] C. Moura, T. Esteves, L. Gano, P. D. Raposinho, A. Paulo, I. Santos, Synthesis, characterization and biological evaluation of tricarbonyl M(I) (M = Re, ^{99m}Tc) complexes functionalized with melanin-binding pharmacophores, *New J. Chem.*, 34 (2010), 2564–2578.

[12] R. Alberto, A. Egli, U. Abram, K. Hegetschweiler, V. Gramlich, P. A. Schubiger, Synthesis and Reactivity of $[NEt_4]_2[ReBr_3(CO)_3]$. Formation and Structural Characterization of the Clusters $[NEt_4][Re_3(\mu_3\text{-}OH)(\mu\text{-}OH)_3(CO)_9]$ and $[NEt_4][Re_2(\mu\text{-}OH)_3(CO)_6]$ by Alkaline Titration, *J. Chem. Soc. Dalton Trans.*, Issue 1 (1994), 2815-2820.

Chapter VII

Coupling Reaction with Iron Oxide Nanoparticles (IONPs)

7.1 Introduction

Since early diagnosis is fundamental for a successful eradication of tumors, the research is moving towards the development of systems which can be exploited both for diagnosis and therapy purposes. In this work the attention was focused on magnetic iron oxide nanoparticles which can ensure the delivery of a platinum prodrug into the cells and can be employed in many fields (*Figure 7.1*), such as cancer therapy hyperthermia and Magnetic Resonance Imaging (MRI), due to their superparamagnetism.

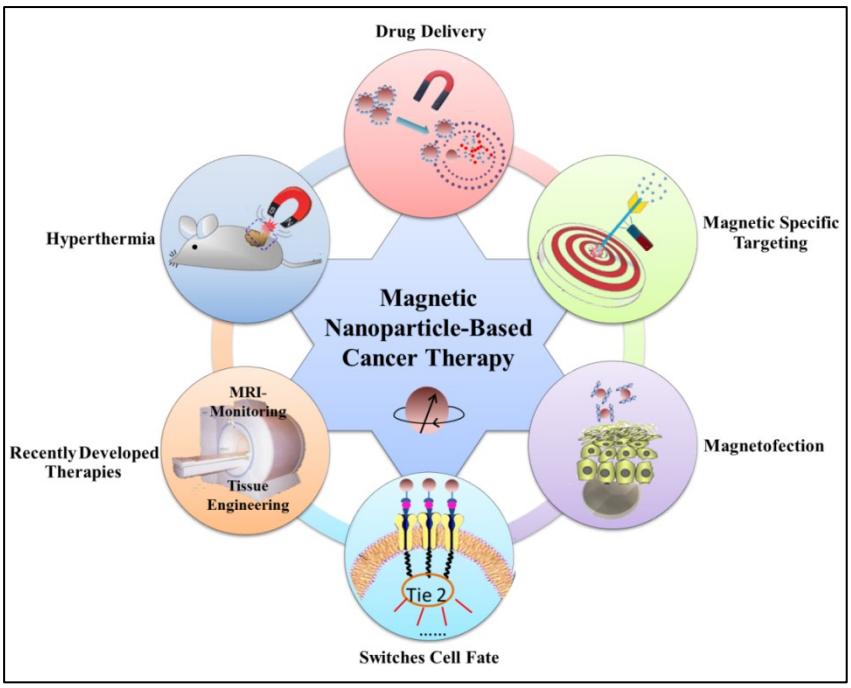

Figure 7.1: Possible cancer treatments based on the use of magnetic nanoparticles. The picture was obtained after a slight modification of that reported in literature [1]

These NPs, since 1987, have been clinically administered to detect spleen and liver diseases by means of MRI. They are composed of magnetite (Fe_3O_4) and maghemite (γ-Fe_2O_3), are considered superparamagnetic because they can be

oriented in the direction of a magnetic field and, after its removal, they restore their initial state, and they are biocompatible. Their biocompatibility is due to the fact that the uptake, excretion and storage of iron are efficiently regulated and the clearance of the excess occurs without serious side effects.

Furthermore, they can be classified into different categories depending on their size. The size role is crucial because the nanoparticles dimensions affect their biodistribution and accumulation into the tumor site:

- size higher than 100 nm may induce embolization and non-specific uptake by the reticuloendothelial system [2],
- diameters higher than 30 nm (SPIO, i.e. small paramagnetic iron oxide), often, have a short blood half-life because they are phagocytosed in liver and spleen and this causes a loss of the signal exploitable for MRI [3],
- dimensions between 1 and 30 nm (USPIO, i.e. ultrasmall paramagnetic iron oxide) avoid early phagocytosis and, therefore, allow to be used as contrast agents and monitoring tool [3].

Feridex, Endorem and Resovist are some examples of clinically administered superparamagnetic iron oxide nanoparticles and, in particular, they are employed in USA (Feridex), Europe (Endorem and Resovist) and Japan (Resovist).

As regards the imaging methods, the MRI is a noninvasive scan of the body and exploits the water molecules hydrogen atoms which, in the presence of an appropriate magnetic field, are excited. After this process, their relaxation occurs and different tissues can be distinguished by different relaxation times T1 and T2. Some contrast agents (based on gadolinium or manganese) act on T1 by shortening it and, therefore, giving rise to a brighter picture (positive contrast). On the contrary, superparamagnetic iron oxide nanoparticles reduce T2 (negative contrast). Therefore, the use of superparamagnetic iron oxide nanoparticles allows to improve the sensitivity of MRI.

In the case of magnetic NPs, a possible exploitable therapy is the hyperthermia, i.e. a locally increase of a tissue temperature. It is known that the physiological temperature is 37 °C and, therefore, higher values can lead the cell to lose its functions and also to its death. In fact, the heat generated by the nanoparticles when placed in an alternative magnetic field can be exploited as an antitumoral treatment. The accumulation of the NPs into the diseased site can be ensured by exploiting an external magnetic field or by ligand-receptor interactions [4], even though in the first case the specific delivery is problematic and side effects may occur (such as the heating of the healthy tissues).

In this work, Iron Oxide Magnetic Nanoparticles (IONPs) functionalized with furan groups were employed in collaboration with Dr. Jérôme Fresnais (Laboratoire de Physico-Chimie des Electrolytes, Colloïdes et Sciences Analytiques, Paris (France)). Furan can be exploited for Diels-Alder cycloaddition. Therefore, in the first synthetic phase of this work, some Pt(IV) complexes bearing a dienophile functionality were prepared. In particular, glycine and maleic anhydride reacted in order to obtain the (*Z*)-4-((carboxymethyl)amino)-4-oxobut-2-enoic acid (**29**). Then, a cyclization reaction allowed to synthesize the 2-(2,5-dioxo-2,5-dihydro-1*H*-pyrrol-1-yl)acetic acid (**30**), which represents the ligand that will be coordinated to the platinum core, in axial or equatorial position (in this latter case, by substitution of a chloride ion of cisplatin), and the dienophile suitable for a Diels-Alder cycloaddition. In particular, four Pt(IV) compounds were prepared: three show the maleimide derivative in equatorial position (**32**, **33**, **34**) and one in axial position (**35**). However, only one of them was chosen for further couplings, due to its high purity and ease of synthesis. Therefore, its cycloaddition reaction was studied in the presence of different dienes, i.e. a furan, a ligand containing a furan group (Furan-Functionalized Phosphonic Acid-Terminated POE

Monomethyl Ether) and iron oxide nanoparticles containing the same ligand (*Figure 7.2*).

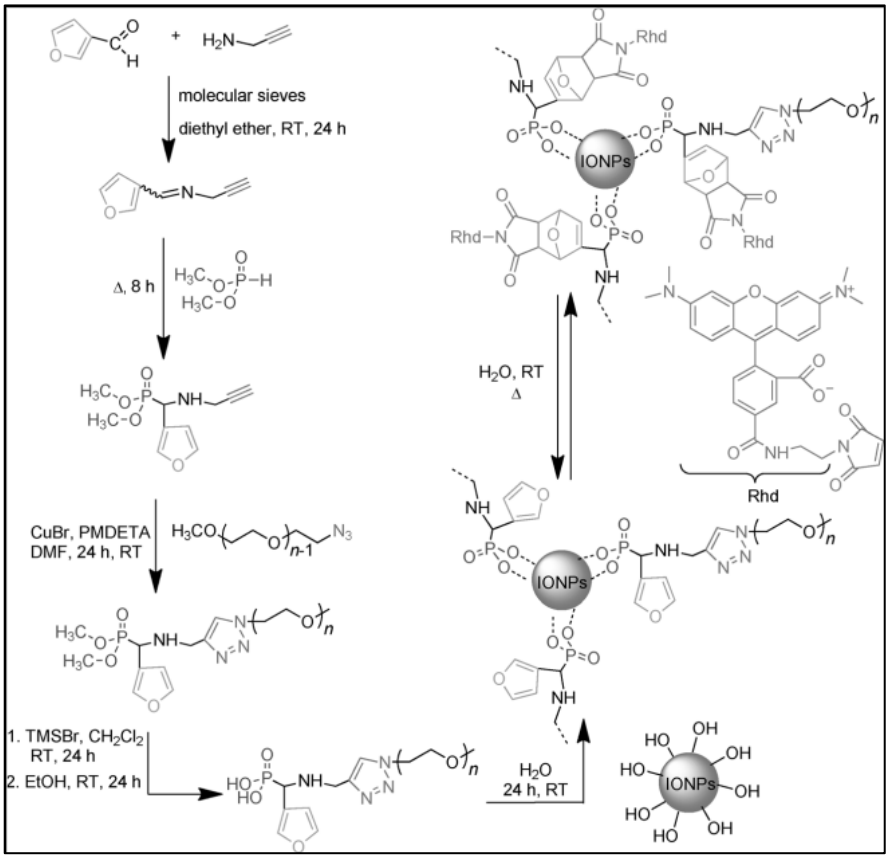

Figure 7.2: Schematic representation of the synthesis and applications of the IONPs [5]. PMDETA = *N*,*N*,*N*′,*N*″,*N*‴-pentamethyldiethylenetriamine and TMSBr = trimethylsilyl bromide

Then, the *in vitro* and *in vivo* biological activity of the Diels-Alder product must be evaluated and, in particular, the hyperthermia treatment.

The synthesized platinum complexes and conjugates are reported here in order of discussion:

- (*Z*)-4-((carboxymethyl)amino)-4-oxobut-2-enoic acid (**29**),
- 2-(2,5-dioxo-2,5-dihydro-1*H*-pyrrol-1-yl)acetic acid (**30**),
- (SP-4-3)-diamminechlorido(2-(2,5-dioxo-2,5-dihydro-1*H*-pyrrol-1-yl)

acetate)platinum(II) (**31**),

- (OC-6-44)-diamminechloridodihydroxido(2-(2,5-dioxo-2,5-dihydro-1*H*-pyrrol-1-yl)acetate)platinum(IV) (**32**),
- (OC-6-44)-diamminedichlorido(2-hydroxyethanolato)(2-(2,5-dioxo-2,5-dihydro-1*H*-pyrrol-1-yl)acetate)platinum(IV) (**33**),
- (OC-6-44)-diammine(4-carboxypropanoato)dichlorido(2-(2,5-dioxo-2,5-dihydro-1*H*-pyrrol-1-yl)acetate)platinum(IV) (**34**),
- (OC-6-44)-diamminedichloridoethanolato(2-(2,5-dioxo-2,5-dihydro-1*H*-pyrrol-1-yl)acetate)platinum(IV) (**35**),
- (OC-6-44)-diamminedichloridoethanolato(2-(1,3-dioxo-3a,4,7,7a-tetrahydro-1*H*-4,7-epoxyisoindol-2(3*H*)-yl)acetate)platinum(IV) (**36**),
- Product of the Diels-Alder cyclization between complex **35** and the furan-functionalized ligand (**37**),
- Product of the Diels-Alder cyclization between complex **35** and IONPs (**38**).

7.2 Synthesis of the (Z)-4-((carboxymethyl)amino)-4-oxobut-2-enoic Acid (29)

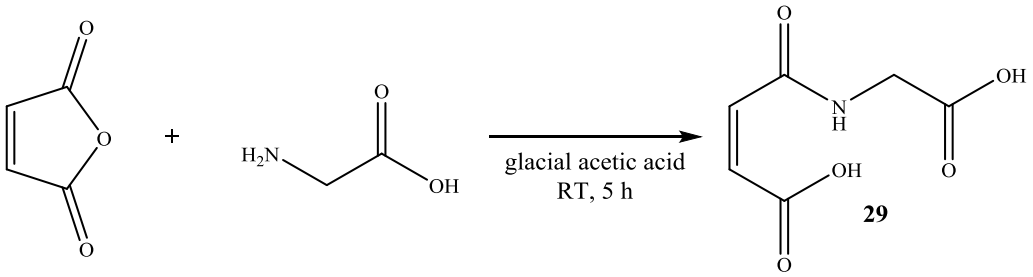

Complex **29** was synthesized according to a previously published procedure [6]. In particular, to a solution of maleic anhydride (1.08 g, 11.1 mmol) in glacial

acetic acid (14 mL), glycine (0.830 g, 11.1 mmol) was added. The suspension was magnetically stirred for 5 hours at room temperature. Then, the product was separated by centrifugation, washed twice with cold ultrapure water and twice with methanol, and dried *in vacuo*.
Yield: 1.76 g, 10.2 mmol, 91.8%.

7.2.1 Characterization of the Compound

RP-HPLC-ESI-MS

The analysis was performed by employing a stationary phase consisting of a C18 Phenosphere-NEXT column 5 μm, 250 × 4.60 mm ID, a mobile phase composed by a 20:80 mixture of a 15 mM aqueous solution of formic acid and pure methanol (by isocratic elution), a flow rate of 0.500 mL/min, a temperature of 37 °C and the UV-Visible detector set at 210 nm. Compound **29** showed a retention time of 8.65 minutes and its identity was attributed by the corresponding ESI-MS spectrum (*Figure 7.3*).

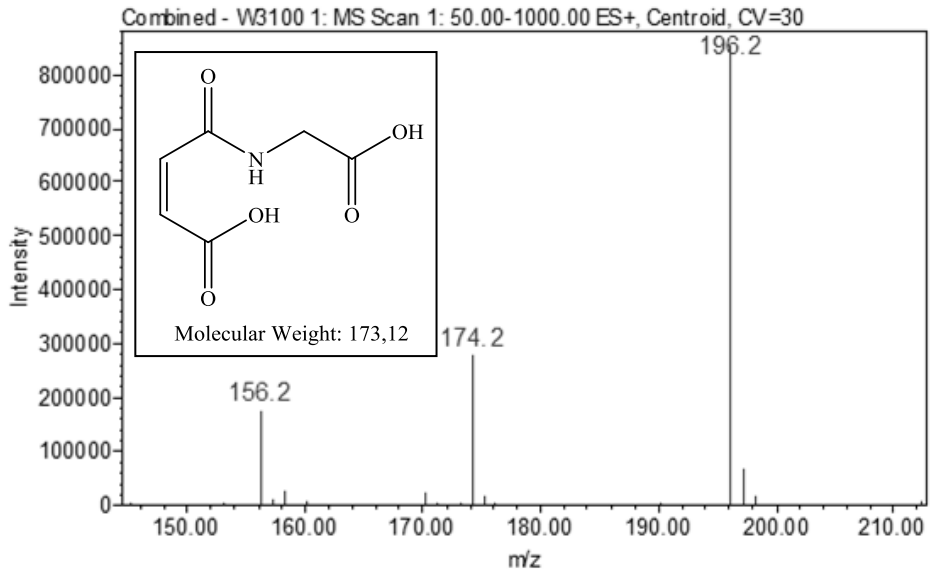

Figure 7.3: ESI-MS spectrum of compound **29**, prepared in methanol

The ESI-MS spectrum of compound **29** (*Figure 7.3*), registered in positive ion mode with a cone voltage of 30V, shows the pseudo-molecular ion $[M+H]^+$ peak at 174.2 m/z and the $[M-OH]^+$ and $[M+Na]^+$ species at 156.2 and 196.2 m/z, respectively.

[1]H-NMR

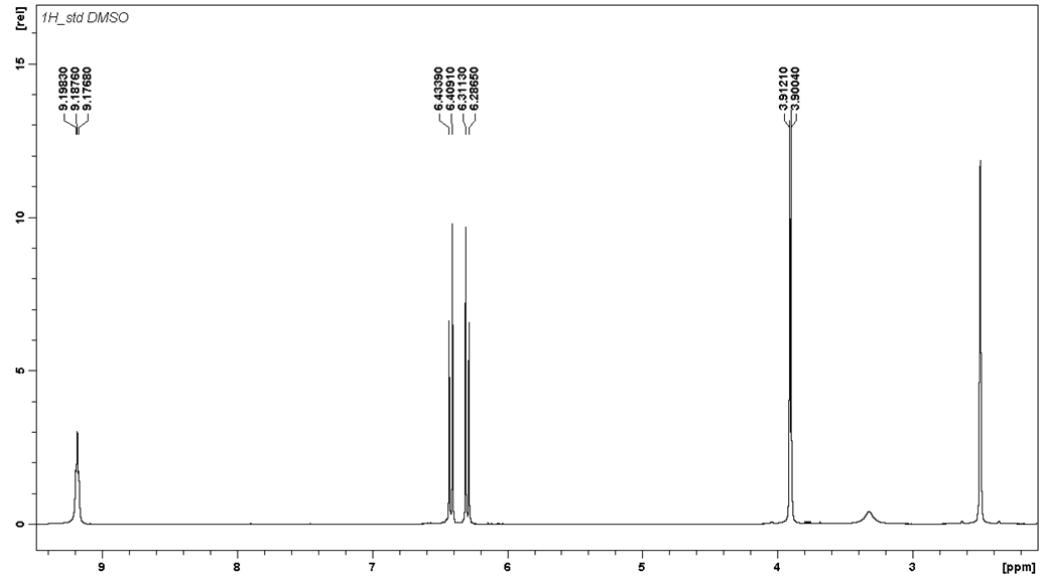

Figure 7.4: [1]H-NMR spectrum of compound **29**, registered in DMSO-d_6

The [1]H-NMR (500 MHz, DMSO-d_6) spectrum of **29** (*Figure 7.4*) shows the following signals, δ: 3.91 (d, 2H, -C*H*$_2$, ^{3}J = 5.85 Hz), 6.31 (d, 1H, -C*H*CO$_2$H, ^{3}J = 12.4 Hz), 6.43 (d, 1H, -C*H*CONH, ^{3}J = 12.4 Hz), 9.19 (t, 1H, -N*H*, ^{3}J = 5.35 Hz) ppm.

^{13}C-NMR

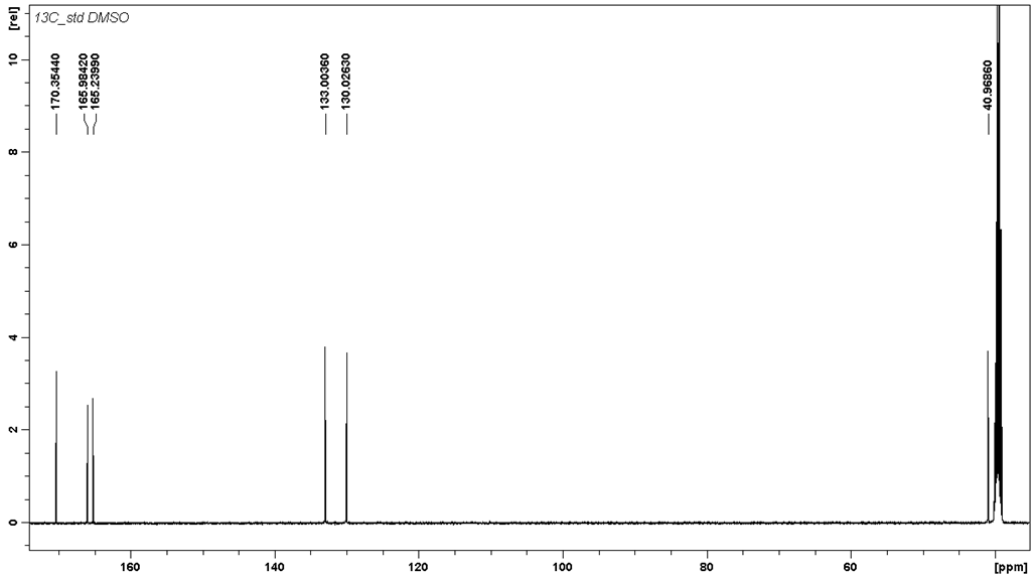

Figure 7.5: ^{13}C-NMR spectrum of compound **29**, registered in DMSO-d_6

The ^{13}C-NMR (125.7 MHz, DMSO-d_6) spectrum of **29** (*Figure 7.5*) shows the following signals, δ: 40.97 (-*C*H_2), 130.0 (-*C*HCONH), 133.0 (-*C*HCO_2H), 165.2 (-CH*C*O_2H, 165.98 (-CH*C*ONH), 170.4 (-CH_2*C*O_2H) ppm.

The product was synthesized in high purity and, therefore, was employed for the preparation of the ligand, which must be coordinated to the Pt in equatorial or axial position.

7.3 Synthesis of the 2-(2,5-dioxo-2,5-dihydro-1H-pyrrol-1-yl)acetic Acid (30)

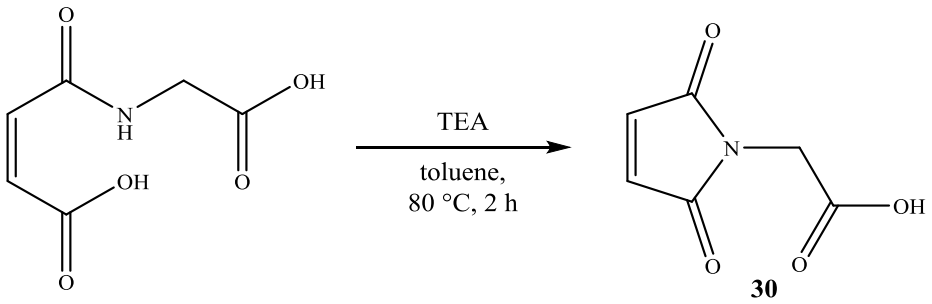

30

The synthetic procedure was reported in literature [7]. Compound **29** (500 mg, 2.89 mmol) was suspended in 75 mL of toluene. Then, after the addition of 1.4 mL of triethylamine (TEA), the suspension was left under vigorous stirring at 80 °C in an oil bath till the reagent was completely dissolved (about 2 hours): the solution became pale yellow and, on the flask bottom, a brownish oil was formed. It was eliminated by centrifugation. Toluene was removed under reduced pressure. Then, the colorless residue was dissolved with ultrapure water (about 50 mL) and the pH was adjusted to 2.0 ± 0.1 with few drops of concentrated HCl. Two extractions with of ethyl acetate were carried out and the organic phase was made anhydrous with anhydrous sodium sulfate and evaporated to dryness by a rotary evaporator.

The product was collected and dried *in vacuo* (it was very hygroscopic).

Yield: 0.322 g, 2.07 mmol, 71.9%.

7.3.1 Characterization of the Compound

RP-HPLC-ESI-MS

The analysis was performed by employing a stationary phase consisting of a C18 Phenosphere-NEXT column 5 μm, 250 × 4.60 mm ID, a mobile phase composed by a 20:80 mixture of a 15 mM aqueous solution of formic acid and pure methanol (by isocratic elution), a flow rate of 0.500 mL/min, a temperature of 37 °C and the UV-Visible detector set at 210 nm. Compound **30** showed a retention time of 8.71 minutes and its identity was attributed by the corresponding ESI-MS spectrum (*Figure 7.6*).

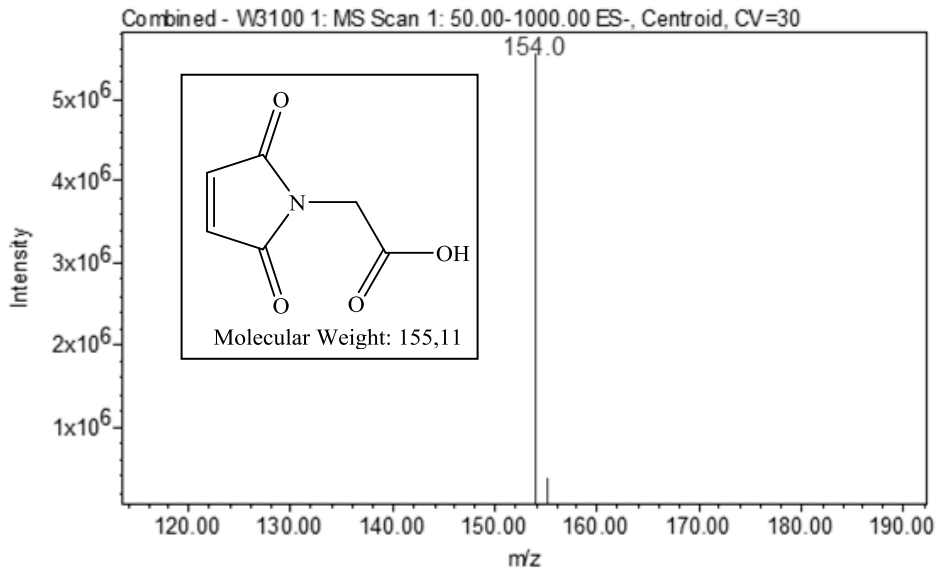

Figure 7.6: ESI-MS spectrum of compound **30**, dissolved in methanol

Figure 7.6 shows the ESI-MS spectrum of compound **30**, registered in negative ion mode with a cone voltage of 30V, and it allows to confirm the presence of the pseudo-molecular ion $[M-H]^-$ at 154.0 m/z.

[1]H-NMR

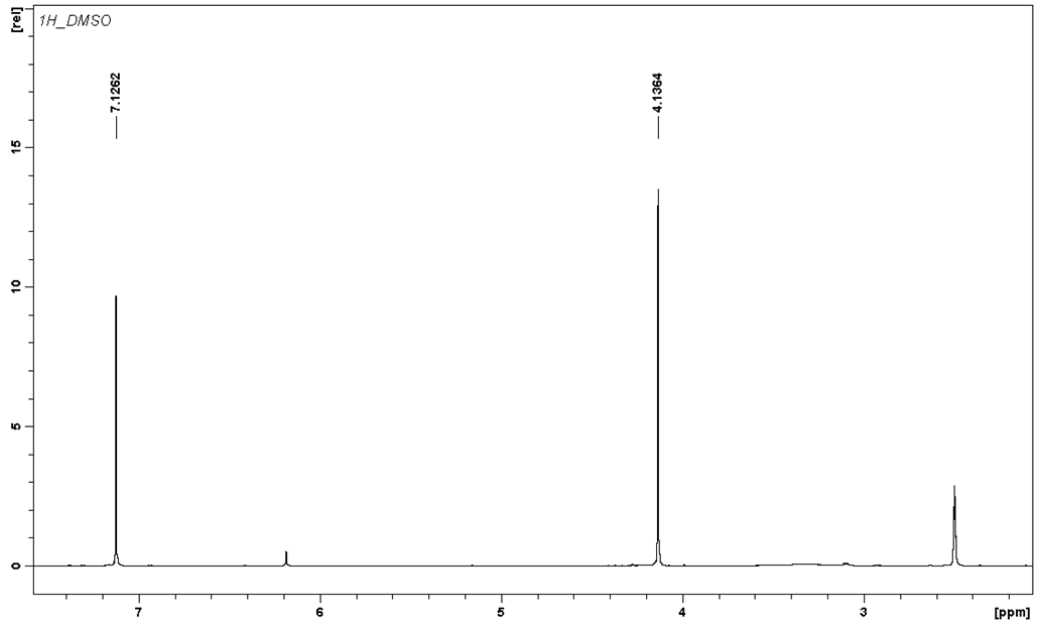

Figure 7.7: [1]H-NMR spectrum of compound **30**, registered in DMSO-d_6

The [1]H-NMR (500 MHz, DMSO-d_6) spectrum of **30** (*Figure 7.7*) shows the following signals, δ: 4.14 (s, 2H, -OCOCH_2), 7.13 (s, 1H, -NCOC*H*) ppm.

^{13}C-NMR

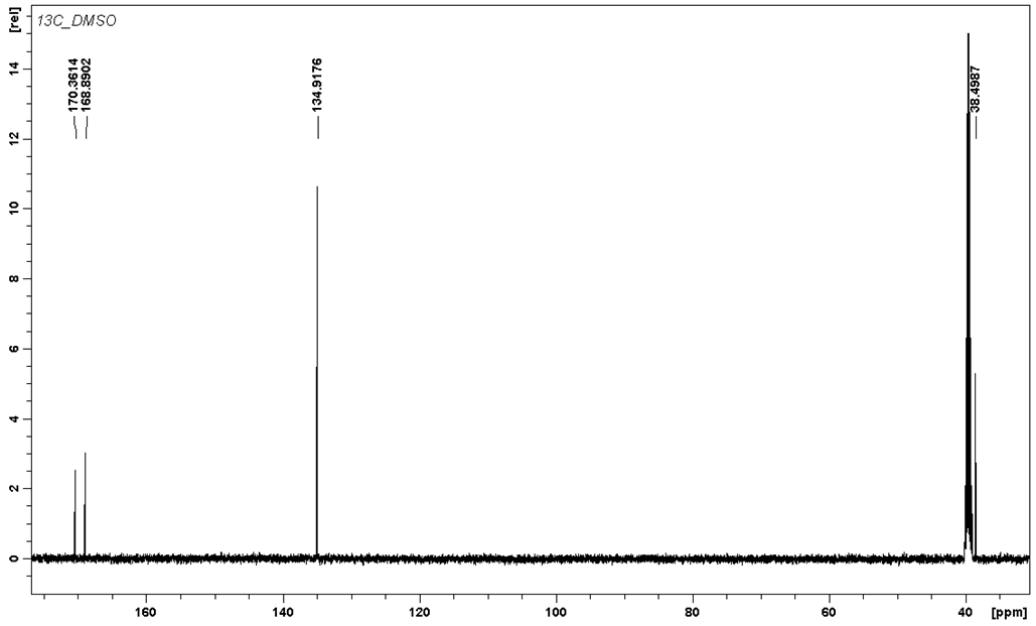

Figure 7.8: ^{13}C-NMR spectrum of compound **30**, registered in DMSO-d_6

The ^{13}C-NMR (125.7 MHz, DMSO-d_6) spectrum of **30** (*Figure 7.8*) shows the following signals, δ: 38.5 (-OCO*C*H_2), 134.9 (-NCO*C*H=*C*H), 168.9 (-O*C*OCH_2), 170.4 (-N*C*OCH=CH) ppm.

The synthesized ligand, obtained in high purity, was used to substitute one of the two leaving groups of cisplatin in order to exploit also the equatorial position for the coupling with another drug or a vector. In particular, the reaction of cisplatin with an almost stoichiometric amount of silver nitrate allows to replace a chloride with a water molecule. Then, this intermediate reacts with a solution containing the salt of the previously prepared ligand (**30**), obtaining as a result a Pt(II) complex which can be functionalized also in equatorial position (**31**). Its synthesis and characterization are reported in the following paragraph.

7.4 Synthesis of the (SP-4-3)-diamminechlorido(2-(2,5-dioxo-2,5-dihydro-1H-pyrrol-1-yl)acetate)platinum(II) (31)

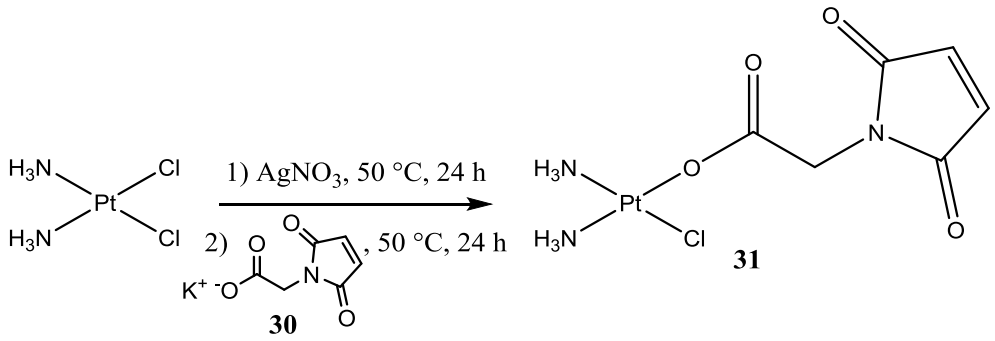

The replacement reaction of one of the two cisplatin chlorides was carried out according to a procedure [8]. In particular, to a suspension of cisplatin (100 mg, 0.333 mmol) in 5 mL of anhydrous DMF, silver nitrate (53.7 mg, 0.317 mmol) was added dropwise and the mixture was magnetically stirred at room temperature for 24 hours in the dark. The suspension was then filtered (PTFE filter with a porosity of 0.45 μm) in order to remove AgCl (precipitated during the displacement of the chloride ligand). The solution was added to a solution of potassium 2-(2,5-dioxo-2,5-dihydro-1*H*-pyrrol-1-yl)acetate in anhydrous DMF. This latter was previously prepared by dissolving compound **30** (57.3 mg, 0.369 mmol) and KOH (20.7 mg, 0.369 mmol) in ultrapure water, by correcting the pH value to about 5-6, by removing water under reduced pressure and by suspending the obtained species in anhydrous DMF. The reaction was carried out at 50 °C for 24 hours in the dark. The mixture was then filtered (0.45 μm porosity) and DMF was removed under reduced pressure. The yellow product was precipitated by adding ethanol/diethyl ether, washed with ethanol and methanol and finally dried *in vacuo*.

Yield: 59.1 mg of not completely pure compound.

7.4.1 Characterization of the Complex

RP-HPLC-ESI-MS

The analysis was performed by employing a stationary phase consisting of a C18 Phenosphere-NEXT column 5 μm, 250 × 4.60 mm ID, a mobile phase composed by a 50:50 mixture of a 15 mM aqueous solution of formic acid and pure methanol (by isocratic elution), a flow rate of 0.500 mL/min, a temperature of 37 °C and the UV-Visible detector set at 210 nm. The chromatogram of the reaction product is reported in *Figure 7.9*.

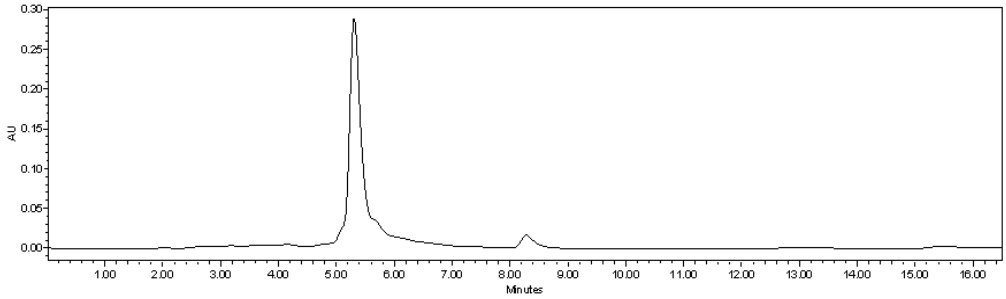

Figure 7.9: Chromatogram of complex **31**, prepared in ultrapure water

The chromatogram shows three main peaks at 5.31, 5.82 and 8.15 minutes, the identity of which is verified by the corresponding ESI-MS spectra (*Figures 7.10-7.12*).

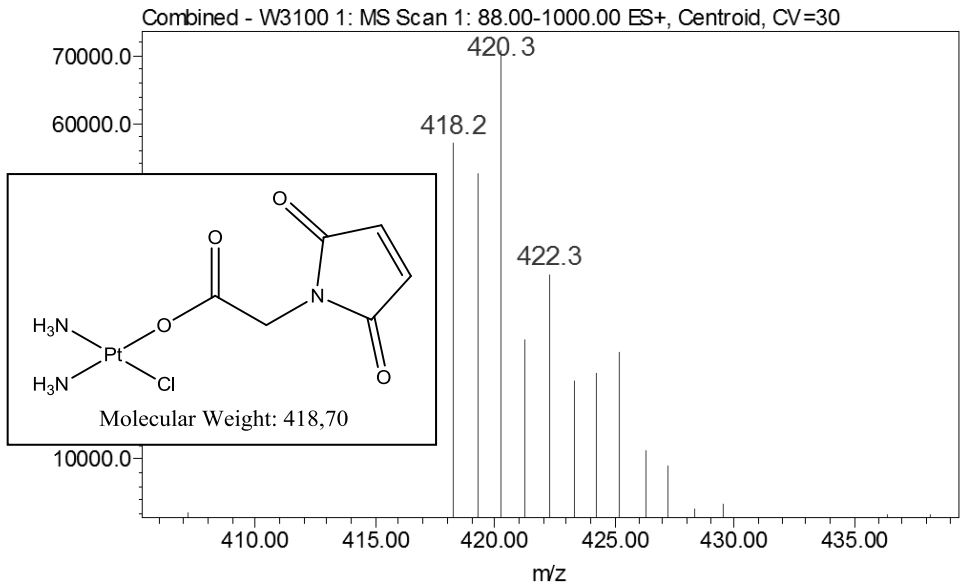

Figure 7.10: ESI-MS spectrum of the species eluted at 5.31 minutes

The ESI-MS spectrum (*Figure 7.10*), registered in positive ion mode with a cone voltage of 30V, shows a value at 420.3 m/z, corresponding to the pseudo-molecular ion $[M+H]^+$ peak of complex **31**.

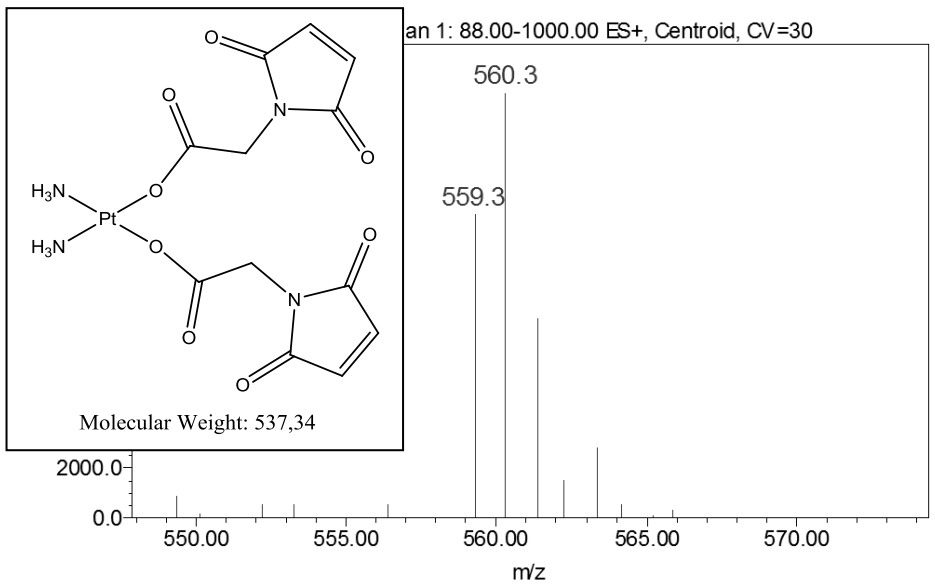

Figure 7.11: ESI-MS spectrum of the species eluted at 5.82 minutes

The ESI-MS spectrum (*Figure 7.11*), registered in positive ion mode with a cone voltage of 30V, shows a value at 560.3 m/z, corresponding to the $[M+Na]^+$ adduct of a Pt(II) complex in which also the second chloride ligand is replaced by another **30** molecule, byproduct.

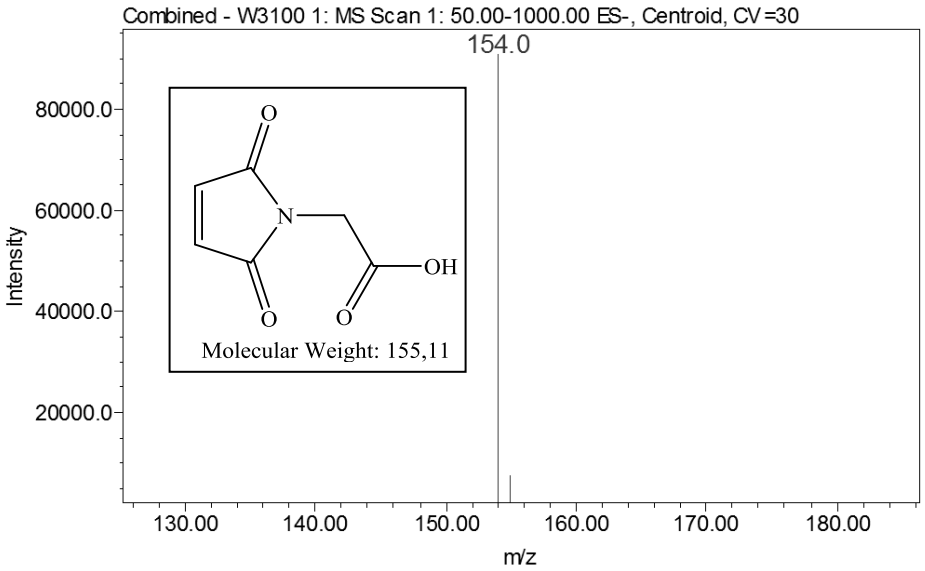

Figure 7.12: ESI-MS spectrum of the species eluted at 8.15 minutes

The ESI-MS spectrum (*Figure 7.12*), registered in negative ion mode with a cone voltage of 30V, shows a value at 154.0 m/z, corresponding to the pseudo-molecular ion $[M-H]^-$ peak of the unreacted 2-(2,5-dioxo-2,5-dihydro-1H-pyrrol-1-yl)acetic acid (**30**).

[1]H-NMR

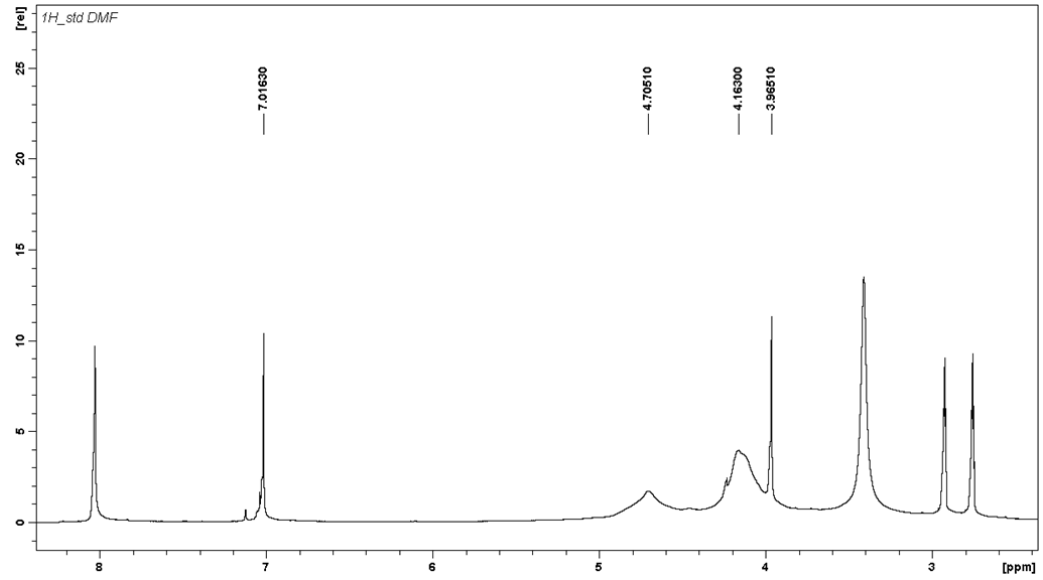

Figure 7.13: [1]H-NMR spectrum of complex **31**, registered in DMF-d_7

The [1]H-NMR (500 MHz, DMF-d_7) spectrum of **31** (*Figure 7.13*) shows the following signals, δ: 3.97 (s, 2H, -OCOCH_2), 4.16 (m, 3H, -NH_3 in *trans* to the carboxylate ligand), 4.70 (m, 3H, -NH_3 in *trans* to the chloride ligand), 7.02 (s, 2H, -C*H*=C*H*CON) ppm.

It is possible to attribute the signals at 4.16 and 4.70 ppm to the protons of the carrier groups in *trans* to the carboxylate and to the chloride ligands, respectively, since literature [9] reports that protons in *trans* to a chloride show a higher chemical shift than the ones of a species in *trans* to a carboxylato group.

^{13}C-NMR

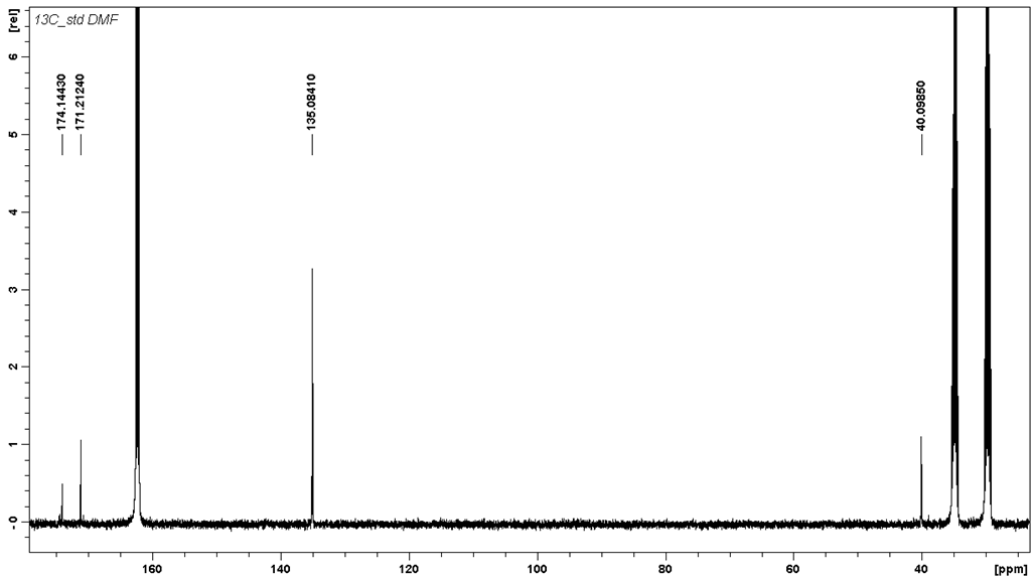

Figure 7.14: ^{13}C-NMR spectrum of complex **31**, registered in DMF-d_7

The ^{13}C-NMR (125.7 MHz, DMF-d_7) spectrum of **31** (*Figure 7.14*) shows the following signals, δ: 40.1 (-OCO*C*H_2), 135.1 (-NCO*C*H=*C*H), 171.2 (-N*C*OCH=CH), 174.1 (-O*C*OCH_2) ppm.

^{195}Pt-NMR

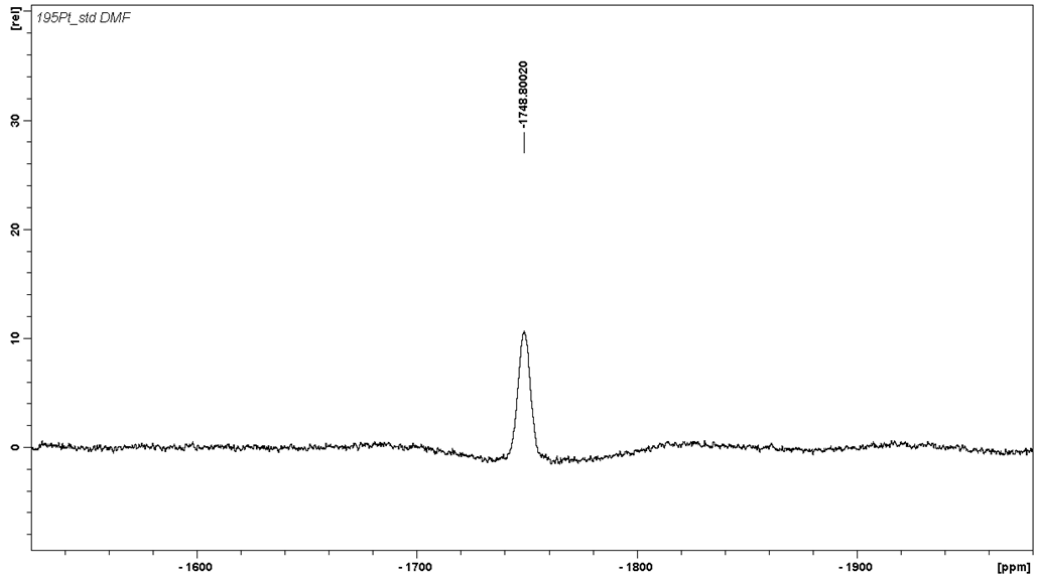

Figure 7.15: ^{195}Pt-NMR spectrum of complex **31**, registered in DMF-d_7

The ^{195}Pt-NMR spectrum of complex **31** (*Figure 7.15*) was registered in DMF-d_7 (at a 107.2 MHz NMR frequency) and shows a signal with a chemical shift value of -1749 ppm, which is consistent with a Pt(II) complex containing a chloride, a carboxylato and two amines.

After a further step of purification, complex **31** was employed as the basis for the synthesis of three Pt(IV) compounds, the axial ligands of which must be exploited for further couplings to other drugs or active species.

In one case, the oxidation reaction was carried out by using hydrogen peroxide in water in order to prepare a symmetrical complex (**32**) with two hydroxido groups in axial position (the first deriving from the H_2O_2 and the second from the solvent).

In the other cases, the *N*-chlorosuccinimide (NCS) was the oxidizing agent: this is a source of "positive chloride ions", which remove two electrons to the Pt(II)

that is then oxidized to Pt(IV) [10]. The second axial ligand is 2-hydroxoethanolato (complex **29**), which derives from the reaction solvent (i.e. ethylene glycol), or 4-carboxypropanoato (compound **30**), deriving from the nucleophile (i.e. succinic anhydride) dissolved in a non-coordinating solvent (acetone). This latter is not completely anhydrous and it is hypothesized that the water present in the solvent has an important role in the reaction mechanism: probably, an hydroxido is at first coordinated to platinum in axial position, by forming an intermediate which then reacts with the anhydride to obtain the final product.

7.5 Synthesis of the (OC-6-44)-diamminechloridodihydroxido(2-(2,5-dioxo-2,5-dihydro-1H-pyrrol-1-yl)acetate)platinum(IV) (32)

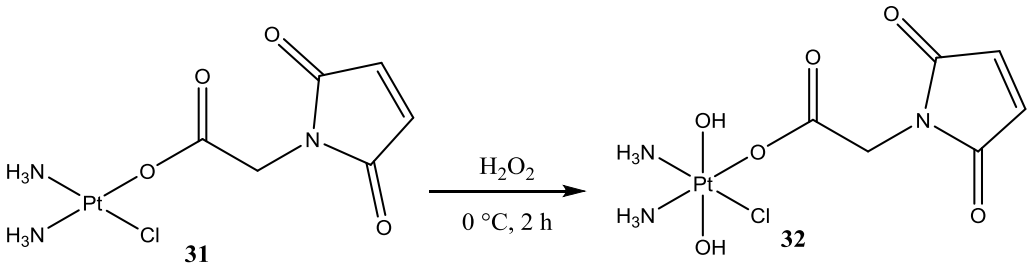

Complex **31** (35.0 mg, 0.0836 mmol) was suspended in 1 mL of a 50% w/w aqueous solution of hydrogen peroxide and the mixture was magnetically stirred in an ice bath for 2 hours. Then the water was removed under reduced pressure and the product was precipitated by acetone/diethyl ether, washed with diethyl ether and dried *in vacuo*.

Yield: 19.7 mg of crude product (see RP-HPLC-ESI-MS results).

7.5.1 Characterization of the Complex

RP-HPLC-ESI-MS

The analysis was performed by employing a stationary phase consisting of a C18 Phenosphere-NEXT column 5 μm, 250 × 4.60 mm ID, a mobile phase composed by a 50:50 mixture of a 15 mM aqueous solution of formic acid and pure methanol (by isocratic elution), a flow rate of 0.500 mL/min, a temperature of 37 °C and the UV-Visible detector set at 210 nm.

The RP-HPLC-ESI-MS characterization allows to verify that the oxidation reaction of complex **31**, in these conditions, was not successful: in fact, the Pt(II) complex is not formed (not even in small amounts). For this reason, this oxidation method was abandoned and other strategies, based on the use of the *N*-chlorosuccinimide, were carried out to obtain an oxidized product.

7.6 Synthesis of the (OC-6-44)-diamminedichlorido(2-hydroxyethanolato)(2-(2,5-dioxo-2,5-dihydro-1H-pyrrol-1-yl) acetate)platinum(IV) (33)

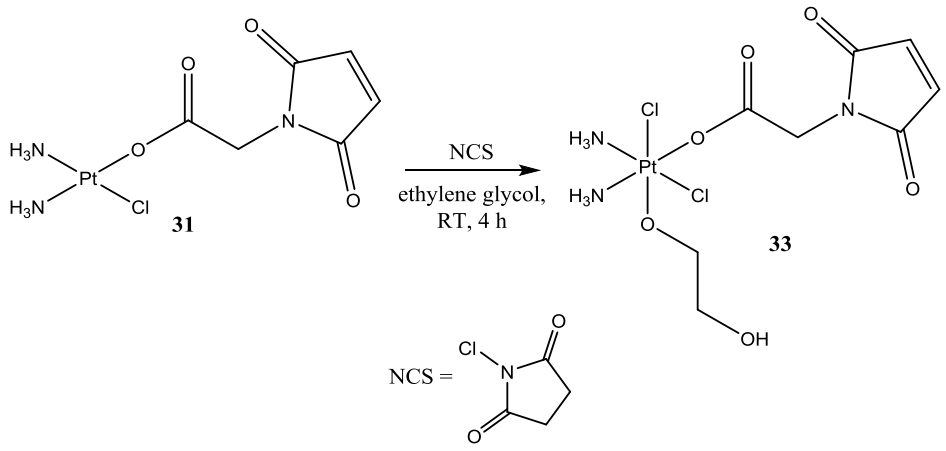

Complex **31** (46.0 mg, 0.110 mmol) was suspended in 1.5 mL of ethylene glycol and was magnetically stirred for 30 minutes. Then a slight excess of *N*-chlorosuccinimide (14.8 mg, 0.111 mmol) was added to the mixture and the reaction was carried out at room temperature for 4 hours in the dark. After the established time, the mixture was filtered and a yellow product was precipitated by adding acetone/diethyl ether, washed with diethyl ether and dried *in vacuo*.
Yield: 35.8 mg of crude product (see RP-HPLC-ESI-MS results).

7.6.1 Characterization of the Complex

RP-HPLC-ESI-MS

The analysis was performed by employing a stationary phase consisting of a C18 Phenosphere-NEXT column 5 μm, 250 × 4.60 mm ID, a mobile phase composed by a 50:50 mixture of a 15 mM aqueous solution of formic acid and pure methanol (by isocratic elution), a flow rate of 0.500 mL/min, a temperature of 37 °C and the UV-Visible detector set at 210 nm.
Also in this case, the RP-HPLC-ESI-MS characterization allows to verify that complex **31** was not oxidized and, for this reason, this oxidation method was modified: in fact, the ethylene glycol was replaced by the use of a non-coordinating solvent (acetone) and of a nucleophile (succinic anhydride) in order to study this oxidation method again but allowing the coordination of another type of second axial ligand.

7.7 Synthesis of the (OC-6-44)-diammine(4-carboxypropanoato)dichlorido(2-(2,5-dioxo-2,5-dihydro-1H-pyrrol-1-yl)acetate)platinum(IV) (34)

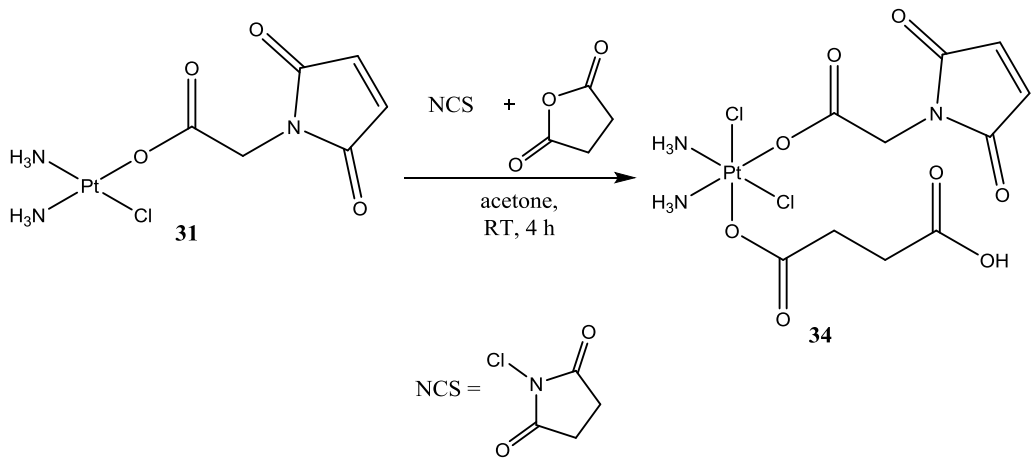

Complex **31** (92.1 mg, 0.220 mmol) and *N*-chlorosuccinimide (29.7 mg, 0.222 mmol) were suspended in 2 mL of anhydrous acetone. Then succinic anhydride (440 mg, 4.40 mmol), dissolved in 14 mL of anhydrous acetone, was added to the mixture and the reaction was carried out at room temperature for 4 hours in the dark. Subsequently, the solid was removed by filtration and the acetone was removed under reduced pressure. The solid was collected and washed several times with diethyl ether and then dried *in vacuo*.

Yield: 42.6 mg of not completely pure compound.

7.7.1 Characterization of the Complex

RP-HPLC-ESI-MS

The analysis was performed by employing a stationary phase consisting of a C18 Phenosphere-NEXT column 5 μm, 250 × 4.60 mm ID, a mobile phase composed by a 50:50 mixture of a 15 mM aqueous solution of formic acid and pure methanol (by isocratic elution), a flow rate of 0.500 mL/min, a temperature of 37 °C and the UV-Visible detector set at 210 nm. Complex **34**, the chromatogram of which is reported in *Figure 7.16*, shows a retention time of 5.75 minutes and its identity is attributed by the corresponding ESI-MS spectrum (*Figure 7.17*). However, the chromatogram allows to evaluate the presence of other species, the identity of which is not attributed, except for the compound eluted at 8.15 minutes which is a residue of **30**.

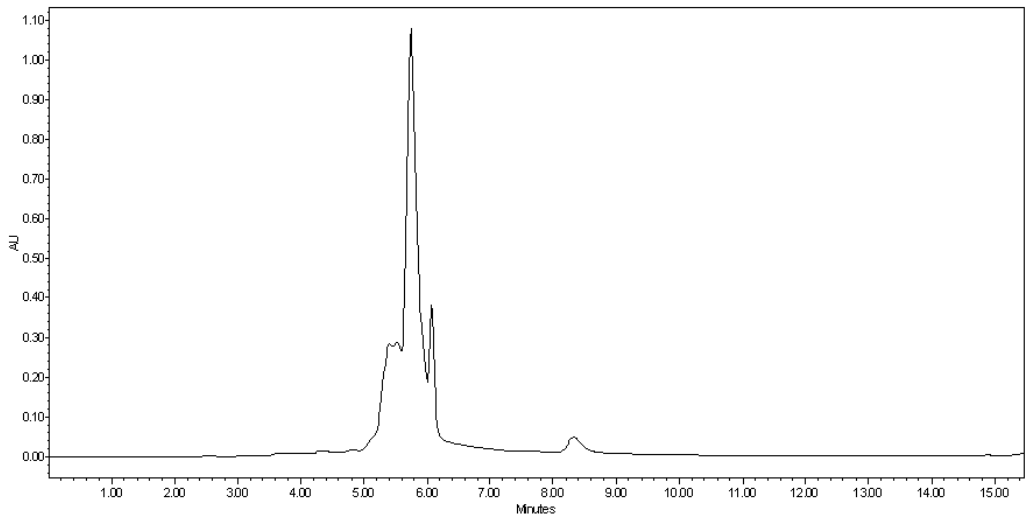

Figure 7.16: Chromatogram of the reaction product, dissolved in a 50:50 mixture of ultrapure water and methanol

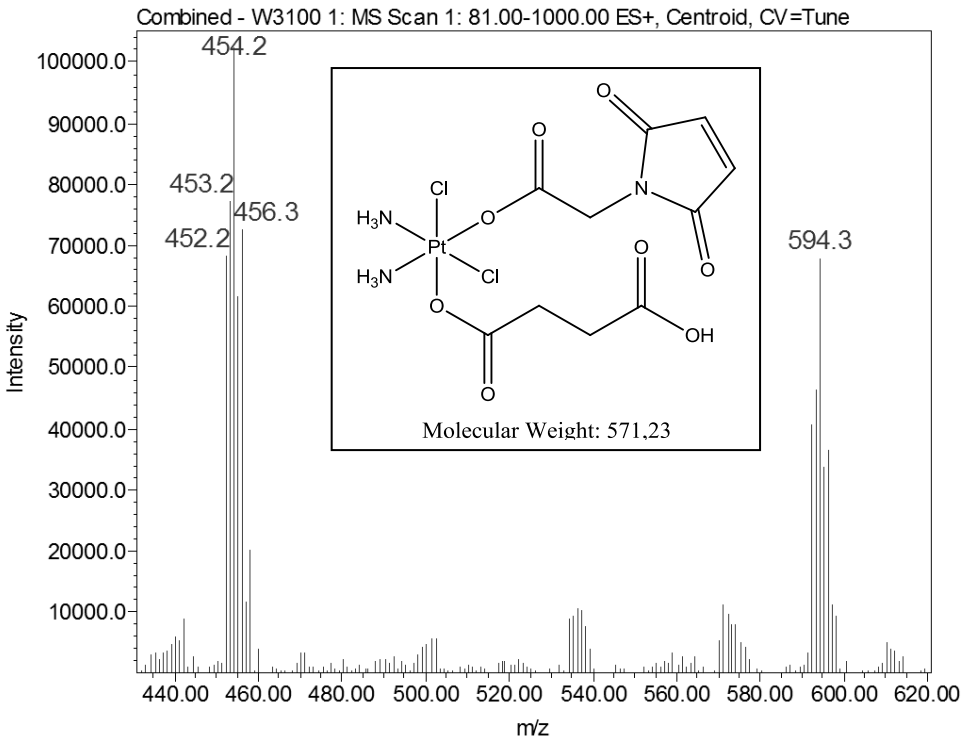

Figure 7.17: ESI-MS spectrum of complex **34**, dissolved in a 50:50 mixture of ultrapure water and methanol

The ESI-MS spectrum reported in *Figure 7.17*, registered in positive ion mode with a cone voltage of 30V, confirms the identity of the product eluted at 5.75 minutes (complex **34**): in fact, it is possible to observe the pseudo-molecular ion $[M+H]^+$ peak at 572.3 m/z, the $[M+Na]^+$ adduct at 594.3 m/z and the fragment $[M\text{-succinate}]^+$ at 454.2 m/z.

The synthesized complex was not pure enough to proceed with its activation and subsequent coupling with a primary amine (model of an amino-functionalized vector). For this reason, the project to prepare a Pt(IV) compound with a 2-(2,5-dioxo-2,5-dihydro-1*H*-pyrrol-1-yl)acetic acid (**30**) coordinated in equatorial

position was abandoned and the axial position of complex **6** (i.e. (OC-6-44)diamminedichloridoethanolatohydroxidoplatinum(IV)) was exploited.

7.8 Synthesis of the (OC-6-44)-diamminedichloridoethanolato(2-(2,5-dioxo-2,5-dihydro-1H-pyrrol-1-yl)acetate)platinum(IV) (35)

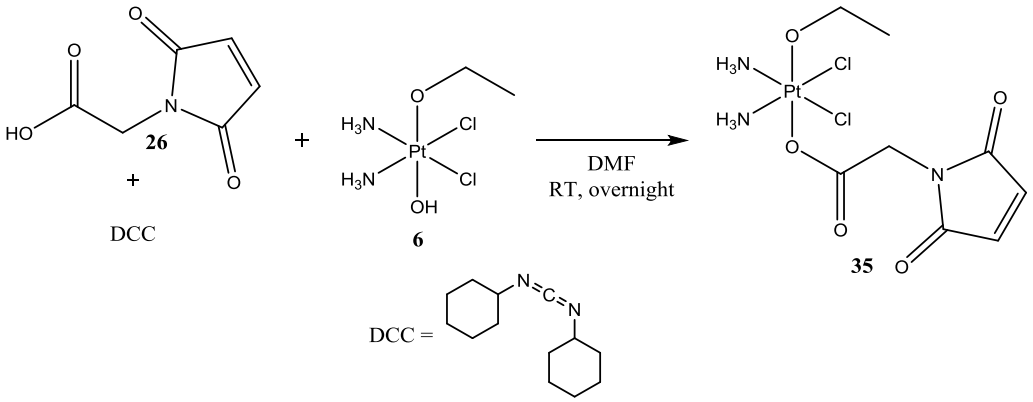

The carboxylic acid of the compound **30** was activated by employing a procedure reported in literature [11]. In particular, a solution of **30** (48.0 mg, 0.309 mmol) and DCC (63.8 mg, 0.309 mmol), dissolved in 1 mL of anhydrous DMF, was sonicated in an ultrasonic bath for 15 minutes at room temperature: the colorless solution became dark red and a white solid (DCU) precipitated. Then the precipitate was separated by centrifugation and the supernatant was added very slowly (dropwise for 30 minutes) to a suspension of **6** (100 mg, 0.276 mmol) in 5 mL of anhydrous DMF. The reaction was carried out overnight at room temperature. The mixture was then cooled, filtered (PTFE filter with a porosity 0.45 μm) and the DMF was evaporated by a rotary evaporator (bath temperature set at < 60 °C). The yellow oil obtained was dissolved in ultrapure water, in order to allow the precipitation of the remained DCU. The yellow solution was filtered (0.45 μm porosity), the water was

removed under reduced pressure and the reaction product was precipitated with acetone/diethyl ether and then dried *in vacuo*.
Yield: 83.2 mg, 0.167 mmol, 60.4%.

7.8.1 Characterization of the Complex

RP-HPLC-ESI-MS

The analysis was performed by employing a stationary phase consisting of a C18 Phenosphere-NEXT column 5 µm, 250 × 4.60 mm ID, a mobile phase composed by a 70:30 mixture of a 15 mM aqueous solution of formic acid and pure methanol (by isocratic elution), a flow rate of 0.500 mL/min, a temperature of 37 °C and the UV-Visible detector set at 210 nm. Compound **35**, the chromatogram of which is shown in *Figure 7.18*, is eluted at 9.20 minutes and its identity is attributed by means of the corresponding ESI-MS spectrum (*Figure 7.19*). However, other two species are eluted at 5.20 and 10.03 minutes and they correspond to cisplatin and compound **30**, respectively.

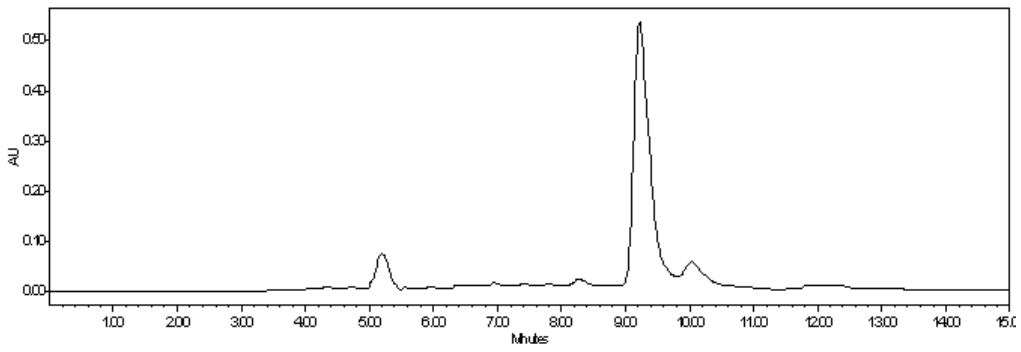

Figure 7.18: Chromatogram of complex **35**, dissolved in ultrapure water

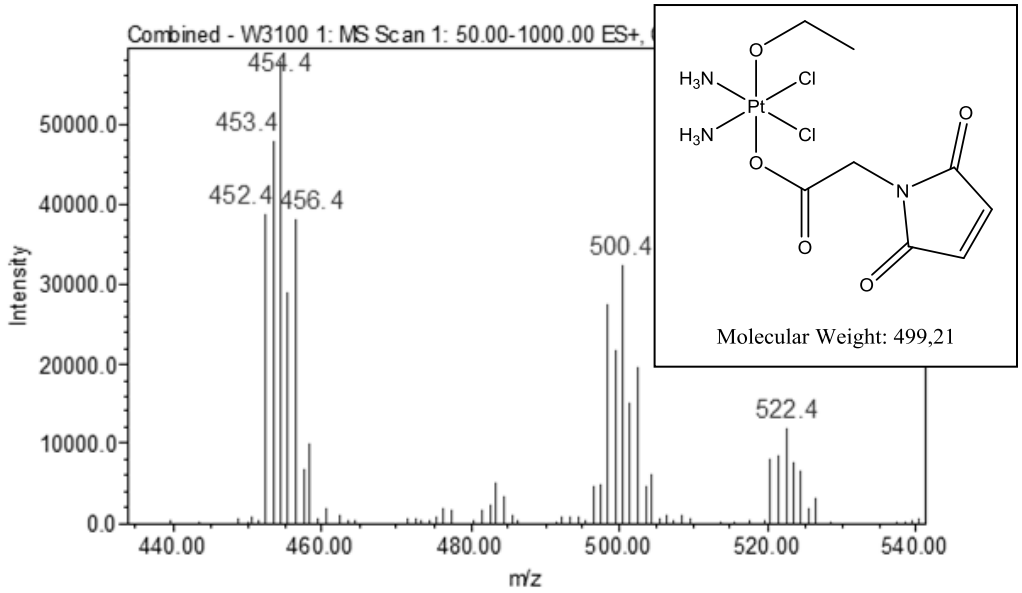

Figure 7.19: ESI-MS spectrum of complex **35**, prepared in ultrapure water

In the ESI-MS spectrum reported in *Figure 7.19*, registered in positive ion mode with a cone voltage of 30V, complex **35** is confirmed by the presence of the pseudo-molecular ion $[M+H]^+$ peak at 500.4 m/z, the adduct $[M+Na]^+$ at 522.4 m/z and the fragment $[M-OCH_2CH_3]^+$ at 454.4 m/z.

^{1}H-NMR

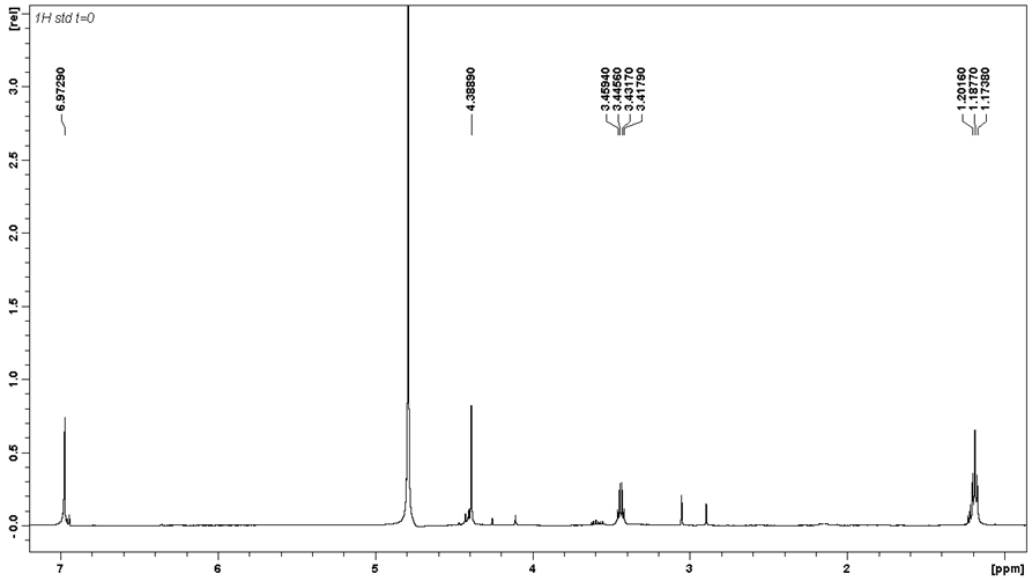

Figure 7.20: ^{1}H-NMR spectrum of complex **35**, registered in D_2O

The ^{1}H-NMR (500 MHz, D_2O) spectrum of **35** (*Figure 7.20*) shows the following signals, δ: 1.19 (t, 3H, -OCH_2CH_3, ^{3}J = 6.95 Hz), 3.43 (q, 2H, -OCH_2CH_3, ^{3}J = 6.95 Hz), 4.39 (s, 2H, -$OCOCH_2$), 6.97 (s, 2H, -NCOC*H*=C*H*) ppm.

The δ signals at 2.85 and 3.01 ppm correspond to –$(CH_3)_2$ of DMF, employed during the synthetic phase and not completely removed.

^{13}C-NMR

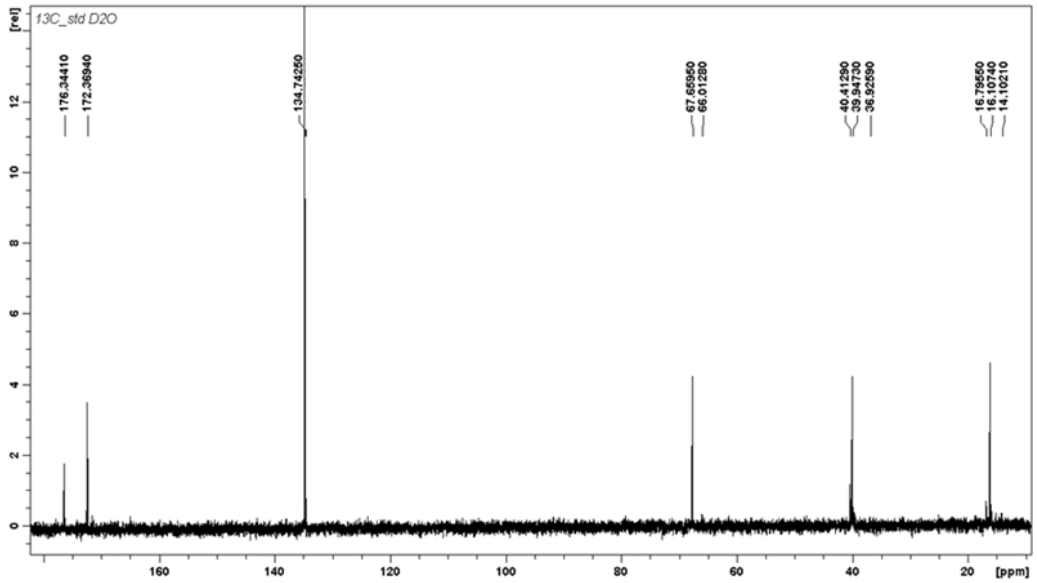

Figure 7.21: ^{13}C-NMR spectrum of complex **35**, registered in D_2O

The ^{13}C-NMR (500 MHz, D_2O) spectrum of **35** (*Figure 7.21*) shows the following signals, δ: 16.11 (-OCH$_2$*C*H$_3$), 39.95 (-OCO*C*H$_2$), 67.66 (-O*C*H$_2$CH$_3$), 134.74 (-NCO*C*H=*C*H), 172.37 (-N*C*OCH=CH), 176.34 (-O*C*OCH$_2$) ppm.

^{195}Pt-NMR

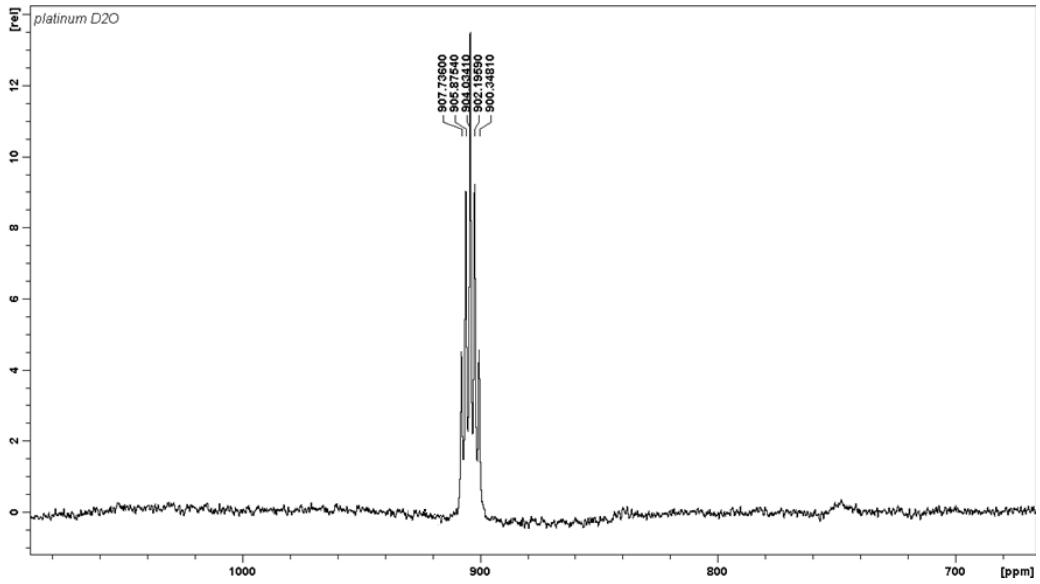

Figure 7.22: ^{195}Pt-NMR spectrum of complex **35**, registered in D_2O

In the ^{195}Pt-NMR spectrum (*Figure 7.22*), registered in D_2O (at a 107.2 MHz NMR frequency), it is possible to observe the presence of an intense signal (in the form of a defined quintuplet, ^{1}J = 197.4 Hz) at 904 ppm which is attributed to complex **35**: in fact, it is consistent with a Pt(IV) complex having coordinated an alkoxido, two chlorides, two amines and a carboxylato.

The signals multiplicity is typical of the coupling of ^{195}Pt (whose spin quantum number I is ½) with two ^{14}N atoms (I = 1) and it is quite broad, due to the coupling with the quadrupolar nucleus ^{14}N.

7.8.2 Stability in Aqueous Solution of Complex 35

In order to evaluate the behavior of **35** in solution (at 25 °C, in the dark), the complex (12.0 mg, 0.0240 mmol) was dissolved in 600 µL of D_2O, transferred in a NMR tube and its stability was followed by means of ^{1}H-NMR

spectroscopy. The spectra, registered at the initial time (t = 0), after 12 and 60 hours, were compared in *Figure 7.23*.

^{1}H-NMR

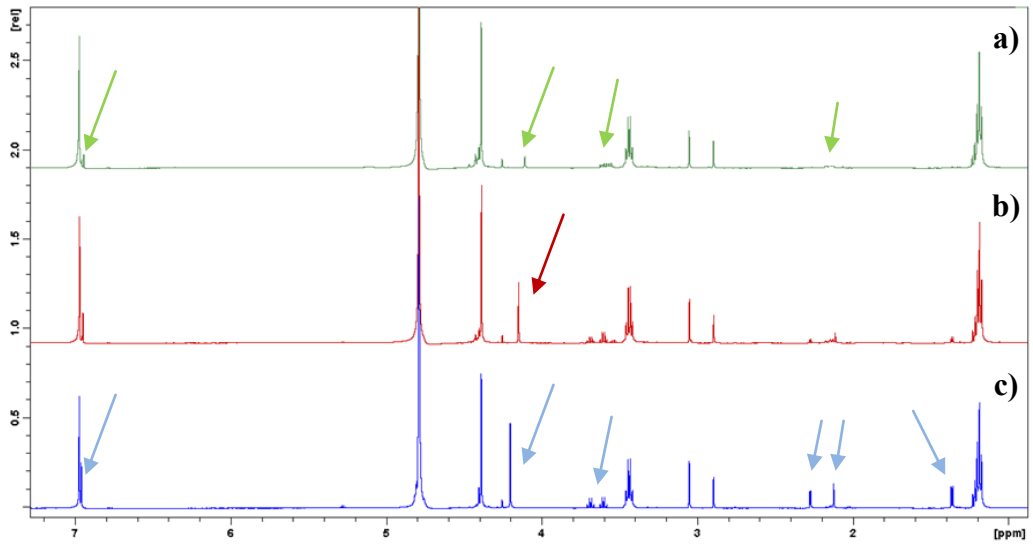

Figure 7.23: ^{1}H-NMR spectra of **35**, registered in D_2O, at a) t = 0, b) t = 12h, and c) t = 60h

In the spectrum, registered at the initial time (*Figure 7.23a*), it is possible to observe the presence of some impurities at about 2.1, 3.6, 4.1 and 4.3 ppm (green indicators). However, after already 12 hours (*Figure 7.23b*), these species grow and the signal at 4.1 ppm (red indicator), in particular, begins to shift at higher values. After 60 hours (*Figure 7.23c*) the δ signals are much higher (light blue indicators) and the species that at first was at about 4.1 ppm underwent a shift of about 0.1 ppm. Therefore, the results show that a degradation of the Pt(IV) complex begins within 12 hours and this suggests that, consequently, the Diels-Alder reaction must be performed within one day, in order to limit the formation of byproducts.

7.9 Diels-Alder Reaction with Furan

In a cycloaddition reaction, two species containing π bonds react to synthesize a cyclic molecule, obtained after the rearrangement of the π electrons and the formation of two new π bonds. The Diels-Alder is one of the most known examples of cycloaddition reaction. Moreover, this latter can be classified by considering the number of π electrons that take part in the process. The Diels-Alder reaction is a cycloaddition [4 + 2] because one compound takes part with its four π electrons and the other one with two π electrons.

In this case, the reaction involved the π electrons of the maleimide derivative present in complex **35** (dienophile) and the ones of furan (conjugated diene). This latter was employed as a model in order to set up the reaction conditions for the cycloaddition. In particular, two different temperatures were compared, i.e. 40 °C and 25 °C, because the first was the same reported in literature [5] and the second was chosen in order to verify the cyclization in the absence of heating. The reaction time was fixed at 5 days [5].

7.9.1 Characterization of Furan

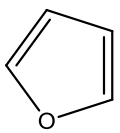

[1]H-NMR

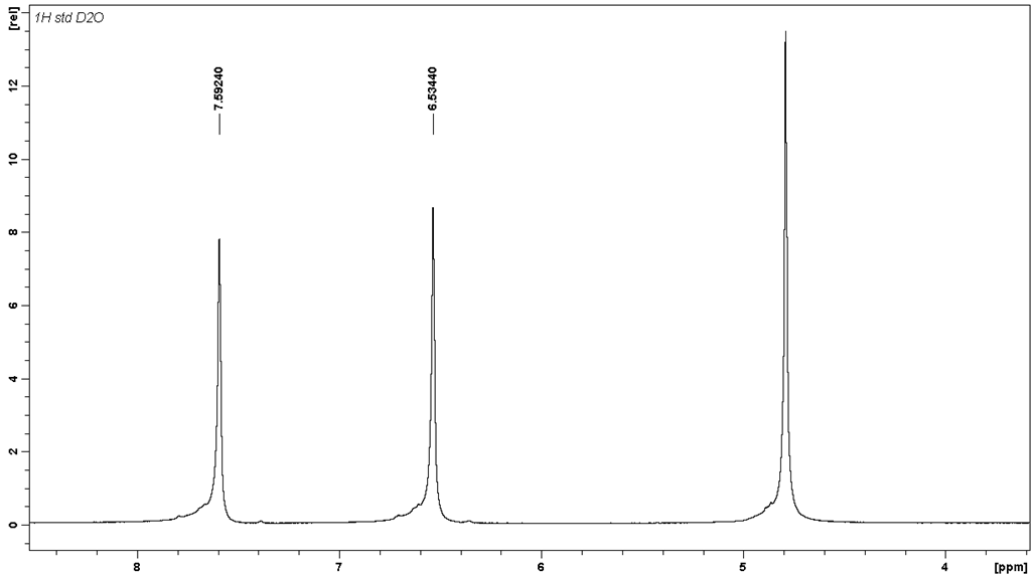

Figure 7.24: [1]H-NMR spectrum of furan, registered in D_2O

The [1]H-NMR (500 MHz, D_2O) spectrum of furan (*Figure 7.24*) was acquired for comparison purposes and shows the following signals, δ: 6.53 (s, 1H, -OCH=C*H*), 7.59 (s, 1H, -OC*H*=CH) ppm.

7.9.2 Synthesis of the (OC-6-44)-diamminedichloridoethanolato(2-(1,3-dioxo-3a,4,7,7a-tetrahydro-1H-4,7-epoxyisoindol-2(3H)-yl) acetate)platinum(IV) (36): I Method

In a NMR tube, furan (1.75 µL, 0.0240 mmol) and **35** (12.0 mg, 0.0240 mmol) were dissolved in 0.6 mL of D_2O and immersed in an oil bath preset at 40 °C. The reaction was followed by [1]H-NMR spectroscopy for 5 days.

At first, when both compounds were dissolved, the t = 0 (initial reaction time) spectrum was registered and compared to the ^{1}H-NMR spectra of free furan and complex **35** (*Figure 7.25*).

^{1}H-NMR

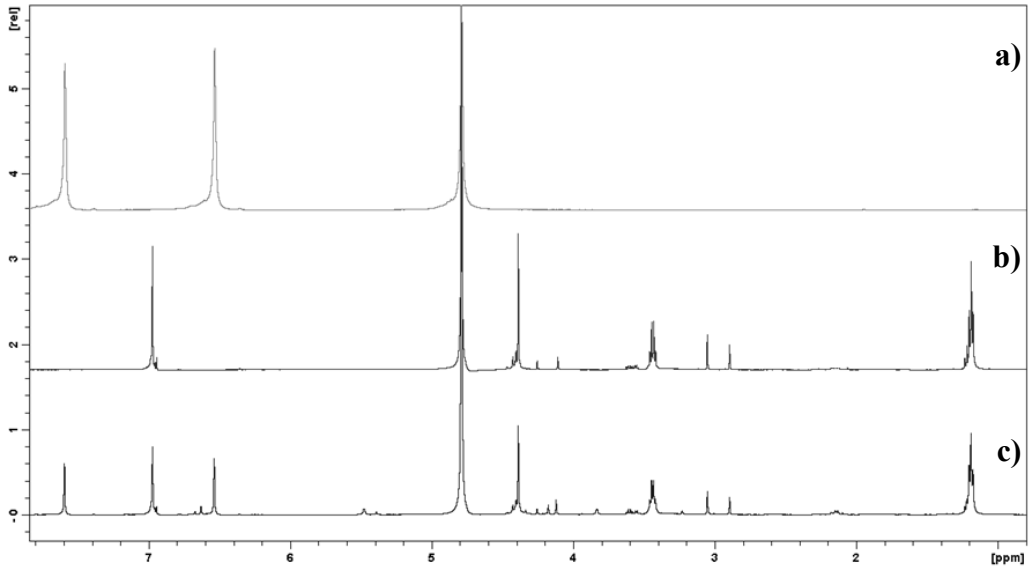

Figure 7.25: ^{1}H-NMR spectrum of the reaction at t = 0 (c)) compared to a) furan and b) complex **35** ^{1}H-NMR spectra. All the spectra were registered in D_2O

Then, the tube was immersed in the oil bath (40 °C) and the reaction started in order to obtain the compound **36** (*Figure 7.26*). The ^{1}H-NMR spectra were registered almost every 12 hours for 5 days; *Figure 7.27* shows the most relevant spectra.

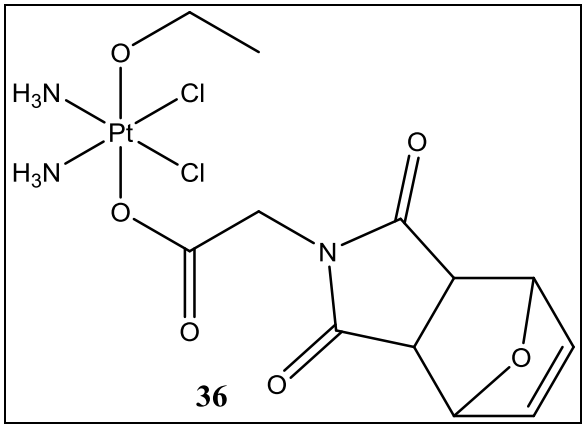

Figure 7.26: Structural formula of the Diels-Alder reaction product (**36**)

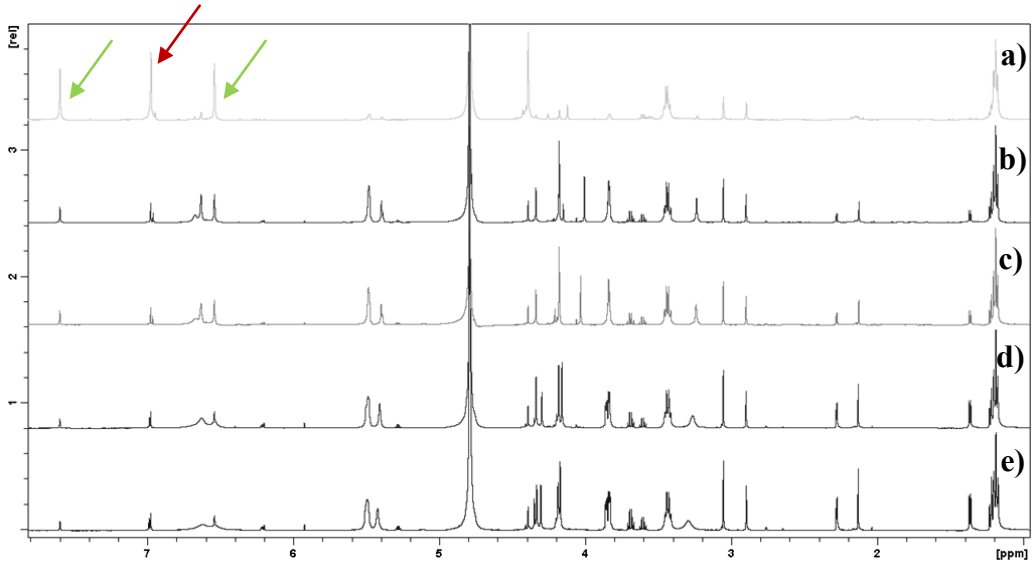

Figure 7.27: ^{1}H-NMR spectra of the Diels-Alder reaction (at 40 °C) at a) t = 0, b) t = 17 h, c) t = 23 h, d) t = 41 h, e) t = 50 h

The ^{1}H-NMR spectra allowed to verify that the Diels-Alder reaction happened: in fact, the signal of maleimide-CH (red indicator in *Figure 7.27a*) and furan-CH (green indicators) gradually disappeared, even though not completely. Probably, a little amount of the two reactants did not react but this does not represent a disadvantage when using IONPs [5], since they can be removed by dialysis in ultrapure water.

Moreover, in the δ range between 5.4 and 5.6 ppm, the two characteristic signals of the bound furan [5] were formed: it is possible to evaluate the progress of the reaction already in the *Figure 7.27a*, after the addition of the furan to the platinum solution. However, in the δ region between 3.5 and 4.5 ppm many new signals can be observed and they have been already seen as regards the study of the stability in solution of complex **35** (*Figures 7.23*).
The right assignment is indicated in *paragraph 7.9.3*.
Furthermore, the solution color changed from yellow at t = 0 (almost unchanged within 24 hours) to the very dark orange of the 5th day. In particular, after the first 24 hours the color became darker and darker: this indicated a degradation of the species present in the mixture. For this reason, it was decided to perform the reaction at 25 °C (II method) to avoid or limit the degradation process.

7.9.3 Synthesis of the (OC-6-44)-diamminedichloridoethanolato(2-(1,3-dioxo-3a,4,7,7a-tetrahydro-1H-4,7-epoxyisoindol-2(3H)-yl) acetate)platinum(IV) (36): II Method

In a NMR tube, furan (1.75 μL, 0.0240 mmol) and complex **31** (12.0 mg, 0.0240 mmol) were dissolved in 0.6 mL of D_2O and the reaction was carried out at 25 °C and followed by ^{1}H-NMR spectroscopy for 5 days.
Also in this case, when both compounds were dissolved in D_2O, the t = 0 ^{1}H-NMR spectrum was registered and compared to the ^{1}H-NMR spectra of furan and of the Pt(IV) complex (*Figure 7.28*).

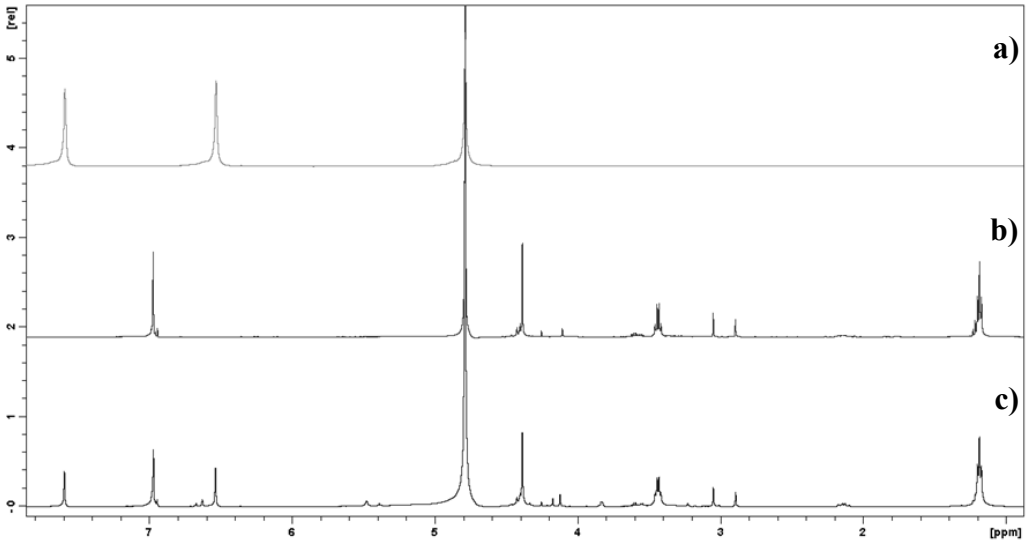

Figure 7.28: ^{1}H-NMR spectrum of the reaction at t = 0 (c)), compared to a) furan and b) complex **31** ^{1}H-NMR spectra. All the spectra were registered in D_2O

Then, the reaction started in order to obtain the compound **36**. ^{1}H-NMR spectra were registered almost every 12 hours for 5 days and compared (*Figures 7.29* and *7.30*).

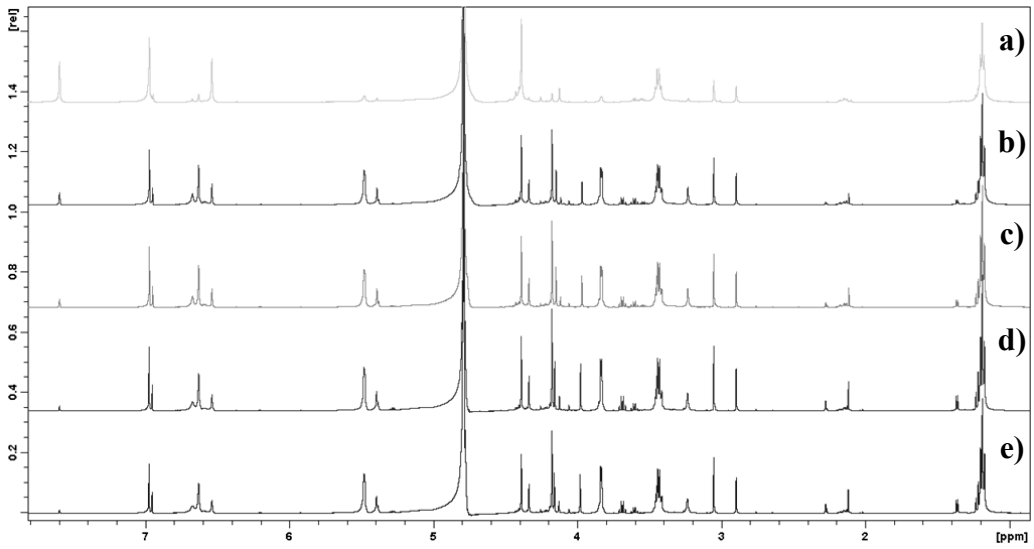

Figure 7.29: ^{1}H-NMR spectra of the Diels-Alder reaction (at 25 °C) at a) t = 0, b) t = 17h, c) t = 23 h, d) t = 41h, e) t = 50h

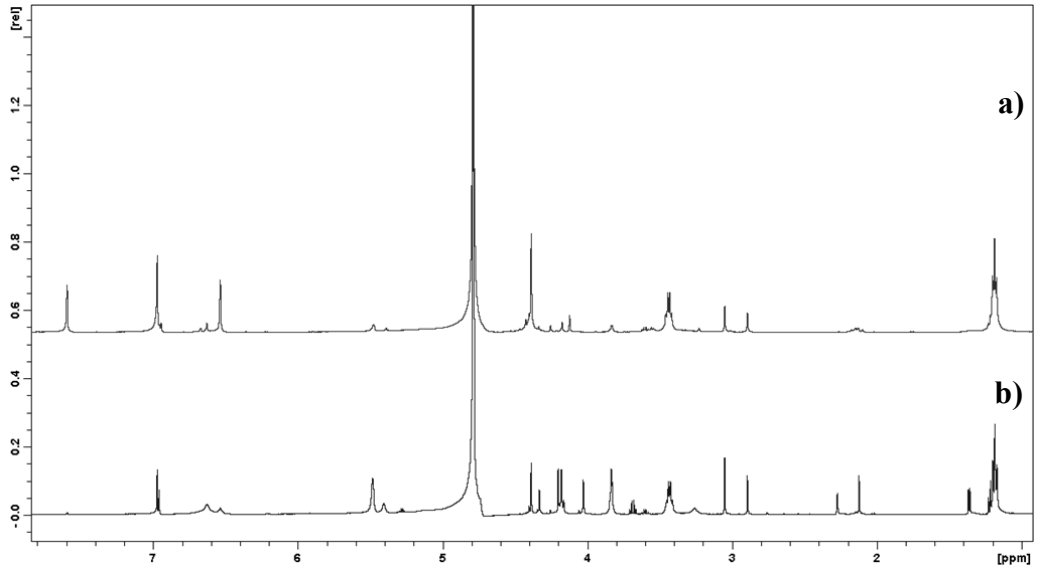

Figure 7.30: ^{1}H-NMR spectra of the Diels-Alder reaction (at 25 °C) at a) t = 0, b) t = 136h

Also in this case, the ^{1}H-NMR spectra show that the Diels-Alder reaction happened: the free furan signals gradually disappeared and, in the δ range between 5.4 and 5.6 ppm, it is possible to find the two characteristic signals of the bonded furan. However, in δ region between 3.5 and 4.5 ppm, many new signals can be observed (they have been already seen in *Figure 7.29b*) and the maleimide-CH signal does not completely disappear.

In this case, the solution color (yellow) remained unchanged during the whole reaction period (5 days).

Furthermore, in *Figure 7.31* the ^{195}Pt-NMR spectrum of the Diels-Alder product (**36**) is reported: it was registered in D_2O (at a 107.2 MHz NMR frequency) after 100 hours from the beginning of the reaction and shows a well-defined signal (^{1}J = 197.7 Hz) at 906 ppm, consistent with a Pt(IV) complex containing an alkoxido, two chlorides, two amines and a carboxylato.

^{195}Pt-NMR

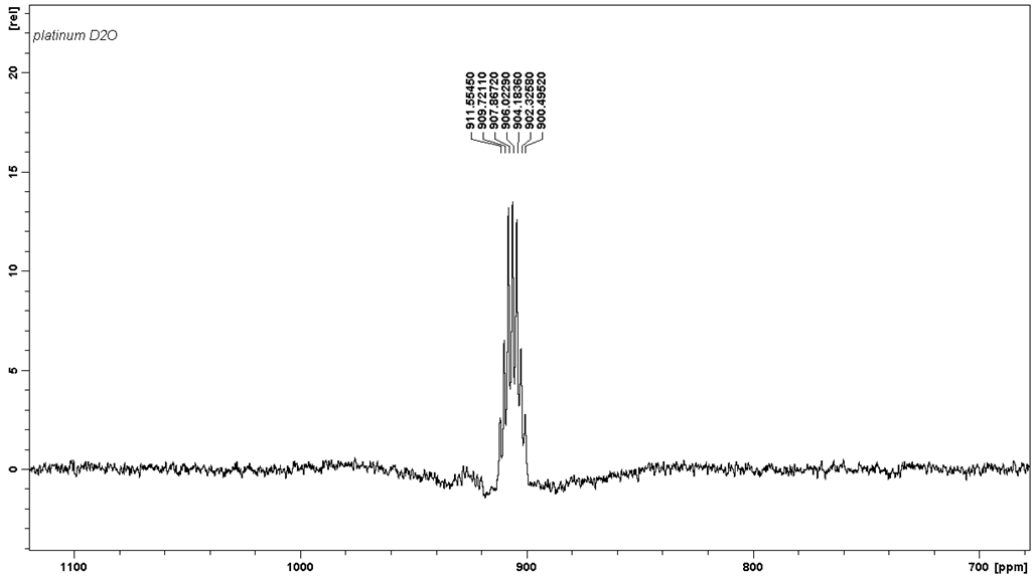

Figure 7.31: ^{195}Pt-NMR spectrum of the Diels-Alder reaction product (**36**) after 100h from the beginning of the reaction, registered in D_2O

The typical signal multiplicity is due to the coupling of ^{195}Pt (I = ½) with two ^{14}N atoms (I = 1) and it is quite broad was caused by the coupling with the quadrupolar nucleus ^{14}N.

The right assignment is allowed by the Heteronuclear Single Quantum Correlation-NMR spectrum (*Figure 7.32*) of the Diels-Alder reaction (at 25 °C), registered after 50 hours from the beginning of the reaction.

The series of double signals is justified by the formation of exo/endo products and their attribution is carried out according to the literature [12].

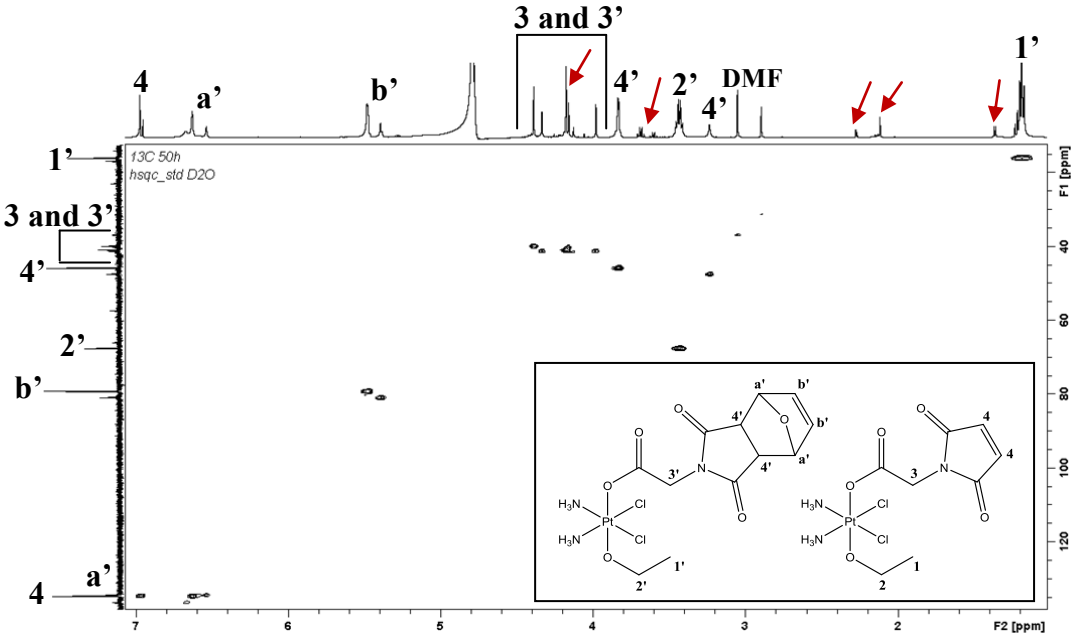

Figure 7.32: HSQC-NMR spectrum of the Diels-Alder reaction at t = 50h, registered in D_2O

The ^{1}H-NMR (500 MHz, D_2O) spectrum of the Diels-Alder reaction, shows the following signals, δ: 1.19 (t, 3H, **H1'**, ^{3}J = 6.95 Hz), 3.23 (m, 1H, **H4'exo**), 3.43 (q, 2H, **H2'**, ^{3}J = 6.95 Hz), 3.83 (m, 1H, **H4'endo**), 5.48 (s, 2H, **Hb'**), 6.63 (s, 2H, **Ha'**) ppm.

The assignment of **H3'** is in the δ region between 3.98 and 4.34 ppm. The signals at 4.39 (**H3**) and 6.97 (**H4**) ppm are due to the unreacted **35**.

In addition, the red indicators are employed to point out the signals that are formed from the free Pt(IV) complex itself.

The portion of the ^{13}C-NMR (125.7 MHz, D_2O) spectrum of **36** reported in *Figure 7.32* shows the following signals, δ: 16.1 (**C1'**), 36.9 or 39.9 (**C3'**), 45.8 (**C4'**), 67.6 (**C2'**), 79.3 (**Cb'**), 134.4 (**Ca'**) ppm.

The signals at 36.9 or 39.9 (**C3**) and 134.7 (**C4**) ppm are due to the unreacted **35**.

The results obtained in *paragraphs 7.9.2* and *7.9.3* allow to verify the occurrence of the Diels-Alder reaction by using furan as a model and to evaluate that the best condition is 25 °C (a higher temperature leads to further degradations).
The presence of unreacted **35** can be solved: in fact, when using IONPs, dialysis can be exploited to removed all the unreacted low MW species.

7.10 Diels-Alder Reaction with the Furan-Functionalized Phosphonic Acid-Terminated POE Monomethyl Ether

The reaction conditions (i.e. 40 °C and 25 °C) used with the maleimide derivative and furan were applied to the case of a ligand containing a furan group: in particular, this ligand was exposed on the surface of the Iron Oxide NanoParticles (IONPs) synthesized by N'Guyen *et al.* [5].

7.10.1 Characterization of the Ligand

^{1}H-NMR spectrum (registered in D_2O) of the furan-functionalized phosphonic acid-terminated PEO (polyethyleneoxide) monomethyl ether (*Figure 7.33*), was registered for comparison purposes.

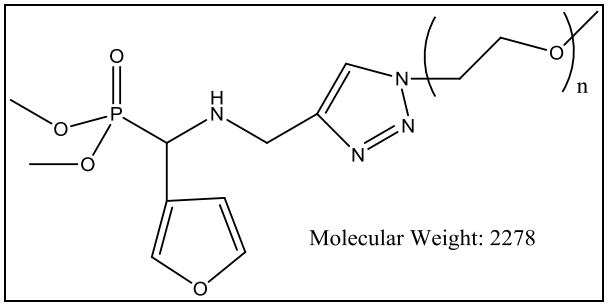

Figure 7.33: Structural formula of the ligand exposed from the IONPs surface

[1]H-NMR

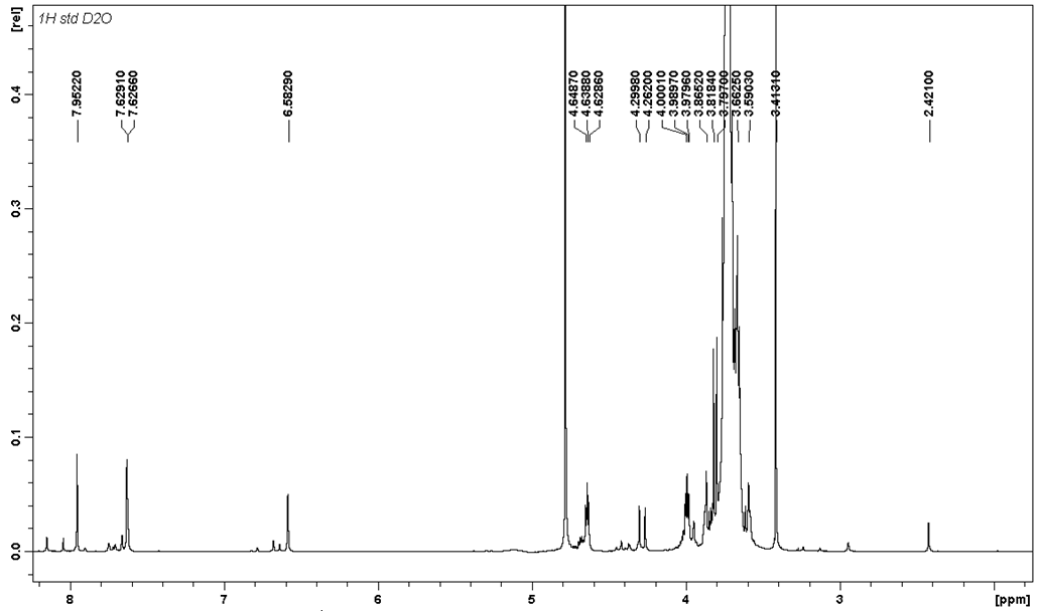

Figure 7.34: [1]H-NMR spectrum of the ligand, registered in D_2O

The signal at 3.41 ppm corresponds to PEO-OCH_3, the protons of POE-OCH_2 resonate in the δ region between 3.5 and 3.9 ppm, the proton of -C*H*P shows a signal at 4.28 ppm, the PEO methylene -NCH_2 has a signal at 4.64 ppm, and the protons of furan and triazole resonate in the δ region between 6.5 and 8 ppm [5].

7.10.2 Diels-Alder Reaction: I Method

In a NMR tube, furan-functionalized phosphonic acid-terminated POE monomethyl ether (54.7 mg, 0.0240 mmol) and complex **35** (12.0 mg, 0.0240 mmol) were dissolved in 0.6 mL of D_2O and immersed in an oil bath preset at 40 °C. The reaction was followed by [1]H-NMR for 5 days.

When both compounds were dissolved in D_2O, the t = 0 ^{1}H-NMR spectrum was registered and compared to the free ligand spectrum (*Figure 7.35*).

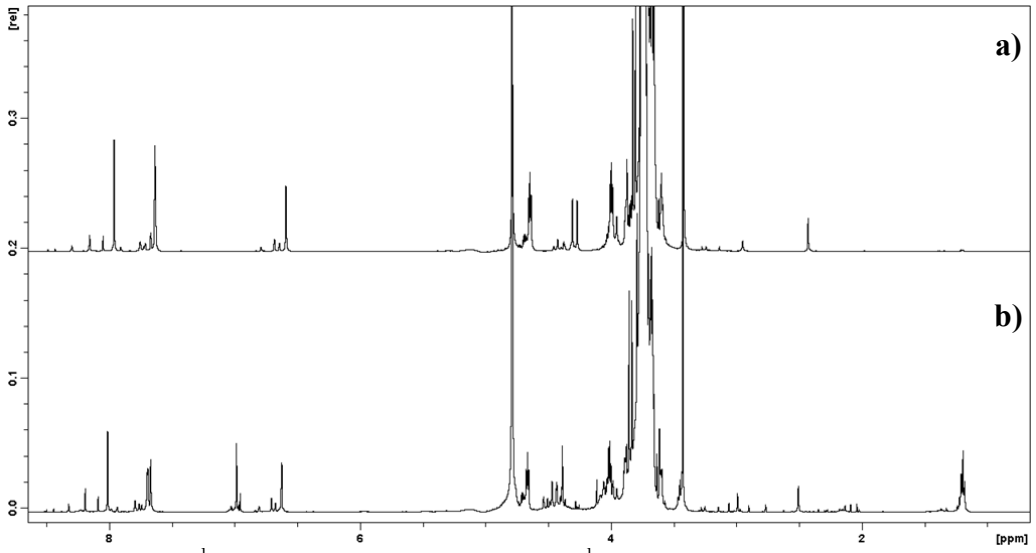

Figure 7.35: a) ^{1}H-NMR spectrum of the ligand, b) ^{1}H-NMR spectrum at t = 0 (initial time reaction)

In *Figure 7.35b* (t = 0) it is possible to observe the signals of the Pt complex together with some changes in the original signals of the ligand (*Figure 7.35a*). Then, the tube was immersed in the oil bath (40 °C) and the reaction started in order to obtain the compound **37** (*Figure 7.36*). The ^{1}H-NMR spectra were registered at t = 1d, t = 2d and t = 5d of reaction (where d = day) and were compared in *Figure 7.37*.

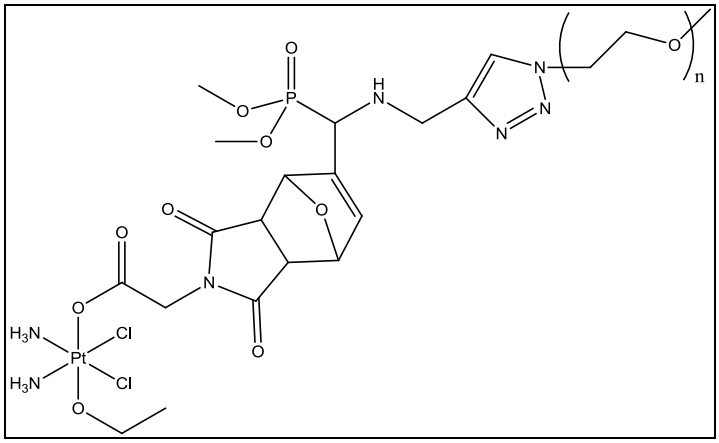

Figure 7.36: Structural formula of the Diels-Alder reaction product (**37**)

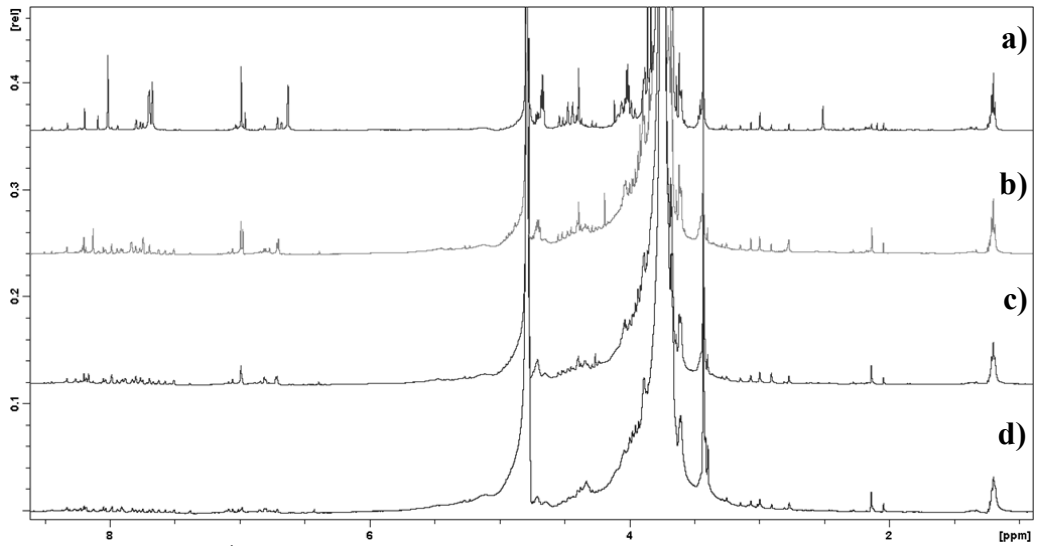

Figure 7.37: ^{1}H-NMR spectra at a) t = 0, b) t = 1d, c) t = 2d, d) t = 5d of reaction

The ^{1}H-NMR (500 MHz, D_2O) spectra indicate that the Diels-Alder reaction happened and, after 2 days, the signals of maleimide-CH disappeared. However, instead of few well-defined signals of the product, a multitude of little signals (in particular, in the δ area between 5 and 8 ppm) can be observed. This is particularly evident in the spectrum of the 5th day (*Figure 7.37d*), together with an overlap in the δ region 3.5-4.5 ppm.

^{195}Pt-NMR

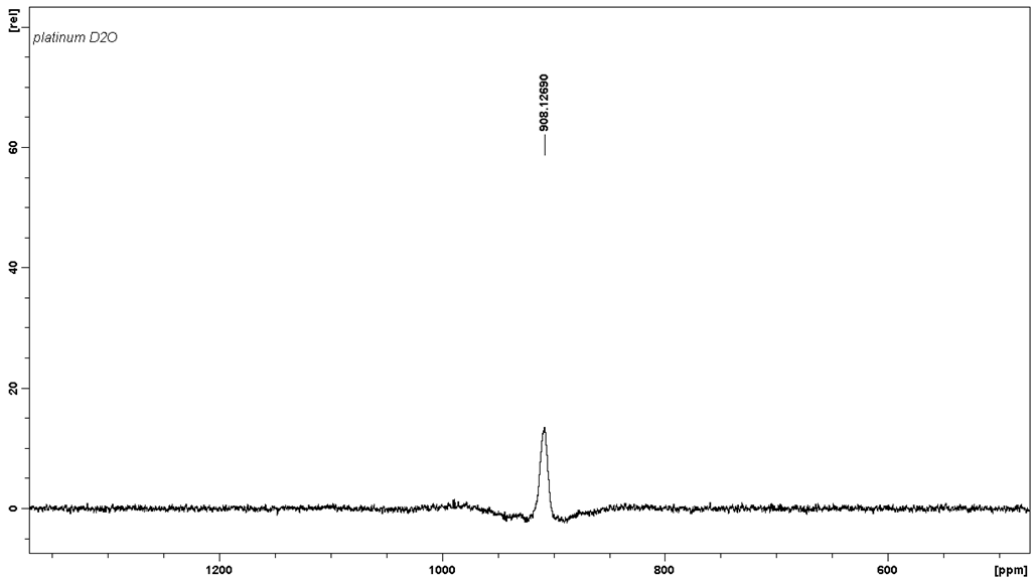

Figure 7.38: ^{195}Pt-NMR spectrum of the Diels-Alder product, registered in D_2O

The ^{195}Pt-NMR spectrum (*Figure 7.38*) of the reaction product, registered in D_2O (at a 107.2 MHz NMR frequency) after five days, shows a signal at 908 ppm, in the form of a not-well defined multiplet. It is consistent with a Pt(IV) complex containing an alkoxido, two chlorides, two amines and a carboxylato, and it is comparable to the results obtained in the case of the Diels-Alder reaction with furan (*Figure 7.31*).

Moreover, the solution color changed from yellow at t = 0 (almost unchanged within 2 days) to the dark orange of the 5th day: probably a degradation was in progress, as observed in *paragraph 7.9.2*.

7.10.3 Diels-Alder Reaction: II Method

In a NMR tube, furan-functionalized phosphonic acid-terminated POE monomethyl ether (54.7 mg, 0.0240 mmol) and complex **35** (12.0 mg, 0.0240 mmol) were dissolved in 0.6 mL of D_2O. The reaction was carried out at 25 °C, to avoid the Pt(IV) complex degradation, and it was followed by ^{1}H-NMR for 7 days.

Also in this case, the t = 0 (initial reaction time) ^{1}H-NMR spectrum was registered and was compared to the spectra of the free ligand and **35** (*Figure 7.39*).

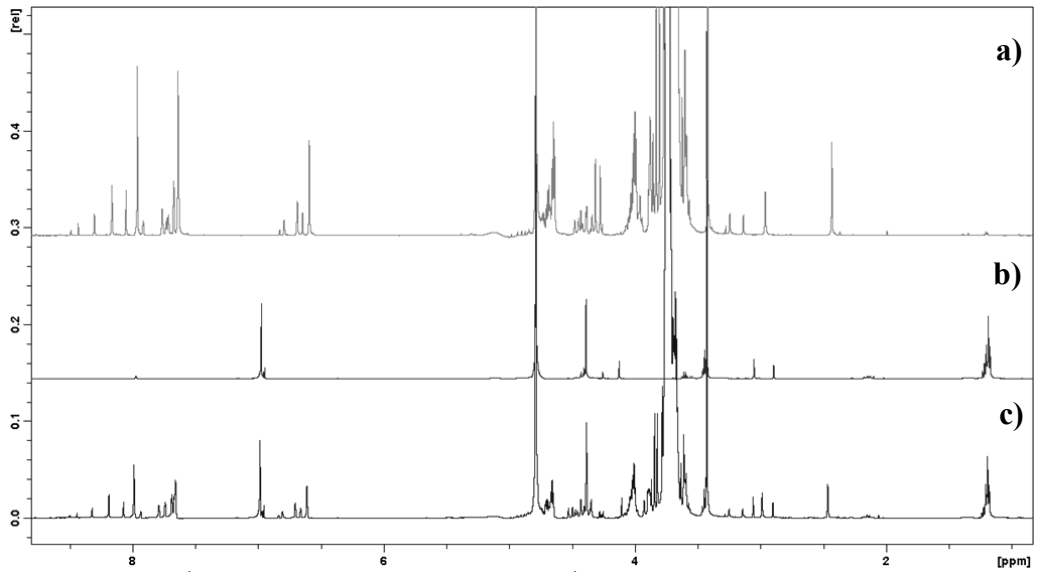

Figure 7.39: a) ^{1}H-NMR spectrum of the ligand, b) ^{1}H-NMR spectrum of the Pt(IV) complex, c) ^{1}H-NMR spectrum at t = 0 (initial time reaction)

In *Figure 7.39c* it is possible to observe the signals of the Pt complex together with some changes in the original signals of the ligand (*Figure 7.39a*).

The reaction started in order to obtain compound **37**. ^{1}H-NMR spectra were registered almost every 12 hours for seven days.

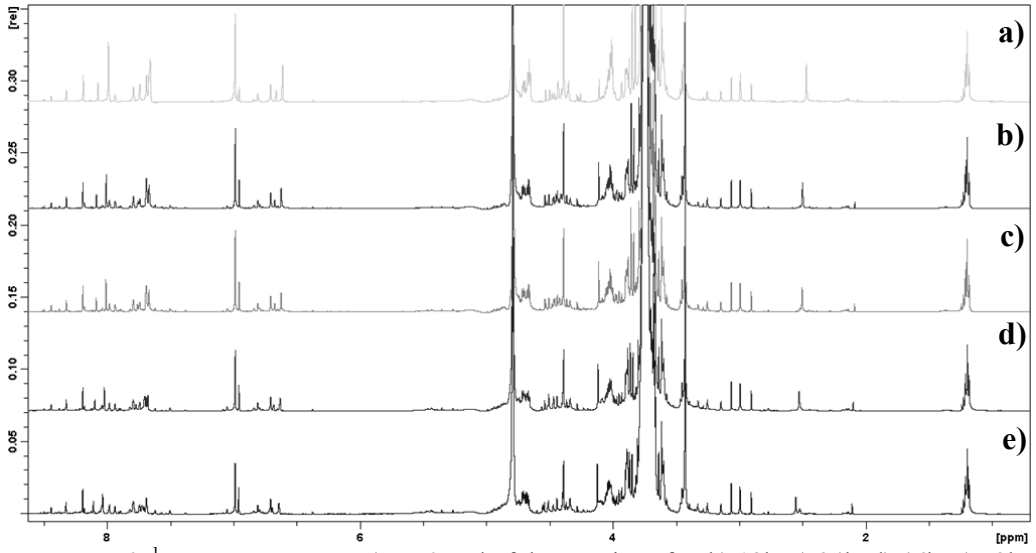

Figure 7.40: ^{1}H-NMR spectra at a) t = 0 and of the reaction after b) 18h, c) 24h, d) 46h, e) 72h

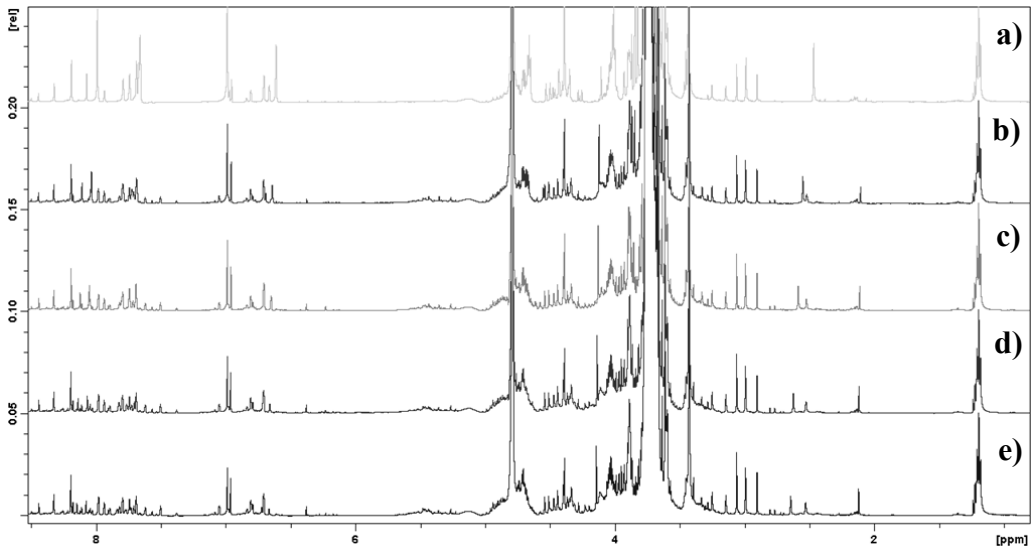

Figure 7.41: ^{1}H-NMR spectra at a) t = 0 and of the reaction after b) 72h, c) 103h, d) 143h, e) 163h

The ^{1}H-NMR (500 MHz, D_2O) spectra (*Figures 7.40-7.41*) allow to evaluate that the Diels-Alder reaction was in progress because the signals of maleimide-CH disappeared, even though slowlier than in the previous case. However,

instead of few well-defined signals of the product, a multitude of little signals is visible (in particular, in the δ region between 7 and 8 ppm). In addition, in the δ region between 5 and 6 ppm some new signals appeared but it is not possible to make a correct attribution.

^{195}Pt-NMR

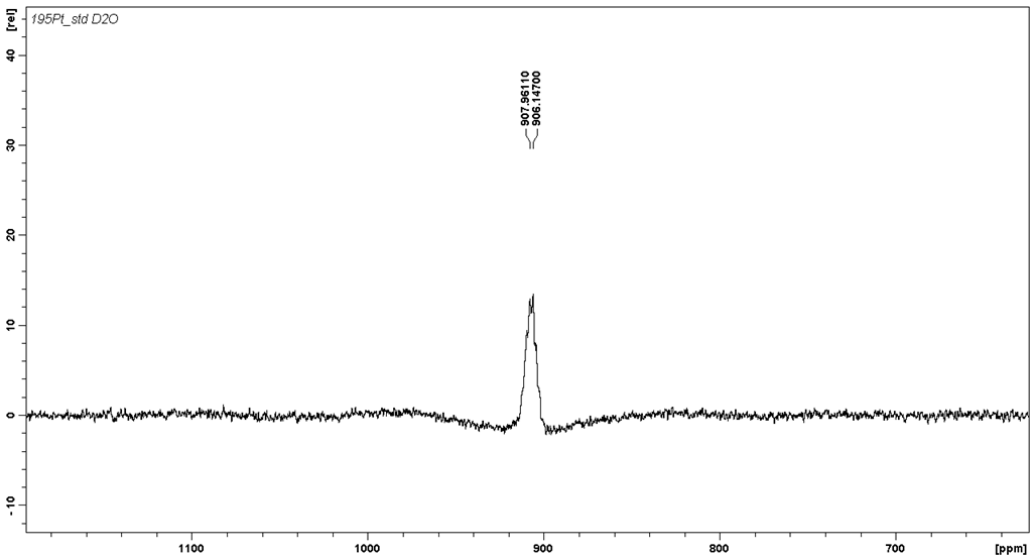

Figure 7.42: ^{195}Pt-NMR spectrum of the Diels-Alder product, registered in D_2O

The ^{195}Pt-NMR spectrum of the reaction product after five days (*Figure 7.42*), registered in D_2O (at a 107.2 MHz NMR frequency) shows a signal at 908 ppm, in the form of a not-well defined multiplet, which is consistent with a Pt(IV) complex having coordinated two chlorides, two amines, an alkoxido and a carboxylato.

Moreover, as verified in *paragraph 7.9.3*, the yellow solution remained unchanged during the five days.

The results reported in *paragraphs 7.10.2* and *7.10.3* allow to verify that, also in this case, the Diels-Alder reaction occurred and, as previously described in *paragraph 7.9*, the best temperature condition is 25 °C.

7.11 Diels-Alder Reaction with IONPs

The results obtained in *paragraphs 7.7* and *7.8* point out that the Diels-Alder reaction must be performed at 25 °C, in order to avoid degradation (even though, in the case of IONPs, not coupled molecules can be removed by dialysis). For this reason, complex **35** and IONPs [5], were reacted in the previously mentioned conditions, both for 24 hours and 5 days (as a comparison).

7.11.1 Main Features of the IONPs

The Iron Oxide NanoParticles, synthesized by Dr. Jérôme Fresnais (Laboratoire de Physico-Chimie des Electrolytes, Colloïdes et Sciences Analytiques, Paris (France)), were provided as water solution with the following features:

- 0.528 % w/w (i.e. 0.528 g of IONPs in 100 g of sample),
- 1 g/mL solution density,
- 1×10^{-4} mol furan/g IONPs,
- 43.1 mM Fe concentration,
- 9 nm as mean diamenter.

7.11.2 Diels-Alder Reaction for 24 Hours

An aliquot of the IONPs (600 μL, 0.317 μmol) was added to complex **35** (7.91 mg, 15.8 μmol) and the mixture was magnetically stirred at 25 °C for 24 hours. Then the sample was collected and dialyzed in ultrapure water for four days by using a dialysis tubing cellulose membrane (the molecular weight cut-off was 1 kDa). An aliquot of the sample (200 μL) was mineralized by acid digestion, with 37% w/w HCl, in an ultrasonic bath at 60 °C for 1 hour. During the mineralization, the color solution changed from the initial brown to a bright yellow. Then the solution was diluted with HNO_3 1% v/v and the Pt content was quantified by means of ICP-OES analysis and, as a consequence, the Pt/furan ratio was determined. In particular, the Pt concentration is 1.00 mM, which corresponds to a Pt/furan ratio was 1.9.

7.11.3 Diels-Alder Reaction for 5 Days

Another IONPs aliquot (600 μL, 0.317 μmol) was added to complex **35** (7.91 mg, 15.8 μmol) and the reaction was carried out at 25 °C for 5 days. After the established time, the sample was processed as described in *paragraph 7.9.2*.
The data show that the Pt concentration is 1.95 mM and the Pt/furan ratio is 3.7.

7.12 Conclusions

In this work, a ligand functionalized with a maleimide derivative (dienophile species) was successfully synthesized and, therefore, it was employed for the preparation of Pt(IV) complexes having one equatorial or axial position occupied by this ligand. The results point out that only complex **35** (in which the

maleimide was axially coordinated) is promising. For this reason, its functionalizable group (alkene) was exploited for Diels-Alder cycloaddition reactions. Furan derivatives were used as a model to set up the reaction conditions and the successful results allowed to apply the synthetic procedure to magnetic iron oxide nanoparticles (IONPs).

The two synthesized conjugates are undergoing *in vitro* biological assays.

At first, hyperthermia therapies will be exploited (by means of the retro-Diels-Alder reaction) in order to release the Pt(IV) prodrug, which, after the so-called activation by reduction, gives rise to the active Pt(II) species.

References

[1] J. Yu, D. Y. Huang, Z. Yousaf Muhammad, Y. L. Hou, S. Gao, Magnetic nanoparticle-based cancer therapy, *Chin. Phys. B.*, 22 (2013), 027506-1-027506-13.

[2] L. Tong, M. Zhao, S. Zhu, J. Chen, Synthesis and application of superparamagnetic iron oxide nanoparticles in targeted therapy and imaging of cancer, *Front. Med.*, 5 (2011), 379-387.

[3] B. Blasiak, F. C. J. M. van Veggel, B. Tomanek, Applications of Nanoparticles for MRI Cancer Diagnosis and Therapy, *J. Nanomater.*, Volume 2013, Article ID 148578, 1-12.

[4] I. Pantic, Magnetic Nanoparticles in Cancer Diagnosis and Treatment: Novel Approaches, *Rev. Adv. Mater. Sci.*, 26 (2010) 67-73.

[5] T. T. T. N'Guyen, H. T. T. Duong, J. Basuki, V. Montembault, S. Pasqual, C. Guibert, J. Fresnais, C. Boyer, M. R. Whittaker, T. P. Davis, L. Fontaine, Functional Iron Oxide Magnetic Nanoparticles with Hyperthermia-Induced Drug Release Ability by Using a Combination of Orthogonal Click Reactions, *Angew. Chem. Int. Ed.*, 52 (2013), 14152-14156.

[6] T. Oishi, K. Kagawa, M. Fujimoto, Synthesis and Polymerization of N-[[[N'-(α-methylbenzyl)amino]carbonyl]methyl]maleimide, *Macromolecules*, 26 (1993), 24-29.

[7] D. Rich, P. Gesellchen, A. Cheung, C. Buckner, Alkylating derivatives of amino acids and peptides. Synthesis of *N*-maleoylamino acids, [1-(*N*-maleoylglycyl)cysteinyl]oxytocin. Effects on vasopressin-stimulated water loss from isolated toad bladder, *J. Med. Chem.*, 18 (1975), 1004-1010.

[8] J. J. Wilson, S. J. Lippard, Synthetic Methods for the Preparation of Platinum Anticancer Complexes, *Chem. Rev.*, 114 (2014), 4470-4495.

[9] S. J. Berners-Price, L. Ronconi, P. J. Sadler, Insights into the mechanism of action of platinum anticancer drugs from multinuclear NMR spectroscopy, *Prog. Nucl. Magn. Reson. Spectrosc.*, 49 (2006) 65-98.

[10] M. Ravera, E. Gabano, G. Pelosi, F. Fregonese, S. Tinello, D. Osella, A New Entry to Asymmetric Platinum(IV) Complexes via Oxidative Chlorination, *Inorg. Chem.*, 53 (2014), 9326-9335.

[11] J. Z. Zhang, P. Bonnitcha, E. Wexselblatt, A. V. Klein, Y. Najajreh, D. Gibson, T. W. Hambley, Facile preparation of mono-, di- and mixed-carboxylato platinum(IV) complexes for versatile anticancer prodrug design, *Chemistry*, 19 (2013), 1672-1676.

[12] M. M. J. Smulders, J. R. Nitschke, Supramolecular control over Diels–Alder reactivity by encapsulation and competitive displacement, *Chem. Sci.*, 3 (2012), 785-788.

Chapter VIII

Drugs Encapsulation into Liposomes

8.1 Introduction

It is known that malignant pleural mesothelioma (MPM) is a tumor which affects the mesothelial cells that line the pleural cavity and it is associated to the exposure to asbestos fibers. Many decades may elapse between the exposure and the disease diagnosis and, despite its rarity, MPM is very aggressive because the median survival goes from 8 to 12 months. In this regard, the Food and Drug Administration accepted a treatment which exploits the combination of cisplatin and pemetrexed (i.e. an antifolate which acts on some enzymes involved in the synthesis of thymidine and purine), which results to partially extend (by a few months) the median survival with respect to a cisplatin-based therapy [1].

Furthermore, since epigenetic modifications play a significant role in neoplastic progression, the research aims to co-administer drugs, which exploit this function, with other chemotherapeutics [2].

One of the epigenetic modifications is the acetylation of histone (i.e. a protein that represents the structural component of chromatin), which is controlled by histone acetyltransferases (HAT) and deacetylases (HDAC) (*Figure 8.1*). These latter enzymes, in particular, remove the acetyl groups from the histone lysines increasing the association of the histone with DNA and preventing the binding of cisplatin to DNA. For this reason, HDAC inhibitors (HDACI) must be employed in order to inhibit deacetylation (and, therefore, the DNA interaction with histones) and to allow the drug to bind to its target. Moreover, the accumulation of acetylated histones activates the transcription of some genes and, when they are expressed, the tumor growth is inhibited and apoptosis is induced [2].

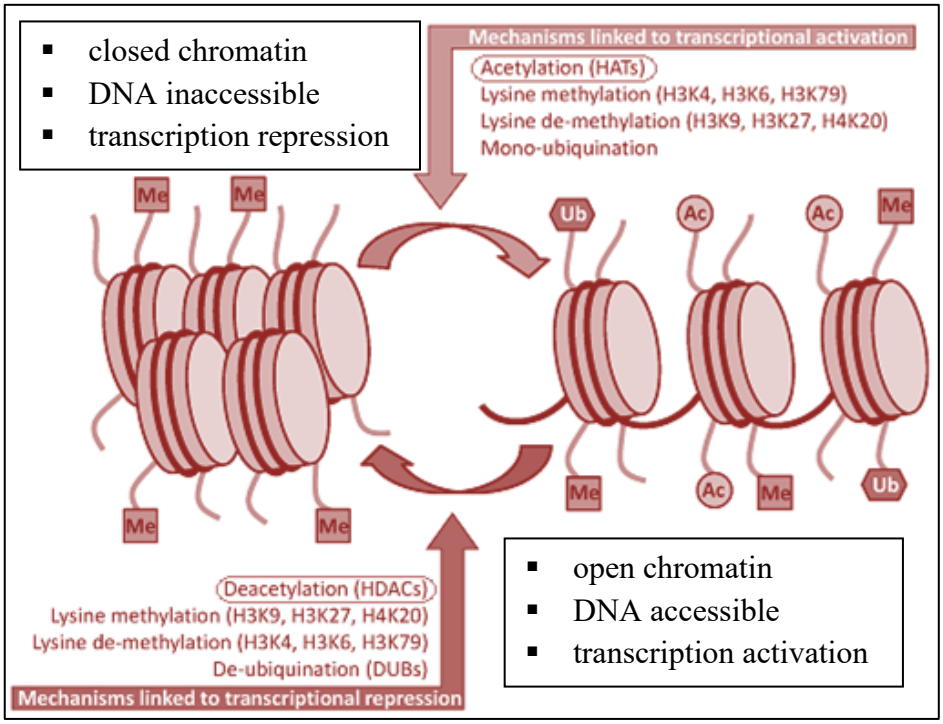

Figure 8.1: Hystone acetylation and deacetylation, which play important roles in gene expression. The picture is adapted from [3]

Hydroxamic acids, such as suberoylanilide hydroxamic acid (SAHA or Vorinostat), and anions of aliphatic acids (such as 2-propylpentanoate or valproate) can be mentioned among the HDACIs. In particular, valproate (clinically employed as an anticonvulsant drug) showed a HDAC inhibition activity and its effect positively influenced the results of the co-administration of cisplatin with pemetrexed in the case of mesothelioma diseases [2]. Moreover, Zanellato *et al.* [4] evaluated the combination index (CI, i.e. a quantitative measure of the efficacy of a drug combination [5, 6]) of valproate and cisplatin:

$$CI = \frac{[cisplatin]}{cisplatin\ IC_x} + \frac{[valproate]}{valproate\ IC_x} + \frac{[cisplatin] \times [valproate]}{(cisplatin\ IC_x) \times (valproate\ IC_x)}$$

(where the drug IC_x is the concentration of the single drug to obtain the x% of cell viability and the [cisplatin] and [valproate] are the concentrations of these drugs within the combination to achieve the same result, i.e. x% viability) on some malignant pleural mesothelioma cell lines. The purpose was to verify if synergistic (CI < 1), additive (CI = 1) or antagonistic (CI > 1) effects occurred: synergy was generally observed.

In this work [7], three types of cationic liposomes (containing cisplatin, valproate sodium salt and the combination of both drugs in an approximative 1:2 molar ratio) were synthesized in order to evaluate if the co-administration of the two drugs encapsulated into the lipid vectors allowed to obtain the same antiproliferative effect of a Pt(IV) complex, the axial ligands of which were both valproate, i.e. (OC-6-33)-diamminedichloridobis(2-propylpentanoate)platinum(IV) (**39**). This latter proved to have a high cytotoxic activity on several tumor cell lines, higher than cisplatin [8]. Moreover, complex **39** was also encapsulated into a forth liposome for comparison.

Furthermore, the combination index of the two liposomes containing the single drugs was evaluated in order to verify if a synergism occurs, as well as in the case of free cisplatin and valproate.

The cellular accumulation of the platinum complexes and liposomes and the DNA platination (i.e. the amount of platinum bound to DNA) of complex **39** were evaluated.

The synthesized platinum(IV) complex and liposome formulations are reported in order of discussion:

- (OC-6-33)-diamminedichloridobis(2-propylpentanoate)platinum(IV) (**39**),
- cationic liposomes without any drugs,
- cationic liposomes encapsulating cisplatin,
- cationic liposomes encapsulating valproate sodium salt,

- cationic liposomes encapsulating both cisplatin and valproate sodium salt,
- cationic liposomes encapsulating complex **39**.

8.2 Synthesis of the (OC-6-33)-diamminedichloridobis(2-propylpentanoate)platinum(IV) (39)

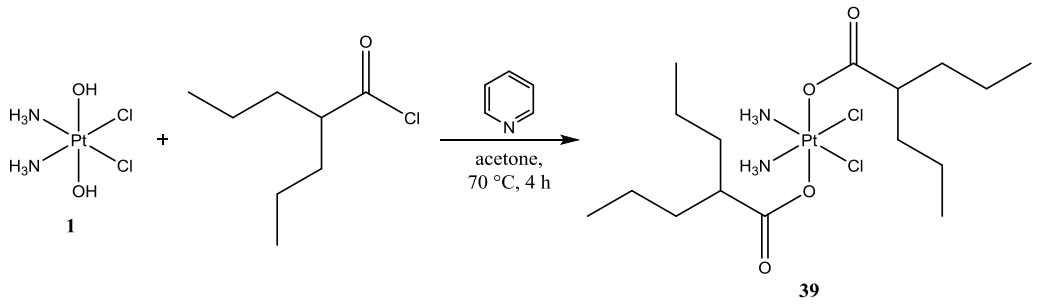

Complex **39** was prepared according to a previously reported procedure [8]. In particular, to a suspension of complex **1** (100 mg, 0.299 mmol) and pyridine (1.00 mL, 12.4 mmol) in 3 mL of acetone, a solution of 2-propylpentanoyl chloride (1.36 mL, 7.81 mmol) in 5 mL of acetone was added dropwise and the reaction was carried out for 4 hours at 70 °C with a reflux condenser. After the established time, 10 mL of hexane were added to the mixture, which was centrifuged and filtered (0.45 μm porosity). The solvent was then removed under reduced pressure. A white solid was precipitated by the addition of diethyl ether, washed several times with ultrapure water and diethyl ether and finally dried *in vacuo*.

Yield: 86.0 mg, 0.147 mmol, 49.0%.

8.2.1 Characterization of the Complex

RP-HPLC-ESI-MS

The analysis was performed by employing a stationary phase consisting of a C18 Phenosphere-NEXT column 5 μm, 250 × 4.60 mm ID, a mobile phase composed by a 20:80 mixture of a 15 mM aqueous solution of formic acid and pure methanol (isocratic elution), a flow rate of 0.500 mL/min, a temperature of 37 °C and the UV-Visible detector set at 210 nm. Compound **39** showed a retention time of 12.70 minutes and its identity was attributed by the corresponding ESI-MS spectrum (*Figure 8.2*).

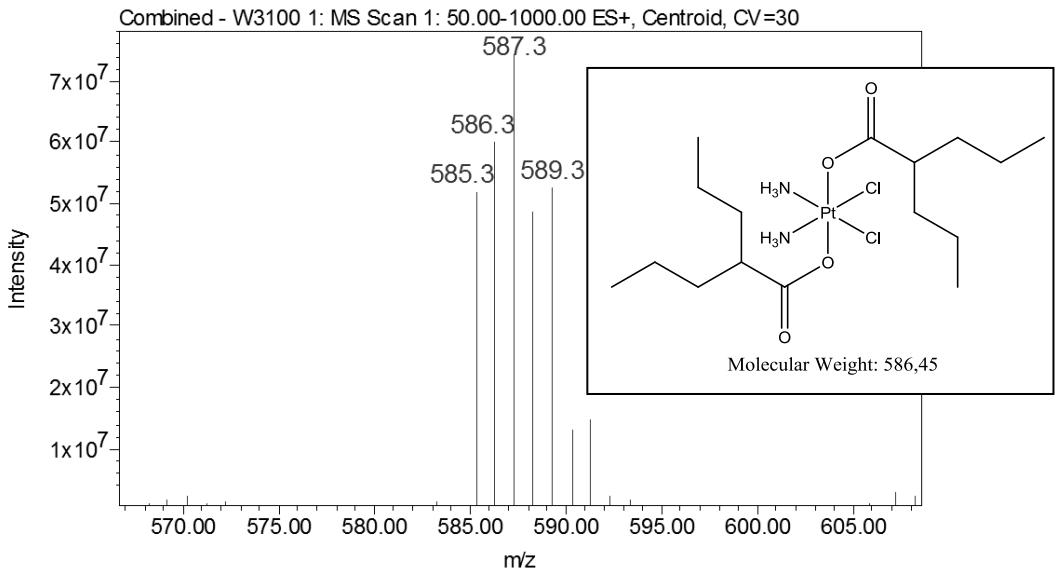

Figure 8.2: ESI-MS spectrum of complex **39**, prepared in methanol

The ESI-MS spectrum of compound **39** (*Figure 8.2*), registered in positive ion mode with a cone voltage of 30V, confirms the success of the reaction: in fact, it shows the pseudo-molecular ion $[M+H]^+$ peak at 587.3 m/z.

^{1}H-NMR

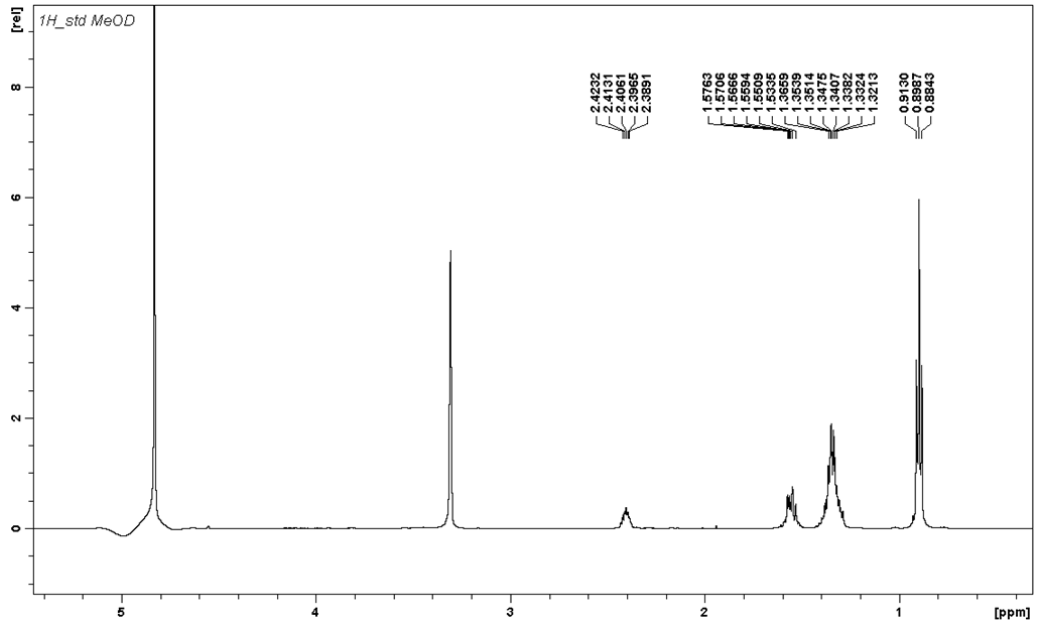

Figure 8.3: ^{1}H-NMR spectrum of complex **39**, registered in MeOD-d_4

The ^{1}H-NMR (500 MHz, MeOD-d_4) spectrum of complex **39** (*Figure 8.3*) shows the following signals, δ: 0.90 (t, -C*H*$_3$, 12H, ^{3}J = 7.2 Hz), 1.35 (m, -C*H*$_2$CH$_3$, 8H), 1.56 (m, -C*H*$_2$CH$_2$CH$_3$, 8H), 2.41 (m, -C*H*, 2H) ppm.

^{13}C-NMR

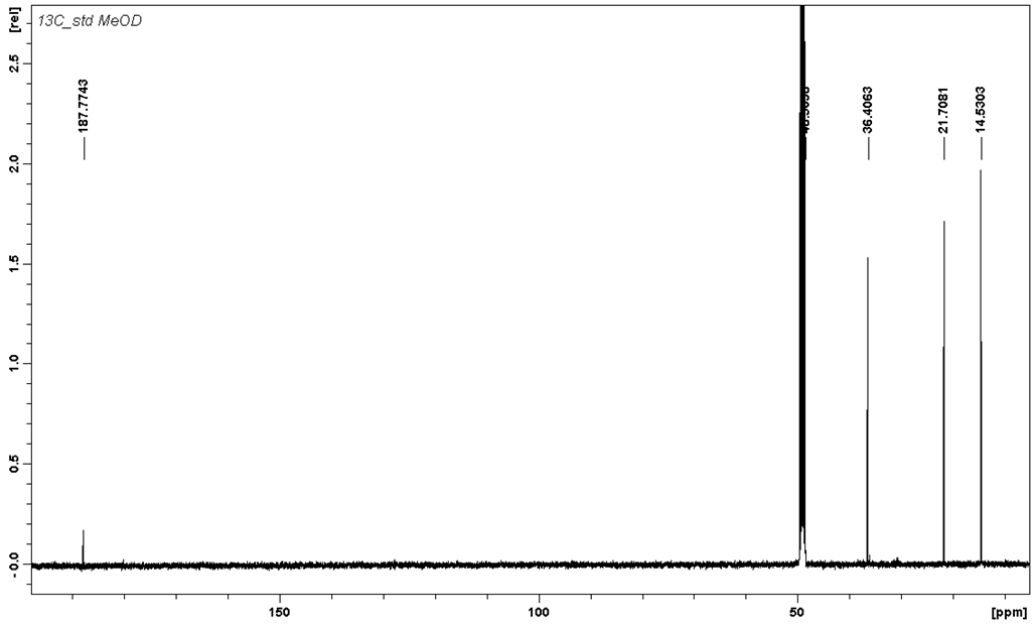

Figure 8.4: ^{13}C-NMR spectrum of complex **39**, registered in MeOD-d_4

The ^{13}C-NMR (125.7 MHz, MeOD-d_4) spectrum of complex **39** (*Figure 8.4*) shows the following signals, δ: 14.5 (-*C*H_3), 21.7 (-*C*H_2CH$_3$), 36.4 (-*C*H_2CH$_2$CH$_3$), 48.5 (-*C*H), 187.8 (-*C*O_2) ppm.

^{195}Pt-NMR

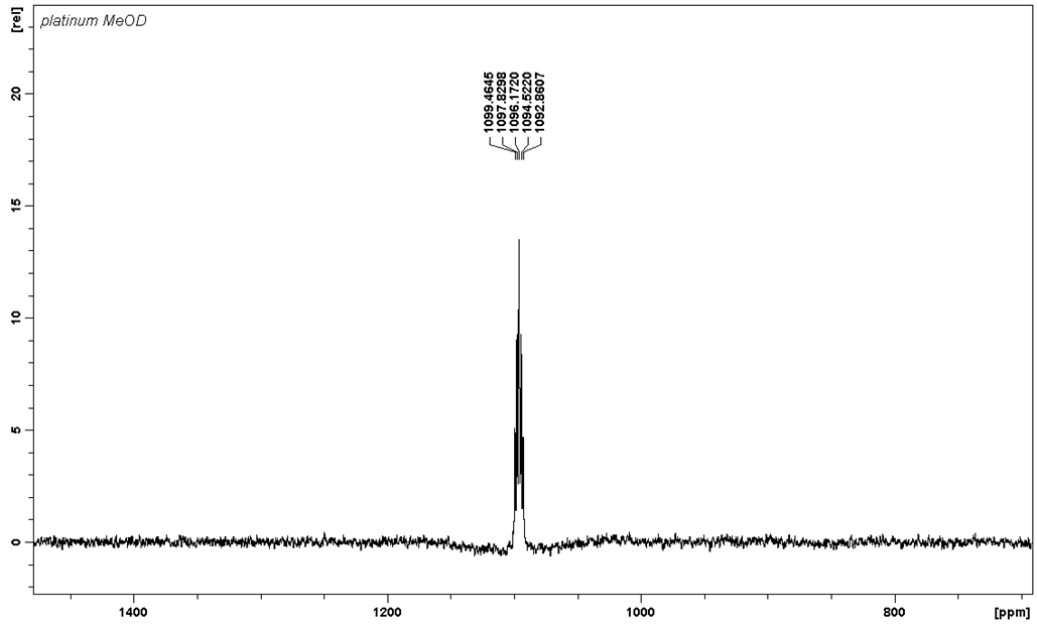

Figure 8.5: ^{195}Pt-NMR spectrum of complex **39**, registered in MeOD-d_4

The ^{195}Pt-NMR spectrum (*Figure 8.5*) of complex **39** (with a 107.2 MHz NMR frequency) showed a well-defined quintuplet at 1096 ppm (^{1}J = 177.7 Hz), consistent with a Pt(IV) complex containing two chlorides, two amines and two carboxylato ligands.

8.3 Preparation of the Liposomes

The liposomes [7] were prepared by the use of two lipids, i.e. the neutral 1,2-dioleoyl-sn-glycero-3-phosphoethanolamine (DOPE) and the cationic 1,2-dioleoyl-sn-glycero-3-ethylphosphocholine (chloride salt) (DOEPC) (*Figure 8.6*), which were dosed to synthesize carriers with a positive charge in order to ensure the adhesion to the cell membrane [9, 10, 11] in the case of *in vitro* assays. In particular, the molar fraction (α) of cationic lipid

$$\alpha = \frac{n_{L^+}}{n_{L^+} + n_{L^0}}$$

was fixed at 0.3 because it represented the best compromise between size and charge of the liposome itself: in fact, when α was 0.2 the diameter was slightly larger (323 ± 11 nm for liposomes encapsulating valproate salt, and 282 ± 6 nm for liposomes encapsulating both drugs), whereas α = 0.1 made the liposome difficult to be suspended in aqueous solution because the too low cationic let the lipophilic effect prevail. For this reason, the formulations based on 0.1 and 0.2 molar fraction of DOEPC were abandoned.

The synthetic procedure was a modification of a reported method [12].

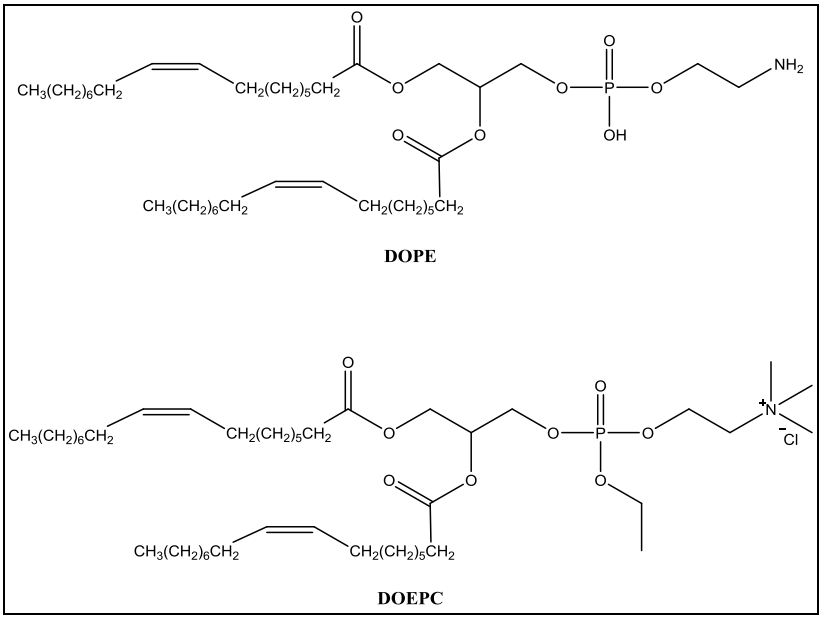

Figure 8.6: Structural formulas of the two lipids employed for the preparation of the liposomes

A mixture of DOPE (13.4 mg, 18.0 mmol) and DOEPC (6.60 mg, 7.76 mmol), representing a 0.3 DOEPC molar fraction (α), was dissolved in 1 mL of chloroform and dried under reduced pressure for 1 hour to obtain a homogeneous lipid film. Then 1 mL of a 20 mM HEPES/20 mM NaCl (pH 7.4)

aqueous solution (as such or containing 1 mM cisplatin and/or 2 mM valproate sodium salt) was added to the previously prepared film, vortexed and sonicated in an ultrasonic bath for 15 minutes in order to obtain a homogeneous suspension. This latter was extruded by means of a 1.5 mL Lipex Extruder (Northern Lipids Inc.) at 40 °C and under a 20 atm Argon pressure: in particular, 15 extrusions were carried out with 400, 200 and 100 nm polycarbonate extrusion membranes (NucleporeTM, Whatman International Ltd.), i.e. 5 extrusions per different membrane size. The prepared liposomes were treated in order to remove the not encapsulated drugs: they were filtered four times by using Centrifree® ultrafiltration devices (regenerated cellulose membrane, the molecular weight cut-off of which was 30 kDa, Merck Millipore) at 2000 g relative centrifugal force. After each centrifugation, the filtrate volume was quantified and the filter unit was refilled with the same volume (with the 20 mM HEPES/20 mM NaCl aqueous solution). The centrifugation of the inverted filter unit allowed to collect the purified liposomes, which were maintained at 4 °C. It was observed that, in these conditions, the liposomes were stable for one month.

The preparation of the liposomes containing complex **39** was slightly different from the previously mentioned one, because this lipophilic compound cannot be dissolved in aqueous solutions. Therefore, a mixture of DOPE, DOEPC and **39** (1 mM) was dissolved in 1 mL of chloroform, dried under reduced pressure and then suspended in 1 mL of HEPES/NaCl solution. The prepared mixture was processed as previously described.

The effective concentrations of the encapsulated Pt complexes and valproate were quantified by ICP-OES and an immunoturbidimetric assay, respectively. In particular, for the first analysis, 20 μL of the liposome suspension were mineralized by adding 200 μL of 70% w/w HNO_3 in an ultrasonic bath for 1 hour at 60 °C. Then the solution was diluted with 1% v/v HNO_3 to the final acid concentration of 1% v/v and the Pt content was measured by ICP-OES (by

selecting the 299.797 nm line). As regards the valproate, after the lysis of 50 µL of the liposomes suspension with 5% Triton X-100 at 72 °C [13], its content was quantified by employing an immunoturbidimetric assay (code MF010, Delta Chemie Biotechnology). This latter is based on the reaction between an antibody and latex particles bound to valproic acid and the analysis is based on turbidimetry: the solution turbidity was measured by exploiting the absorption and reflection at a specific wavelength (i.e. 600 nm). The turbidity produced is directly proportional to the valproic acid concentration present in the sample.

8.3.1 Size and Stability Investigations

The dimensional analyses of the liposomes were performed by DLS and TEM techniques (*paragraphs 4.2* and *5.5*).

The preparation of the sample for the DLS analysis consisted of the dilution of 20 µL of purified sample with the 20 mM HEPES/20 mM NaCl aqueous solution to the final volume of 1 mL. Then, the suspension was transferred into a quartz cuvette to perform the analysis (for each sample, five measurements were carried out).

For TEM analysis, 100 µL of the sample were dispersed in 200 µL of 4% low melting point agarose and, in order to ensure the polymerization of this latter, the suspension was maintained at 4 °C for 1 hour. By employing a single edge razor blade, the prepared sample was cut in small cubes of about 1-2 mm^3. Then the sample was divided into two batches: in particular, in one of them 2% of a potassium permanganate solution was added and it was incubated for 1 hour at 4 °C under gentle shaking, whereas the other one was fixed in 2.5% glutaraldehyde in HEPES overnight at 4 °C and, subsequently, in 1% osmium tetroxide solution for 1 hour. Then, each aliquot was washed several times with distilled water and dehydrated in graded ethanol series (from 30 to 100%),

embedded in Epon-Araldite resin and ultrathin sections were cut with a diamond knife in a Leica Ultracut UCT Ultramicrotome, double-stained with uranyl acetate and lead citrate, observed through a Philips CM 10 Transmission Electron Microscope, which operated at 60 kV.

The ζ potential analysis allowed to evaluate the suspension stability of each sample and was performed after the dispersion of 20 μL of liposomes in a 20 mM HEPES aqueous solution (without NaCl) to the final volume of 1 mL. Then the suspension was transferred into a cuvette and the analysis was carried out (five measurements).

The results of the analyses are shown in *Table 8.1*.

Liposome containing	DLS diameter	ζ potential
no drugs	166 ± 5 nm	58 ± 4 mV
cisplatin	163 ± 2 nm	58 ± 6 mV
sodium valproate	190 ± 9 nm	64 ± 2 mV
both cisplatin and sodium valproate	192 ± 17 nm	59 ± 4 mV
39	273 ± 14 nm	56 ± 8 mV

Table 8.1: Size and suspension stability results of the five types of liposomes

The data show that the encapsulation of cisplatin did not cause an increase in size, with respect to empty liposomes: in fact, in both cases, the diameters are about 160 nm. However, the inclusion of sodium valproate or complex **39** led to an increase to about 190 nm and 270 nm, respectively.

The ζ potential data (about +60 mV) show that all the liposomes exceed the threshold of stability (+30 mV): these results indicated that a very high stability was ensured for these systems and this aspect may increase the adhesion to the cellular membrane.

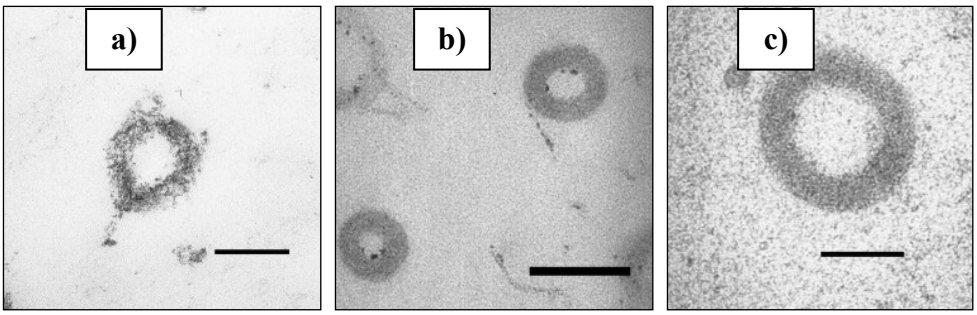

Figure 8.7: TEM micrographs of a) empty liposome after the treatment with $KMnO_4$, b) empty liposome after the treatment with OsO_4, c) cisplatin liposome after the treatment with OsO_4. The bars represent 200 nm in a) and b), whereas 100 nm in c)

The TEM micrographs (*Figure 8.7*) confirm the DLS analysis data. The results reported in *Chapters IV* and *V* point out that DLS diameters are larger than the TEM ones. However, in this case, the two dimensional analyses allow to obtain similar values: probably, the treatments employed for the liposomes led to an increase in the vector size.

8.4 Spontaneous Drug Release from Liposomes

The drug release from liposomes containing cisplatin, sodium valproate or complex **39** was evaluated in abiological conditions. In particular, the prepared nanosystems were kept at 37 °C for 4 hours in HEPES/NaCl solution and then filtered by means of Centrifree® ultrafiltration devices, centrifuged at 2000 g relative centrifugal force. Then, the previously described procedure for the liposomes purification was here followed: the filtrate volume was quantified, the filter unit was refilled with the same volume and the centrifugation of the inverted filter unit allowed to collect the liposomes.

These latter were employed for the quantification of the Pt or valproate residual concentration by ICP-OES and immunoturbidimetric assay, respectively, and

the released amount was determined by means of the difference between the initial and the residual concentrations.
The test showed that the drug release was 15 ± 5 % from the liposomes containing cisplatin, 10 ± 3 % from the liposomes encapsulating sodium valproate and 3 ± 1 % from the liposomes containing complex **39**.

8.5 Biological In Vitro Studies

After the phase of characterization, liposomes and complex **39** were tested *in vitro* to evaluate their ability in the inhibition of the cellular proliferation, their accumulation into the cells, their platination of DNA and, in particular, to evaluate the combination index of the different liposomes.

8.5.1 The Antiproliferative Activity (IC_{50})

The liposomes, cisplatin, valproate sodium salt and complex **39** were tested on A2780 human ovarian carcinoma cell line, grown in RPMI 1640 medium, which was supplemented with L-glutamine (2 mM), penicillin (100 IU/mL), streptomycin (100 mg/L) and 10% fetal bovine serum (FBS). The continuous treatments (72 hours) were performed at 37 °C in a 5% CO_2 humidified chamber and, after treating the cells with the compounds, the resazurin reduction assay was employed [14] in order to verify the remaining cells viability. The details are reported in *paragraph 4.19.1*.
The IC_{50} values (expressed as means of at least three independent replicates) were obtained from the dose-response sigmoids. Moreover, the data were normalized to 100% of viability for not-treated cells and the fluorescence/absorbance of the medium without cells was used as blank. The

results are summarized in *Table 8.2* and the curve-response curves are shown in *Figure 8.8*.

Compound	IC_{50} (µM) considering the Pt concentration	IC_{50} (µM) considering the valproate concentration
cisplatin	0.46 ± 0.11	-
sodium valproate	-	1833 ± 434
39	0.011 ± 0.003	0.022 ± 0.003
cisplatin liposome	0.13 ± 0.02	-
sodium valproate liposome	-	6.0 ± 1.2
cisplatin and sodium valproate liposome	0.07 ± 0.01	0.14 ± 0.02
39 liposome	0.007 ± 0.002	0.014 ± 0.003

Table 8.2: IC_{50} values of four liposomes compared to cisplatin, valproate sodium salt and complex **39**

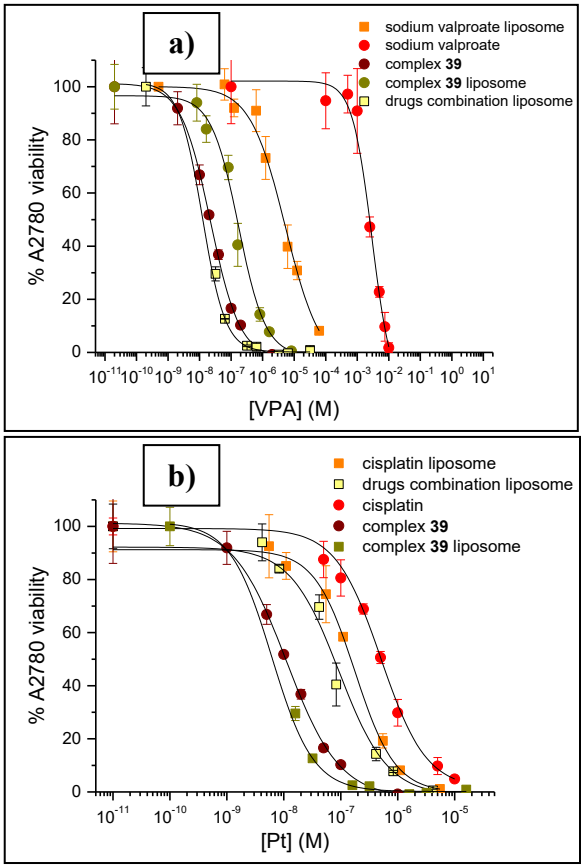

Figure 8.8: Dose-response curves of a) cisplatin, complex **39**, liposomes with cisplatin, complex **39** and both the drugs, and b) valproate sodium salt, complex **39**, liposomes with valproate sodium salt and both drugs

In almost all the cases (except for the liposomes containing both the drugs), it is possible to verify that the use of liposomes led to an increased cytotoxic activity with respect to free cisplatin and valproate: this is due to the fact that these vectors ensure a more efficient accumulation of the drug into the cells. In fact, the comparison between free and encapsulated into liposomes cisplatin show that the employment of the lipid carrier led to a 3.5 times higher efficacy. The antiproliferative activity of sodium valproate is enhanced by about 300 times when it is included into the liposomes.

As regards the system encapsulating two drugs, the presence of the HDAC inhibitor doubles the cytotoxicity of the cisplatin liposome, whereas the presence of cisplatin enhances the one of the valproate of about 40 times.
Complex **39**, however, results to be about six times more active than the liposome with the combined drugs, even though both contain the two drugs in the same ratio: in fact, complex **39** is a cisplatin-based Pt(IV) with two valproate coordinated in the axial positions, and the lipid vehicle contains cisplatin and valproate in a 1:2 molar ratio.
As regards the liposome containing **39**, instead, the lipid carrier did not significantly increase the antiproliferative activity of the free complex.

Furthermore, in order to verify the type of effect of the combination of the liposomes formulations, the Combination Index (CI) was evaluated. It is plotted as a function of the Affected Fraction, which represents the amount of residual viability after each combined treatment and is expressed as a numerical value from 0 (100% residual viability) to 1 (0% residual viability).
In this experiment the liposomes containing both cisplatin and valproate or the combined liposomes containing the single drugs were compared to the liposomes containg the single drugs. The resulting CI plot are reported in *Figure 8.9*.

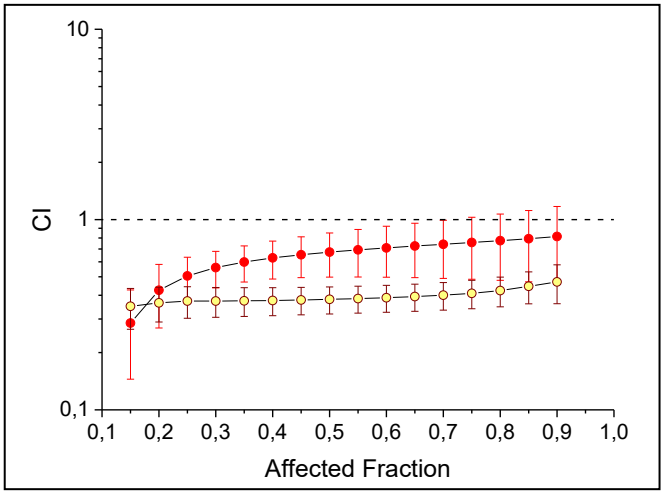

Figure 8.9: Combination Index *vs.* Affected Fraction of the liposome containing the drugs combination with respect to cisplatin-liposome and valproate-liposome (red balls) and combination index of the mixture of the cisplatin-liposome and the valproate-liposome with respect to cisplatin-liposome and valproate-liposome (yellow balls)

CI is always lower than 1, pointing out a synergism of the two drugs both in the case of a co-administration of the two separate liposomes and also when the two drugs are encapsulated in the same carrier, as previously demonstrated for free cisplatin and sodium valproate [4].

8.5.2 The Cellular Accumulation

The cellular accumulation of the synthesized compounds was expressed as Accumulation Ratio (AR) [15].

In particular, 10 μM cisplatin and complex **39** and 1 μM (expressed as Pt concentration) suspensions of liposomes (those containing platinum) were employed for the several treatments (4 h CT, 4 h CT + 20 h recovery (R) and 24 h CT) on A2780 human ovarian carcinoma cell line. After the established time, 100 μL of culture medium were harvested to measure the neat extracellular platinum concentration following adsorption to sterile plasticware. After the

treatment, cells were washed three times with PBS, detached from the 25 cm^2 flasks using 1 mL of 0.05% Trypsin 1X + 2% EDTA and harvested in fresh complete medium. Then, an automatic cell counting device was employed to measure the cells number and the mean diameter from every cell count. About 5 × 10^6 cells were transferred into a glass tube and spun at 1100 rpm for 5 minutes at room temperature. The supernatant was removed by aspiration and, in order to limit the cellular loss, about 200 µL of the supernatant were left. Each cell pellet was stored at -20 °C and, after defrosting it, 350 µL of HNO_3 70% w/w were added and mineralized for 1 hour at 60 °C in an ultrasonic bath. Then the sample was diluted with a 1% v/v aqueous solution of HNO_3 (by adding 5650 µL) to a final 4 % v/v of acid concentration and the platinum content of each solution was quantified by means of ICP-MS.

The results were expressed as Pt µg/L (ppb) and then divided by the platinum atomic mass (195 u) to determine the corresponding µM Pt concentration.

The data processing, after the normalization of the intracellular platinum content upon the cells number and volume (calculated from the actual mean cell diameter measured for each sample), allowed to determine the intracellular platinum concentration. The ratio between the intra- and extracellular Pt concentrations allowed to obtain the AR value of each sample (*Figure 8.10*).

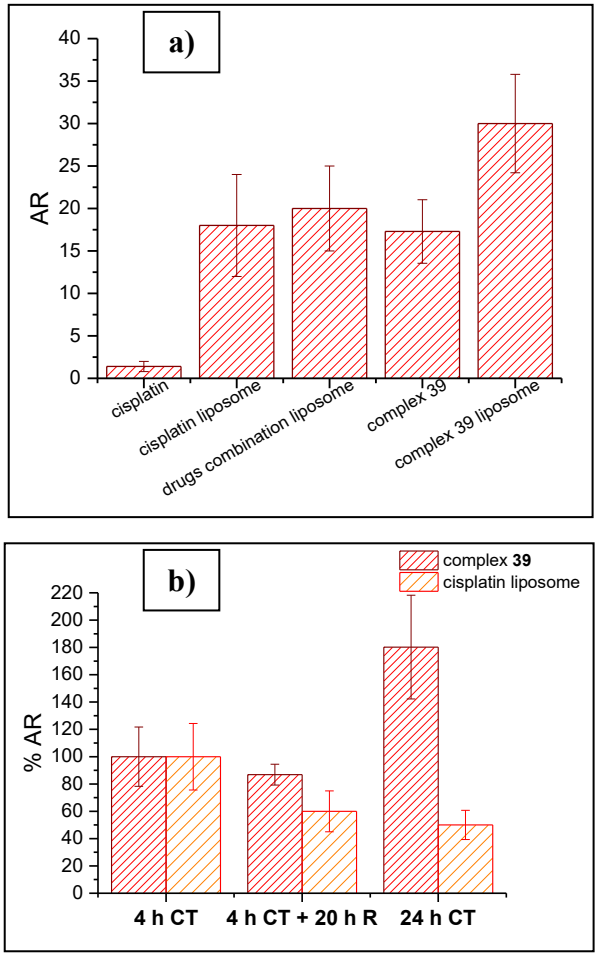

Figure 8.10: Bars graphs of the AR values of a) cisplatin, complex **39** and liposomes containing cisplatin, both the drugs and complex **39**, and b) complex **39** and cisplatin liposome as a function of time

The bars graph in *Figure 8.10a* shows that, after 4 hours of continuous treatment (CT), the liposomes containing only cisplatin and both cisplatin and valproate have AR values similar to those of complex **39** but about 15 times higher than cisplatin. On the contrary, the liposome containing **39** gives the highest cellular accumulation results, even though there are no remarkable improvements on the efficacy, probably due to an incomplete drug release in the cell cytosol.

The *Figure 8.10b* points out that the AR of complex **39** results increased by passing from a 4 hours to a 24 hours CT (as expected for a lipophilic compound) and slightly decreased after 4 hours of treatment, followed by 20 hours of recovery (R) in fresh medium. This latter study, in particular, aimed to evaluate the efficiency of the drug efflux: in fact, the lipophilicity of some platinum(IV) species allows them to remain into the cells and to continue to bind DNA [16]. Cisplatin (released by the cisplatin liposome), instead, was rapidly removed from the cells by efficient detoxification pathways, being a hydrophilic compound.
Furthermore, it was possible to observe a decrease of the accumulation ratio values of the cisplatin liposome by passing from a 4 hours to a 24 hours CT and, as expected, after a recovery period in fresh medium.

8.5.3 The DNA Platination

The measurements of DNA platination is the phase that follows the cellular accumulation and consists of the binding of the considered drug to the DNA. This parameter must be normalized for the extracted amount of DNA because the extraction efficiency is not constant and can be expressed as Pt pg/DNA μg or Pt pg/(1×10^6) cells. This latter can be obtained multiplying the DNA platination by 6.550 (in fact, female cells, such as A2780 cells, contain 6.550 μg DNA/10^6 cells; on the contrary, male cells contain 6.436 μg DNA/10^6 cells).
In particular, a 10 μM ethanol solution of complex **39** was employed for three different treatments of A2780 cells: 4 hours of continuous treatment (CT), 24 hours of CT, or 4 hours of CT followed by 20 hours recovery (R, i.e. suspension of the cells in fresh medium). About 5×10^6 cells, from each experiments, were collected for cellular accumulation quantification, whereas about 20×10^6 cells were used to quantify the DNA platination.

After the fixed time, the cells were transferred into a plastic microcentrifuge tube and centrifuged at 1100 rpm for 5 minutes at room temperature: the supernatant was removed by aspiration, and the total genomic DNA was extracted from the cell pellet. In particular, during cell lysis, DNA was purified by RNAse A and proteinase K treatment, then extracted on silica-based centrifugation columns and eluted in 300 µL of elution buffer. 8 µL of sample or elution buffer (used as blank) were diluted in TE buffer (10 mM Tris-HCl, 1 mM EDTA, pH 8.0) to the final volume of 80 µL. The absorbance values at 260 nm (A_{260}, relative to nucleic acids) and at 280 nm (A_{280}, relative to proteins) were recorded from triplicate wells. Then, the two previously mentioned values (i.e. A_{260} and A_{280}) were corrected by subtraction of the background absorbance (A_{340}), and subsequently the samples purity was verified by means of the A_{260}/A_{280} ratio. In all the cases, this ratio resulted to be higher than 2: this indicated that only nucleic acids were present and this avoided the occurrence of complexes-proteins interactions, which can modify the results. After the subtraction of mean A_{260} of blank wells, the DNA concentration was calculated from the corrected A_{260} by means of a calibration curve obtained with calf thymus DNA. Under these conditions, an absorbance = 1 at 260 nm corresponds to 100 µg of DNA per mL. The remaining amount of DNA elution buffer was transferred into a borosilicate glass tube, its precise volume was obtained by weight in order to determine the total amount of DNA, and the sample was stored at -20 °C. After defrosting, the samples were mineralized according to the procedure described in *paragraph 8.4.2* but, in this case, 100 µL of HNO_3 70% w/w were added and, after the mineralization, the sample was diluted with a 1% v/v aqueous solution of HNO_3 (by adding 1800 µL) to a final 3.7 % v/v of acid concentration and the platinum content of each solution was quantified by means of ICP-MS.

The platination data (expressed as Pt pg/ DNA μg of a mean of at least three independent replicates) are reported in *Figure 8.11*.

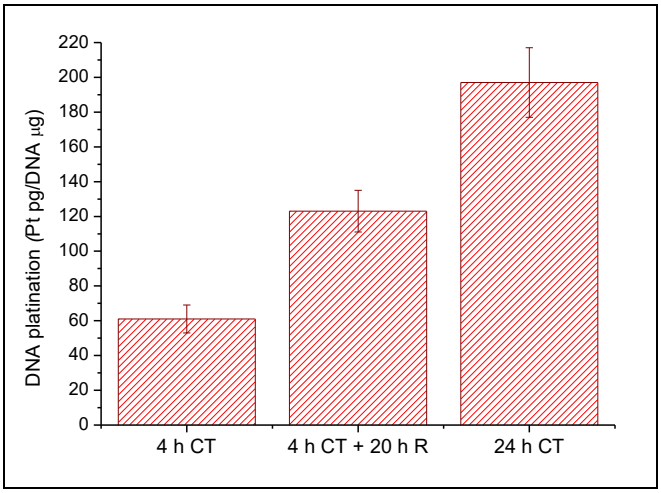

Figure 8.11: Bars graph of the DNA platination of complex **39** after 4 h of continuous treatment (CT), 4 h of CT summed to 20 h of recovery, and 24 h of CT

Complex **39** shows an increasing time-related platination: the lipophilicity of the compound ensured its permanence into the cells and the platination occurred because the Pt(IV) was activated to the Pt(II) metabolite, which continued to bind DNA [7, 16].

8.6 Conclusions

In this work, cationic liposomes containing cisplatin, sodium valproate, their combination or complex **39** (i.e. a cisplatin-based Pt(IV) with two valproate ligands coordinated in axial position) were successfully prepared. By the determination of the Combination Index (CI), it was verified that both the liposome formulation of the two free drugs and the co-administration of the two separate liposomes (in both cases with 1:2 cisplatin/valproate molar ratio)

resulted to be synergic. Moreover, the antiproliferative activity of all the liposomes was evaluated on A2780 cell line and compared with free cisplatin, valproate and complex **39**. The results pointed out that the use of liposomes enhances the cytotoxicity of the drugs, except when cisplatin and sodium valproate are combined: in fact, in this case, this formulation resulted to be less active than complex **39**.

The encapsulation of complex **39**, instead, increased its cellular accumulation but the corresponding antiproliferative activity was not significantly improved, probably because the drug was not completely released at cellular level.

Complex **39** increased its accumulation ratio passing from 4 hours to 24 hours of treatment, whereas the liposome encapsulating cisplatin showed the opposite behavior.

Furthermore, the DNA platination of complex **39** resulted to be increased by three times after 24 hours of treatment, with respect to the results obtained after 4 hours: in fact, being **39** a lipophilic compound, it was not removed by the cells (unlike cisplatin) and, therefore, after its reduction to the active species, it continued to bind DNA.

References

[1] N. J. Vogelzang, J. J. Rusthoven, J. Symanowski, C. Denham, E. Kaukel, P. Ruffie, U. Gatzemeier, M. Boyer, S. Emri, C. Manegold, C. Niyikiza, P. Paoletti, Phase III study of pemetrexed in combination with cisplatin versus cisplatin alone in patients with malignant pleural mesothelioma, *J. Clin. Oncol.*, 21 (2003), 2636-2644.

[2] F. Vandermeers, P. Hubert, P. Delvenne, C. Mascaux, B. Grigoriu, A. Burny, A. Scherpereel, L. Willems, Valproate, in Combination with Pemetrexed

and Cisplatin, Provides Additional Efficacy to the Treatment of Malignant Mesothelioma, *Clin. Cancer Res.*, 15 (2009), 2818-2828.

[3] S. A. Bassett, M. P. G. Barnett, The Role of Dietary Histone Deacetylases (HDACs) Inhibitors in Health and Disease, *Nutrients*, 6 (2014), 4273-4301.

[4] I. Zanellato, I. Bonarrigo, E. Gabano, M. Ravera, N. Margiotta, P. G. Betta, D. Osella, Metallo-drugs in the treatment of malignant pleural mesotelioma, *Inorg. Chim. Acta*, 393 (2012), 64-74.

[5] T. C. Chou, P. Talalay, Quantitative analysis of dose-effect relationships: the combined effects of multiple drugs or enzyme inhibitors, *Adv. Enzyme Regul.*, 22 (1984), 27-55.

[6] T. C. Chou, Theoretical Basis, Experimental Design, and Computerized Simulation of Synergism and Antagonism in Drug Combination Studies, *Pharmacol. Rev.*, 58 (2006), 621-681.

[7] M. Ravera, E. Gabano, I. Zanellato, A. Gallina, E. Perin, A. Arrais, S. Cantamessa, D. Osella, Cisplatin and valproate released from the bifunctional $[Pt^{(IV)}Cl_2(NH_3)_2(valproato)_2]$ antitumor prodrug or from liposome formulations: who does what?, *Dalton Trans.*, 46 (2017), 1559-1566.

[8] M. Alessio, I. Zanellato, I. Bonarrigo, E. Gabano, M. Ravera, D. Osella, Antiproliferative activity of Pt(IV)-bis(carboxylato) conjugates on malignant pleural mesothelioma cells, *J. Inorg. Biochem.*, 129 (2013), 52-57.

[9] S. Salatin, S. M. Dizaj, A. Y. Khosroushahi, Effect of the surface modification, size, and shape on cellular uptake of nanoparticles, *Cell Biol. Int.*, 39 (2015), 881-890.

[10] C. B. He, Y. P. Hu, L. C. Yin, C. Tang, C. H. Yin, Effects of particle size and surface charge on cellular uptake and biodistribution of polymeric nanoparticles, *Biomaterials*, 31 (2010), 3657-3666.

[11] V. Forest, M. Cottier and J. Pourchez, Electrostatic interactions favor the binding of positive nanoparticles on cells: A reductive theory, *Nano Today*, 10 (2015), 677-680.

[12] M. Munoz-Ubeda, A. Rodriguez-Pulido, A. Nogales, O. Llorca, M. Quesada-Perez, A. Martin-Molina, E. Aicart, E. Junquera, Gene vectors based on DOEPC/DOPE mixed cationic liposomes: a physicochemical study, *Soft Matter*, 7 (2011), 5991-6004.

[13] M. Sila, S. Au, N. Weiner, Effects of Triton X-100 concentration and incubation temperature on carboxyfluorescein release from multilamellar liposomes, *Biochim. Biophys. Acta - Biomembranes*, 859 (1986), 165-170.

[14] E. Magnani, E. Bettini, Resazurin detection of energy metabolism changes in serum-starved PC12 cells and of neuroprotective agent effect, *Brain Res. Protocol.*, 5 (2000), 266-272.

[15] A. Ghezzi, M. Aceto, C. Cassino, E. Gabano, D. Osella, Uptake of antitumor platinum(II)-complexes by cancer cells, assayed by inductively coupled plasma mass spectrometry (ICP-MS), *J. Inorg. Biochem.*, 98 (2004), 73-78.

[16] M. Ravera, E. Gabano, I. Zanellato, I. Bonarrigo, M. Alessio, F. Arnesano, A. Galliani, G. Natile, D. Osella, Cellular trafficking, accumulation and DNA platination of a series of cisplatin-based dicarboxylato Pt(IV) prodrugs, *J. Inorg. Biochem.*, 150 (2015), 1-8.

Conclusions and Perspectives

During the Ph.D. thesis, most attention was focused on the synthesis and characterization of several Pt(IV) complexes, containing suitable functionalities to be exploited in coupling reactions with vectors (*Figure 1*) useful for passive Drug Targeting and Delivery strategies, in order to improve the selective accumulation of such antitumor prodrugs.

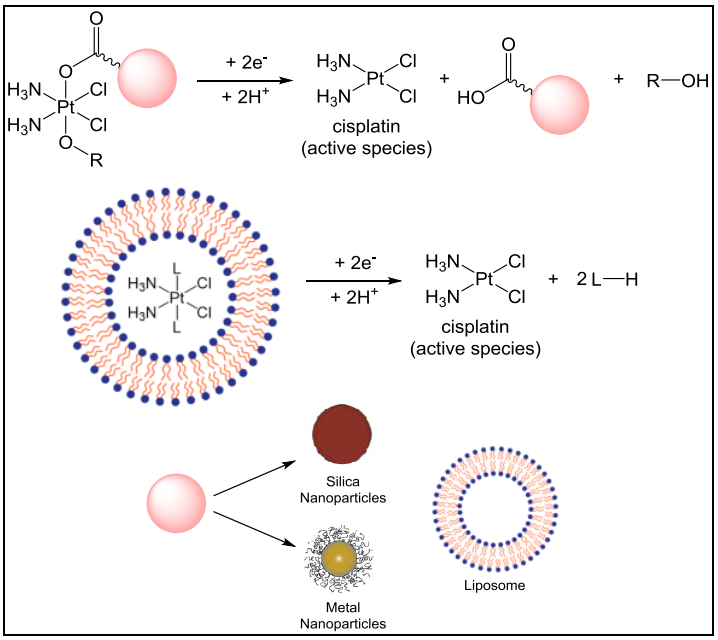

Figure 1: Schematic representation of different types of platinum drug targeting methods, which ensure a more selective accumulation of the drugs into the cells

Some of the employed nanosystems (i.e. silica nanoparticles, modified chitosan and liposomes) were synthesized as part of this work, whereas other vectors (i.e. fluorescent silica nanoparticles and iron oxide nanoparticles) were provided

thanks to the collaboration with the research groups of Prof. M. Laus (Università del Piemonte Orientale, DiSIT) and Dr. J. Fresnais (Sorbonne-Université, Paris). The synthesized Pt-nanoparticle conjugates were characterized from a chemical point of view by SEM, TEM, DLS and ζ potential techniques, and by ICP-MS and ICP-OES analyses to determine the amount of the loaded species. The biological *in vitro* experiments, instead, were performed in cell culture laboratory at DiSIT (Università del Piemonte Orientale).

In particular, the coupling reactions with different kinds of amino-functionalized silica nanoparticles allowed to prepare conjugates with significant *in vitro* efficacy against A2780 human ovarian carcinoma cell line. The employed nanoparticles proved to be suitable vectors for Pt(IV) antitumors prodrugs and, as a future perspective, the synthesized nanosized system should be tested *in vivo*, in order to verify the exploitation of the EPR effect. Moreover, other platinum complexes could be loaded on the nanoparticles in order to study the effect of the modification of the employed prodrugs, trying to avoid the occurrence of side effects.

The conjugates obtained with the couplings of the previously prepared Pt(IV) complexes with chitosan and chitosan derivatives were completely characterized from a chemical point of view and the *in vitro* tests are now in progress, in collaboration with the Radiopharmaceutical Sciences Group of Dr. A. Paulo (Instituto Superior Técnico, Sacavém, Portugal).

The synthesis and characterization of Pt(IV) prodrugs able to link magnetic iron oxide nanoparticles and their coupling reactions with such vectors were successful. Moreover the prepared conjugates are now undergoing *in vitro* experiments. Based on the results of these experiments new complexes could be synthesized and tested as prodrugs to be linked to such nanoparticles.

Finally, the synthesis of cationic liposomes and the following encapsulation of antitumor drugs were carried out and their *in vitro* studies were performed.

Future perspectives of this work can include the encapsulation of other drugs and/or the setting up and following exploitation of different liposome formulations.

In almost all the carried out projects, the results confirmed that these nanosized systems are vectors able to ensure a more enhanced *in vitro* cellular accumulation and antiproliferative activity than the corresponding free Pt complex.

List of Publications

- M. Ravera, E. Perin, E. Gabano, I. Zanellato, G. Panzarasa, K. Sparnacci, M. Laus, D. Osella, Functional fluorescent nonporous silica nanoparticles as carriers for Pt(IV) anticancer prodrugs, *Journal of Inorganic Biochemistry*, **2015**, *151*, 132-142.

- M. Ravera, E. Gabano, I. Zanellato, E. Perin, A. Arrais, D. Osella, Polyanionic Biopolymers for the Delivery of Pt(II) Cationic Antiproliferative Complexes, *Bioinorganic Chemistry and Applications*, **2016**, *2016*, Article ID 2380540, 1-7.

- M. Ravera, E. Gabano, I. Zanellato, E. Perin, A. Arrais, D. Osella, Functionalized nonporous silica nanoparticles as carriers for Pt(IV) anticancer prodrugs, *Dalton Transactions*, **2016**, *45*, 17233-17240.

- M. Ravera, E. Gabano, I. Zanellato, A. Gallina, E. Perin, A. Arrais, S. Cantamessa, D. Osella, Cisplatin and valproate released from the bifunctional $[Pt^{(IV)}Cl_2(NH_3)_2(valproato)_2]$ antitumor prodrug or from liposome formulations: who does what?, *Dalton Transactions*, **2017**, *46*, 1559-1566.

Acknowledgements

Un ringraziamento particolare va al Prof. Mauro Ravera, mio supervisore, ed al Prof. Domenico Osella per la loro infinita disponibilità e la proficua collaborazione nel corso di questi anni.

Un ringraziamento speciale va alla Dott.ssa Elisabetta Gabano, la quale è stata assiduamente disponibile, infinitamente paziente e sempre pronta a dare fruttuosi consigli sia dal punto di vista lavorativo che in fase di stesura della tesi. La ringrazio anche per la buona compagnia in occasione di alcuni congressi a cui abbiamo entrambe partecipato.

Ringrazio ancora questo mio gruppo di ricerca per avermi appassionata e coinvolta attivamente già a partire dal tirocinio della Laurea Triennale in Chimica, per avermi dato l'opportunità di svolgere i progetti prima descritti e per avermi fatto crescere sia dal punto di vista chimico che umano.

Altro ringraziamento va al Dott. Stefano Tinello con cui ho condiviso tutto il persorso universitario e che si è dimostrato sempre pronto ad aiutarmi ogni qual volta sia stato necessario.

Un ringraziamento va alla Dott.ssa Ilaria Zanellato, al Dott. Andrea Gallina e alla Dott.ssa Beatrice Rangone per aver testato *in vitro* i composti da me preparati, per la loro disponibilità nel chiarire ogni eventuale dubbio e per il rapporto di amicizia instauratosi nel corso degli anni.

Ringrazio il Dott. Claudio Cassino, persona estremamente preparata in ogni ambito chimico (non solo NMR) e dalla infinita disponibilità e gentilezza.

Altro ringraziamento va al Dott. Davide Musso per la sua disponibilità e per aver collaborato con me per le analisi effettuate mediante ICP-MS e ICP-OES.

Ringrazio la Dott.ssa Francesca Trivero, con la quale si è instaurata da subito una bella amicizia, la Dott.ssa Sabrina Bianco, la quale mi ha insegnato molto e mi ha dato preziosi consigli, il Dott. Federico Fregonese e la Dott.ssa Manuela Alessio, con cui ho condiviso parte del percorso di Dottorato.
Ringrazio Loredana, Emanuela, Davide e Valeria, con cui ho condiviso il laboratorio di Chimica Bioinorganica negli ultimi mesi, per la buona compagnia.
Ringrazio i ragazzi che ho seguito in laboratorio (sia di ricerca e che di didattica), nel corso di questi tre anni, poiché mi hanno permesso di crescere, di maturare la capacità di gestire le situazioni ed il lavoro altrui, e con cui si sono instaurati ottimi rapporti.
Un ringraziamento molto speciale va alla mia famiglia che mi è sempre stata vicina e mi ha sempre supportata in ogni mia scelta, dandomi tanta forza e incoraggiandomi in ogni occasione.
Infine, ringrazio la Compagnia di San Paolo (progetto BIPLANES) che ha supportato la ricerca svolta.